Author:
Kim, Dongik

Title:
Analysis of climate change using century-long reanalysis data over South Korea

Analysis of climate change using century-long reanalysis data over South Korea

By

Dong-Ik Kim BSc

A Dissertation submitted to the University of Bristol in accordance with the requirements of the degree of Doctor of Philosophy in the Faculty of Engineering.

Department of Civil Engineering

January 2019

Approximately 58327 words

ABSTRACT

Long-term climate data play a vital role in climate change analysis, but *in situ* observations are spatio-temporally limited in many regions throughout the world – including South Korea. A lack of data may lead to considerable uncertainties in hydrological applications and make it difficult to detect nonstationarity that can significantly affect future risk estimation. This challenge is especially the case in rainfall frequency analysis. This thesis aims to analyse the climate change impact, especially for rainfall intensity change, by adopting globally available century-long reanalysis data. Although a few century-long reanalyses have been developed, there is still a knowledge gap on the suitability of such data for regional-scale studies. Due to the systematic errors in the data, bias correction should be considered before any applications. Accordingly, this thesis mainly consists of three parts: 1) the assessment of the reanalysis data in regional-scale analyses, 2) the bias correction of the century-term reanalysis data to reduce design rainfall uncertainty, and 3) the reanalysis-data-based nonstationary rainfall frequency analysis.

The first part evaluates the long-term reanalyses in South Korea, which is the selected study region in this thesis. Multi-decadal reanalyses (ERA-20cm, ERA-20c, ERA-40, and 20CR) for monthly mean precipitation and temperature were first assessed in South Korea compared with the global gridded observations (CRUv3.23 and GPCCv7). This analysis showed that reanalysis data could statistically reproduce observations well, but all products should be locally adjusted before their hydrological applications. A two-step approach was followed for the bias correction of the century-long reanalysis data: 1) a quantile mapping (QM) method using a composite gamma-Pareto distribution for the reference period (1973–2010) and 2) a trend-preserving QM method (i.e. quantile delta mapping method) for the whole 20th century. The evaluation suggested that the proposed bias correction scheme was useful for a regional-scale modelled data with a limited network of rain gauges. Meanwhile, the century-long data contributed to the reduction of design rainfall uncertainty. The final part presents a reanalysis-product-based nonstationary analysis. This new approach suggested that the stationary approach could underestimate future risk in many areas. The findings in this thesis show that despite the biases, reanalysis data can provide valuable information that helps researchers to understand an area's climate change impact using limited observations.

Keywords | *Bayesian approach, bias correction, composite distribution, nonstationarity, precipitation, quantile delta mapping, reanalysis, uncertainty*

AUTHOR'S DECLARATION

I declare that the work in this thesis was carried out in accordance with the requirements of the University's Regulations and Code of Practice for Research Degree Programmes and that it has not been submitted for any other academic award. Except where indicated by specific reference in the text, the work is candidate's own work. Work done in collaboration with, or with the assistance of, others, is indicated as such. Any views expressed in the dissertation are those of the author.

SIGNED:…… DATE:……..……

ACKNOWLEDGEMENTS

I would like to express my deepest gratitude to my supervisor, Prof. Dawei Han for his continuous and tremendous support. Over the past three years, he has always guided me in the right research direction and encouraged me to successfully finish my work. The logical thinking, enthusiasm and confident attitude I have leant from him will benefit me for my life.

My sincere gratitude should also go to Dr. Francesca Pianosi, the reviewer of my PhD study, for her support, advice, and guidance in reviewing my research work.

Special thanks must also go to Prof. Hyun-Han Kwon, who led and guided me to bias correction studies. I am also grateful to Prof. Taesam Lee for his valuable suggestions on nonstationary analysis. They gave me valuable advice in research throughout my PhD study.

Earnest thanks should go to Dr. Kue Bum Kim and Mr. Moonhyuk Kwon for their support during my PhD study. With their active help and selfless support, I could have confidence during my PhD study. I would also like to thank every research group member since I joined, Dr. ASMM Rahman, Dr. Fanny Sarrazin, Dr. Joost Iwema, Dr. Jun Zhang, Dr. Null Nanding, Dr. Qiang Dai, Dr. Sherien Al-Azerji, Dr. Yang Song, Dr. Otto Chen, Ms Ludovica Beltrame, and Mr. Charles West for sharing their insights, knowledge, and discussions.

I would like to thank the European Centre for Medium-range Weather Forecasts (ECMWF), the National Oceanic and Atmospheric Administration (NOAA), the Climatic Research Unit (CRU) and the Global Precipitation Climatology Centre (GPCC) and the Korea Meteorological Administration (KMA) for providing their datasets to my work.

Finally, but by no means least, I owe my deepest appreciation and heartfelt gratitude to my beloved wife Seoungyeon Lee and only child Jitae Kim. Their love is beyond expression. My research would not have been completed without their ardent support and constant encouragement.

The Government of South Korea provided financial support for carrying out the study.

January 2019 (Dong-Ik Kim)

LIST OF PUBLICATIONS

(Kim D.-I. carried out all the analyses and wrote the papers, and co-authors discussed and checked the manuscripts.)

< Journal papers >

1. Kim, D.-I. and Han, D., 2018. Comparative study on long term climate data sources over South Korea. J. Water Clim. Chang. https://doi.org/10.2166/wcc.2018.032

2. Kim, D.-I., Kwon, H.-H., and Han, D., 2018. Exploring the Long-Term Reanalysis of Precipitation and the Contribution of Bias Correction to the Reduction of Uncertainty over South Korea: A Composite Gamma-Pareto Distribution Approach to the Bias Correction. Hydrol. Earth Syst. Sci. Discuss., https://doi.org/10.5194/hess-2018-36

3. Kim, D.-I. and Han, D., Evaluation of ERA-20cm reanalysis dataset over South Korea. J. Hydro-environ. Res. (under revision)

4. Kim, D.-I., Kwon, H.-H., and Han, D., Exploring the long-term reanalysis of precipitation and its bias correction using a composite gamma-Pareto distribution approach over South Korea. Hydrol. Res. (accepted under minor revision)

5. Kim, D.-I., Han, D., and Lee, T., Reanalysis-product-based nonstationary frequency analysis for estimating extreme design rainfall. J. Hydrol. (in review)

6. Kim, D.-I., Kwon, H.-H., and Han, D., Exploration of intensity change in daily precipitation using bias-corrected ERA-20c in South Korea for the 20th century (1900-2010). Clim. Dyn. (in review)

< Conferences >

7. Kim, D.-I., Kwon, H.-H., and Han, D., 2018. Exploration of intensity change in daily precipitation using bias-corrected ERA-20c in South Korea over the whole 20th century. EGU General Assembly 2018, Vienna, Austria. (Poster presentation).

8. Kim, D.-I. and Han, D., 2017. Comparative study on long term climate data sources over South Korea. EGU General Assembly 2017, Vienna, Austria. (Poster presentation).

TABLE OF CONTENTS

LIST OF FIGURES

LIST OF TABLES

LIST OF ABBREBIATIONS

AIC	Akaike information criterion
AMR	Annual maximum rainfall
BIC	Bayesian information criterion
BM	Block maxima method
CDF	Cumulative distribution function
CRU	Climatic Research Unit at the University of East Anglia
CRUv3.23	CRU model data version 3.23
CV	Coefficient of variation
ECMWF	European Centre for Medium-range Weather Forecasts
En0 (En9)	Ensemble member 0 (Ensemble member 9) of ERA-20cm
ENE	Expected number of exceedance
ENSO	El Niño-Southern Oscillation
ERA-20c	ECMWF 20th century reanalysis assimilating surface observations only
ERA-20cm	ECMWF 20th century atmospheric model ensemble
ERA-40	ECMWF 45-year reanalysis
EWT	Expected waiting time approach
GEV	Generalised extreme value distribution
GLUE	Generalised likelihood uncertainty estimation
GPCC	Global Precipitation Climatology Centre
GPCCv7	GPCC precipitation data version 7
GPD	Generalised Pareto distribution
gpQM	Quantile mapping based on a combined distribution of gamma and GPD
gpQM95	gpQM with the 95th percentile as the upper threshold
gpQM99	gpQM with the 95th percentile as the upper threshold

gQM	Quantile mapping based on a gamma distribution
GUM	Gumbel distribution
IDW	Inverse distance weighting method
IM-PCM	Interpolation method based on parameter contour maps
IPCC	Intergovernmental Panel on Climate Change
KMA	Korea Meteorological Administration
LOGN	Log-normal distribution
MCMC	Markov Chain Monte Carlo algorithm
MH	Metropolis-Hastings sampler
NOAA	National Oceanic and Atmospheric Administration
NSE	Nash–Sutcliffe efficiency
NWP	Numerical weather prediction
Obs	Observation for the reference period in each chapter
Obs0	Observation from 1974–2017
Obs95a/Obs99a	Design rainfall uncertainties using prior distribution for the shape parameter of GEV informed by QDM95v0/QDM99v0
Obs95b/Obs99b	Design rainfall uncertainties using prior distributions for location and scale parameters of GEV informed by QDM95v0/QDM99v0
Obs95c/Obs99c	Design rainfall uncertainties using prior distributions for all parameters of GEV informed by QDM95v0/QDM99v0
ONI	Oceanic Niño Index
PDF	Probability density function
POT	Peak over threshold
QM	Quantile mapping
QM95/QM99	QM approaches based on a composite distribution of gamma and GPD with the 95^{th} /99^{th} percentiles as the upper thresholds
gevQM	QM approach based on a GEV distribution
gamQM	QM approach based on a gamma distribution
gumQM	QM approach based on a Gumbel distribution

QDM	Quantile delta mapping
QDM95/QDM99	QDM approaches based on a composite distribution of gamma and GPD with the 95^{th} /99^{th} percentiles as the upper thresholds
QDM95v1	Design rainfall uncertainty derived from the bias-corrected AMRs by using QDM95 from 1974 to 2010
QDM99v1	Design rainfall uncertainty derived from the bias-corrected AMRs by using QDM99 from 1974 to 2010
QDM95v0	Design rainfall uncertainty derived from the bias-corrected AMRs by using QDM95 from 1900 to 2010
QDM99v0	Design rainfall uncertainty derived from the bias-corrected AMRs by using QDM99 from 1900 to 2010
gevQDM	QDM approach based on a GEV distribution
gamQDM	QDM approach based on a gamma distribution
gumQDM	QDM approach based on a Gumbel distribution
SQM	Stationary quantile mapping
SQM95/SQM99	SQM approaches based on a composite distribution of gamma and GPD with the 95^{th} /99^{th} percentiles as the upper thresholds
gevSQM	SQM approach based on a GEV distribution
gamSQM	SQM approach based on a gamma distribution
gumSQM	SQM approach based on a Gumbel distribution
RMSE	Root mean square error
SST	Sea surface temperature
TH	(cut-off) Threshold
WEI	Weibull distribution
20CR	NOAA 20^{th} century reanalysis data

CHAPTER 1 Introduction

1.1 Background and motivation

Long-term climate change is a fundamental issue in scientific and engineering disciplines. Previous studies have addressed that climate change has impacted a wide range of fields such as agriculture, environment, health, economy and water resources (IPCC, 2014; Nelson et al., 2009; Patz et al., 2005; Vörösmarty et al., 2000). A long-term change in climate variables such as precipitation and temperature can affect crop growth, the ecosystem, human diseases, and water-related hazards. Of these impacts, water-related hazards are closely linked to changes in rainfall intensity, which are of primary concern to water resource managers. Especially, in South Korea, flood events have happened frequently and caused the economic losses as well as severe casualties (MOLIT, 2013). Moreover, it is anticipated that the frequency and intensity of the extreme rainfall in South Korea will increase in the future (Jung et al., 2013). From this vein, it is essential to reliably evaluate the flood risk in the future in order to adapt and mitigate the climate change impact in South Korea.

To systematically assess and mitigate climate change impacts, modellers should collect reliable long-term climate data. Generally, local gauged data play an essential role in a certain catchment, and such data have been considered to provide accurate values in the modelling process. However, it has been widely acknowledged that observed climate data are coarse in space, and long-term climate data are not readily available in many countries around the world (Becker et al., 2013; Simmons et al., 2004). In other words, gauged values are commonly available at best from the 1950s or 1960s, and the density of the observation network depends on the region. For instance, South Korea, the study region in this thesis, has an area of about 100,032 km^2. However, only a few dozen stations have continuous records of daily scales over the past 40 years, and fewer than 15 stations have records over 50 years. Climate change analysis based on such limited observations cannot consider the early 20^{th} century and may involve significant uncertainty associated with sampling error.

Given this environment, this thesis suggests retrospective global data sources, especially reanalysis data, as an approach to expanding climatic records such as precipitation – one of the essential parameters in hydrological applications. Here, 'reanalysis' refers to a process of retrospectively generating atmospheric model data using a numerical weather prediction (NWP) model and modern data assimilation techniques (Parker, 2016). A benefit of reanalysis products is that they can globally provide consecutive climate records with daily or sub-daily resolution. Notably, a few datasets –such as ERA-20c by the European Centre for Medium-range Weather Forecasts (ECMWF) – can cover the entire 20th century in which the gauged data cannot be reached.

Conceptually, these datasets are not directly taken from the gauged records, and the atmospheric models consider ensemble to account for the main sources of the uncertainties. This implies that understanding the feature of reanalysis ensemble is an important issue in reanalysis-data-based analyses. For this reason, it is essential to assess both the quality of reanalysis data and the feature of the ensemble before applying these products in a regional climate change study. However, due to the lack of comparative studies, knowledge gaps still exist about the suitability of reanalysis data in many regions around the world. For instance, in a few trials that applied reanalysis products to climate change analysis in South Korea, the datasets had been adopted to estimate the features of a comparable region like East-Asia, not the features of South Korea itself (Choi et al., 2016; Ho et al., 2003; Jeong et al., 2015). For ensemble, previous studies have generally applied the mean values for climate change analyses (Donat et al., 2016; Poli et al., 2016). Meanwhile, there has been little interest in the feature of ensemble predictions due to data accessibility. In this context, this thesis first focuses on assessing century-long global datasets in a region lacking such studies (i.e. South Korea) to fill the knowledge gaps.

Even if reanalysis products reproduce the local gauged observations well, removing the biases contained in the data is still an essential issue in the hydrological applications based on the model outputs. Previous studies have also documented that long-term reanalysis datasets may include the systematic errors varying in space (Bao and Zhang, 2013; Bosilovich et al., 2008; Gao et al., 2016; Ma et al., 2009). Thus, researchers who want to apply reanalysis products to hydrological applications should consider the bias correction involved.

In one bias correction scheme that is commonly adopted in hydrological modelling such as quantile mapping (QM), the model data are typically corrected by using the distributional properties such

as quantiles compared with the corresponding observation data. The conventional bias correction approach corrects the mean value well, but often fails to reproduce extreme values such as heavy rainfalls. Moreover, as *in situ* records are limited in certain regions like South Korea, the conventional QM method is also limited in that it cannot be applied directly to the ungauged basin (or the period beyond the observed period) in which a one-to-one relationship between the observed and the modelled data does not exist. Consequently, modellers need to establish an alternative method for the synthesis of unpaired data in areas with limited observation networks. Given this, one of the main goals of this thesis is to build up a bias correction scheme in a region with a limited observation network. For practical purposes, this thesis mainly deals with the bias correction of daily precipitation (i.e. the 24-hour accumulated amount of rain) data, especially for extreme rainfalls, which are commonly adopted in hydrological applications such as rainfall frequency analysis.

In design rainfall estimation using long-term reanalysis data, a change in the uncertainty range may be one of the additional effects. Previous studies have indicated that the use of more extended data in the hydrologic frequency analysis can substantially reduce the uncertainty of design rainfall estimation associated with sampling error (Coles et al., 2003; Huard et al., 2010; Overeem et al., 2008; Tung and Wong, 2014; Van de Vyver, 2015). That is, a century-long reanalysis-based frequency analysis may provide less uncertain design rainfall quantiles than those produced by multi-decadal observation-based estimation. In this context, this thesis also analyses the contribution of reanalysis-product-based frequency analysis to the reduction of 24-hour design rainfall uncertainty.

The other major issue in hydrological models under climate change is the time-dependent feature of a target climate variable – namely, ‘nonstationarity’. Current researches have indicated that many regions throughout the world have experienced the pattern change of climatic extremes, especially for heavy rainfall (Alexander et al., 2006; IPCC, 2014). However, due to the lack of sample data, the time-dependent nature may not be sufficiently identified by the classic approach based on the local gauged data. Consequently, future hazards like heavy rainfall may be estimated using the stationary assumption. Under a climate change environment, this stationary approach can misrepresent future risk in some regions. For instance, if a significant increasing trend for extreme rainfalls exists in an area, the conventional approach may underestimate the design

rainfalls in the viewpoint of the future, leading to misrepresentation of future flood risk. Thus, to reliably evaluate future risk change, it is necessary to consider the nonstationarity of a target climate variable in hydrological applications. A benefit of century-long reanalysis data is that the time series can go back into the early 20th century, even in a region with limited historical records. If the reanalysis data can plausibly represent the real change in a region after bias correction, researchers may easily detect nonstationarity by using the century-long values and then implement nonstationary analysis. This thesis analyses the 24-hour design rainfall changes under the nonstationary condition using bias-corrected century-long reanalysis data.

In summary, the main topics presented in this thesis are in three parts: (1) to assesses the quality of long-term reanalysis data in regional-scale analysis, (2) to evaluate bias correction of century-long reanalysis data and its contribution to the reduction of design rainfall uncertainty, and (3) to analyse design rainfall changes under nonstationary conditions by using century-long reanalysis data. The results of the proposed approach in this thesis may be used to make decisions for climate change strategies. To mitigate climate change impact, structural flood prevention methods such as dam construction and expansion of sewage drainage have been applied based on multi-decadal rainfall observations under stationary assumption in South Korea. However, under the climate change environment, these measurements based on the conventional approach can underestimate future hazards. On the other hand, policymakers would like to exactly estimate the potential flood risk which can demonstrate the necessity of the new investment on the infrastructure or an optimised alternative. Given this, clarifying the impact of climate change based on the longer data period would be the first step in effectively responding to future changes. Figure 1-1 illustrates this thesis' proposed approach to the decision-making process of climate change strategies compared with the conventional approach.

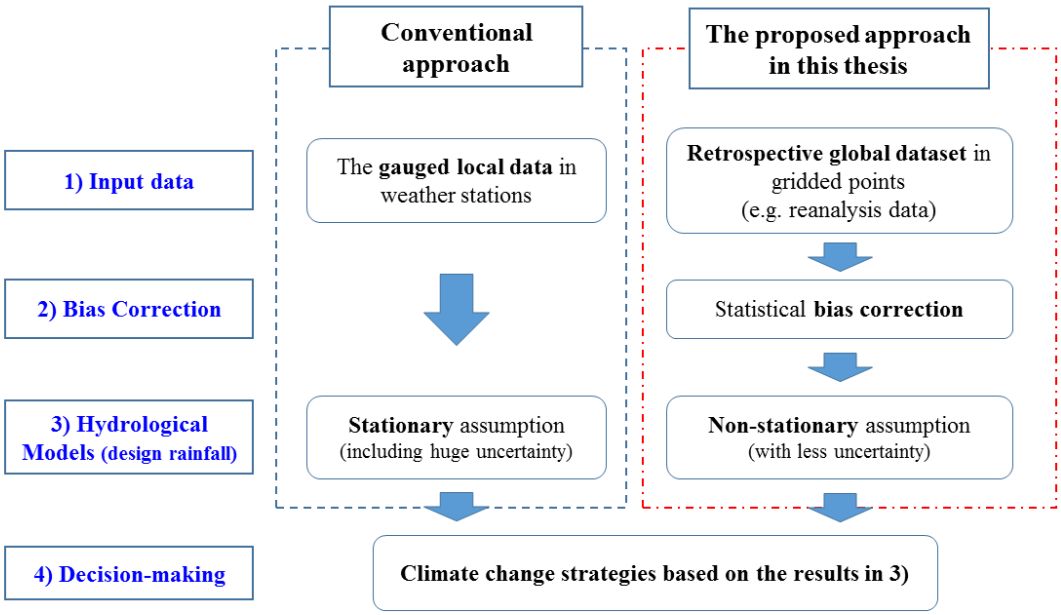

Figure 1-1 A flowchart for the decision-making process of climate change strategies. The red dash-dot line box indicates the parts which are mainly addressed in this thesis, while the blue dash line box shows the conventional approach.

1.2 Scope and objectives

The primary aim of this thesis is to supplement limited observations with long-term reanalysis products and evaluate the climate change impact – especially on estimation of design rainfall with 24-hour duration (hereafter in this thesis 'design rainfall') – by using the model data. The main objectives addressed in this study are detailed as follows:

1. Assess the temporal and statistical suitability of long-term reanalysis data for precipitation and temperature, which are commonly adopted in climate change studies, in a region lacking such study (i.e. South Korea);

2. Create a new bias correction scheme for reanalysis daily precipitation in South Korea with a spatio-temporally limited observation;

3. Evaluate the contribution of bias-corrected century-long data to the reduction of design rainfall uncertainty in South Korea; and

4. Analyse rainfall intensity change under nonstationary condition by using century-long reanalysis datasets covering South Korea.

1.3 Thesis structure

To effectively achieve the outlined objectives, this thesis is structured as illustrated in Figure 1-2. First, Chapter 2 undertakes a brief literature review on retrospective global data sources and bias correction. Basic concepts for uncertainty estimation and nonstationary analysis are also described in this chapter. Chapter 3 presents the details for the study region and datasets used in this thesis. The main three parts of this PhD work are displayed from Chapter 4 onwards. Chapter 4 assesses the long-term global data sources in monthly precipitation and temperature within the context of temporal and statistical reliability. The bias correction scheme with a limited observation, especially for daily precipitation, is addressed in Chapters 5 and 6. Using the bias-corrected values, design rainfall change and its uncertainty reduction are also shown based on the conventional frequency analysis in Chapter 6. Finally, Chapter 7 mainly addresses the nonstationary design rainfall estimation using the long-term data. Detailed descriptions for these main chapters are presented as below:

To assess the quality of retrospective datasets in South Korea, Chapter 4 comparatively evaluates multi-decadal reanalysis datasets (ERA-20cm, ERA-20c, ERA-40, and NOAA 20th century reanalysis (20CR)) and global gridded observations (CRUv3.23 and GPCCv7) for monthly mean precipitation and temperature within the context of the temporal and statistical accuracy. Since reanalysis products can reproduce various variables such as temperature, precipitation and wind, this chapter assesses not only precipitation but also temperature, which has been commonly adopted in climate change studies. Further study is also explored on the ERA-20cm ensemble that accounts for the uncertainty.

Chapter 5 focuses on a bias correction scheme to improve ERA-20c daily precipitation for the reference period (1973–2010). A preliminary assessment for ERA-20c daily precipitation has

indicated that ERA-20c has two main biases: (1) overestimated wet-day frequency and (2) underestimated extreme values. Thus, this chapter applies a cut-off threshold to reduce the former. Then, a QM method based on a composite of gamma and Pareto distribution is introduced to improve the wet-day distribution, especially for extreme rainfalls. To carry out bias correction in ungauged catchments, I additionally propose an interpolation method based on the parameter contour map. The bias-corrected values are evaluated according to the error estimations in 48 stations over South Korea for the reference period.

Since Chapter 5 mainly focuses on the bias correction for the reference period, Chapter 6 begins with bias correction of ERA-20c daily precipitation for the entire 20^{th} century by applying the quantile delta mapping (QDM) method, a trend-preserving bias correction scheme. Using the bias-corrected values, the spatio-temporal design rainfall changes and reduction of the uncertainty are evaluated based on the Bayesian principle. The rainfall intensity changes over the 20^{th} century are also assessed under stationary condition.

Chapter 7 mainly deals with the reanalysis-product-based nonstationary frequency analysis for estimating design rainfall. In this chapter, I first correct the annual maximum rainfalls (AMRs) of reanalysis data, not all wet-day data. I then detect the nonstationarity of the bias-corrected AMRs from 1900 to 2010. To confirm the nonstationarity of the AMRs in South Korea, two different reanalysis datasets, ERA-20c and 20CR, are analysed. This thesis then carries out nonstationary frequency analysis based on a time-varying parameter approach using the bias-corrected values.

Finally, the conclusions and recommendations for future work are outlined in Chapter 8. In particular, further studies are proposed in connection with the limitations of this thesis.

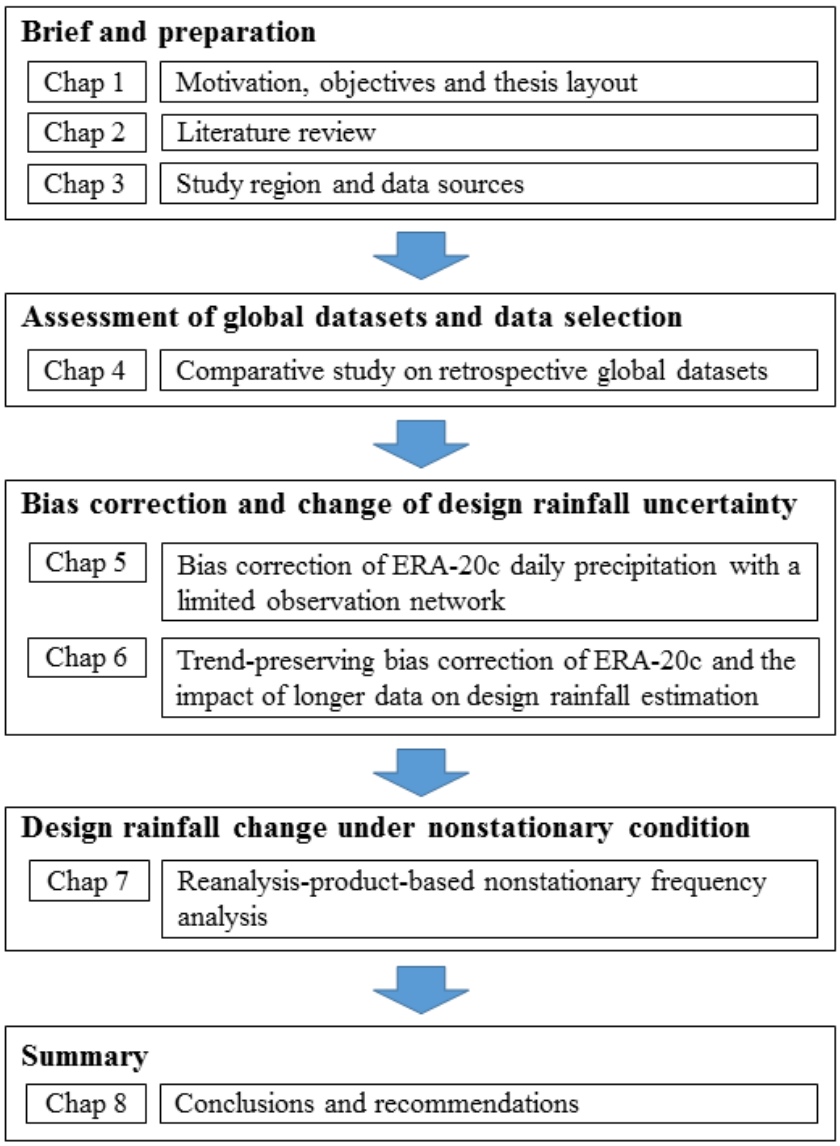

Figure 1-2 Thesis layout and structure.

CHAPTER 2 Literature review

2.1 Introduction

As stated in Chapter 1, this thesis mainly deals with (1) the assessment of century-long reanalysis data, (2) the bias correction of long-term data and its contribution to the change of design rainfall uncertainty and (3) reanalysis-data-based nonstationary frequency analysis for estimating design rainfall. In this context, this chapter introduces the basic knowledge for retrospective global data sources such as reanalysis, and literature review on bias correction, uncertainty analysis and nonstationary analysis for design rainfall estimation. More specifically, this chapter is categorised as follows. In Section 2.2, retrospective global data sources – including reanalysis data – are presented. Section 2.3 describes bias correction methods for precipitation. The concept of uncertainty estimation in hydrology is described in Section 2.4. Finally, Section 2.5 presents the nonstationary frequency analysis for estimating extreme rainfalls.

2.2 Retrospective global dataset

In a changing climate, long-term data have a vital role in understanding current changes and estimating future risks. However, long-term climate change analysis may not be possible in certain areas where climate data are lacking. For this reason, several retrospective global datasets have been developed based on observation, and they can be mainly divided into two types (Becker et al., 2013; Compo et al., 2011; Donat et al., 2016; Harris et al., 2014; Poli et al., 2016). One type includes global gridded observations using interpolation techniques. The second type of dataset includes reanalysis datasets using data assimilation techniques. This section presents the details of these two global data sources.

2.2.1 Global gridded observation

To reliably assess global, continental, or national climate change, a single dataset that can homogeneously cover the study area should be estimated (Huffman et al., 1997). However, as local gauged observations are limited in time and sparse in space, the importance of the availability of highly accessible and reliable gridded datasets has been identified in global climate change studies since the 1980s, especially for precipitation and temperature (Becker et al., 2013). For this purpose, several monthly datasets for precipitation and temperature have been developed based on interpolation of observation data throughout the world (Becker et al., 2013; Chen et al., 2002; Harris et al., 2014; Huffman et al., 1997). In the initial stage, the Global Precipitation Climatology Project developed monthly precipitation datasets on a 2.5°×2.5° latitude-longitude grid, covering the period from 1979 to the present (Huffman et al., 1997). The National Oceanic and Atmospheric Administration (NOAA) also reconstructed global monthly precipitation over land (PREC/L) spanning the period from 1948 to the present (Chen et al., 2002). Recently addressing, another research group, the Climatic Research Unit (CRU) at the University of East Anglia, developed monthly precipitation and temperature datasets which can go back to the early 20th century with the 0.5°×0.5° resolution (Harris et al., 2014). The Global Precipitation Climatology Centre (GPCC) also constructed monthly precipitation datasets on a 0.5°×0.5° grid (Becker et al., 2013).

Conceptually, these global gridded datasets are provided by observation-based interpolation, and they can plausibly represent the actual climatic values of the surface. Thus, many studies have applied these datasets to trend analysis in areas lacking local observations or to global climate change analysis (Dinku et al., 2008; Donat et al., 2016, 2014; Fekete et al., 2004; Nicholson et al., 2003; Nikulin et al., 2012; Sheffield et al., 2012; Simmons et al., 2004; Zhang and Zhou, 2011). However, as observation sites are mainly located on the ground, these datasets are typically provided only on land. Moreover, these gridded observations may include uncertainties due to various reasons such as the heterogeneity of data quality, the inconsistency of the data density being used over time, and the sampling error in the interpolation process (Becker et al., 2013). More specifically, there exists spatial and temporal discontinuity of climate records associated with changes in observational methods and differences in measurement techniques used in different countries, resulting in the heterogeneity of data quality. The different densities of valid data over time can also affect the accuracy of gridded observations. Generally, observations in the

early 20th century are sparse, while much more data are available since the 1970s. The density of the observation network also varies over the region, and consequently, the uneven distribution of observation sites can result in sampling errors. Therefore, if one would like to apply these gridded observations in a regional-scale study, the accuracy of these datasets is still an important issue. For the comparison with reanalysis data, this thesis employs the century-long gridded observations, monthly precipitation datasets by the GPCC and the CRU, and temperature datasets by the CRU. The specific analysis is described in Chapter 4.

2.2.2 Reanalysis

The other surrogates for local observations are long-term datasets derived from a process called 'retrospective analysis' or 'reanalysis' using a numerical weather prediction (NWP) model and modern data assimilation techniques (Parker, 2016). Generally, data assimilation can be defined as a process in which all the information is used to reproduce the state of a system as accurately as possible (Talagrand, 1997). In atmospheric data assimilation, this information generally refers to both the various types of observations and the forecasts from NWP models which are based on physical laws (Parker, 2016; Talagrand, 1997). More specifically, the NWP forecast provides a first-guess of atmospheric state and then, the state is updated by the observations (Parker, 2016).

Since the 1990s, numerous reanalysis datasets have been developed by research institutes such as the ECMWF and the NOAA. In the early stage, most reanalysis datasets were only able to cover the period from the mid-twentieth century to the present (Compo et al., 2011). Examples of this include the first National Centres for Environmental Prediction/National Centre for Atmospheric Research reanalysis : 1948–present (Kalnay et al., 1996); the ECMWF 45-year reanalysis (ERA-40): 1975 – 2002 (Uppala et al., 2005); the Japan Meteorological Agencies reanalysis: 1979 – present (Onogi et al., 2007); and the ECMWF reanalysis interim: 1989 – present (Dee et al., 2011). However, a few recent reanalyses extended the data period to cover the entirety of the 20th century, such as the NOAA 20th century reanalysis v2c (20CR), the ECMWF 20th century atmospheric model ensemble (ERA-20cm), and the ECMWF 20th century reanalysis assimilating surface observations only (ERA-20c) (Compo et al., 2011; Hersbach et al., 2015; Poli et al., 2016). These century-long reanalysis products are not directly taken from the gauged values, so ensemble is invoked to represent the main sources of the uncertainties (Poli et al., 2016). ERA-20c and ERA-20cm by the ECMWF adopt 10-member ensembles, whereas 20CR produces 56 ensemble

members (Compo et al., 2011; Hersbach et al., 2015; Poli et al., 2013). However, ERA-20c and 20CR only provide single-member prediction or ensemble means to the public. Therefore, end users cannot adopt specific ensemble predictions for them (for the 20CR, ensemble range is available). On the other hand, ERA-20cm provides ten ensemble member predictions via the website.

All century-long reanalysis productions can globally provide daily or sub-daily scale precipitation data, but there are differences in the assimilation techniques and spatial-temporal resolution. The products from the ECMWF (i.e. ERA-20c and ERA-20cm) are based on the same model, the Integrated Forecasting System version Cy38r1, and they can provide data with the finest resolution of 0.125°×0.125°. The difference between ERA-20c and ERA-20cm is that the former assimilates pressure and wind observations, while the latter does not consider them in the modelling process (Donat et al., 2016; Hersbach et al., 2015; Poli et al., 2016). On the other hand, the available spatial resolution (i.e. 1.875°×1.9°) for 20CR processed by an Ensemble Kalman Filter technique (Compo et al., 2011) is coarser than the other century-long reanalysis products.

A primary advantage of these reanalyses is that compared with the observed, they can provide finer scale data over time, such as daily or sub-daily, for the entire 20th century. Moreover, this atmospheric reanalysis model can produce both surface parameters – such as precipitation and sea surface temperature – and atmospheric parameters such as pressure and wind at different altitudes. However, despite their benefits and unlike real observation, these products may not be directly applied due to their errors. Previous studies have shown that reanalysis datasets contain systematic errors which vary in space and time (Bao and Zhang, 2013; Bosilovich et al., 2008; Gao et al., 2016; Ma et al., 2009). Thus, to apply a reanalysis dataset instead of local gauged data to hydrological applications in regional-scale studies, it is essential to accurately assess their qualities and remove the biases.

Several comparative studies have assessed the quality of reanalysis datasets, but they were mainly based on global or continental scales (Befort et al., 2016; Donat et al., 2016; Poli et al., 2016; Zhang et al., 2013). To use reanalysis datasets in regional-scale analyses, it is important that comparative studies cover a wide range of locations around the world, and knowledge gaps should be filled for the sites lacking such studies so that a clear pattern can be understood. However, many regions – including South Korea – have not sufficiently employed the century-long reanalysis

datasets. Little attention has been given to the characteristics of the ensemble. In this context, this thesis assesses four multi-decadal reanalyses (ERA-20c, ERA-20cm, ERA-40, and 20CR) for monthly mean precipitation and temperature over South Korea in Chapter 4. This chapter also explores the feature of ERA-20cm ensemble members.

2.3 Bias correction methods

In statistics, 'error' can be defined as any difference between a measured value of a quantity and its true value. Errors have two additive parts: (1) random errors and (2) systematic errors. A random error (or random variation) is due to factors which cannot or will not be controlled. Systematic errors are errors that are not determined by chance but are introduced by an inaccuracy inherent to the system. Unlike random errors, systematic errors are easier to correct. 'Bias' is defined as the difference between the prediction of the model and the correct value which we are trying to predict. Sometimes, systematic error is referred to as bias. 'Variance' is a value of how spread is the measured data. The error due to variance is taken as the variability of a model prediction for a given data point. In statistics, the mean square error (MSE) of a model prediction can be expressed by the sum of variance and the squared bias ($MSE = Var + Bias^2$).

In a climate model, a bias at time *t* can be defined as the systematic difference between a simulated output and an observed value (Maraun and Widmann, 2018). As numerical weather prediction-based model outputs such as reanalysis datasets cannot perfectly reproduce observed properties, the model data include systematic errors. Previous researches have documented that the systematic errors (i.e. biases) in climate model data may misrepresent temporal variability and intensity of extreme events (Befort et al., 2016; Brands et al., 2012; Donat et al., 2016; Krueger et al., 2013; Poli et al., 2013). In other words, reanalysis data without an attempt to adjust the bias can be problematic for many hydrologic applications.

To remove the errors in climate model data, various concepts have been applied, ranging from mean-based corrections to QM methods (Maraun, 2016; Maraun and Widmann, 2018; Teutschbein and Seibert, 2012). For precipitation, which is the primary concern of this thesis, Teutschbein and Seibert (2012) introduced four different bias correction schemes: (1) linear scaling (Lenderink et

al., 2007), (2) local intensity scaling (Schmidli et al., 2006a), (3) power transformation (Leander et al., 2008; Leander and Buishand, 2007), and (4) QM method (Piani et al., 2010). Conceptually, all the schemes begin with estimating distributional properties (e.g. means, variances, and quantiles) of both model outputs and observations. The techniques then catch a transfer function that fits the model properties onto observed properties (Maraun, 2016; Maraun and Widmann, 2018). The linear scaling approach proposed by Lenderink et al. (2007) corrects the errors in the mean by multiplying the ratio between the long-term means of the observed and the modelled data. Local intensity scaling, one of the mean-correction approaches, adjusts rainfall through both the mean and rainfall frequencies (Schmidli et al., 2006a). Power transformation method improves the variance and the mean of precipitation data (Leander et al., 2008; Leander and Buishand, 2007), and QM approach matches the quantiles of the model data to those observed. Although each method has its own merits and limitations, previous studies have documented that bias correction methods were generally capable of reducing systematic errors in numerical model outputs and, among them, QM method showed better performance than other approaches, especially for precipitation (Fang et al., 2015; Maraun and Widmann, 2018; Teutschbein and Seibert, 2012; Themeßl et al., 2012). This thesis also adopts QM approaches for bias correction of daily precipitation data. The details of the above approaches for daily precipitation are described in Sections 2.3.1 to 2.3.4.

2.3.1 Linear scaling method

The linear scaling approach adjusts the relative mean values between the observed and model data (Lenderink et al., 2007). More specifically, the simulated precipitation is scaled by the ratio of long-term mean between the model output and the corresponding observation, as follows:

$$P_{cor} = P_{mod} \times \left[\frac{\mu_m(P_{obs})}{\mu_m(P_{mod})}\right] \quad (2\text{-}1)$$

Here, P_{mod} and P_{cor} represent the raw model data and the bias-corrected model data respectively, and $\mu_m(P_{obs})$ and $\mu_m(P_{mod})$ indicate the long-term mean of the observed and simulated data, respectively.

This scaling approach assumes that the scaling factor (i.e. the ratio of long-term mean) is constant and the model data already have reliable higher moments (Maraun and Widmann, 2018). However,

this approach does not adjust the intensities and frequencies of model precipitation, which can affect the quality of the bias-corrected values.

2.3.2 Local intensity scaling

Unlike linear scaling method, the local intensity scaling approach proposed by Schmidli et al. (2006) adjusts both the mean and wet-day frequencies for daily precipitation using the three-step approach as follows:

(1) First, this method equalises the number of wet-days between the observed and model precipitation by applying a cut-off threshold. Typically, simulated precipitation overestimates the frequency of low-intensity rainfall. In this process, the model values less than the threshold are set to zeros, as shown:

$$P_{mod} = \begin{cases} 0, & \text{if } P_{mod} < P_{th} \\ P_{mod}, & otherwise \end{cases} \quad (2\text{-}2)$$

Here, P_{th} indicates a cut-off threshold. This process prevents distortion due to overestimated low-intensity precipitation. QM method also adopts a cut-off threshold.

(2) The second step is to estimate the scaling factor based on the long-time mean precipitation. Here, the mean values are calculated using wet-day data only (i.e. observations larger than 0mm and the model precipitation over a cut-off threshold (P_{th})). Consequently, the linear scaling factor (*f*) is estimated using the following equation:

$$f = \frac{\mu_m(P_{obs}|P_{obs} > 0\ mm)}{\mu_m(P_{mod}|P_{mod} > P_{th})} \quad (2\text{-}3)$$

(3) Finally, the bias-corrected values are estimated by multiplying the scaling factor to the simulated precipitation, as in the linear scaling method in Section 2.3.1.

$$P_{cor} = P_{mod} \times f \quad (2\text{-}4)$$

2.3.3 Power transformation

Conceptually, linear scaling approaches ignore the biases in the higher-order moments such as variance, but climate model biases generally affect both the mean and the variance. Thus, to

account for the differences in variance, the power transformation approach applies a nonlinear scaling correction expressed by an exponential form $P_{cor} = a \cdot P_{mod}^{b}$ (Leander et al., 2008; Leander and Buishand, 2007). Here, the parameter b is estimated by matching the coefficient of variation (*CV*) of the observed precipitation (P_{obs}) with the *CV* of the simulated precipitation for each month *m*, as follows:

$$CV_m\,(P_{obs}) = CV_m\left(P_{mod}^{b_m}\right) \tag{2-5}$$

Finally, by applying $P_{mod}^{b_m}$ instead of P_{mod} in Eq. 2-1, the bias-corrected values are estimated using the following equation.

$$P_{cor} = P_{mod}^{b_m} \times \left[\frac{\mu_m(P_{obs})}{\mu_m(P_{mod}^{b_m})}\right] \tag{2-6}$$

2.3.4 Quantile mapping

A main concept of QM referred to as 'distribution mapping' or 'probability mapping' is to map the modelled data to the observed data in the probability space. More generally, cumulative distribution functions (CDFs) of the modelled data are mapped to that of the observed, which is considered 'true' (Rabiei and Haberlandt, 2015; Teutschbein and Seibert, 2012). In other words, the distribution of simulated values is fitted to the true distribution, the relationship of which is established in the advanced stages of bias correction, as follows:

$$P_{cor} = F_{obs}^{-1}[F_{mod}\{P_{mod}(t)\}] \tag{2-7}$$

Here, F_{obs} and F_{mod} represent the CDF of the observed and the modelled, respectively. For daily precipitation, since the simulated data typically have too many wet days of low-intensity rainfall as stated in 2.3.2, a cut-off threshold is considered to adjust the frequency before applying a QM method.

QM methods for daily precipitation have involved transfer functions that are based on parametric and nonparametric distributions (Cannon et al., 2015; Eum and Cannon, 2017; Kim et al., 2015a, 2015b; Teutschbein and Seibert, 2012). Some studies have adopted non-parametric QMs, but they can lead to an increase of bias in the upper quantile for the extreme values (Maraun, 2016; Maraun

and Widmann, 2018). For parametric QMs, previous studies have commonly adopted a gamma distribution with two parameters since it can describe the main features of daily precipitation (Kim et al., 2015a, 2015b; Piani et al., 2010; Teutschbein and Seibert, 2012). The gamma distribution and its transfer function for the QM can be expressed as follows:

$$F(x|\alpha,\beta) = \frac{1}{\beta^{\alpha}\Gamma(\alpha)}\int_0^x t^{\alpha-1}e^{-t/\beta}dt\,;\ \ x \geq 0;\ \alpha,\beta > 0 \tag{2-8}$$

$$x_{cor} = F^{-1}[F(x_{mod};\alpha_{mod},\beta_{mod});\alpha_{obs},\beta_{obs}] \tag{2-9}$$

Here, x_{cor} and x_{mod} are the corrected data and the uncorrected (or modelled) data in the baseline period. F is a gamma CDF, and F^{-1} is its inverse function, while α and β are the shape and scale parameters of the gamma distribution, respectively. To account for the seasonality, it is common to have bias correction models for each month that are independent of the others (Kim et al., 2015b).

However, this gamma-based QM approach also often fails to represent the extreme values (Maraun, 2016; Maraun and Widmann, 2018; Volosciuk et al., 2017). Thus, the bias correction for the extreme tail of rainfall distribution requires special care. Moreover, as a QM approach requires a one-to-one relationship between the observed and modelled, the bias correction in a region with spatio-temporally limited observations may be a complicated problem. In these contexts, Chapters 5 and 6 deal with the limitations of the conventional approach and propose new approaches for bias correction of long-term daily precipitation – especially for extreme rainfalls.

2.4 Uncertainty analysis in hydrology

In hydrology, uncertainty can be defined as a quantitative indication of reliability for a given hydrological value, either observed or modelled (Montanari, 2011). As knowing the uncertainty in the model prediction allows hydrologists to better understand the limitation of the model output, uncertainty analysis has become a core feature in hydrological models. In order to systematically review the uncertainty issue, this thesis first introduces the sources of uncertainty in hydrological models. It then explains the uncertainty assessment methods.

2.4.1 Sources of uncertainty

The various reasons behind the presence of uncertainty in hydrology can be divided into two main groups: (1) natural variability and (2) knowledge uncertainty (Dai, 2014; Merz and Thieken, 2005; Montanari, 2011; Teng et al., 2017). Natural variability, called aleatory variability, refers to the inherent randomness in the natural system across time and space. Due to this randomness, natural variability cannot be reduced or described using a deterministic approach. On the other hand, knowledge uncertainty represents the uncertainty caused by data/parameter errors, misunderstanding and lack of knowledge about the hydrological process. More specifically, knowledge uncertainty can be categorised into four groups: (1) data uncertainty, (2) model parameter uncertainty, (3) model structure uncertainty, and (4) operation uncertainty (Montanari, 2011; Teng et al., 2017). The detailed explanations about these uncertainties are as follows.

Data uncertainty, also known as measurement uncertainty, mainly stems from the imperfection of the measuring technique and observers (Hayes, 2011). More specifically, the number of measurements, the spatial or temporal variability between measurements, the accuracy of the monitoring device, and the skill of the observer can affect the uncertainty. Hydrological models are simulated with this imperfect data, and consequently, the model outputs include errors. However, as it is difficult to exactly estimate data uncertainty and it is independent on model structure, most studies either assume that the observation is ‘true’ or this data uncertainty is attributed to parameter uncertainty (Dai, 2014).

Model parameter uncertainty occurs when there is a lack of good quality data series or when the model’s optimisation algorithm is inefficient (Montanari, 2011). In most hydrological models, the model parameters are typically estimated from a calibrated process. This process depends on limited or unrepresentative calibration data. As a result, the model based on the parameters results in imperfect model outputs. Since a model commonly consists of several parameters, quantifying how much individual parameters impact the uncertainty is a major issue. In recent studies, sensitivity analysis is commonly used to discover the contribution of individual parameters (Dai, 2014; Montanari, 2011; Teng et al., 2017). This thesis analyses the sensitivity of individual parameters for GEV distribution in design rainfall estimation in Chapter 6.

Model structural uncertainty arises from incomplete configuration of the model (Dai, 2014; Hayes, 2011). The real world is so complicated that it is impossible to correctly optimise the real world in a model structure. Even if modellers can construct a complex model to closely reproduce the real world, the model would require a larger number of parameters and input data, which may result in more uncertainties in model output. Thus, a model algorithm should not be too complicated, and consequently, the model structure cannot perfectly represent the real world.

Operation uncertainty, also called decision uncertainty, happens when end-users such as decision makers apply the model results. This uncertainty is mainly attributed to unexpected human changes such as human goals and conditions (Dai, 2014; Montanari, 2011). For instance, decision makers can change the primary goal of a project from high safety to cost reduction according to people's needs. In this case, this change may affect the model structure, and it can cause obvious uncertainty. Thus, the modellers should be aware of this uncertainty when they apply the model.

2.4.2 Uncertainty assessment

As stated in Section 2.4.1, there are various sources of uncertainty in hydrological models. Many methods have been proposed in the literature to estimate individual or whole uncertainties in a model, and they can be classified into three different approaches: (1) analytical methods, (2) probabilistic methods and (3) non-probabilistic methods (Dai, 2014; Hayes, 2011; Montanari, 2011, 2007).

The analytical approach generally assesses the uncertainty of model output by directly deriving the statistics of the system response from a knowledge of the statistical values of the system and input data (Langley, 2000; Montanari, 2011). However, this approach may confront two major problems for a complex model (Montanari, 2011). First, the derivation of the response statistics of the simulated data can face significant mathematical and numerical difficulties. Second, the statistical values of the system and the input data may not be available. For these reasons and due to the development of probabilistic and non-probabilistic methods, analytical approaches are not widely used in recent studies (Dai, 2014).

Probabilistic methods assess uncertainty in a hydrological model by employing strict probability theory. In this approach, the uncertainty is identified by probabilities associated with the events. Although there are several variations, the formal Bayesian approaches can represent probabilistic

methods in hydrology (Montanari, 2011; Montanari et al., 2009). The Bayesian methods adopt formal probability distributions for the priors and formal likelihood measures, and this approach can provide statistically rigorous confidence intervals under certain conditions (Hall et al., 2011; Teng et al., 2017). The Bayesian principle typically requires massive computation, but together with current advances in technology, this approach has been commonly applied in the hydrologic community.

Non-probabilistic methods represent the various generalisations of probability theory, including the generalised likelihood uncertainty estimation (GLUE), fuzzy set theory, and possibility theory (Hayes, 2011; Montanari, 2007). The GLUE method is based on probability theory, but it is less formally invoked. Fuzzy set theory is based on possibility theory. Fuzzy set theory and possibility theory have received considerable attention in hydrology since human reasoning in the hydrological system is considered 'possibilistic' rather than strictly probabilistic (Montanari, 2011). However, broadly speaking, the most commonly applied methodologies in hydrology are the GLUE method and the Bayesian approaches (Dai, 2014; Stephens and Bates, 2015; Teng et al., 2017; Vrugt et al., 2009). Thus, this thesis pays more attention to the comparison of these two favourite methods.

The GLUE method proposed by Beven and Binley (1992) has been commonly adopted for estimating uncertainties in environmental models, especially in hydrological models. This is because it is theoretically simple, easy to implement, and does not require modifications of existing source codes (Vrugt et al., 2009). The GLUE method estimates model uncertainty by using a combined concept of Monte Carlo analysis and Bayesian estimation. Compared with the formal Bayesian methods, GLUE applies the more flexible pseudo-likelihood function that partitions the parameter space into acceptable and non-acceptable (Stephens and Bates, 2015; Teng et al., 2017). This difference has led to a debate about the choice between the probabilistic methods (i.e. the formal Bayesian approach) and the non-probabilistic methods (i.e. the GLUE approach) (Beven, 2006; Beven et al., 2007, 2008; Mantovan and Todini, 2006; Montanari, 2007, 2005). The major criticism of GLUE is that it requires relatively subjective decisions in the process and is statistically incoherent. Meanwhile, criticism about probabilistic methods mainly expresses the concern that the assumptions of classical statistics cannot be justified in some cases. From the literature, Montanari et al. (2009) summarised that a probabilistic statistical method is preferable when

sufficient information is available to support statistical hypotheses with corresponding statistical tests. Meanwhile, they confirmed, the GLUE method is applicable when expert knowledge is needed due to data scarcity. In this thesis, I apply the Bayesian approaches to assess the uncertainty change in design rainfall by using long-term reanalysis data in Chapters 6 and 7. To be more specific, the parameters of distribution functions are estimated within a Bayesian modelling framework, and the derived posterior distributions of the parameters are further used to estimate design rainfalls and their uncertainties. Theoretically, the posterior distribution, $p(\boldsymbol{\theta}|\mathbf{R})$, of the parameter vector ($\boldsymbol{\theta}$) is described as follow:

$$p(\boldsymbol{\theta}|\mathbf{R}) = \frac{p(\boldsymbol{\theta},\mathbf{R})}{p(\mathbf{R})} = \frac{p(\mathbf{R}|\boldsymbol{\theta})p(\boldsymbol{\theta})}{p(\mathbf{R})} = \frac{p(\mathbf{R}|\boldsymbol{\theta})p(\boldsymbol{\theta})}{\int p(\boldsymbol{\theta})p(\mathbf{R}|\boldsymbol{\theta})d\theta} \propto p(\mathbf{R}|\boldsymbol{\theta})p(\boldsymbol{\theta}) \quad (2\text{-}10)$$

Here, **R** indicates the vector of the AMRs in a given daily precipitation, $p(\mathbf{R}|\boldsymbol{\theta})$ is the likelihood function, and $p(\mathbf{R})$ and $p(\boldsymbol{\theta})$ are the marginal distribution and prior distribution, respectively.

2.5 Nonstationary frequency analysis

Based on the historical records, design rainfall has been commonly estimated from the precipitation intensity-duration-frequency (IDF) relationship using the stationary assumption (Cheng and Aghakouchak, 2014; Li et al., 2017). More generally, the notion of return period and risk has been routinely applied to hydrologic extreme events analysis, such as heavy rainfalls. The conventional approach typically estimates the return period and risk based on the observed extremes under the stationary condition. As a result, design rainfall estimated in this approach is commonly used to estimate floods or to design a water-related infrastructure. However, recent researches have indicated that many regions throughout the world have experienced a pattern change of climatic extremes, especially in heavy rainfall (Alexander et al., 2006; IPCC, 2014). Numerous studies have commonly adopted the time-varying parameter scheme to consider nonstationarity in hydrologic extreme event estimations for heavy rainfall or floods (Cannon, 2010; Cunderlik and Burn, 2003; El Adlouni et al., 2007; Leclerc and Ouarda, 2007; Panagoulia et al., 2014; Son et al., 2017). Conceptually, this time-varying parameter approach assumes that a climate variable like precipitation has the same distribution function type, typically GEV distribution in block maxima (BM) approach. However, the parameter values are dependent on time. In this

concept, a return period ($T_t = 1/(1 - F_z(z_{q0}, \theta_t))$ with a certain design quantile (z_{q0}) at time *t* can be derived from a cumulative distribution (F_z) with the time-varying parameters (θ_t) (Du et al., 2015). However, as estimating a quantile with a target period (e.g. 100-year) varies by time, the use of the 'return period' concept can be meaningless under nonstationary conditions (Cheng et al., 2014; Du et al., 2015; El Adlouni et al., 2007). Nevertheless, since the return period can still provide intuitive information to engineers, numerous studies have addressed this issue and two different approaches have been proposed: (1) the expected waiting time (EWT) approach and (2) the expected number of exceedance (ENE) approach (Du et al., 2015; Obeysekera et al., 2016; Read and Vogel, 2015; Salas et al., 2018; Salas ad Obeysekera, 2014). EWT focuses on the 'expected waiting time' for the first occurrence exceeding the design rainfall (z_{q0}). The ENE approach obtains the target value by setting the expected number of exceedances over the design life *T*. Both concepts should be numerically solved to estimate the design quantile with a target return period under nonstationary conditions. This section describes the details of the classic stationary approach and two nonstationary approaches (i.e. EWT and ENE) in design rainfall estimation.

2.5.1 The conventional concept for extreme events

The conventional approach for determining the return period and risk of extreme hydrologic events begins with two assumptions (Leadbetter, 1983): (1) extreme events follow a stationary distribution; and (2) their occurrences are independent or weakly dependent. Under stationary conditions, the extreme rainfalls denoted by the random variable *Z* have a CDF $F_z(z, \theta)$, where θ is the constant parameter set. Here, the return period (*T*) and exceedance probability of a given design rainfall *z* are simply estimated based on the observation at a specific year that is normally the initial year of the modelling (Du et al., 2015; Salas and Obeysekera, 2014). To be more specific, design rainfall at the initial year (i.e. $t = 0$) is denoted by z_{q_0}, and the corresponding non-exceedance probability and exceedance probability are denoted by q_0 and $p_0 = 1 - q_0$ respectively, as illustrated in Figure 2-1(a). Researchers are commonly interested in the probability of the first occurrence of rainfall exceeding the design rainfall z_{q_0} to design a project. Nonetheless, the first event may occur in year 1, 2, 3, or so on. If the random variable representing the year of the first occurrence is denoted by *X*, the first occurrence that exceeds the design rainfall z_{q_0} in year

$X = x$ follows the geometric probability law (Obeysekera and Salas, 2014; Salas and Obeysekera, 2014).

$$f(x) = P(X = x) = (1 - p_0)^{x-1} p_0, \qquad x = 1,2, \ldots \tag{2-11}$$

The expected value of X – the mean expected waiting time (or the mean number of years that will take for the first occurrence of a rainfall exceeding the design rainfall) – is known as the return period T, and it can be expressed as follows (Du et al., 2015; Salas and Obeysekera, 2014):

$$T = E(X) = \sum_{x=1}^{\infty} x f(x) = 1/p_0 \tag{2-12}$$

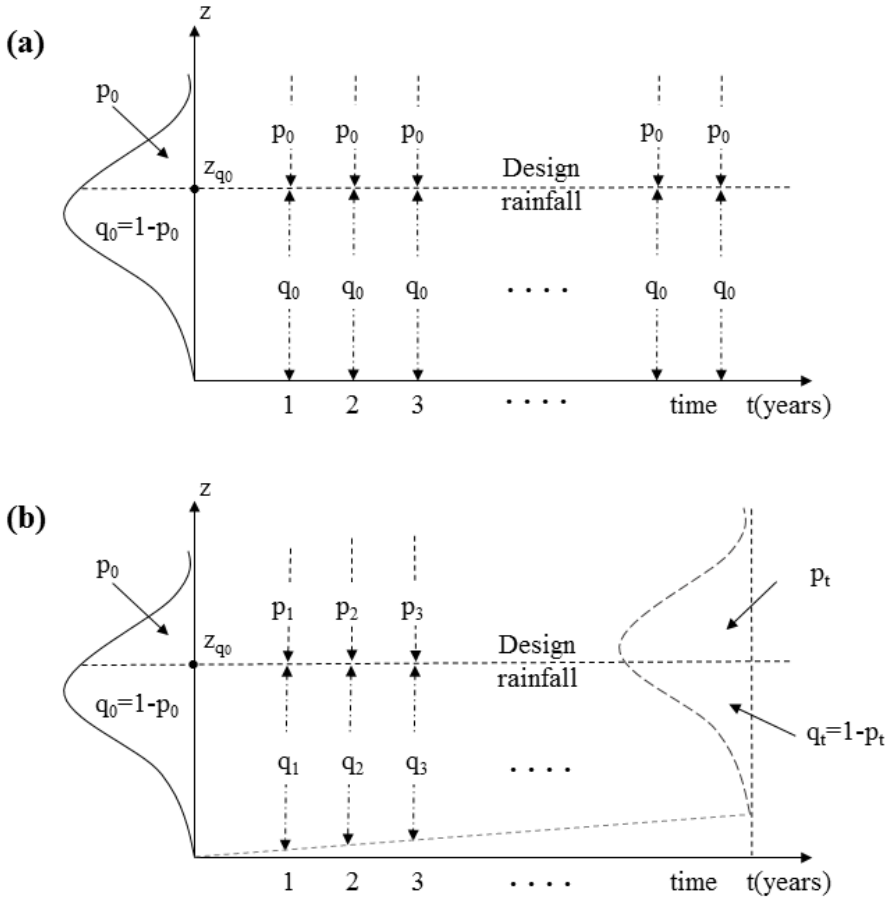

Figure 2-1 Schematic depicting of the design rainfall quantile (z_{q_0}), with (a) being constant exceedance probabilities (p_0) and non-exceedance probabilities (q_0) and (b) being time-varying exceedance probabilities (p_t) and non-exceedance probabilities (q_t) through year 1 to *t*.

Generally, extremes of hydrological values such as precipitation and flood are modelled in two main ways: (1) the BM approach and (2) the peak over threshold (POT) approach. The BM method estimates the design quantile by using the maximum value series in a given period (which is typically one year), while the POT method uses all extreme events above a selected threshold. The POT scheme is expected to provide a larger sample than the BM approach when estimating design events. However, due to the subjectivity of threshold selection, complexity of modelling, and potentiality of loss for some annual maximum series below the threshold, the BM approach has generally been used in actual practice (Salas et al., 2018). For this reason, this thesis applies the BM method to practically estimate design rainfall.

In the BM approach, various probability distributions such as gamma, Gumbel, and GEV have been applied for extreme events, but among them, GEV distribution has been widely adopted in design quantile estimation (Coles, 2001; Leclerc and Ouarda, 2007; Panagoulia et al., 2014). For GEV, the exceedance probability (p_0) corresponding to the design quantile (z_{q0}) is expressed as follows:

$$p_0 = 1 - \ exp\left\{-\left[1 + \xi\left(\frac{z_{q0} - \mu}{\sigma}\right)\right]^{-\frac{1}{\xi}}\right\} \tag{2-13}$$

Here, μ, σ, and ξ are location, scale and shape parameter of GEV distribution, respectively. Under stationary condition, the GEV parameters are constant and the exceedance probability (p_0) can be easily calculated in Eq. 2-13. Then, the return period is taken from Eq. 2-12.

2.5.2 Expected waiting time (EWT) approach

Unlike the conventional approach, real extreme rainfalls may change over time, in which case the exceedance probability is time-dependent as illustrated in Figure 2-1(b). Under the nonstationary condition, the first occurrence exceeding the design quantile (z_{q0}) in year $X = x$ is described as follows (Du et al., 2015; Salas et al., 2018; Salas and Obeysekera, 2014):

$$\begin{aligned} f(x) = P(X = x) &= (1 - p_1)(1 - p_2)(1 - p_3)\cdots(1 - p_{x-1})p_x \\ &= p_x \prod_{t=1}^{x-1}(1 - p_t), \qquad x = 1, 2, \cdots, \infty \end{aligned} \tag{2-14}$$

The expected waiting time (EWT) for the first event exceeding z_{q0} – i.e. return period (T) – is obtained as follows:

$$T = E(X) = \sum_{x=1}^{\infty} xf(x) = \sum_{x=1}^{\infty} xp_x \prod_{t=1}^{x-1}(1-p_t) \tag{2-15}$$

Here, return period *T* under nonstationary condition is a function of time-varying exceedance probabilities (p_t), unlike the stationary approach in which return period *T* is only a function of constant p_0. For GEV distribution, the CDF can be expressed as a CDF $F_z(z,\theta_t)$ with time-dependent parameters (θ_t) in Eq. 2-16. Its time-varying exceedance probabilities (p_t) can be described as the time-dependent parameters in Eq. 2-17.

$$F(z_{q_0},\theta_t) = exp\left\{-\left[1+\xi_t\left(\frac{z_{q0}-\mu_t}{\sigma_t}\right)\right]^{-\frac{1}{\xi_t}}\right\} \tag{2-16}$$

$$p_t = 1 - exp\left\{-\left[1+\xi_t\left(\frac{z_{q0}-\mu_t}{\sigma_t}\right)\right]^{-\frac{1}{\xi_t}}\right\} \tag{2-17}$$

Here, μ_t, σ_t, and ξ_t represent the time-varying location, scale, and shape parameters of GEV distribution. By applying p_t in Eq. 2-17 to Eq. 2-15, this approach can numerically estimate the design quantile with a target return period such as 100-year for a project. In general, most studies have assumed that location parameter only or location and scale parameters are time-dependent while shape parameter is constant due to its sensitivity (Cannon, 2010; Leclerc and Ouarda, 2007; Salas and Obeysekera, 2014).

2.5.3 Expected number of exceedance (ENE) approach

Unlike the EWT scheme, the ENE approach focuses on the expected number of exceedances over the design life (i.e. return period *T*). If *M* is denoted as the random variable representing the number of exceedances in *T* years, under nonstationary condition, the expected number of exceedances is described as (Du et al., 2015; Salas et al., 2018):

$$E(M) = \sum_{j=1}^{T} P(Z_t < z_{q_0}) = \sum_{j=1}^{T} F_z(z_{q_0},\theta_t) = \sum_{j=1}^{T} p_t \tag{2-18}$$

As exceedance probabilities p_t under nonstationary condition can be described as in Eq. 2-17, for GEV distribution, the return period *T* of the first occurrence exceeding the design quantile (z_{q0}) can be numerically estimated by applying *E(M)* = 1 in Eq. 2-18.

Both methods, the EWT and ENE, are applicable for nonstationary events, but the EWT approach has the drawback of conceptually requiring information beyond the design lifetime of a certain infrastructure to numerically solve the problem (Du et al., 2015; Obeysekera and Salas, 2016; Salas et al., 2018). For this reason, this thesis applies the ENE interpretation for estimating the design quantile (z_{q0}) with 10- to 200-year return periods in Chapter 7.

CHAPTER 3 Study region and data sources

3.1 Description of South Korea

All the analyses applied in this thesis have been conducted only in one region – South Korea. South Korea is located in the northeast part of Asia, lying with all of its islands between latitudes 33°-39°N and longitudes 125°-132°E. The total area is approximately 100,032 km^2, and its annual average rainfall is about 1,277 mm. In particular, two-thirds of the annual precipitation is concentrated in the summer, from June to September, which is the monsoon season. This rainfall pattern frequently causes water-related hazards such as floods in the summer. Additionally, due to the generally steep land grade, rainfall runs-off into the ocean rapidly (MOLIT, 2013). This environment has made water management more challenging in South Korea and the South Korea government has invested in large scale infrastructure projects such as dams, drainage systems, embankments etc. to minimise the flood damage.

The recent changing climate also makes it difficult to prevent water-related hazards. These days, the localised heavy rain with high intensity is occurring more frequently due to the climate change (Jung et al., 2013; MOLIT, 2013). For instance, Seoul, the capital of South Korea, witnessed inundation for 3 consecutive years from 2010 to 2012. Busan, South Korea's second largest city, experienced severe casualties and property damage estimated about 0.5 billion BP in the latter part of July, 2014, due to the flash flooding which peaked at a rate of 130mm per hour. It is also anticipated that the frequency and intensity of the extreme rainfall will increase in the future (Jung et al., 2013). Under this environment, it is a key factor of water policy to pre-emptively diagnose the causes of flood and make adaptation strategies.

In South Korea, hundreds of local weather gauging stations are available. However, most of them have been installed after the 1970s, and fewer than 15 stations can provide long-term daily climate records for more than 50 years. This thesis uses the mainland of South Korea as a study region. The thesis excludes oceans and islands, since the most long-term weather stations are only available in mainland areas, and the reanalysis dataset in the ocean may be heterogeneous to the

reanalysis data on land (Donat et al., 2016; Hersbach et al., 2015; Poli et al., 2016). Figure 3-1 illustrates an overview of the mainland of South Korea.

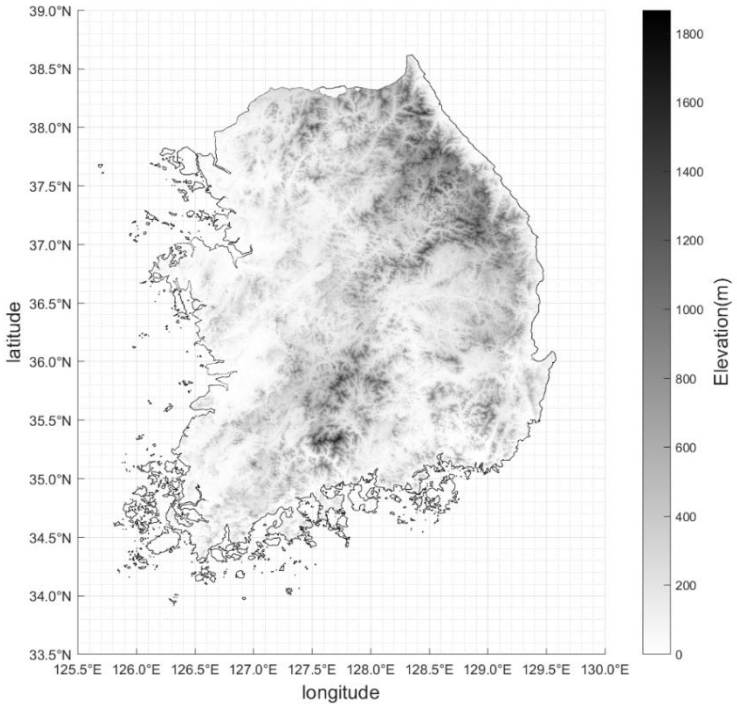

Figure 3-1 A map showing the study area. The grey shading on the map indicates elevations.

3.2 Local gauged data

To evaluate the model data, this thesis uses the local gauged precipitation and 2-m air temperature data, which are derived from the data archive of the Korea Meteorological Administration (KMA) (https://data.kma.go.kr/cmmn/main.do). Depending on the purpose and target model data, this thesis applies the data for the different period as follows.

Chapter 4 collects daily precipitations and daily mean 2-m air temperatures from 13 ground weather stations, covering 1961–2010. It then merges them into monthly values to assess the several reanalysis datasets and global gridded observations. Since global gridded observations are typically provided monthly, this chapter evaluates the monthly values of precipitation and temperature, which are generally adopted in hydrological modelling.

In Chapter 5, I mainly focus on the bias correction of ERA-20c daily precipitation for the reference period including spatial interpolation. Thus, a larger number of weather stations (48 stations) are used. However, due to limited data availability, the data period is limited to 1973–2010 in this chapter.

Chapter 6 also employs daily precipitation in 48 stations for bias correction of ERA-20c data, but the data period is slightly different from that in Chapter 5. More specifically, to remove biases in ERA-20c for the entire 20th century (1900–2010), I apply quantile delta mapping (QDM) method. QDM needs the relative change of quantiles between the reference period and the projected period, which are set to the same length. As ERA-20c data is 111-years-long, this chapter first sets the reference period to 1974–2010 (37 years) and then divides the past projected period (1900–1973) into two periods to make the intervals equal to the reference period (i.e. 1900–1936 and 1937–1973). For this reason, Chapter 6 adopts the observed data in 48 stations for the reference period (i.e. 1974–2010). For the validation of the bias-corrected values, this chapter also uses the longest historical records (1910–2010) for 7 stations out of 48 stations.

Chapter 7 applies the observed data in 48 stations from 1974 to 2010 for QDM bias correction method as in Chapter 6. However, as this chapter aims to analyse nonstationary frequency analysis for design rainfall based on a BM principle, only the AMRs of the observations are adopted. To detect the time-dependent characteristic, this chapter examines the AMRs of the observed both for the reference period (1974–2010) and the extended period (1974–2017).

3.3 Global gridded observation

As stated in Section 2.2, there are several global gridded observation datasets for monthly precipitation and temperature based on their own interpolation techniques, and these datasets have been applied to long-term climate change studies. To assess the reliability of century-long reanalysis datasets, this thesis employs a few century-long global gridded observations that cover the whole 20th century. More specifically, Chapter 4 adopts monthly precipitation of the CRU TS v.3.23 (CRUv3.23) and GPCC Full Data Reanalysis Product Version 7 (GPCCv7)) and temperature datasets of CRUv3.23. From the global gridded observations at a 0.5°×0.5° grid, the monthly temperature and precipitation values over South Korea from 1901 to 2010 are extracted and compared with the reanalysis data and local gauged data. The CRU and GPCC datasets are

supplied from their websites, https://crudata.uea.ac.uk/cru/data/hrg/ and http://gpcc.dwd.de, respectively.

3.4 Reanalysis data

As described in Section 2.2, several reanalysis datasets have been developed since the 1990s, but only a few recent reanalysis datasets – such as 20CR by the NOAA, and ERA-20cm and ERA-20c by the ECMWF – can span the period of the whole 20th century (Compo et al., 2011; Hersbach et al., 2015; Poli et al., 2016). As one of the main goals in this thesis is to extend the climate data, I adopt the century-long reanalysis datasets that can provide the most extended data period. A detailed explanation of the reanalysis data used in the chapters is offered below.

Chapter 4 assesses the reliability of monthly precipitation and temperature for ERA-20cm, ERA-20c, and 20CR, compared with the global gridded observations (GPCCv7 and GRUv3.23) and the local gauged data. Thus, these century-long reanalysis datasets are collected for the common data period of 1901–2010. ERA-40 is adopted as a benchmark for a half-century reanalysis data from 1961 to 2001. Among these long-term reanalyses, only ERA-20cm can provide all ensemble predictions which can account for the uncertainty in the reanalysis data. Thus, the individual ensemble members of ERA-20cm are specifically explored. The reanalysis daily data are collected at a 0.5°×0.5° grid – except 20CR with the resolution of 1.875°×1.9°. They are then merged into monthly data.

Chapter 5 mainly focuses on bias correction of reanalysis daily precipitation for the reference period of 1973 to 2010. All century-long reanalyses (i.e. ERA-20c, ERA-20cm, and 20CR) can globally provide daily or sub-daily scale precipitation data, but differences exist in the assimilation techniques and spatial-temporal resolution. The products from the ECMWF (such as ERA-20c and ERA-20cm) are based on the same model. They can provide data with the finest resolution of 0.125°×0.125°, which are more relevant in regional-scale studies in South Korea. However, unlike ERA-20c, ERA-20cm does not include a data assimilation process using observations. Therefore, ERA-20cm is limited in reproducing the actual synoptic situation (Gao et al., 2016; Hersbach et al., 2015). For 20CR based on Ensemble Kalman Filter technique, the available spatial resolution

(i.e. 1.875°×1.9°) is much coarser than ERA-20c and ERA-20cm. As this thesis conducts bias correction in a regional-scale site (i.e. South Korea), this chapter applies the ERA-20c daily precipitation data for the reference period at a 0.125°×0.125° grid over the mainland of South Korea.

Chapter 6 also employs the ERA-20c daily precipitation at a 0.125°×0.125° grid. However, this chapter adopts the extended period of 1900–2010 because it aims to improve the reanalysis data for the entire 20th century and analyse the design rainfall change using the corrected data.

Chapter 7 carries out reanalysis-product-based nonstationary frequency analysis for design rainfall estimation. In this nonstationary approach, it is crucial to identify the long-term trend of a target variable preliminarily. To reliably detect the long-term trend of the AMRs for the whole 20th century, this chapter uses two different century-long reanalysis datasets: ERA-20c by the ECMWF and 20CR by the NOAA. With the bias-corrected AMRs of these two datasets, this chapter analyses the design rainfall change under nonstationary conditions in South Korea.

3.5 Summary of datasets used in each chapter

In summary, Chapter 4 adopts monthly precipitation and temperature taken from three different data types: (1) the local gauged data, (2) global gridded observations (GPCCv7 and GRUv3.23), and (3) multi-decadal reanalyses (ERA-20c, ERA-20cm, 20CR, and ERA-40). Chapter 5 and Chapter 6 focus on ERA-20c daily precipitation in terms of bias correction and design rainfall change. Meanwhile, Chapter 7 uses both ERA-20c and 20CR daily precipitation to reliably conduct nonstationary frequency analysis based on the long-term reanalysis data. The detailed information of the datasets used in the chapters is summarised in Table 3-1.

Table 3-1 Data information used in this thesis.

Chapter	Variable (Unit)	Data Type	Data Source	Resolution	Period
Ch. 4	Temperature (°c/month), Precipitation (mm/month)	Local gauged data	KMA	13 stations	1961–2010
		Global gridded observation	CRUv3.23, GPCCv7[1)]	0.5°×0.5°	1901–2010
		Reanalysis	ERA-20c, ERA-20cm, 20CR, ERA-40	ERAs[4)]: 0.5°×0.5° 20CR: 1.875°×1.9°	1901–2010 (ERA-40: 1961–2001)
Ch. 5	Precipitation (mm/day)	Local gauged data	KMA	48 stations	1973–2010
		Reanalysis	ERA-20c	0.125°×0.125°	1973–2010
Ch. 6	Precipitation (mm/day)	Local gauged data	KMA	48 stations	1974–2010[2)]
		Reanalysis	ERA-20c	0.125°×0.125°	1900–2010
Ch. 7	Precipitation (mm/day)	Local gauged data	KMA	48 stations	1974–2010 1974–2017[3)]
		Reanalysis	ERA-20c, 20CR	ERA-20c: 0.125°×0.125° 20CR: 1.875°×1.9°	1900–2010

[1)] GPCCv7 only provides monthly precipitation data.

[2)] The longest historical records in 7 stations are additionally used for validation.

[3)] The gauged data from 1974 to 2017 is applied for detecting the long-term trend of the AMRs.

[4)] ERAs: ERA-20c, ERA-20cm and ERA-40

CHAPTER 4 [1,2]Assessment of retrospective global datasets in monthly precipitation and temperature in South Korea

4.1 Motivation

Long-term climate data play a key role in reliably assessing water-related hazards to adapt and mitigate climate change. In regional-scale hydrological analyses, researchers typically adopt local *in situ* records, but they are usually sparse in space and limited in the time (Becker et al., 2013; Simmons et al., 2004). Given this, I suggest retrospective global datasets, especially reanalysis data, as an alternative to the *in situ* data in regional-scale climate change studies. This chapter aims to assess the reliability of these datasets which can cover the whole 20th century in South Korea.

As stated in Section 2.2, retrospective global datasets can be categorised into two groups: (1) global gridded observation and (2) reanalysis data (Becker et al., 2013; Chen et al., 2002; Compo et al., 2011; Donat et al., 2016; Harris et al., 2014; Hersbach et al., 2015; Poli et al., 2016; Uppala et al., 2005). The former datasets, which generally provide monthly precipitation and temperature, have been developed by interpolation of observations worldwide, and some can go back to the early 20th century, such as precipitation and temperature by the CRU and precipitation by the GPCC. For the latter data (i.e. reanalysis products), 20CR by the NOAA and ERA-20c and ERA-20cm by the ECMWF can representatively provide the daily or sub-daily data covering the 20th century (Compo et al., 2011; Hersbach et al., 2015; Poli et al., 2016). However, since both data types are not directly taken from weather stations, their qualities are still an important issue in regional-scale hydrological applications.

---

[1] Kim, D.-I. and Han, D., 2018. Comparative study on long term climate data sources over South Korea. J. Water Clim. Chang. https://doi.org/10.2166/wcc.2018.032

[2] Kim, D.-I. and Han, D., Evaluation of ERA-20cm reanalysis dataset over South Korea. J. Hydro-environ. Res. (under revision)

More specifically, to use these global datasets in regional-scale analyses, it is important to fully understand their features through studies in different regions of the world. However, many regions – including South Korea – have not sufficiently tested century-long reanalysis data. Some comparative studies have been carried out, but they were mainly global or continental-scale investigations (Befort et al., 2016; Donat et al., 2016; Poli et al., 2016; Zhang et al., 2013). To fill in the knowledge gaps for the sites lacking such studies, especially in South Korea, this chapter assesses multi-decadal reanalyses (ERA-20cm, ERA-20c, ERA-40, and 20CR) and gridded observations (CRUv3.23 and GPCCv7) for monthly mean precipitation and temperature for South Korea. Here, ERA-40 is selected as a benchmark for a half-century reanalysis. The evaluation is performed within the context of temporal variability, long-term trend, and statistical agreement.

For century-long reanalysis products, the ensemble is invoked to represent the main sources of the uncertainties. Thus, understanding the feature of reanalysis ensemble can be an important issue. However, previous global climate change studies have typically adopted the mean values only (Donat et al., 2016; Poli et al., 2016). Also, due to data accessibility, public users cannot collect ensemble predictions – except in ERA-20cm, as discussed in Section 2.2 (Compo et al., 2011; Hersbach et al., 2015; Poli et al., 2013). Given this, this chapter analyses the general feature of ERA-20cm ensemble members in terms of temporal variability, long-term trend, and statistical agreement. The chapter also explores the goodness of the ensemble spread and the relationship between the spread and the El Niño-Southern Oscillation (ENSO).

4.2 Data

4.2.1 Observed local data

This chapter adopts daily total precipitation and daily temperature from 13 ground gauge stations that are evenly distributed over South Korea excluding islands. The data were collected from KMA server and merged into monthly values. For comparison, I collected data for the common period. More specifically, overall comparison with different data sources (i.e. global gridded observations and reanalyses) adopts the data from 1961 to 2001, while the ERA-20cm ensemble comparison uses data from 1961 to 2010. There are no empty values in local observations during the

comparison period except three stations which are available from 1966 (St.4), 1968 (St.3) and 1973 (St.8), respectively. The quality of the gauged records is strictly controlled by the KMA. The detailed on the location and data period of the stations is provided in Figure 4-1 and Table 4-1.

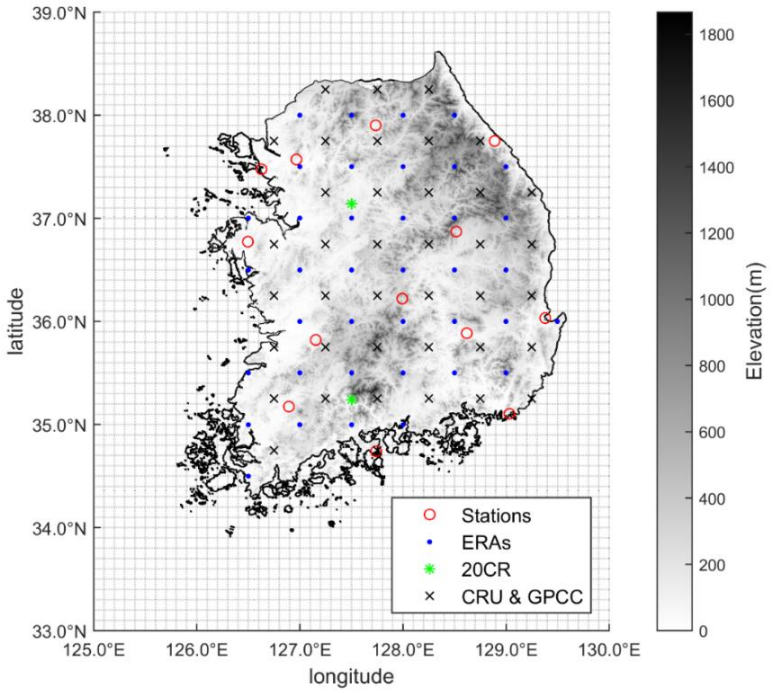

Figure 4-1 Locations of 13 weather stations shown in Table 4-1 and gridded points of ERAs (ERA-20cm, ERA-20c, and ERA-40), 20CR, CRUv3.23 (CRU), and GPCCv7 (GPCC).

Table 4-1 Longitude, latitude, and observation period of the selected stations in Chapter 4.

No.	Name	Longitude	Latitude	Observation period	Elevation (m. asl)
1	Seoul	126-57-56 E	37-34-17 N	1961–2010	11.1
2	Incheon	126-37-29 E	37-28-39 N	1961–2010	69.6
3	Seosan	126-29-45 E	36-46-25 N	1968–2010	30.3
4	Chuncheon	127-44-08 E	37-54-09 N	1966–2010	79.1
5	Gangneung	128-53-27 E	37-45-05 N	1961–2010	27.4
6	Jeonju	127-09-17 E	35-49-17 N	1961–2010	54.8
7	Chupungnyeong	127-59-40 E	36-13-11 N	1961–2010	246.1
8	Yeongju	128-31-00 E	36-52-18 N	1973–2010	212.2
9	Gwangju	126-53-29 E	35-10-22 N	1961–2010	73.8
10	Yeosu	127-44-26 E	34-44-21 N	1961–2010	66.0
11	Daegu	128-37-08 E	35-53-06 N	1961–2010	65.5
12	Pohang	129-22-46 E	36-01-57 N	1961–2010	3.7
13	Busan	129-01-55 E	35-06-16 N	1961–2010	71.0

4.2.2 Reanalysis data

ERA-20c is one of the atmospheric 20th-century reanalyses provided by the ECMWF. This single-member dataset, covering the period of 1900–2010, was produced by assimilating observations of surface pressure and surface marine winds only (Poli et al., 2016). Considering the data availability and resolution of the other data sources, I extracted total precipitation from the 24-hour accumulated forecasts and 2-m air temperature from 6-hourly analysis data at a 0.5×0.5º grid from January 1901 to December 2010 via the ECMWF web server. The products in South Korea have been accumulated into monthly data. The values over the sea have been excluded, because the comparable long-term weather stations are available on land areas and the ocean grid points would be heterogeneous to the land points for averaging (Donat et al., 2016; Hersbach et al., 2015; Poli et al., 2016).

In addition to ERA-20c, The ECMWF also provided ERA-20cm data with 10-member ensemble from January 1900 to December 2010 (Hersbach et al., 2015). This dataset was produced with the Integrated Forecasting System version Cy38r1 like ERA-20c, but ERA-20cm assimilates no atmospheric observations (Donat et al., 2016). For a specific comparison of the ensemble, I employed ten individual ensemble members for 3-hourly total precipitation and 2-m air temperature at a 0.5°×0.5° grid from January 1901 to December 2010 via the ECMWF server. Note that ERA-20cm adopted the mean for overall comparison with the different data sources and further comparison between individual ensemble members was analysed separately. Here, the mean of ERA-20cm is calculated by averaging the time series data of ten ensemble members. The products over South Korea were accumulated into monthly data, and the values on the sea were excluded as well. In the ensemble analysis, the 10 different kinds of ensemble values are abbreviated as from En0 to En9 hereafter, while the mean is denoted as Mean.

20CR is one of the long-term reanalysis datasets provided by the NOAA. Its latest version 2c, spanning the period of 1850–2014 with a resolution of 1.875×1.9º, was produced by assimilating only surface pressures and using the Ensemble Kalman Filter technique to produce 56 ensemble members (Donat et al., 2016). For public users, each ensemble prediction is not available, but the mean of the ensemble members and the ensemble spread can be collected via the web server. In this chapter, I collected 8-times daily ensemble means for total precipitation and 2-m air temperature from 1901 to 2010 and accumulated them on a monthly basis. Thus, in this analysis,

20CR data represents the mean of 20CR ensemble data. As with other datasets, the data over the sea were ignored.

To identify the difference between reanalysis products having different data periods, I applied ERA-40 data covering the period from September 1957 to August 2002 (Uppala et al., 2005). The data was extracted from the ECMWF archive in the same way as ERA-20c. More specifically, I collected the 6-hourly convective precipitation data, large-scale precipitation data and 2-m air temperature data on a 0.5×0.5º grid from 1961 to 2001. The total precipitation was produced by the sum of convective and large-scale precipitation, excluding the values on the sea, and the products were aggregated into monthly data.

4.2.3 Gridded observations by CRU and GPCC

CRUv3.23 is land-only dataset from 1901 to 2014, which covers all over the world except for the Antarctic (Harris et al., 2014). This dataset was constructed by using the Climate Anomaly Method based on worldwide observations providing monthly total precipitation and monthly mean 2-m air temperature with its highest resolution (0.5×0.5º latitude/longitude) (Harris et al., 2014). For comparison with the other data sources, this chapter extracted the data over South Korea for the period of 1901–2010.

GPCC has produced the global land-surface precipitation data, and its 7th version, GPCCv7, covers a 113-year analysis period from 1901 to 2013 based on the rain gauge database over 51,000 stations worldwide (Schneider et al., 2015). Here, this chapter took the monthly total precipitation product with the highest resolution of 0.5×0.5º over South Korea from 1901 to 2010.

4.3 Methodology

4.3.1 Evaluation of interannual variability

To explore the temporal variability of model outputs (i.e. reanalysis data and gridded observations), the Pearson's linear correlation coefficients (r) between the global data sources and observations in 13 stations were calculated for the reference period of 1961–2001 for comparison of all data sources and 1961–2010 for ERA-20cm ensemble comparison (hereafter in this chapter referred to

as 'reference period'). Due to the lack of weather stations with long-term data, this chapter paid more attention to the comparison of the mean values averaged over the whole region. This method has been widely used to measure the degree of collinearity between the observed and the modelled data in multi-decadal climate variability studies, although it is oversensitive to high extreme values and insensitive to proportional gaps between two variables (Deser et al., 2004; Dickinson et al., 2006; Gholami et al., 2015; Herrmann et al., 2005; Legates and McCabe Jr., 1999; Wang et al., 2015; Wu et al., 2010). Here, this chapter focuses on the variability between the observation and modelled datasets by using *r*, while the absolute differences between them are simply explored through figures on seasonal/annual change. For this analysis, seasonal/yearly total precipitation and mean temperature variables were derived from all the datasets. Every seasonal dataset was collected for spring from March to May, summer from June to August, autumn from September to November, and winter from December to February.

For the calculation of *r* in a given station, due to the difference in coordinate and resolution between datasets (seen in Figure 4-1), I interpolated the model data at grids into each station point by using an inverse distance weighting (IDW) method which is one of the most applied deterministic methods (Babak and Deutsch, 2009). Compared with another preferred method, kriging, the IDW method is simple to calculate, more applicable to spatial estimation with small-sized observation networks, and does not require prior information such as a semi-variogram model (Babak and Deutsch, 2009; Lu and Wong, 2008; Tomczak, 1998). For this reason, this chapter applied the IDW method as follows:

$$\boldsymbol{w(x,y)} = \sum_{\boldsymbol{i=1}}^{\boldsymbol{N}} \boldsymbol{\alpha_i w_i}\,, \qquad \boldsymbol{\alpha_i} = \frac{\left(\frac{\mathbf{1}}{\boldsymbol{d_i}}\right)^{\boldsymbol{p}}}{\sum_{\boldsymbol{i=1}}^{\boldsymbol{N}}\left(\frac{\mathbf{1}}{\boldsymbol{d_i}}\right)^{\boldsymbol{p}}} \tag{4-1}$$

Here, *N* is the number of the grids used in the calculation, *w* is the evaluated value from the data product in each station point, w_i is the *i*-th data point among the selected values, d_i is the distance from the station to the *i*-th grid, and *p* is the specified weighting power. In this equation, the weighting parameter (*p*) can vary from 0 to infinite, and when the value increases, the estimated is less influenced by the further stations (Chang et al., 2006). In this analysis, all inland gridded values were used and the most common value, 2, was applied for the power p (Babak and Deutsch, 2009; Teegavarapu and Chandramouli, 2005). After calculating the *r* in 13 stations, the mean *r*

values were compared. The standards for the agreement of the *r* values between the modelled and the observed data applied in this chapter are suggested in Table 4-2.

Table 4-2 Standards for the agreement of correlation coefficients (*r*) between observations and models.

Standard	Agreement
***r* > 0.9**	Very high (Very well)
0.9>= *r* > 0.7	High
0.7>= *r* >0.4	Moderate
***r* < 0.4**	Low

For ERA-20cm, the *r* values between ensemble members for annual variables were evaluated in the same way to identify the independence of ten ensemble members. Since the ensemble members are forced by realisations related with the sea surface temperature (SST) (Hersbach et al., 2015), to discover the relationship between the El Niño-Southern Oscillation (ENSO) and the ensemble spread of ERA-20cm, this chapter assesses the *r* values between 3 month moving ensemble spread and the Oceanic Niño Index (ONI), which is the standard that NOAA applies for detecting El Niño and La Niña events. The ONI is the difference between a three-month running average of the sea surface temperature averaged over an area of the east-central equatorial Pacific Ocean – called the Nino-3.4 region (5S to 5N; 170W to 120W) – and the long term average for the same three months. When the three month running means of SST anomalies exceed a threshold of ±0.5°C for at least 5 consecutive months, the first month of them is considered as the start of El Niño/ La Niña.

4.3.2 Trend test

The correlation coefficient *r* does not assess the time-dependent characteristic, although it shows the relationship between the observed and the model. Thus, to find out the significance of the long-term trend in each dataset, the Mann–Kendall test was applied for the reference period. The trends of century-long datasets from 1901 to 2010 were also examined to assess long-term patterns throughout the 20th century. The Mann–Kendall trend test created by (Mann, 1945) and (Kendall, 1955) is one of the widely used nonparametric tests for detecting the trends of hydrological variables such as precipitation, temperature and streamflow (Bae et al., 2008; Shadmani et al.,

2012; Xu et al., 2005; Zang and Liu, 2013). Compared with parametric tests such as linear regression which needs data normality as well as independence, this method only requires the independence of data (Hamed and Rao, 1998; Xu et al., 2005). In the Mann–Kendall test, the test statistic *S* and the standardised test statistic *Z* are estimated by the related equations as follows:

$$\boldsymbol{S = \sum_{i=1}^{n-1} \sum_{j=i+1}^{n} sgn(x_j - x_i)} \tag{4-2}$$

$$\boldsymbol{sgn(x) = \begin{cases} 1 \ for\ x > 0 \\ 0 \ for\ x = 0 \\ -1 \ for\ x < 0 \end{cases}} \tag{4-3}$$

$$\boldsymbol{V(S) = \frac{n(n-1)(2n+S) - \sum_{i=1}^{m} t_i(t_i-1)(2t_i+5)}{18}} \tag{4-4}$$

$$\boldsymbol{Z = \begin{cases} \frac{S-1}{\sqrt{V(S)}} & for\ S > 0 \\ 0 & for\ S = 0 \\ \frac{S+1}{\sqrt{V(S)}} & for\ S < 0 \end{cases}} \tag{4-5}$$

Here, $x_1, x_2, x_3, \ldots, x_n$ are the time series of length *n*, *V*(*S*) is the variance of *S*, *m* is the number of tied groups, t_i is the number of ties for the *i*-th value, and *Z* means a standard normal distribution (Xu et al., 2008). The significance of trends is evaluated by comparing *Z* with the standard normal variate at the desired significance (Hamed and Rao, 1998). When $|Z| > Z_{1-\alpha/2}$, where $Z_{1-\alpha/2}$ is the standard normal deviates in which the significance level is α, the null hypothesis is rejected, and it means that there is a significant trend in the time series in the test. In this analysis, the most commonly used values –0.05 and 0.10 – were applied for α, although significance levels could vary from 0.1 to 0.001 according to the literature (Bae et al., 2008; Hamed and Rao, 1998; Jung et al., 2011; Xu et al., 2005; Zang and Liu, 2013). In this method, the magnitude of a linear trend is estimated by the Theil–Sen approach – sometimes referred to as 'Kendall Slope Estimator' – defined by the median value of the ranked slope estimates as follows (Sen, 1968; Theil, 1950; Xu et al., 2008; Zang and Liu, 2013):

$$\boldsymbol{\beta = Median\left(\frac{x_j - x_i}{j - i}\right), \quad \forall i < j} \tag{4-6}$$

In this equation, the positive value of β represents an increasing trend over time, while the negative value means an opposite trend. The advantage of this method is that it is less sensitive to outliers or extreme values than the least-square method (Sayemuzzaman and Jha, 2014; Shadmani et al., 2012).

4.3.3 PDF-based evaluation method

To assess the statistical similarity between the observation and each dataset for the reference period, I estimated the skill score based on the probability density function (PDF) suggested by Perkins et al. (2007). By calculating the overlapped area between two distributions at each bin, this method estimates how much the climate dataset distribution is similar to the observed data. If a dataset matches the observed values perfectly in PDF, the skill score will be 1, which equals the sum of the probability. Otherwise, if the skill score is close to zero, it means that there is no common area between the model values and observations. In other words, the more overlapped the two curves, the closer to 1 this score is. The skill score is calculated as follows:

$$\boldsymbol{S_{score}} = \sum_{\mathbf{1}}^{\boldsymbol{n}} \boldsymbol{minimum}(\boldsymbol{P_m}, \boldsymbol{P_0}), \tag{4-7}$$

where n is the number of bins for the calculation, P_m is the frequency of values in a given bin from a comparison target, and P_0 is the frequency values in a given bin from observations. In this study, the square root of 1mm month^{-1} (sqrt(mm/month)) for precipitation and 1°C for temperature are considered the intervals of bins for the monthly dataset analysis to effectively compare the PDFs, as in previous studies (Gao et al., 2016; Perkins et al., 2007). This method is simple but powerful in capturing the relative compatibility between observation and model distribution. Moreover, compared with the traditional mean-based method, this performance shows more credible climate variations, and it is flexible to collect data with different time periods from multiple stations (Gao et al., 2016; Perkins et al., 2007). The standards for the agreement of skill scores between the modelled and the observed data applied in this chapter are suggested in Table 4-3.

Table 4-3 Standards for the agreement of skill scores (*S*) between observations and models.

Standard	Agreement
$S > 0.9$	Very high (Very well)
$0.9 >= S > 0.7$	High
$0.7 >= S > 0.5$	Moderate
$S < 0.5$	Low

4.3.4 Criterion for the goodness of ERA-20cm ensemble

For ERA-20cm ensemble, the goodness of ensemble spread from 1961 to 2010 is evaluated by the percentage of observations within the ensemble interval, which is identical to the P-95CI method used by Li et al. (2010). This index is simply calculated as follows:

$$\boldsymbol{P}(\%) = \frac{\boldsymbol{N_{in}}}{\boldsymbol{n}} \times \mathbf{100} \tag{4-8}$$

Here, n is the number of bins, and N_{in} is the number of observations bracketed by the upper and the lower boundaries. In this analysis, the closeness of the *P* to 100% judges the goodness of predictions. In Li et al. (2010), the 95% confidence interval was derived from thousands of simulations. However, since ERA-20cm has only ten ensemble predictions, the current analysis considered the lowest and highest values at a given bin as the lower and the upper boundaries (i.e. ensemble interval).

4.4 Results

4.4.1 Precipitation

4.4.1.1 Interannual variability

Table 4-4 quantitatively explains the correlation of seasonal/annual precipitation between the observation and global data sources from 1961 to 2001. In the seasonal mean comparison, the *r* values for CRUv3.23 and GPCCv7 exceeded 0.9 in every season, and ERA-20c, ERA-40 and 20CR performed moderate to high correlations ($0.4 < r < 0.9$). Among seasonal values, spring and

winter were more correlated than summer and autumn. However, the simulations for ERA-20cm are located between -0.110 and 0.284, which means that there is little temporal correlation with the observation for precipitation. An annual mean comparison describes a similar result. CRUv3.23 and GPCCv7 performed very well with the *r* over 0.9, and ERA-20c followed with 0.621. 20CR and ERA-40 had moderate correlations with 0.498 and 0.445, respectively, but the *r* value for ERA-20cm, 0.091, was close to zero.

Table 4-4 Correlation coefficient (*r*) for seasonal and annual total precipitation of various datasets averaged over all regions from 1961 to 2001.

Type	Seasonal comparison				Annual comparison
	Spring	Summer	Autumn	Winter	
ERA-20cm	-0.110	0.070	0.014	0.284	0.091
ERA-20c	0.762	0.600	0.665	0.829	0.621
ERA-40	0.821	0.466	0.647	0.883	0.445
20CR	0.744	0.407	0.562	0.638	0.498
CRUv3.23	0.963	0.922	0.942	0.960	0.929
GPCCv7	0.970	0.938	0.952	0.966	0.945

Figure 4-2, which illustrates the seasonal and annual precipitation changes of the simulated datasets from 1961 to 2001, supports this result. For seasonal comparison, the fluctuations of ERA-20cm had little correlation with the observations in all seasons, while GPCCv7 and CRUv3.23 performed almost in similar movements with the observed values (Figure 4-2(a)). For ERA-20c, ERA-40, and 20CR, their movements had significant similarities to the observations, but the values themselves of each dataset were slightly different. For example, ERA-40 and 20CR had lower rainfall than the observation, especially in summer and autumn, whereas ERA-20c was relatively close to the observation (Figure 4-2(a)). This result means that in terms of interannual variability, ERA-20c is less biased than ERA-40 and 20CR in South Korea. The annual change showed a similar result with the seasonal trend. The annual pattern of ERA-20cm was totally different from that of the observation, while CRUv3.23 and GPCCv7 performed very well (Figure 4-2(b)). For ERA-20c, ERA-40, and 20CR, they had partial similarity to the observation in the annual comparison, but only ERA-20c had comparable values with the observed in Figure 4-2(b). In other words, the annual rainfalls of ERA-40 and 20CR were underestimated compared with the observation. These results are summarised in the Taylor diagram (Figure 4-3) that provides the correlation coefficient, centred root-mean-square error, standard deviation, and bias.

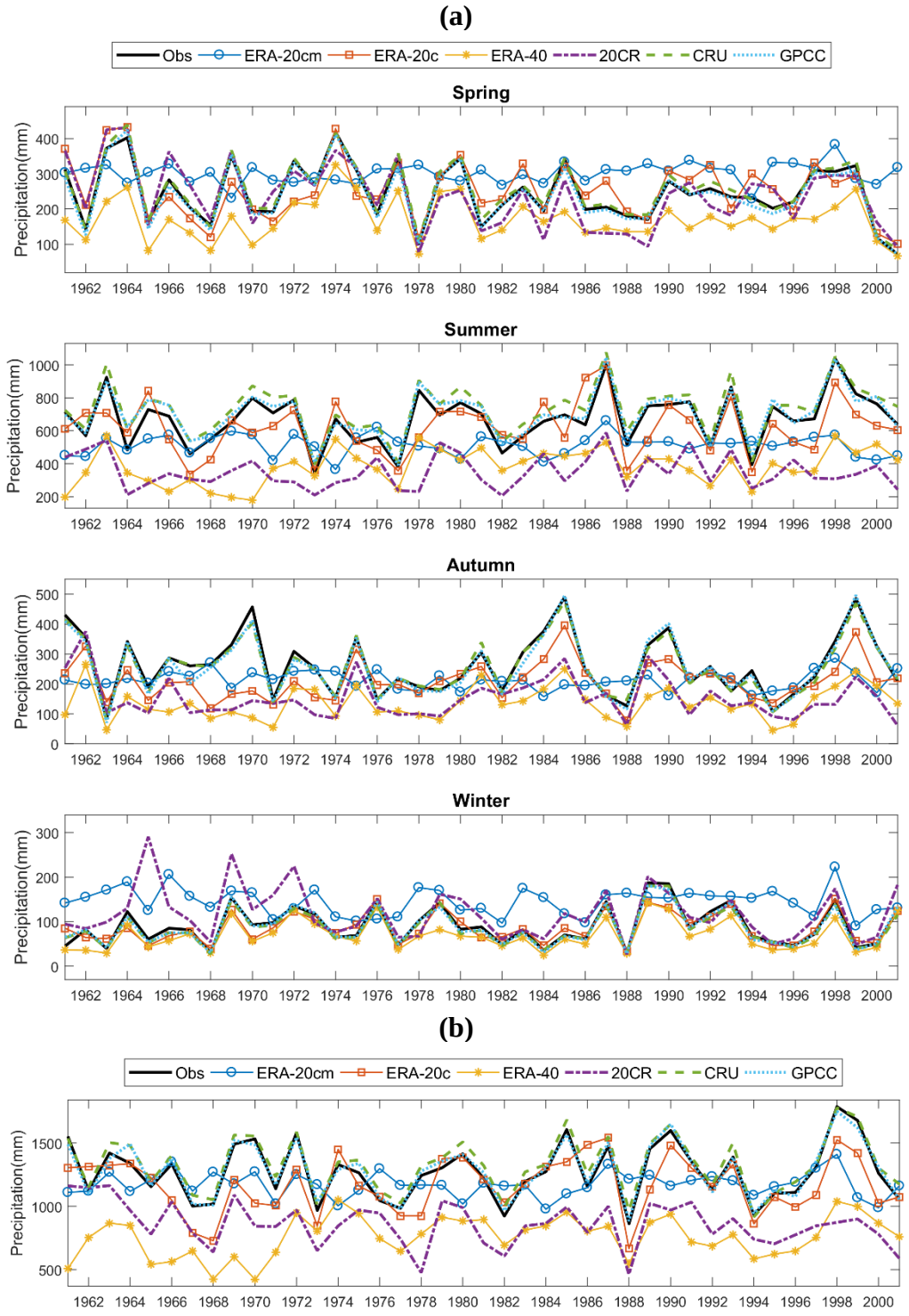

Figure 4-2 Total precipitation change of observation (Obs), ERA-20cm, ERA-20c, ERA-40, 20CR, CRUv3.23 (CRU), and GPCCv7 (GPCC) over the whole region from 1961 to 2001. (a) The seasonal total precipitation change (from above, spring, summer, autumn, and winter) and (b) The annual total precipitation change.

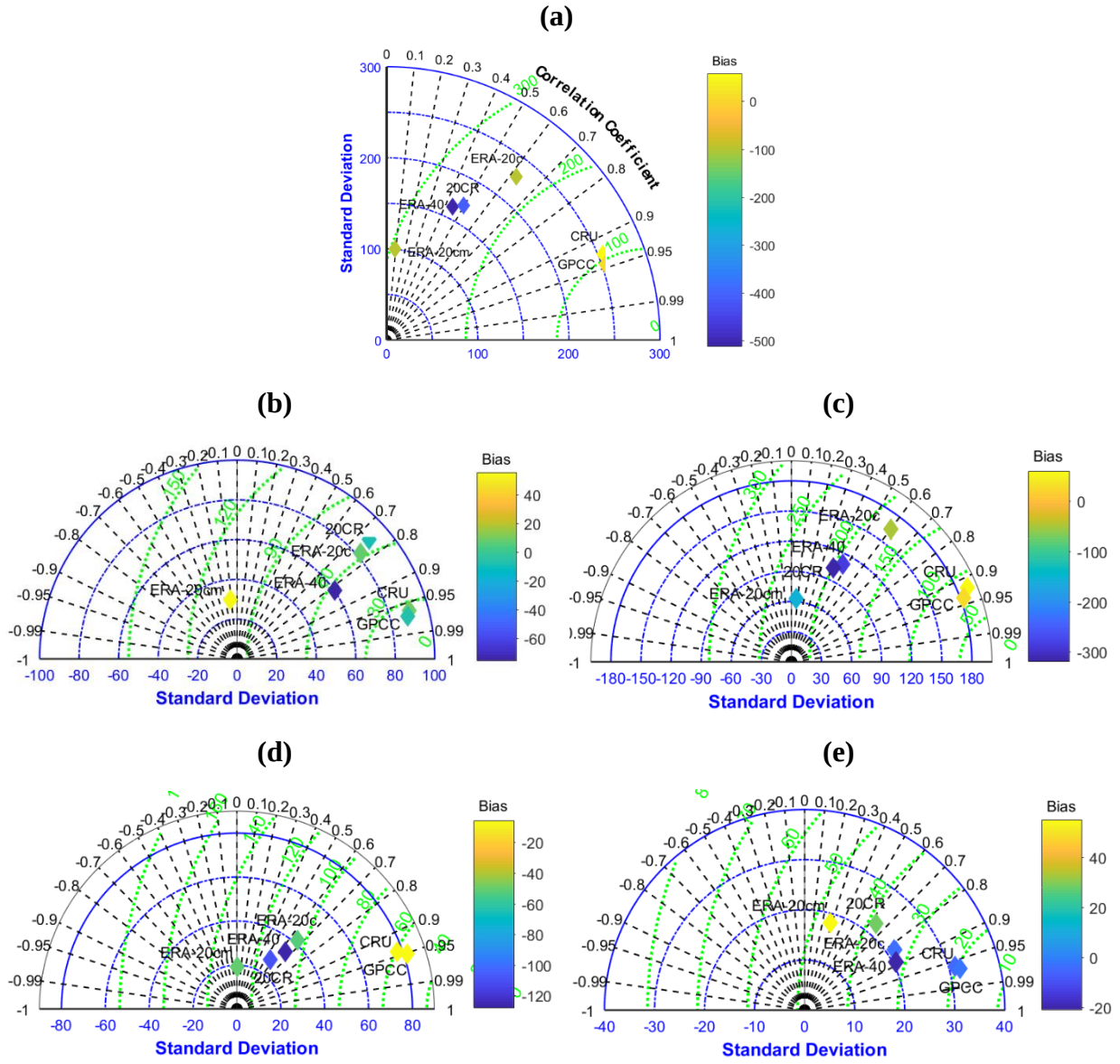

Figure 4-3 Taylor diagram of ERA-20cm, ERA-20c, ERA-40, 20CR, CRUv3.23 (CRU), and GPCCv7 (GPCC) for total precipitation over the whole region from 1961 to 2001. (a) represents the annual change and (b) ~ (e) indicate the seasonal change [(b) spring, (c) summer, (d) autumn, and (e) winder].

For ERA-20cm ensemble, further analysis for temporal variability of individual members has been carried out. Table 4-5 quantitatively explains the seasonal or annual correlation between the observation and ensemble members from 1961 to 2010. In the seasonal comparison, the *r* values for all ten ensemble members were between -0.174 and 0.228, and Mean had the values between -0.039 and 0.278. This analysis indicates that there are little temporal correlations between ERA-

20cm ensemble members as well as Mean and the observations for precipitation. The annual comparison also suggested the similar result. The highest value was 0.160 for En6, the lowest one was -0.069 for En1, and Mean performed 0.109. In other words, the *r* values of ERA-20cm ensemble predictions and Mean were overall close to zero.

Table 4-5 Correlation coefficient (*r*) for seasonal and annual total precipitation between the observation and ERA-20cm ensemble members averaged over all regions from 1961 to 2010.

Type	Seasonal				Annual
	spring	summer	autumn	winter	
Mean	-0.010	0.077	-0.039	0.278	0.109
En0	0.066	0.220	-0.154	0.185	0.155
En1	-0.046	-0.090	0.035	0.138	-0.069
En2	-0.171	0.094	-0.008	0.170	0.082
En3	0.049	0.001	0.029	-0.033	0.083
En4	-0.044	0.041	0.057	0.177	-0.021
En5	0.008	-0.062	-0.108	0.193	-0.012
En6	0.133	0.104	-0.065	0.129	0.160
En7	-0.174	0.056	0.002	0.046	0.060
En8	-0.002	-0.085	0.017	0.226	-0.055
En9	0.135	0.065	0.023	0.228	0.118

Figure 4-4, illustrating the seasonal and annual precipitation change of ERA-20cm ensemble members from 1961 to 2010, supports this result. In seasonal changes, it was difficult to observe the similarity between Mean or each member and observation as well as between ensemble predictions in any season (Figure 4-4(a)). Moreover, the simulations for spring and winter had generally higher rainfalls than the observations, while summer rainfalls were overall underestimated. For the magnitude of interannual variability, Mean fluctuated less than any other datasets including the observations. The annual change was similar to the seasonal trend (Figure 4-4(b)). However, due to the aggregation effect of all seasonal values, the gap between ERA-20cm and the observation was mitigated, although there was no significant correlation between them. These results are also illustrated in the Taylor diagram of Figure 4-5.

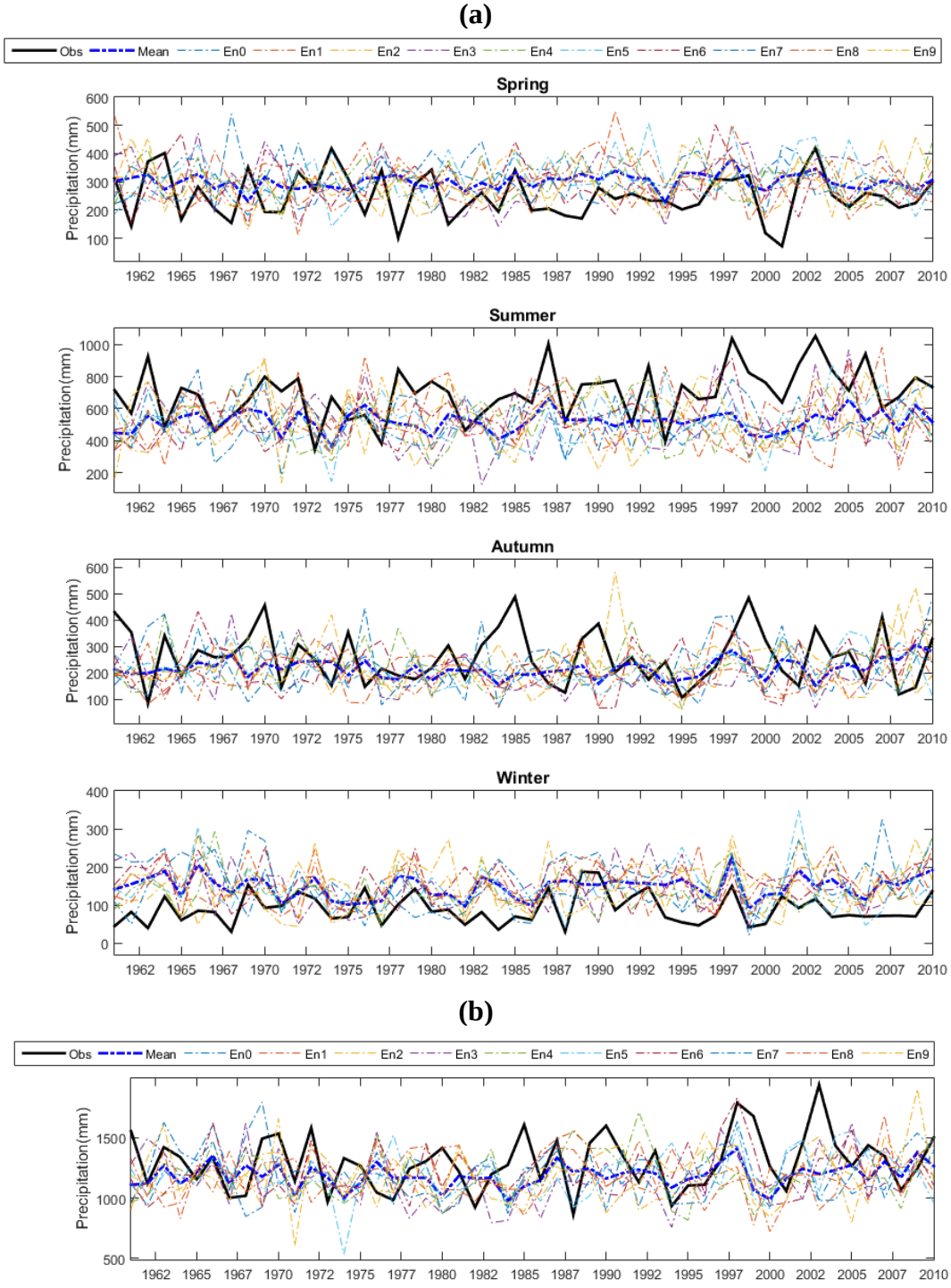

Figure 4-4 Total precipitation change of observation (Obs), mean of ERA-20cm (Mean), and ERA-20cm ensemble members (En0 to En9) averaged over the whole region from 1961 to 2010. (a) The seasonal total precipitation change (from above, spring, summer, autumn, and winter) and (b) The annual total precipitation change.

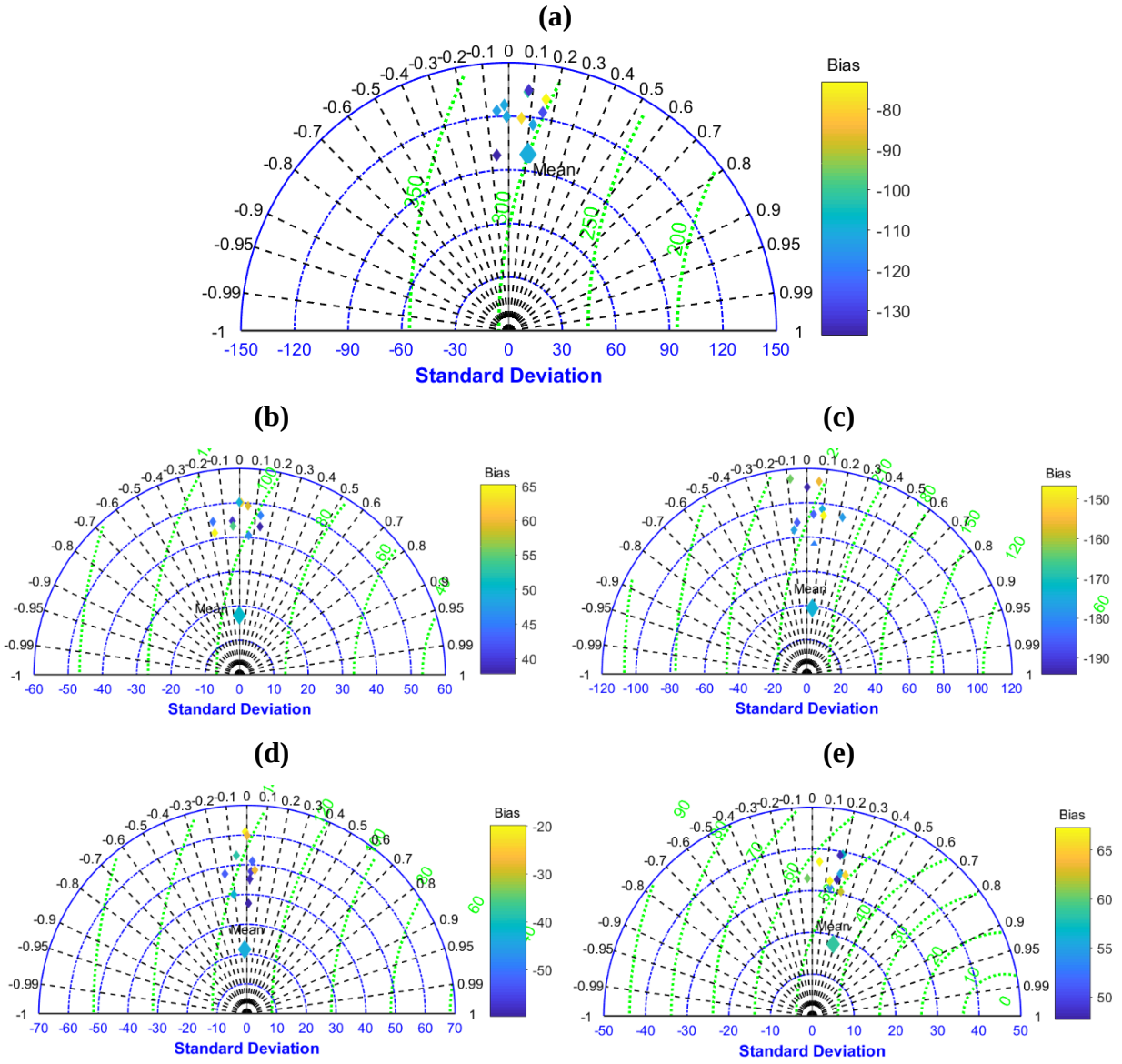

Figure 4-5 Taylor diagram of mean of ERA-20cm (Mean), and ERA-20cm ensemble members (En0 to En9) for precipitation averaged over the whole region from 1961 to 2010. (a) represents the annual change and (b) ~ (e) indicate the seasonal change [(b) spring, (c) summer, (d) autumn, and (e) winder]. Here, the big diamond marker represents Mean and small diamond markers mean ensemble members.

To identify the relationship among ERA-20cm ensemble members, the correlation coefficients between ensemble member predictions were assessed based on annual total precipitation analysis (Table 4-6). The *r* values are between -0.120 and 0.348, which suggests that each ensemble member of ERA-20cm has little correlation with others. This result implies that the ensemble members of ERA-20cm for precipitation over South Korea are generally independent.

Table 4-6 Correlation coefficient (*r*) for annual total precipitation between ERA-20cm ensemble members from 1961 to 2010.

	En0	**En1**	**En2**	**En3**	**En4**	**En5**	**En6**	**En7**	**En8**	**En9**
En0	-	0.178	0.299	0.126	0.217	0.097	0.348	0.164	0.079	0.099
En1	0.178	-	0.282	-0.012	0.330	0.097	0.090	-0.088	0.078	0.122
En2	0.299	0.282	-	0.180	0.047	0.107	0.202	-0.120	0.061	0.305
En3	0.126	-0.012	0.180	-	0.232	0.106	0.346	0.216	-0.062	0.114
En4	0.217	0.330	0.047	0.232	-	0.156	0.112	0.307	0.081	0.074
En5	0.097	0.097	0.107	0.106	0.156	-	0.292	0.228	0.036	0.104
En6	0.348	0.090	0.202	0.346	0.112	0.292	-	0.115	0.171	0.066
En7	0.164	-0.088	-0.120	0.216	0.307	0.228	0.115	-	-0.011	0.328
En8	0.079	0.078	0.061	-0.062	0.081	0.036	0.171	-0.011	-	0.022
En9	0.099	0.122	0.305	0.114	0.074	0.104	0.066	0.328	0.022	-

Figure 4-6 describes the relationship between the ensemble spread of ERA-20cm and ENSO. For El Niños, there were strong events in 1972–73, 1982–83, and 1997–98, as seen in Figure 4-6. However, it was difficult to find out ensemble variance which had patterns correlating with El Niños. Likewise, there were strong La-Niñas in 1973–76, 1988–89 and 1998–2001, but the two graphs had no significant agreement. The *r* value between the 3-month moving average spread of ERA-20cm and the ONI, 0.052, confirmed that there was no correlation between them. In other words, ERA-20cm ensemble spread was independent to ENSO over South Korea.

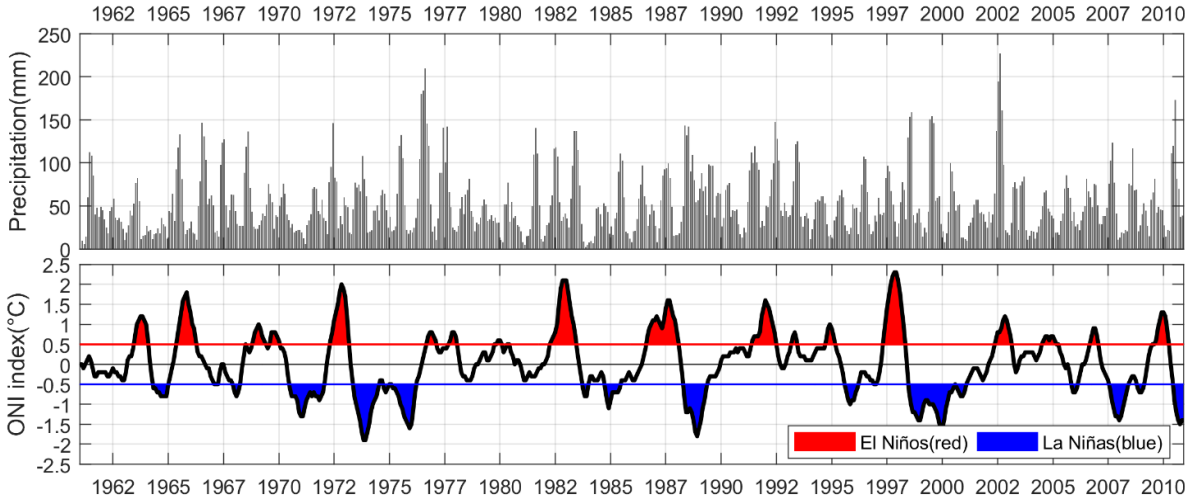

Figure 4-6 Relationship between the 3-month moving average of ERA-20cm ensemble variance for precipitation in South Korea (top) and El Niños/La Niñas events (bottom) from 1961 to 2010.

4.4.1.2 Long-term trend

Table 4-7 shows the long-term trends of the local observation and global data sources derived by the Mann–Kendall test. The standardised statistics (Z) from 1961 to 2001 stated that there were no significant seasonal/annual trends at 90 or 95% confidence level for ERA-20cm, ERA-20c, CRUv3.23, and GPCCv7, as well as the observation. Only ERA-40 in summer and 20CR in spring had an increasing and decreasing trend at 95% confidence level, respectively. With 90% confidence level, a further declining trend was found in the annual trend for 20CR.

The analysis from 1901 to 2010 showed more obvious trends in Table 4-7. ERA-20cm had significant increasing trends in spring, winter and annual simulations, while CRUv3.23 and GPCCv7 showed clear trends in summer and annual values. For ERA-20c, it performed the obvious increasing movement in every test and had a stronger increasing trend than CRUv3.23 and GPCCv7 in the annual test. This result implies that ERA-20c could have the potential to exaggerate the long-term trend for annual/seasonal precipitation than those by the other datasets. On the other hand, 20CR performed downward trends in the summer, autumn and annual test. That is, the long-term trend of 20CR contrasted with the movements of other datasets.

Table 4-7 Mann–Kendall test results for precipitation trend of the observation and global data sources.

Dataset	Spring		Summer		Autumn		Winter		Annual	
	Z	β	Z	β	Z	β	Z	β	Z	β
1961–2001										
Observation	–1.00	–1.38	1.13	2.78	–0.51	–0.74	0.30	0.14	–0.08	–0.39
ERA-20cm	1.49	0.42	–0.48	–0.48	–0.30	–0.19	–0.93	–0.38	–0.12	–0.27
ERA-20c	–0.33	–0.43	0.19	0.45	1.20	1.06	0.62	0.26	0.39	1.43
ERA-40	–0.21	–0.16	2.01[a]	3.44	1.43	1.02	0.39	0.16	1.47	3.95
20CR	–1.99[a]	–2.83	0.15	0.21	–0.46	–0.27	–0.86	–0.75	–1.83[b]	–5.11
CRUv3.23	–1.00	–1.43	1.20	2.36	–0.55	–0.78	–0.01	–0.02	–0.10	–0.42
GPCCv7	–1.02	–1.40	0.86	1.40	–0.12	–0.33	–0.06	–0.05	0.00	0.11
1901–2010										
ERA-20cm	2.58[a]	0.20	0.52	0.11	1.19	0.12	1.82[b]	0.15	2.14[a]	0.60
ERA-20c	4.95[a]	1.21	3.97[a]	2.04	4.53[a]	1.01	5.97[a]	0.55	6.09[a]	5.00
20CR	–0.11	–0.02	–2.19[a]	–0.76	–2.32[a]	–0.48	1.84[b]	0.25	–1.76[b]	–1.13
CRUv3.23	0.80	0.19	3.00[a]	1.70	1.51	0.46	–0.68	–0.07	2.72[a]	2.13
GPCCv7	0.54	0.11	3.42[a]	1.79	1.51	0.46	–1.35	–0.16	2.86[a]	2.14

[a]: Significant trend at the 0.05 significance level; [b]: Significant trend at the 0.10 significance level.
β(trends for precipitation) are in $\mathrm{mm/yr}$.

Table 4-8 shows the long-term trends of the ERA-20cm ensemble derived by the Mann-Kendall test. The standardised statistics (Z) for the period of 1961 to 2010 described that there were no significant seasonal/annual trends in ensemble members and Mean except for a few cases, whereas observation had the significant increasing trend in summer at 95% confidence level. Although the slopes (β) of ensemble members indicate the positive or opposite values, it does not mean that there are significant trends. Of the members, only En2 in autumn and En6 in summer showed significant increasing trends during the baseline period (i.e. 1961-2010).

The longer-term analysis on ERA-20cm ensemble from 1901 to 2010 showed the relatively different result. Mean indicated the significant upward trends in spring, winter, and annual tests, but there was no ensemble member which had the same pattern as Mean. Between the ensemble members, it was also challenging to find out the similarity. More specifically, En3 and En5 had significant increasing trends in spring at 95% confidence level, while En2 and En6 showed them

in autumn. En4 had the positive trend in both spring and autumn at 90% confidence level. In summer, En3 and En9 indicated a significant increasing trend and opposite trend, respectively. En7 showed an obviously increasing trend in the winter simulation at 95% confidence level, whereas En9 was the only ensemble with an upward trend in the annual test, except for Mean. On the other hand, En0, En1, and En8 had no significant trends in all simulations. The trend difference between ensemble members implies that ERA-20cm reanalysis data for precipitation have difficulty in representing the real temporal variability.

Table 4-8 Mann–Kendall test results for precipitation trend of the ERA-20cm ensemble.

Dataset	Spring		Summer		Autumn		Winter		Annual	
	Z	*β*	*Z*	*β*	*Z*	*β*	*Z*	*β*	*Z*	*β*
1961-2010										
Observation	-0.23	-0.34	2.19 [a]	3.46	-0.74	-0.73	0.28	0.09	0.82	2.25
Mean	0.70	0.16	0.43	0.31	1.14	0.44	0.20	0.07	1.36	1.35
En0	0.52	0.40	0.33	0.61	1.30	0.96	0.64	0.46	0.87	1.67
En1	0.92	0.62	-0.65	-0.93	0.69	0.72	1.37	0.69	0.82	1.43
En2	0.80	0.70	0.33	0.57	1.69 [b]	1.33	1.57	0.97	1.39	2.78
En3	1.30	1.24	-0.79	-1.73	-0.33	-0.28	-0.40	-0.29	-0.18	-0.56
En4	0.03	0.04	0.40	0.46	1.47	1.18	-0.13	-0.06	0.80	1.60
En5	0.95	0.72	0.99	1.36	0.42	0.30	-0.05	-0.03	1.29	2.49
En6	-0.94	-0.76	2.16 [a]	3.14	0.72	0.64	0.00	-0.01	1.05	2.17
En7	-0.62	-0.51	-0.05	-0.09	-0.07	-0.07	-1.05	-0.69	-0.32	-0.60
En8	-0.79	-0.57	-0.40	-0.66	-0.17	-0.11	0.38	0.21	-0.55	-1.12
En9	0.37	0.32	0.59	1.06	-0.67	-0.51	0.00	0.00	1.36	2.34
1901-2010										
Mean	2.58 [a]	0.20	0.52	0.11	1.19	0.12	1.82 [b]	0.15	2.14 [a]	0.60
En0	0.11	0.02	0.80	0.38	-0.60	-0.13	0.24	0.04	0.30	0.18
En1	-0.68	-0.15	-0.07	-0.02	-0.54	-0.13	0.70	0.10	0.01	0.01
En2	0.74	0.17	-0.94	-0.48	2.19 [a]	0.51	0.50	0.09	0.65	0.37
En3	2.58 [a]	0.57	-1.90 [b]	-0.89	-0.23	-0.06	1.42	0.25	-0.12	-0.06
En4	1.79 [b]	0.39	-0.85	-0.39	1.83 [b]	0.43	1.01	0.16	0.95	0.58
En5	2.36 [a]	0.55	0.81	0.41	-0.56	-0.12	0.37	0.05	1.20	0.85
En6	0.24	0.04	1.44	0.70	1.96 [a]	0.45	0.26	0.05	1.55	0.97
En7	1.25	0.27	-0.09	-0.05	0.77	0.19	2.09 [a]	0.36	1.30	0.79
En8	1.32	0.30	-0.01	-0.01	-0.84	-0.16	1.29	0.19	0.79	0.52
En9	0.22	0.06	2.04 [a]	1.00	0.09	0.02	0.50	0.08	2.57 [a]	1.39

[a]: Significant trend at the 0.05 significance level; [b]: Significant trend at the 0.10 significance level.
β(trends for precipitation) are in $\mathrm{mm/yr}$.

4.4.1.3 Statistical comparability

For statistical comparison between different datasets, I adopted a PDF-based skill score test. Figure 4-7 describes the statistical agreement between the observation and global data sources from 1961 to 2001. Note that the skill scores were estimated from the PDFs of monthly precipitation data for the reference period. In this analysis, CRUv3.23 and GPCCv7 performed the best simulations with the skill score of approximately 0.94, and ERA-20c followed them closely with 0.93. This result indicates that ERA-20c has statistical similarity with the observed data at almost the same level as CRUv3.23 and GPCCv7. The scores for 20CR and ERA-40 were 0.82 and 0.85, respectively, which showed high agreements. ERA-20cm had a distinctly smaller value, 0.66.

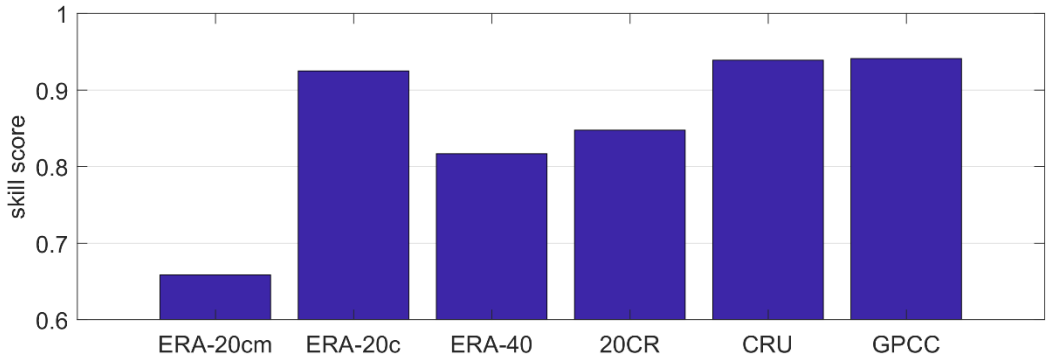

Figure 4-7 PDF-based skill score for precipitation for ERA-20cm, ERA-20c, ERA-40, 20CR, CRUv3.23 (CRU), and GPCCv7 (GPCC) averaged over the whole region from 1961 to 2001.

The specific discrepancies of individual datasets are described in Figure 4-8(a) which illustrates the PDFs of the observation and each dataset in South Korea from 1961 to 2001, and Figure 4-8(b) representing seasonally subdivided PDFs. ERA-20c, as well as CRUv3.23 and GPCCv7, is one of the most fitted datasets to the observation with little discrepancies. However, the other datasets had partial gaps from the observation. For 20CR, the PDF in Figure 4-8(a) showed that it underestimated over 200 mm month^{-1} and overestimated in the range of 36–100 mm month^{-1}. This result was mainly due to the underestimated values in summer, as seen in Figure 4-8(b). The left-biased summer rainfalls led to the overestimation of moderate values and underestimation of intensive values. The PDF of ERA-40 in Figure 4-8(a) overall exaggerated the frequency under 50 mm month^{-1} and underestimated over 200 mm month^{-1}. It came from the generally underestimated distributions in all seasons, especially in summer (Figure 4-8(b)). In the case of ERA-20cm, the dry months and intensive rainfall months were underestimated but the moderate

months were overestimated in Figure 4-8(a). This evaluation suggests that all datasets showed significant agreement with the observation, albeit some of them still needed a cautious approach to use in the frequency analysis.

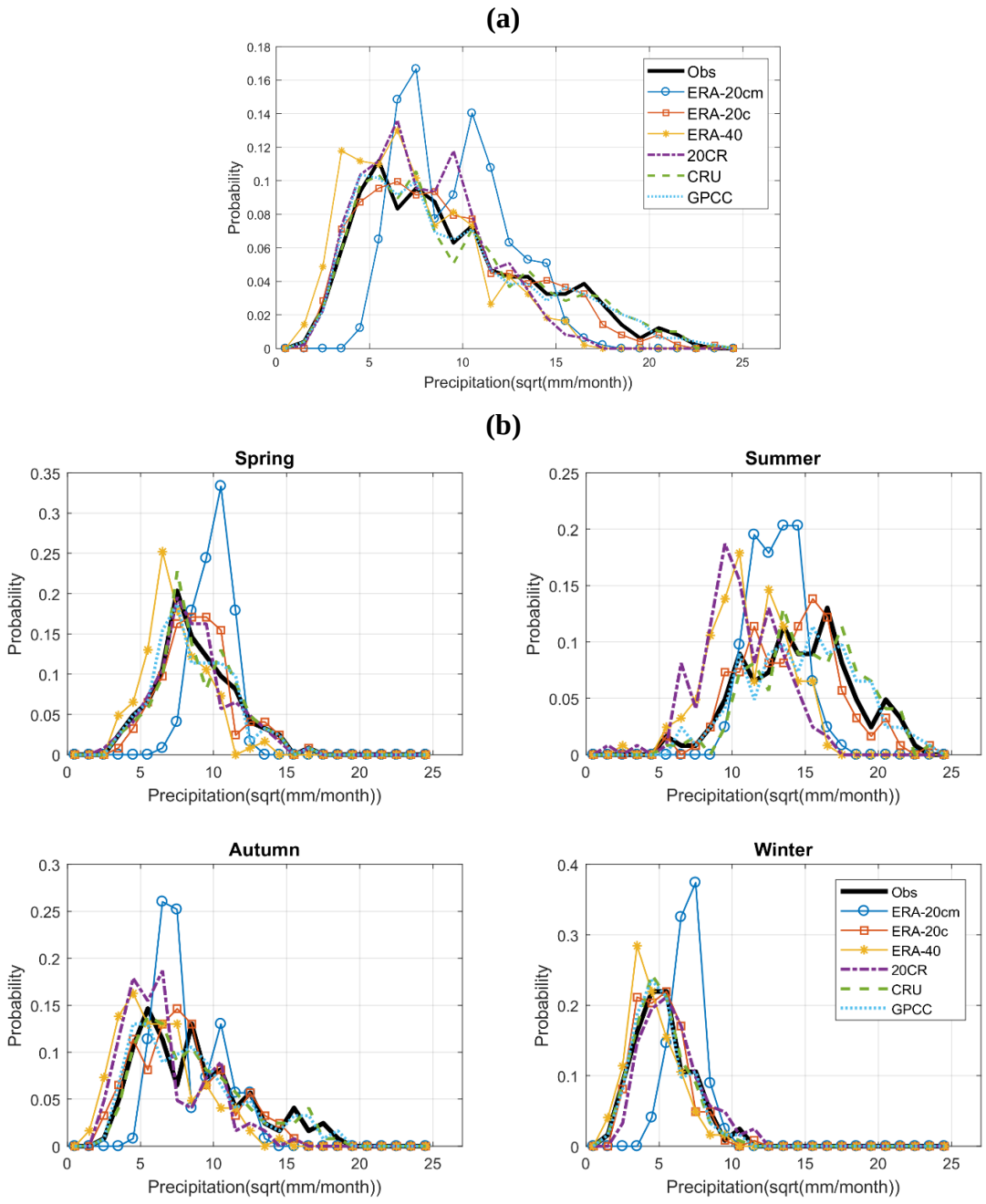

Figure 4-8 PDFs for monthly precipitation for observation (Obs), ERA-20cm, ERA-20c, ERA-40, 20CR, CRUv3.23 (CRU), and GPCCv7 (GPCC) over South Korea. (a) PDFs for monthly total precipitation from 1961 to 2001 and (b) PDFs for seasonally subdivided monthly total precipitation from 1961 to 2001.

This thesis assesses the statistical agreement of ERA-20cm ensemble members as well. Despite the inconsistency of temporal change shown in Sections 4.4.1.1 and 4.4.1.2, Figure 4-9 suggests that there are statistically significant agreements between observation and individual ensemble members from 1961 to 2010. The skill scores of all ten ensemble members exceeded 0.8, and the minimum and maximum values were 0.81 for En6 and 0.86 for En2, respectively. Interestingly, the mean of ERA-20cm (i.e. Mean) indicated 0.67, which was less than any ensemble predictions.

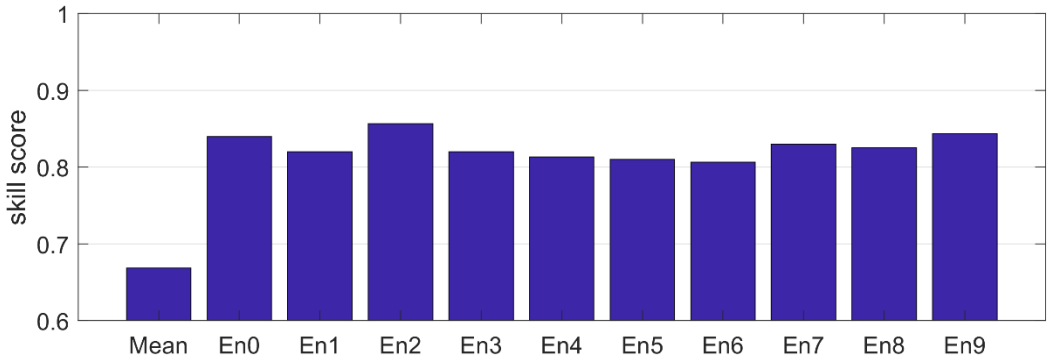

Figure 4-9 PDF-based skill score for monthly precipitation for the ERA-20cm mean (Mean) and ensemble members (En0 to En9) averaged over the whole region from 1961 to 2010.

The specific reason for low skill score for the ERA-20cm ensemble is shown in Figure 4-10 which compares PDFs of the observation with those of the ensemble members and Mean over South Korea from 1961 to 2010. It was evident that all ensemble predictions slightly underestimated the probability of dry months and intensive rainfall months and overestimated the moderate months in Figure 4-10(a). Especially, Mean had the obviously overestimated probability for the moderate intensity, which stemmed from temporally smoothed values in Figure 4-4. Seasonally, spring and winter rainfalls for ensemble members were generally overestimated, and the PDFs of summer rainfalls for ten members were in the left of the PDF of the observation (Figure 4-10(b)). Compared with ensemble predictions, Mean had the more exaggerated moderate values in every season. This evaluation suggests that Mean for ERA-20cm requires a cautious approach to use in the frequency analysis, albeit it as well as all ensemble members show significant agreements with the observation.

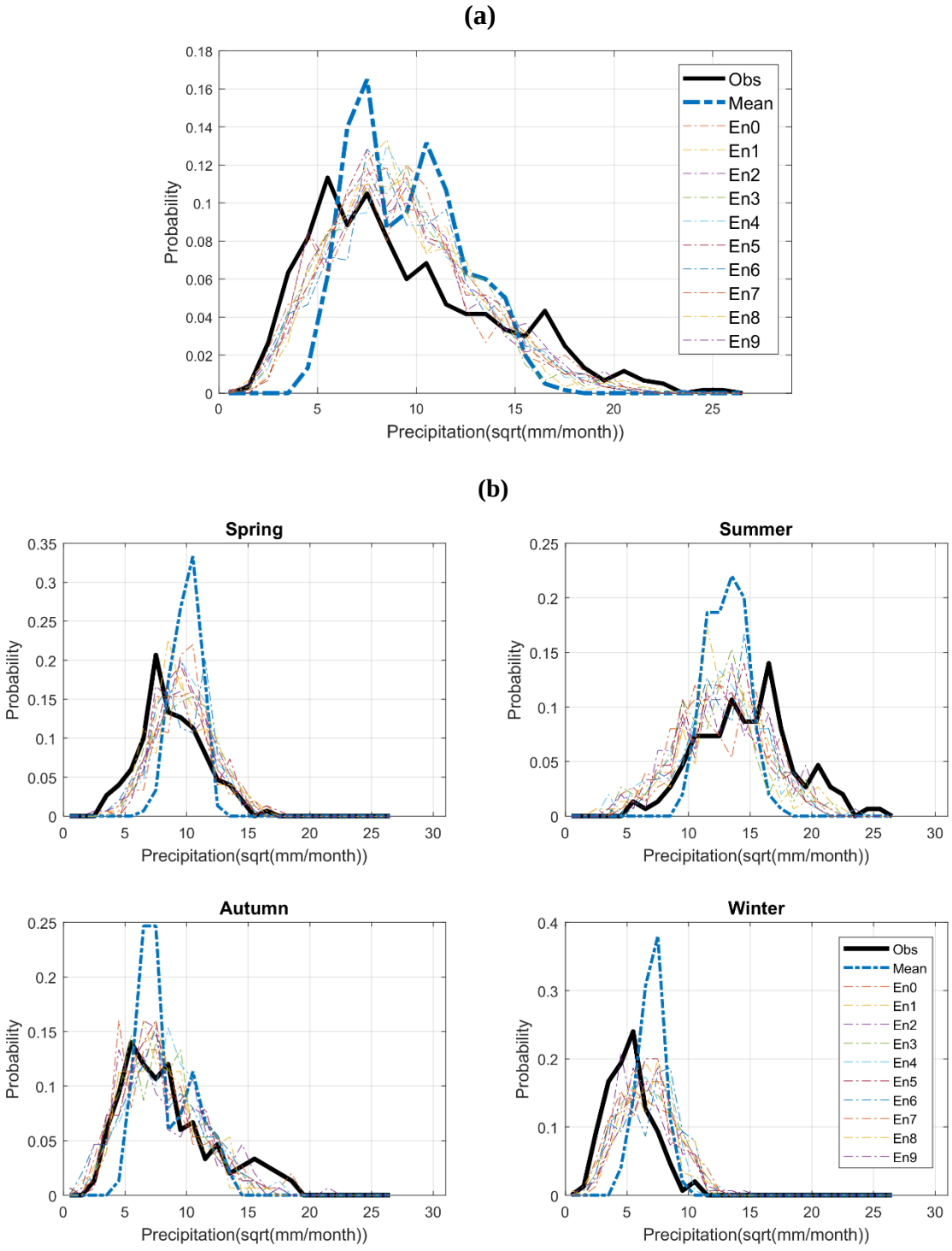

Figure 4-10 PDFs of monthly total precipitation for observation (Obs) and ERA-20cm ensemble over South Korea. (a) PDFs for monthly total precipitation from 1961 to 2010 and (b) PDFs for seasonally subdivided monthly total precipitation from 1961 to 2010.

4.4.1.4 The goodness of ERA-20cm ensemble

To evaluate the suitability of the ensemble spread for ERA-20cm, this thesis has calculated the percentage of observations bracketed by ensemble intervals. Table 4-9 represents the result of this analysis. Regarding the spread for temporal change, the values indicated the moderate to high goodness with the percentage between 56 and 74. This result implies that the ensemble for precipitation is quite well spread to reproduce the real world, but it still needs the improvement to cover the whole observation curve for the period of 1961–2010 as illustrated in Figure 4-4. For the statistical analysis, the *P* value (%), 42.3, seems to indicate the moderate goodness but it decreases to 34.6 if on-boundary values are excluded. This result indicates that the coverage of the ensemble is not statistically well-spread, although each ensemble dataset has the significant agreement with the observation.

Table 4-9 The percentage of the observation for precipitation bracketed by the ERA-20cm ensemble intervals.

Type	Interannual					PDF
	Spring	Summer	Autumn	Winter	Annual	
P(%)	66.0	56.0	74.0	60.0	70.0	42.3 (34.6*)

*: The percentage excluding the number of observations on-boundary

4.4.2 Temperature

4.4.2.1 Interannual variability

Table 4-10 describes the *r* values between the gauged temperature and model outputs from 1961 to 2001. In seasonal comparison, CRUv3.23 and ERA-40 had the highest values over 0.9 in every season and ERA-20c followed closely with 0.830 to 0.914. 20CR had the moderate to high correlations ($0.6 < r < 0.9$) and ERA-20cm were generally the lowest ones with the moderate correlations ($0.4 < r < 0.7$) in four seasons. Of the four seasons, winter had the highest value except for ERA-20cm in which spring showed the best. Theses seasonal findings were similar to the annual simulations. In the annual comparison, CRUv3.23 and ERA-40 showed the most fitted correlations with the *r* values over 0.92, and ERA-20c closely followed them with 0.879. 20CR had the 0.808, and ERA-20cm was the lowest with 0.714.

Table 4-10 Correlation coefficient (*r*) for seasonal and annual mean temperature for global data sources averaged over all regions from 1961 to 2001.

Type	Seasonal comparison				Annual comparison
	Spring	Summer	Autumn	Winter	
ERA-20cm	0.671	0.597	0.578	0.407	0.714
ERA-20c	0.830	0.867	0.895	0.914	0.879
ERA-40	0.924	0.943	0.908	0.963	0.923
20CR	0.654	0.785	0.798	0.875	0.808
CRUv3.23	0.933	0.964	0.945	0.976	0.950

Figure 4-11 demonstrates the seasonal and annual mean temperature trends of several data sources over South Korea from 1961 to 2001. In Figure 4-11, each dataset showed similar movements to the observations, but the values themselves were different depending on the dataset, except for ERA-40. For ERA-20cm and ERA-20c, the seasonal/annual variations seemed to have partial correlations, but the model values were generally about 1–2 ºC lower than those of observations, except the winter season. In the case of CRUv3.23, the mean temperature was about 2 ºC lower than the observation in every comparison, although the trends had similarity to the observations in Table 4-10. On the other hand, 20CR had higher values than the observation in the annual comparison, affected by the autumn and winter temperature. Only ERA-40 was very well fitted to the observed values in every comparison. This result implies that, despite the significant correlations between the observation and each dataset, bias correction should be considered before using them in hydrological applications. Figure 4-12 summarised the evaluation results in the form of the Taylor diagram.

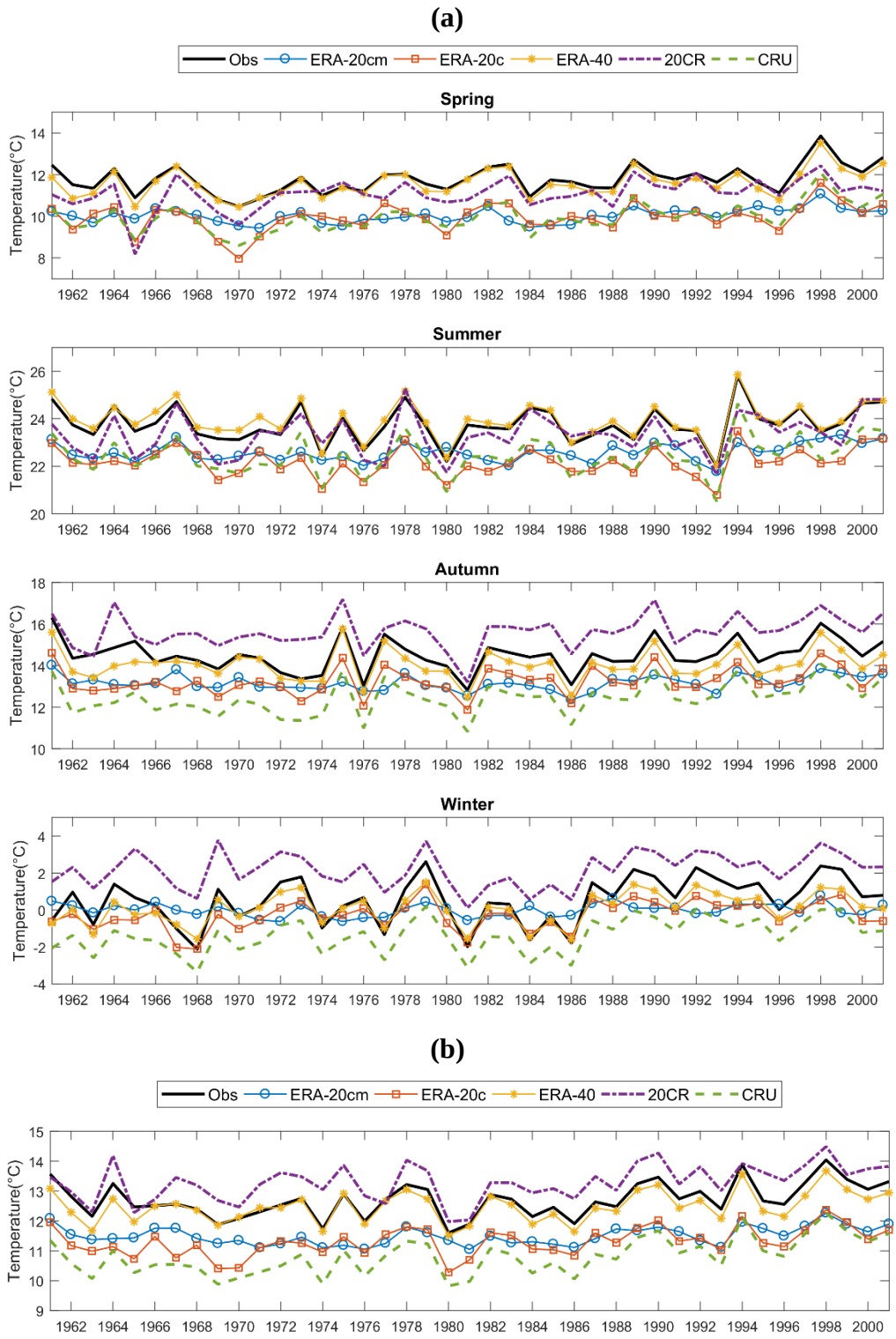

Figure 4-11 Temperature change for observation (Obs), ERA-20cm, ERA-20c, ERA-40, 20CR, and CRUv3.23 (CRU) averaged over South Korea from 1961 to 2001. (a) The seasonal change (from above, spring, summer, autumn, and winter) and (b) The annual change.

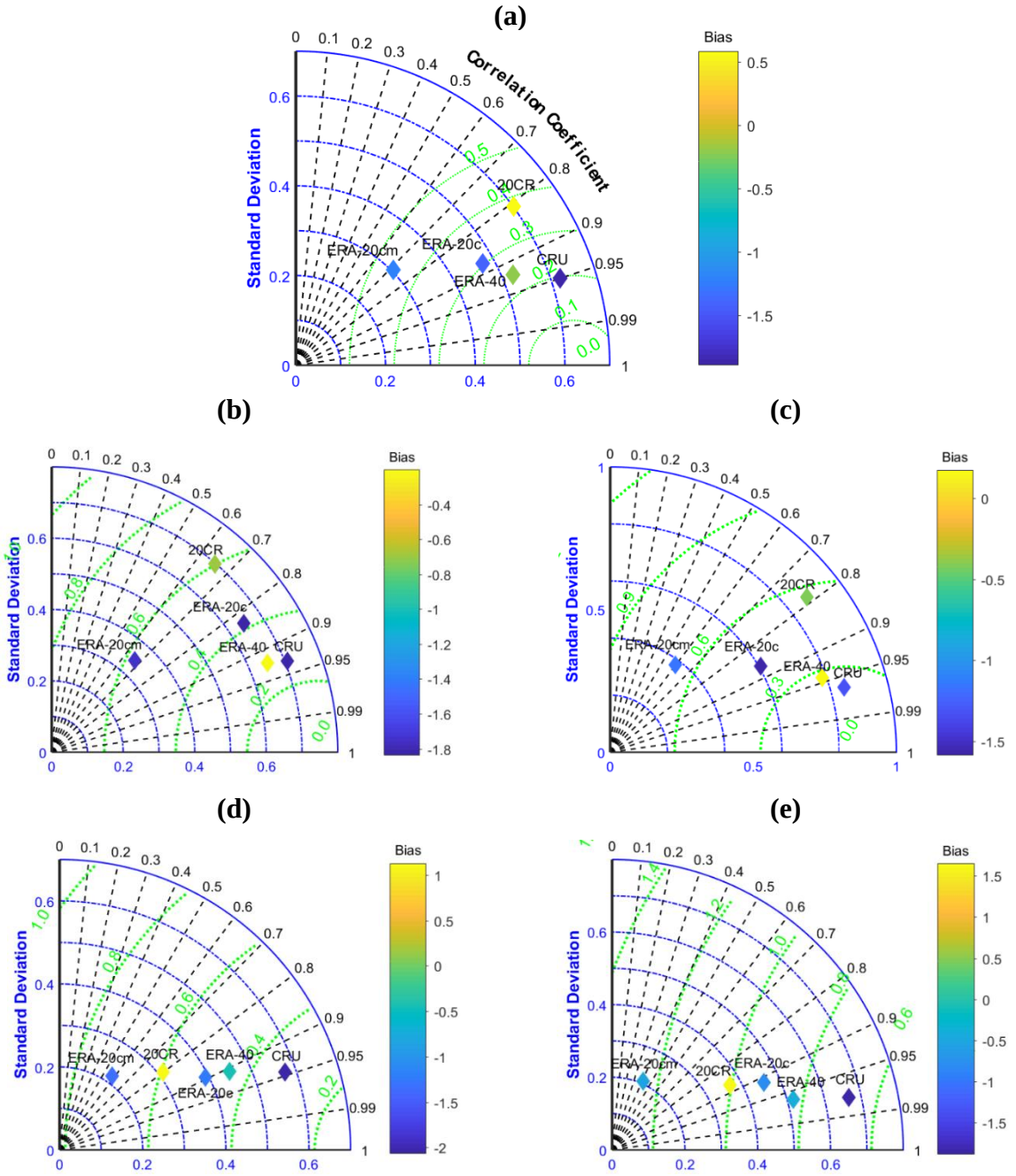

Figure 4-12 Taylor diagram of ERA-20cm, ERA-20c, ERA-40, 20CR, and CRUv3.23 (CRU) for temperature over the whole region from 1961 to 2001. (a) represents the annual change and (b) ~ (e) indicate the seasonal change [(b) spring, (c) summer, (d) autumn, and (e) winder].

This thesis performed the further analysis on ERA-20cm ensemble in monthly temperature. Table 4-11 describes the *r* values between the gauged temperature and the temperature of ERA-20cm ensemble members from 1961 to 2010. In seasonal simulations, ERA-20cm ten ensemble members generally had low to moderate values with 0.045 to 0.521 in four seasons, whereas Mean performed moderate correlation with the highest values between 0.471 and 0.689. To be more specific, spring and summer generally had the highest values except for En4, while winter had the weakest correlation in each dataset. In the annual comparison, Mean addressed the high correlation with the observation (0.746), whereas all ten members showed the moderate correlations ($0.437 < r < 0.602$).

Table 4-11 Correlation coefficient (*r*) for seasonal and annual mean temperature between the observation and ERA-20cm ensemble members averaged over all regions from 1961 to 2010.

Type	Seasonal				Annual
	spring	summer	autumn	winter	
Mean	0.689	0.569	0.611	0.471	0.746
En0	0.504	0.253	0.318	0.241	0.591
En1	0.502	0.388	0.238	0.070	0.519
En2	0.413	0.478	0.410	0.414	0.544
En3	0.348	0.441	0.403	0.045	0.437
En4	0.300	0.350	0.480	0.238	0.523
En5	0.445	0.344	0.425	0.338	0.560
En6	0.366	0.521	0.409	0.191	0.585
En7	0.514	0.355	0.429	0.277	0.580
En8	0.333	0.472	0.389	0.322	0.544
En9	0.397	0.435	0.390	0.351	0.602

Figure 4-13 details the seasonal and annual mean temperature patterns for ERA-20cm ensemble in South Korea from 1961 to 2010. For the seasonal comparisons, the movements of individual ensemble members in a given season had partial similarity with the observation (Figure 4-13(a)). In terms of values themselves, each member was generally lower than the real in all seasons except for winter. More specifically, the mean values for ensemble members were about 1 to 2 Celsius degrees lower than the observations from spring to autumn, and even in winter, gaps were observed since 1988 (Figure 4-13(a)). From this seasonal feature, it is clearly shown that the ERA-20cm annual data have the cooler temperature than the annual mean of the observed temperature, albeit there are some partial correlations between them (Figure 4-13(b)). Figure 4-14 summarised the results in the Taylor diagram.

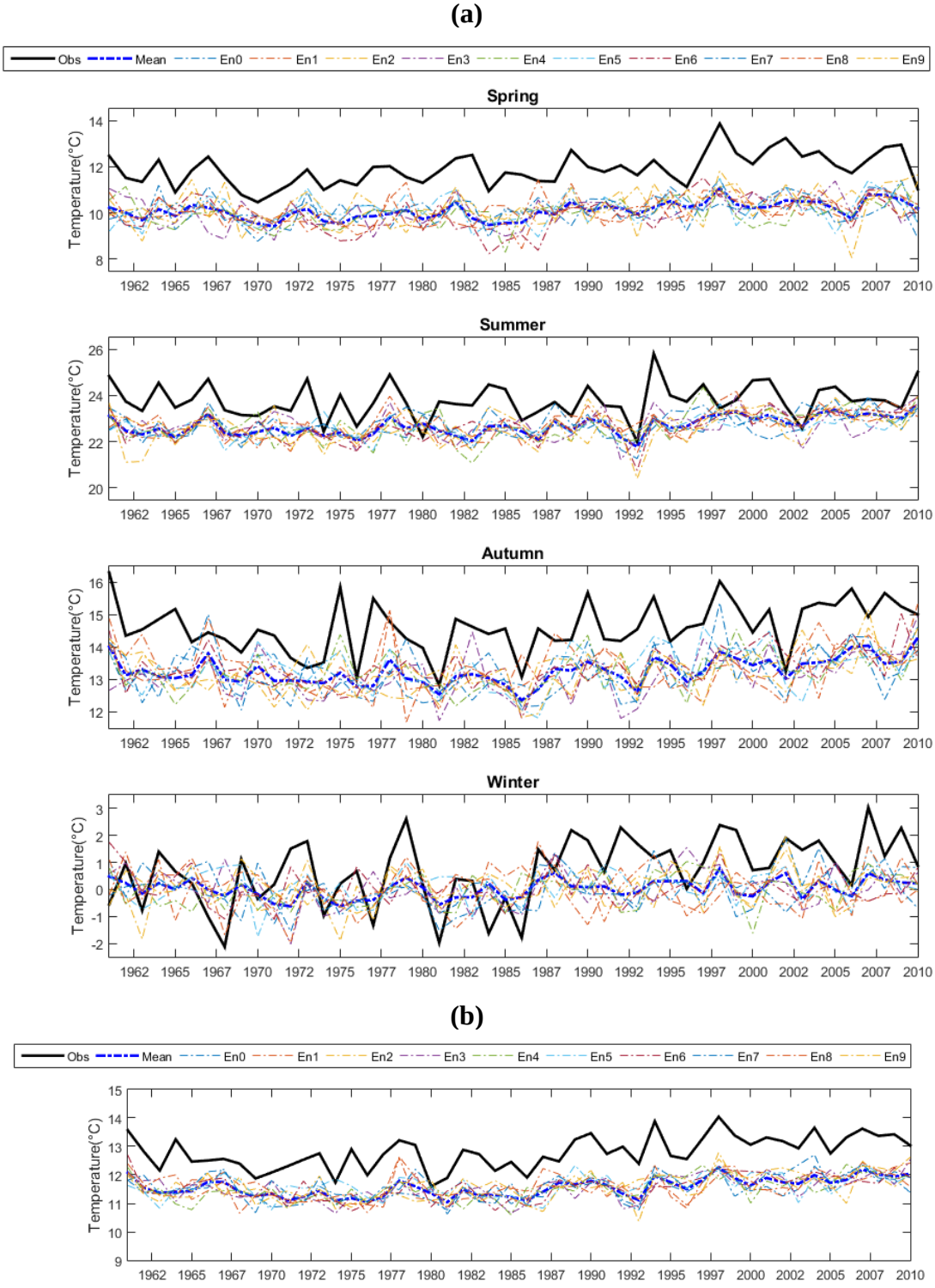

Figure 4-13 Mean temperature change for observation (Obs), Mean of ERA-20cm, and ERA-20cm ensemble members (En0 to En9) from 1961 to 2010. (a) The seasonal change (from above, spring, summer, autumn, and winter) and (b) The annual change.

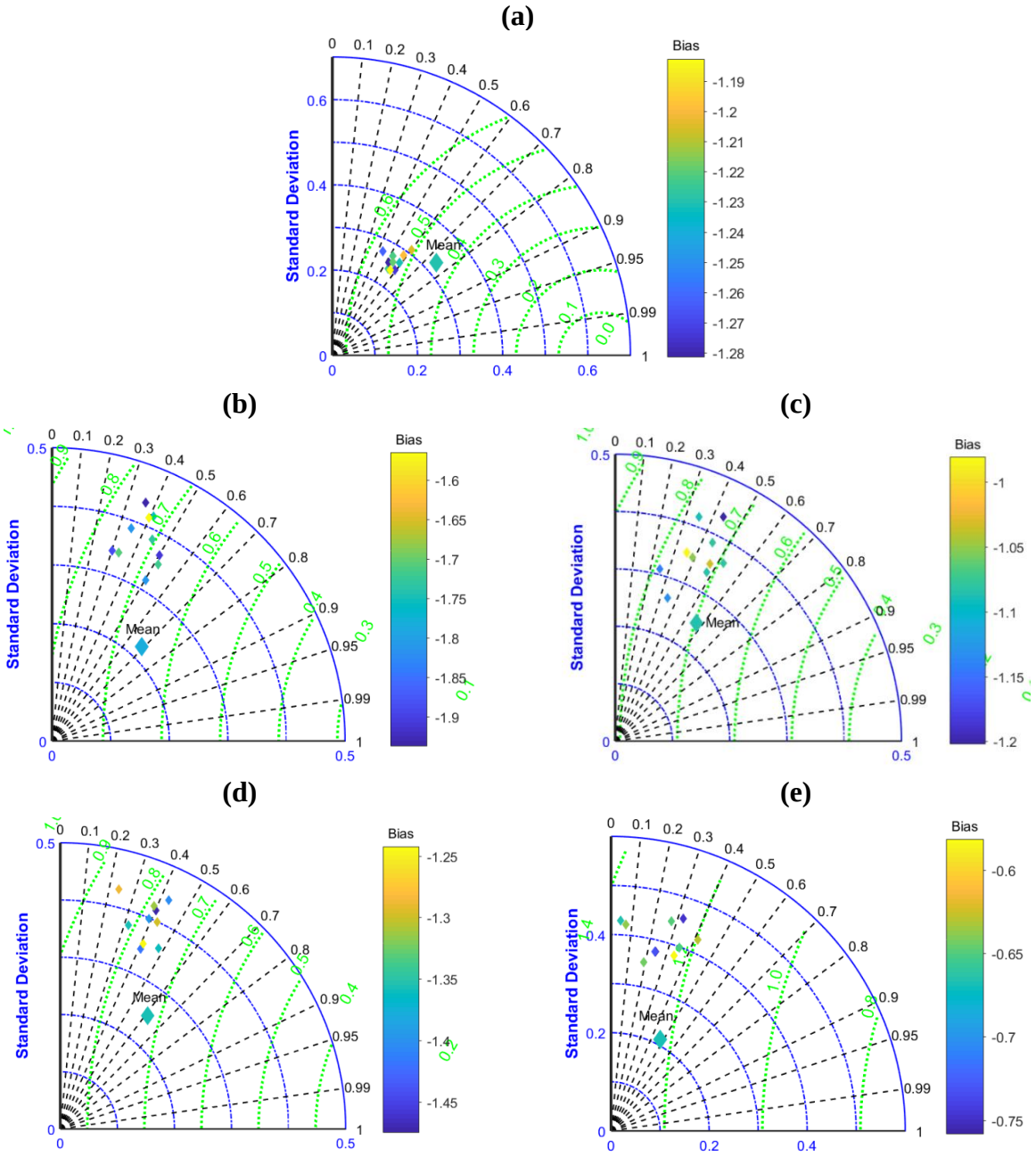

Figure 4-14 Taylor diagram of mean of ERA-20cm (Mean), and ERA-20cm ensemble members (En0 to En9) for temperature averaged over the whole region from 1961 to 2010. (a) represents the annual change and (b) ~ (e) indicate the seasonal change [(b) spring, (c) summer, (d) autumn, and (e) winder]. Here, the big diamond marker represents Mean and small diamond markers mean ensemble members.

To determine the independence among the ten members, the *r* values between ERA-20cm ensemble predictions were estimated based on an annual mean temperature analysis from 1961 to 2010 (Table 4-12). The coefficients were generally low to moderate with the values between 0.259 and 0.686. The most correlated members were En6 and En9 with 0.686, while the least ones were En2 and En4. This analysis suggests that for temperature, there is a partial covarying relationship between ensemble members as well as between the ensemble and observation.

Table 4-12 Correlation coefficient (*r*) for annual mean temperature between ERA-20cm ensemble members from 1961 to 2010.

	En0	**En1**	**En2**	**En3**	**En4**	**En5**	**En6**	**En7**	**En8**	**En9**
En0	-	0.572	0.476	0.568	0.533	0.489	0.602	0.618	0.509	0.613
En1	0.572	-	0.466	0.443	0.509	0.319	0.493	0.430	0.567	0.523
En2	0.476	0.466	-	0.416	0.259	0.436	0.383	0.449	0.354	0.519
En3	0.568	0.443	0.416	-	0.635	0.345	0.567	0.440	0.414	0.627
En4	0.533	0.509	0.259	0.635	-	0.287	0.490	0.416	0.380	0.591
En5	0.489	0.319	0.436	0.345	0.287	-	0.461	0.470	0.292	0.536
En6	0.602	0.493	0.383	0.567	0.490	0.461	-	0.565	0.479	0.686
En7	0.618	0.430	0.449	0.440	0.416	0.470	0.565	-	0.491	0.609
En8	0.509	0.567	0.354	0.414	0.380	0.292	0.479	0.491	-	0.370
En9	0.613	0.523	0.519	0.627	0.591	0.536	0.686	0.609	0.370	-

Figure 4-15 illustrates the relationship between the ensemble spread of ERA-20cm for temperature and ENSO. As aforementioned for precipitation, the strong El Niños happened in 1972–73, 1982–83, and 1997–98 and La-Niñas happened in 1973–76, 1988–89 and 1998–2001. In the comparison between this pattern with the ensemble spread, there was little correlation between them. The r value between the 3-month moving average spread of ERA-20cm and the ONI, -0.006, also supports this result. I.e., the ensemble spread of ERA-20cm for temperature may be not affected by ENSO over South Korea.

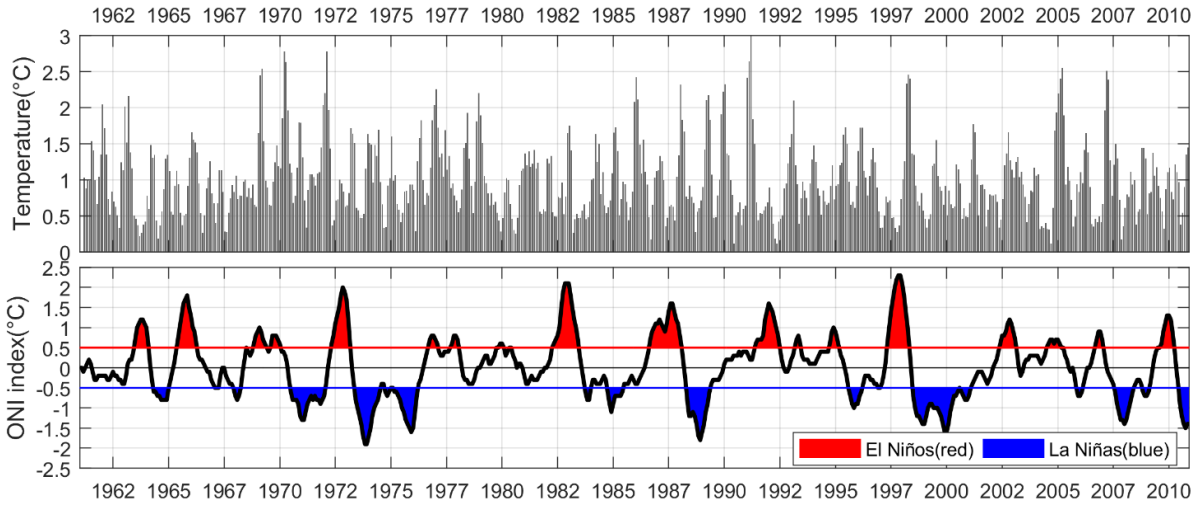

Figure 4-15 Relationship between the 3-month moving average of ERA-20cm ensemble variance for temperature in South Korea (top) and El Niños/La Niñas events (bottom) from 1961 to 2010.

4.4.2.2 Long-term trend

Table 4-13 describes the seasonal and annual patterns of mean temperature for the local records and global data sources by the Mann–Kendall approach. In the first analysis from 1961 to 2001, the result suggested that only ERA-40 had increasing trends in spring, winter and annual simulations, as same as the observations. Seasonally, the other datasets also had an upward trend in spring, but they showed different trends in other seasons. For CRUv3.23 and ERA-20c, there were significant increasing trends in spring, autumn and winter, whereas 20CR had obvious trends in spring and autumn. ERA-20cm had increasing trends in spring and summer at 95% confidence level, not in winter. In terms of annual analysis, all datasets showed upward trends for the reference period (i.e. 1961–2001). ERA-20c, 20CR, and CRUv3.23 showed significant upward trends at 95% confidence level, and ERA-40 and ERA-20cm suggested them at 90% confidence level. For the slope of the annual comparison, those of CRUv3.23 and 20CR were higher than that of observation, while ERA-20c and ERA-40 were slightly smaller than the observed. In the case of ERA-20cm, the slope showed less than half of that for the observation.

The second analysis for the entire 20th century (1901–2010) indicated obvious increasing trends in all seasonal and annual simulations at 95% confidence level in Table 4-13. This result implies that the mean temperature in South Korea has increased obviously over the past 100 years. The only

difference between datasets was the intensity of the slopes. As with the first analysis, the increasing magnitudes (β) of 20CR and CRUv3.23 were generally higher than those of the others.

Table 4-13 Mann–Kendall test results for temperature in the observation and global data sources.

Dataset	Spring		Summer		Autumn		Winter		Annual	
	Z	β	Z	β	Z	β	Z	β	Z	β
1961–2001										
Observation	2.62[a]	2.53	0.57	0.64	0.84	0.70	2.30[a]	3.65	3.66[a]	2.09
ERA-20cm	2.62[a]	1.17	2.12[a]	1.31	0.78	0.59	0.75	0.33	1.81[b]	0.86
ERA-20c	1.67[b]	1.40	0.46	0.33	1.92[b]	1.30	2.62[a]	2.38	2.71[a]	1.80
ERA-40	2.55[a]	2.22	–0.08	–0.12	0.46	0.52	2.26[a]	2.41	1.81[b]	1.47
20CR	2.82[a]	2.20	1.54	1.86	2.41[a]	2.18	1.38	1.99	2.77[a]	2.34
CRUv3.23	3.36[a]	3.07	1.61	1.38	2.62[a]	2.16	2.86[a]	3.53	3.31[a]	2.91
1901–2010										
ERA-20cm	8.69[a]	1.02	7.60[a]	0.91	6.61[a]	0.81	6.61[a]	0.79	9.38[a]	0.95
ERA-20c	3.25[a]	0.66	2.94[a]	0.49	4.06[a]	0.86	6.15[a]	1.55	7.02[a]	1.04
20CR	6.73[a]	1.71	5.14[a]	1.35	6.11[a]	1.43	6.36[a]	2.09	8.15[a]	1.80
CRUv3.23	7.93[a]	1.99	3.77[a]	0.85	5.96[a]	1.51	5.15[a]	1.62	7.85[a]	1.61

[a]: Significant trend at the 0.05 significance level; [b]: Significant trend at the 0.10 significance level.
β(trends for temperature) are in $10^{-2}°C/yr$

The next step was to analyse the long-term trend of the ERA-20cm ensemble. Table 4-14 describes the seasonal and annual patterns for mean temperature of ensemble members by the Mann-Kendall approach. The seasonal analysis from 1961 to 2010 suggested that the observation and ensemble predictions have different trends. In winter, the observation had a most strongly increasing trend at 0.05 significance level, but for ensemble members, there were no significant trends except En0 and En4. In contrasts, in summer, there was no significant trend for the observation, but ensemble members except En3 had the obvious upward trends. Likewise, Mean had the increasing trend at 95% confidence level in summer, but there was no significant trend in winter. In terms of annual analysis, each member, as well as the observation and Mean, showed a significant upward trend at 95% confidence. However, the slopes of annual trends for Mean and the members were generally less than that of the observation. This result suggests that the discrepancy between ERA-20cm

ensemble and the observation for temperature has been widened during the study period, as shown in Figure 4-13(b).

Table 4-14 Mann–Kendall test results for temperature trend of the ERA-20cm ensemble.

Dataset	Spring		Summer		Autumn		Winter		Annual	
	Z	β	Z	β	Z	β	Z	β	Z	β
1961-2010										
Observation	3.45 [a]	2.54	0.89	0.59	2.24 [a]	1.82	3.09 [a]	3.63	3.66 [a]	2.09
Mean	3.85 [a]	1.44	4.00 [a]	1.72	2.79 [a]	1.26	1.59	0.54	3.75 [a]	1.34
En0	1.74 [b]	0.89	2.31 [a]	1.18	1.30	1.02	1.84 [b]	1.00	2.56 [a]	1.16
En1	2.91 [a]	1.72	3.58 [a]	1.94	1.82 [b]	1.31	-1.12	-0.88	1.97 [a]	1.13
En2	2.19 [a]	1.44	2.12 [a]	1.22	1.52	0.90	0.77	0.53	2.78 [a]	1.11
En3	2.33 [a]	1.71	1.22	0.95	2.61 [a]	1.68	0.72	0.45	2.64 [a]	1.31
En4	2.53 [a]	1.18	2.88 [a]	1.99	1.87 [b]	1.20	2.12 [a]	1.56	3.73 [a]	1.56
En5	1.49	0.97	2.94 [a]	1.17	1.89 [b]	1.31	0.65	0.43	2.66 [a]	1.12
En6	1.91 [b]	1.53	4.28 [a]	2.41	2.99 [a]	1.68	-0.28	-0.10	3.06 [a]	1.36
En7	2.23 [a]	1.47	2.43 [a]	1.43	1.42	1.07	0.38	0.35	2.29 [a]	1.15
En8	2.28 [a]	1.31	2.84 [a]	1.49	0.62	0.33	0.67	0.50	2.88 [a]	1.11
En9	3.28 [a]	2.05	3.45 [a]	2.35	2.96 [a]	1.96	1.25	0.94	3.93 [a]	2.04
1901-2010										
Mean	8.69 [a]	1.02	7.60 [a]	0.91	6.61 [a]	0.81	6.61 [a]	0.79	9.38 [a]	0.95
En0	4.90 [a]	1.02	4.02 [a]	0.60	4.17 [a]	0.80	3.19 [a]	0.61	6.33 [a]	0.80
En1	4.18 [a]	0.79	6.45 [a]	1.13	4.25 [a]	0.87	3.59 [a]	0.81	6.89 [a]	0.99
En2	5.48 [a]	1.11	5.75 [a]	0.98	4.23 [a]	0.72	4.84 [a]	1.05	7.80 [a]	1.03
En3	4.86 [a]	0.93	4.52 [a]	0.85	3.49 [a]	0.66	2.84 [a]	0.61	6.10 [a]	0.84
En4	4.42 [a]	0.67	5.80 [a]	1.16	4.48 [a]	0.85	4.57 [a]	0.92	7.17 [a]	0.96
En5	6.05 [a]	1.24	4.45 [a]	0.70	4.45 [a]	0.89	4.19 [a]	0.87	7.38 [a]	1.02
En6	2.85 [a]	0.62	5.16 [a]	0.95	3.72 [a]	0.64	2.06 [a]	0.44	5.33 [a]	0.70
En7	5.66 [a]	1.08	5.99 [a]	1.09	3.14 [a]	0.64	4.09 [a]	0.87	7.00 [a]	1.04
En8	6.05 [a]	1.27	5.06 [a]	0.85	4.25 [a]	0.93	2.96 [a]	0.70	6.77 [a]	0.99
En9	6.48 [a]	1.39	4.91 [a]	0.88	4.74 [a]	0.99	3.75 [a]	0.80	7.29 [a]	1.13

[a]: Significant trend at the 0.05 significance level; [b]: Significant trend at the 0.10 significance level.
β(trends for temperature) are in $10^{-2}°C/yr$

Unlike the analysis for the period of 1961–2010, the simulations for the entire 20th century (1901-2010) indicated that all ensemble members had obvious increasing trends at 0.05 significance level in every season in Table 4-14. To be more specific about seasonal intensities (β), the values for spring and summer were generally higher than those for winter, although all the slopes were between 0.44 and 1.39 °C per 100 years. In case of the annual simulation, all simulations showed

significant upward trends at 95% confidence level, and the extent of increase for the ensemble was close to 1°C per 100 years, which was slightly weaker than those of the first simulation from 1961 to 2010. Reminding the obvious increasing trends in different century-long data sources as described in Table 4-13, this analysis implies that in the long term, the temperature over South Korea has been rising, and ERA-20cm ensemble can represent the overall trend in temperature despite the substantial biases.

4.4.2.3 Statistical comparability

Figure 4-16 represents the PDF-based skill score for reanalyses and gridded observations for monthly mean temperature from 1961 to 2001. The estimate of ERA-40 was approximately 0.90, and 20CR, ERA-20c, and CRUv3.23 followed with 0.74, 0.69, and 0.69, respectively. In other words, ERA-40 had a probability density distribution approximately equal to the observed, and 20CR, ERA-20c, and CRUv3.23 also had significant agreements with the local records. ERA-20cm also had a meaningful agreement, but the skill score was the lowest with 0.58. Remembering the high r values for ERA-20c and CRUv3.23 in the annual comparison ($r > 0.87$ in Table 4-10), this result confirms that, despite the high correlation with the observation, ERA-20c and CRUv3.23 are biased, and they, as well as other datasets, need bias correction before hydrological applications.

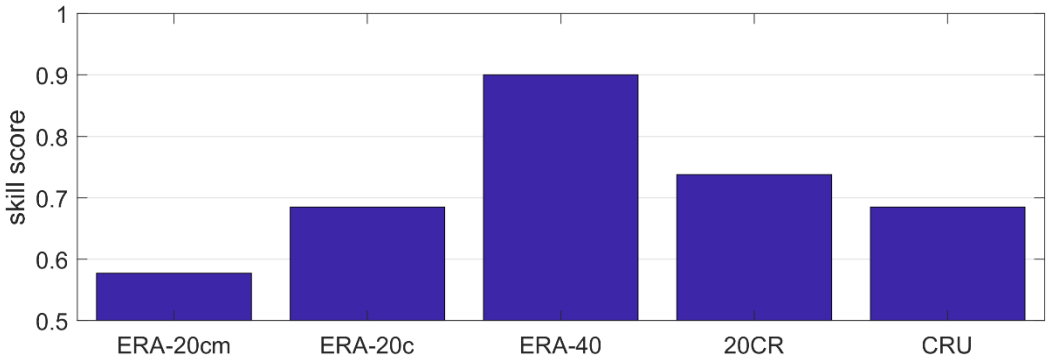

Figure 4-16 PDF-based skill score for monthly mean temperature for ERA-20cm, ERA-20c, ERA-40, 20CR, and CRUv3.23 (CRU) averaged over the whole region from 1961 to 2001.

Figure 4-17 illustrating the PDFs of local gauged values and modelled datasets for temperature supports the skill score analysis. The performance of ERA-40 generally showed high agreement in all comparisons with the observations, but the other datasets had seasonally biased distributions.

The seasonally subdivided PDFs help to understand the difference of each dataset by comparing the peaks of them (Figure 4-17(b)). It should be noted that the three peaks seen in spring and autumn were due to the rapid change in monthly mean temperature. For ERA-20cm and ERA-20c, the distributions were located in the left of the observation in seasonal comparisons except for winter in Figure 4-17(b). Likewise, for CRUv3.23, the PDFs were located in the left side of the observation in every season (Figure 4-17(b)) and caused the generally left-biased distribution in Figure 4-17(a). In the case of 20CR, the PDF in Figure 4-17(a) seemed to perform well, except for the underestimation of the range of below 0 ºC and partial discrepancies, but the seasonal PDFs showed that this result had been refined in the process of combining seasonal discrepancies (Figure 4-17(b)). For instance, the second and third peaks of 20CR in spring represent the lower temperature than the real, but the PDF for winter shows warmer temperature than the observation. This analysis suggests that statistical usage of 20CR without considering this seasonal deviation could distort the simulation.

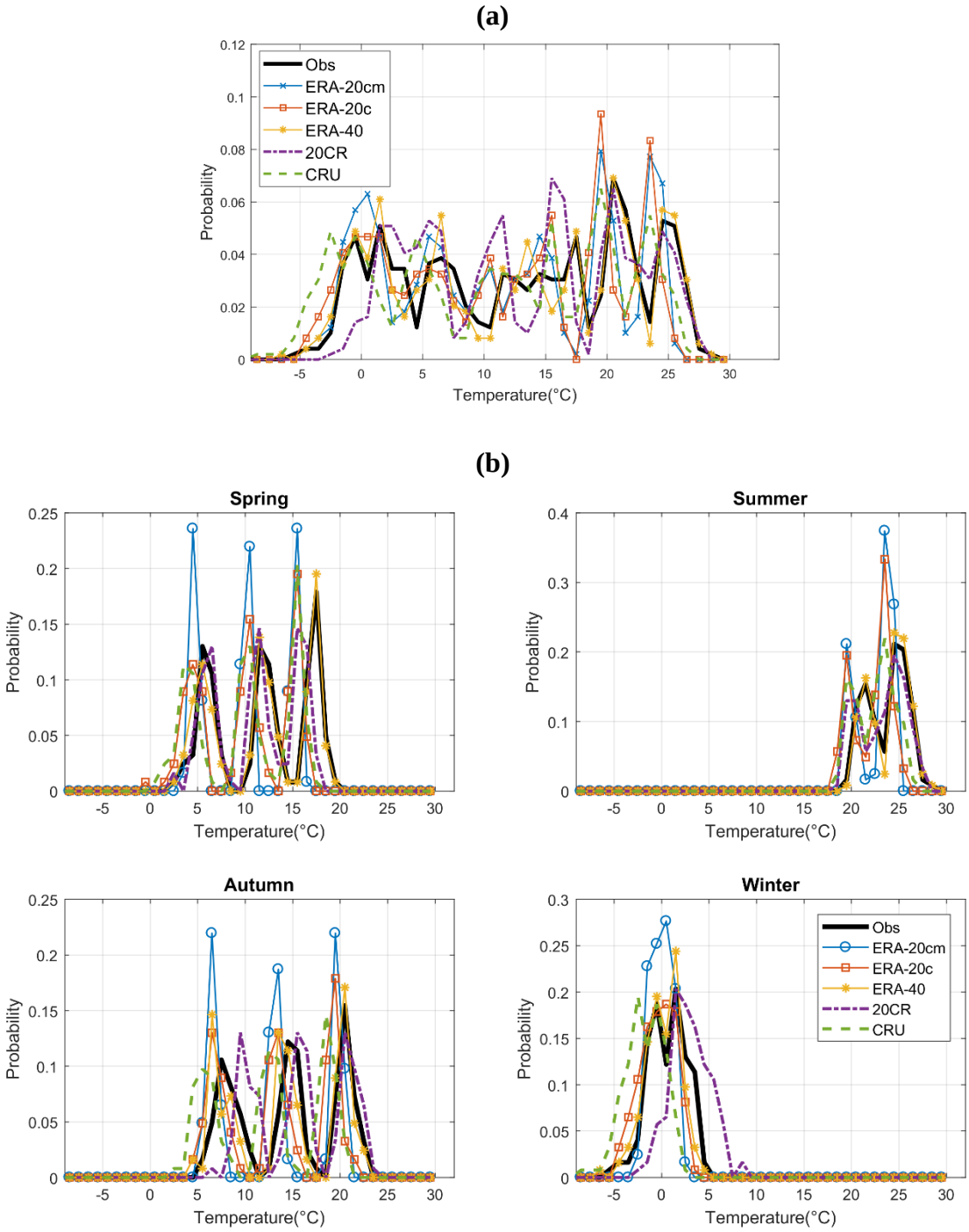

Figure 4-17 PDFs for monthly mean temperature for observation (Obs), ERA-20cm, ERA-20c, ERA-40, 20CR, and CRUv3.23 (CRU) over South Korea. (a) PDFs for monthly mean temperature from 1961 to 2001, and (b) PDFs for seasonally subdivided monthly mean temperature from 1961 to 2001.

The detailed analysis for ERA-20cm ensemble members from 1961 to 2010 is represented in Figure 4-18. The estimates of all ensemble predictions were between 0.69 and 0.75, while Mean represented 0.59 which was the lowest value among the results. This analysis indicates that each ensemble prediction has a meaningful agreement with the observation, but it still needs significant improvement, especially for Mean.

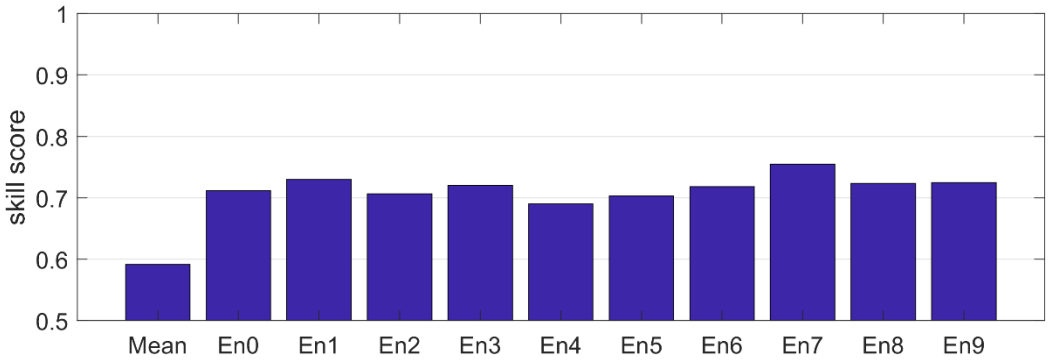

Figure 4-18 PDF-based skill score for monthly temperature for the ERA-20cm mean (Mean) and ensemble members (En0 to En9) averaged over the whole region from 1961 to 2010.

Figure 4-19 which specifies the PDFs of the observed and ERA-20cm ensemble for temperature supports the result shown in Figure 4-18. In Figure 4-19(a), the ensemble members showed high agreements in the range of below -2°C. However, there was a clear discrepancy in the range of about -2°C to 15°C, and over 15°C, the PDFs for the members were left-biased compared with that for the observation. The seasonal comparison showed the points of the discrepancies more clearly. In Figure 4-19(b), compared the peaks of each PDF, the seasonal distributions for all ten members were generally located in the left side of the observations except for winter. This result reconfirms that ERA-20cm ensemble may represent the statistically significant agreement with the observation, but it needs some bias correction before using them in hydrological applications for temperature. Moreover, the magnitude of the peaks for Mean was higher than those of other predictions, especially in spring and autumn, which comes from the temporally averaged values in Figure 4-13. It means that Mean can narrowly interpret the seasonal or annual temperature variability of ERA-20cm data in frequency analysis over South Korea.

(a)

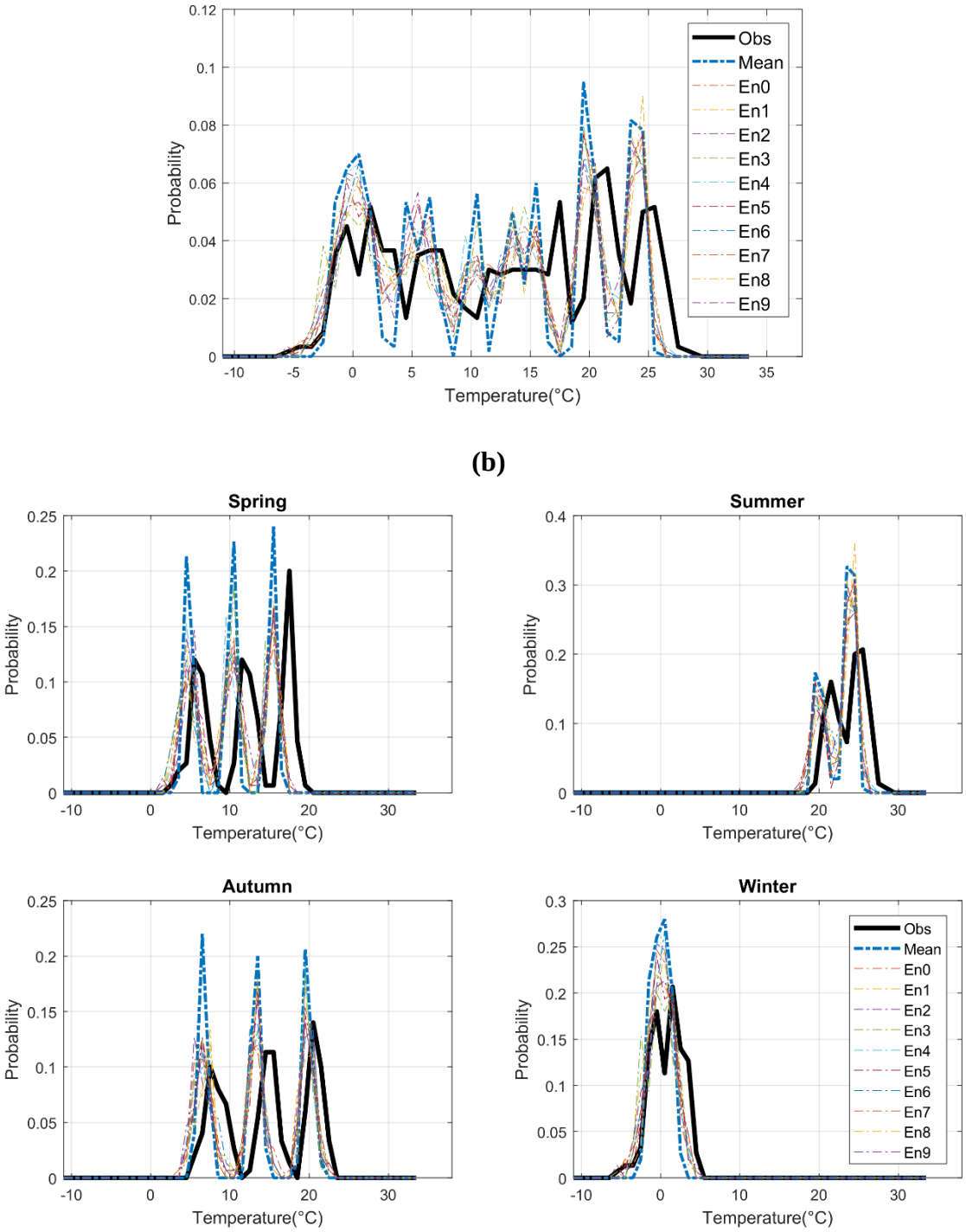

Figure 4-19 PDFs of monthly temperature for observation (Obs) and ERA-20cm ensemble over South Korea. (a) PDFs for monthly total precipitation from 1961 to 2010 and (b) PDFs for seasonally subdivided monthly total precipitation from 1961 to 2010.

4.4.2.4 The goodness of ERA-20cm ensemble

For the evaluation of the suitability of the ERA-20cm ensemble spread for temperature, the percentage of observations bracketed by the ensemble intervals was calculated (Table 4-15). For temporal comparison, the seasonal/annual *P* (%) values represented low performances except for winter. That is, the ERA-20cm ensemble for temperature in South Korea cannot cover the historical climate change well, as shown in Figure 4-13 illustrating the lower temperature of the ensemble than the real. For the statistical test, the value was 37.1%, but it went down to 28.6% when excluding on-boundary values. This result indicates that the spread for the ERA-20cm ensemble is too narrow and biased to represent observation in South Korea, although each ensemble dataset has the good skill score.

Table 4-15 The percentage of the observation for temperature bracketed by the ERA-20cm ensemble intervals.

Type	Interannual					PDF
	Spring	Summer	Autumn	Winter	Annual	
P(%)	4.0	28.0	22.0	42.0	4.0	37.1 (28.6*)

*: The percentage excluding the number of observations on-boundary

4.5 Summary and discussion

This chapter has evaluated multi-decadal reanalysis datasets (ERA-20cm, ERA-20c, ERA-40 and 20CR) and two century-long gridded observations (CRUv3.23 and GPCCv7) for South Korea. More specifically, I have mainly focused on the temporal and statistical applicability of monthly mean values for precipitation and temperature, which are the most commonly used data in climate change studies (Gao et al., 2016). For ERA-20cm ensemble, this thesis additionally explored the goodness of the ensemble spread, and the relationship between the spread and ENSO.

In the temporal variability comparison for precipitation, the *r* values for ERA-20cm mean and ensemble members were close to 0. This result reconfirms a well-known feature of ERA-20cm, in that it cannot reproduce the actual synoptic situation for precipitation (Hersbach et al., 2015). On the other hand, gridded observations (CRUv3.23 and GPCCv7) showed the best performance with

the values over 0.9 in every seasonal/annual comparison. The other reanalyses (ERA-20c, ERA-40, and 20CR) had moderate to high correlations ($0.4 < r < 0.9$). However, ERA-40 and 20CR had seasonal gaps compared with the observations. This analysis suggests that it is of importance to consider the local accuracy in national-scale studies using these datasets.

For the trend test for precipitation, there was no significant trend except ERA-40 in summer and 20CR in the spring and annual simulations for the period of 1961–2001. Apart from En6 and the observation in summer and En2 in autumn from 1961 to 2010, ERA-20cm ensemble members also had no obvious trend. However, the simulation from 1901 to 2010 shows different trends depending on the dataset. CRUv3.23 and GPCCv7 had identically increasing trends in summer and 12-month average simulations. Meanwhile, ERA-20c showed upward tendencies in all tests and 20CR had decreasing trends in summer, autumn, and annual simulations. For ERA-20cm, each ensemble member has its own trend. For instance, Mean had increasing trends in spring, winter, and 12-month average simulations, but En0, En1, and En8 had no trends. It is clear that the results of the trend analysis can vary depending on the study period and regions in South Korea (Bae et al., 2008). Nevertheless, previous long-term trend researches have shown that summer precipitation observed in Korea has generally increased (Chang and Kwon, 2007; Choi et al., 2009; Jung et al., 2011; Wang et al., 2006). Chang and Kwon (2007) and Jung et al. (2011) documented that all stations had increasing summer rainfalls since 1973. Choi et al. (2009) compared the gauged rainfalls of ten Asian countries from 1955 to 2007 and discovered significantly increasing summer rainfall in South Korea at a 95% confidence level. The longest trend analysis on Seoul, the capital of South Korea, also indicated a significant upward trend from 1778 to 2004, although the estimate for the pre-1950 period suggested no significant trend (Wang et al., 2006). Hence, the decreasing tendency of 20CR implies that despite the meaningful correlation with the observation, 20CR can provide distorted information in the long-term trend analysis. In the same vein, the weak trends in summer for ensemble members and Mean of ERA-20cm imply that ERA-20cm may misrepresent the climate change patterns in South Korea. That is, the ERA-20cm ensemble may not be a proper dataset to detect the long-term trend for precipitation, although previous global-scale study showed a fair agreement with long-term temperature trend (Hersbach et al., 2015).

In terms of the intensity of the annual trend from 1901 to 2010, CRUv3.23 and GPCCv7 had significant increasing annual slopes (mm/yr) of 2.13 and 2.14, respectively. These values were

different from Harris et al. (2014), who documented 0.005 for CRU TS3.10 (CRUv3.10) (the earlier version of CRUv3.23) and -0.019 for GPCC version 5 (the earlier version of GPCCv7) in East Asia from 1901 to 2009. However, by evaluating the observations for the 1955–2007 period, Choi et al. (2009) showed that South Korea had a significant increasing trend (2.45). This trend was much higher than those shown in the other East Asian countries, China (0.33) and Japan (-1.75). This literature supports the fact that the slopes of CRUv3.23 and GPCCv7 have reliability.

For statistical evaluation for precipitation, there were significant agreements between the monthly averaged observations derived from 13 gauged stations and each dataset. The skill scores for ERA-20c and gridded observations (CRUv3.23 and GPCCv7) exceeded 0.9, and the other reanalyses were over 0.8 – except for ERA-20cm (0.66) – for the period of 1961–2001. This evaluation indicates that all the reanalyses, including ERA-20cm, can be applied in statistical applications such as rainfall frequency analysis after proper bias corrections. For ERA-20cm ensemble from 1961 to 2010, all ten ensemble members exceed 0.8. This concurs with Gao et al. (2016), who concluded that despite the spatial variability, all ten ensemble members of ERA-20cm for precipitation had high skill scores (> 0.8) in China. The interesting point is that Mean for ERA-20cm had the lowest value (0.67) from 1961 to 2010 because it exaggerated the moderate intensity more than any other members. In other words, the temporally averaged precipitation can show smoothed movement in Figure 4-4, but this results in misrepresenting the statistical weights (Figures 4-9 and 4-10). In some comparative studies, the mean of ERA-20cm represented the ERA-20cm ensemble itself (Donat et al., 2016; Poli et al., 2016). However, the findings in this thesis show that the mean can underestimate the dry and intensive rainfall season in a regional-scale analysis. Hence, it could be concluded that the mean of the ERA-20cm ensemble should be carefully used in the regional study.

For ERA-20cm ensemble for precipitation, there are no temporal correlations between ensemble members. According to Hersbach et al. (2015), the ten members were designed to represent the different realisations and account for uncertainties based on the random plausible SST ensemble. In this vein, the result of the current analysis reconfirms the independence of ensemble members. On the other hand, the *P* values representing the goodness of the spread showed significant goodness for temporal variability, but they statistically had low agreement with the observation. Considering the purpose of the ensemble, which is to account for uncertainties in model data (Poli

et al., 2016), this result shows that the spread has difficulty in representing the real rainfall in South Korea. In other words, it needs to be widened in its coverage. In the comparison between ensemble spread and the ONI, the result showed that the spread for precipitation had no correlation with El Niño or La Niña. Remembering the fact that ERA-20cm was generated by using SST as the boundary condition, it can be hypothesised that the relationship may influence the ERA-20cm spread. However, unlike previous studies – which have verified the significant relationships between the rainfall patterns in Korea and El Niño/La Niña (Jin et al., 2005; Son et al., 2014) – the result shown in this thesis indicated no correlation between the spread and ENSO. Jin et al. (2005) suggested that La Niña phenomena correlate with monthly rainfall with a lag time of 4 or 5 months in Korea. Son et al. (2014) addressed that there was a significant positive correlation between El Niño and winter precipitation, especially strong in early winter.

For temporal temperature comparisons, the interesting point is that the most fitted dataset is ERA-40, not CRUv3.23 which represents the interpolated gridded observation. In CRUv3.23, ERA-20c, and 20CR, there were obvious gaps compared with the observed temperature. The previous comparative study for temperature from 1958 to 2001 described that CRUTEM2v, the earlier version of CRUv3.23, had significantly lower temperature than ERA-40 in the northern hemispheres from 1958 to 1967 because of the limited availability of observations (Simmons et al., 2004). However, the annual discrepancy in the current analysis is shown in South Korea over the whole period 1961–2001, although it has been narrowed over time. In the temperature trend test, ERA-40 showed identical tendencies to the observed, having upward trends in spring, winter, and annual simulations for the 1961–2001 period. Apart from autumn values, ERA-20c, 20CR, and CRUv3.23 also have similarities. In case of ERA-20cm, Mean has moderate correlations with the seasonal/annual observations, while ten members have low to moderate correlations. Compared with the result for precipitation, these values seem to show a significant relationship between the ensemble and the observed. However, the temperature trends from 1961 to 2010 indicate that the ensemble predictions have different trends from the observation. More specifically, excepting a few cases, ERA-20cm ensemble members and Mean showed significant increasing movements in spring and summer. Meanwhile, there were no clear trends in winter, excluding En0 and En4. Previous analyses in South Korea for the late 20th century suggested that the winter and annual mean temperature had significant upward trends, but the summer trend was weak (Choi et al., 2009; Chung and Yoon, 2000; Jung et al., 2002). Comparing these studies with the current

analysis applied in this thesis, it could be deduced that ERA-20cm ensemble (which showed strong summer and weak winter trends) has little reliability in terms of long-term trend.

The interesting point is that the century-long trend assessment of gridded observation (CRUv3.23) and reanalysis datasets from 1901 to 2010 indicated significant warming trends in all the simulations at the 0.95 confidence level, although the intensities of the slopes varied depending on the dataset. Recent studies have also shown the same trend. Donat et al. (2016) suggested warming world trends in their comparative analysis from 1901 to 2010. Likewise, Harris et al. (2014) detected an annual warming trend in East Asia, 0.11 ºC/decade, by using CRUv3.10 from 1901 to 2008. Thus, with ERA-20cm as an exception, the increasing trends of global data sources over 100 years in this analysis have reliability, although the slopes still have some uncertainty. For ERA-20cm ensemble, despite the significant trends, the relatively weak slopes in winter still suggest that it requires a cautious approach.

In the case of PDFs analysis for temperature, ERA-40 performed the best with a skill score of 0.90. 20CR, ERA-20c, and CRUv3.23 had significant agreements to the observation with values between 0.69 and 0.74. For ERA-20cm, all ensemble members had the moderate to high agreements to the observation with values between 0.69 and 0.75. Meanwhile, Mean showed the lowest value of 0.59 due to the averaging effects. This result indicates that global retrospective datasets have significant reliability for monthly frequency for temperature in South Korea. Nonetheless, it is challenging to directly apply them – especially ERA-20cm mean – in hydrological applications. In terms of regional applicability, in an evaluation on ERA-20cm over China, Gao et al. (2016) showed that the skill scores of all ten ensemble members exceeded 0.9 for temperature averaged over all regions. However, the scores in the current analysis were lower than these. This result suggests that the quality of reanalysis data, especially for ERA-20cm ensemble, may vary by region.

For the ERA-20cm ensemble in temperature, the *r* values between ensemble members showed moderate correlations with the values between 0.268 and 0.682, although they were generated from the random SST ensemble (Hersbach et al., 2015). On the other hand, the goodness test for the spread showed low agreement in both temporal and statistical comparisons. This result implies that the spread for temperature is too narrow to cover the actual data. In terms of the relationship between the spread and ENSO, this thesis suggests no correlation between them, although a recent

research by Lee and Julien (2016) suggested that a teleconnection between ENSO and the temperature was clearly identified over South Korea. This finding implies that El Niño and La Niña did not affect the ensemble spread of ERA-20cm for temperature and precipitation.

Due to the improved assimilation and ensemble technique, it is easy to hypothesise that the latest reanalysis datasets would be sufficiently accurate in terms of temporal and statistical variability. However, the results in this thesis indicate that each dataset has its own biases, and the degree of the agreement of each data can vary in space and time – as shown in previous studies (Bao and Zhang, 2013; Bosilovich et al., 2008; Ma et al., 2009; Simmons et al., 2004). Various reasons may exist for this data uncertainty. First, the inhomogeneity of input data for the simulated datasets may be one of the causes (Donat et al., 2016; Thorne and Vose, 2010). In other words, the farther a representation is from the present, the fewer number of stations are available. This could logically explain the reason for the increase of uncertainty in the reanalyses and gridded observations (Becker et al., 2013; Ferguson and Villarini, 2012; Harris et al., 2014; Zhang et al., 2013). Second, significant inconsistencies in extreme climate events could be one of the causes (Befort et al., 2016; Donat et al., 2016; Krueger et al., 2013). Befort et al. (2016) indicated that century-long reanalysis such as ERA-20c had difficulty in representing low-frequent extra-tropical cyclones and windstorms. Donat et al. (2016) documented that for heavy precipitation, the local agreement of century-long reanalyses was spatially variable, while the global time series performed well. Third, regional climate regime could also be one of the causes. Shah and Mishra (2014) documented that reanalysis like ERA-20cm displayed errors for precipitation and temperature in monsoon season for India. Fourth, the elevation difference between the model and actual terrain could affect the result in mountainous regions such as South Korea (Gao et al., 2014a, 2014b, 2012; Zhao and Fu, 2006). Finally, the scale difference between weather stations (point scale) and grid points (area average) may influence the biases, especially for the extreme (Maraun, 2013). As the gridded data can be smoothed, the comparison with the weather station could be biased.

There are numerous reasons for the uncertainty of the datasets, and it is challenging to reliably assess the climate change impact in a region by directly using single modelled data. Thus, to prevent misinterpretation, researchers should carefully apply this product in regional-scale climate change studies, and it is crucial to evaluate the quality of various data sources in sites lacking such regional studies.

4.6 Conclusion

This chapter evaluated key century-long climate datasets and ERA-20cm ensemble for precipitation and temperature in South Korea. The major results obtained in the analyses are summarised as follows:

1. For gridded observations, GPCCv7 and CRUv3.23 for precipitation showed the best performance in all comparisons, while CRUv3.23 for temperature showed a clear gap compared with the observations in South Korea. This result implies that not only reanalyses but also gridded observations (which are generally accepted as the true values in global climate change studies) can be substantially biased.

2. Reanalysis datasets excepting ERA-20cm (i.e. ERA-40, ERA-20c, and 20CR) have significant agreements with the observation in terms of temporal and statistical comparisons. ERA-20c for precipitation showed better results than the others, and ERA-40 for temperature also performed the best. However, they still include a certain degree of errors, so substantial improvement of the quality should be conducted before hydrological applications are carried out. This analysis also suggests that the accuracy of reanalysis data, especially for ERA-20cm, may vary depending on the region.

3. ERA-20cm has difficulty in providing useful information on the long-term trend and the temporal variability for temperature and precipitation in South Korea, although the temperature ensemble has a moderate correlation with the observation. Statistically, all ensemble predictions showed significant agreements to the observed, but they still need a certain degree of improvement for application in South Korea.

4. It is found that the ERA-20cm mean may misrepresent ten individual members, even in the statistical estimate. The ensemble does not spread well enough to cover all observations, especially for temperature, and there is no relationship between the spread and ENSO. This result implies that researchers who want to apply the ERA-20cm mean (which has been often adopted in global-scale climate change analyses) to a regional-scale study should treat this dataset with caution.

The analysis in this chapter has mainly explored the monthly/seasonal/annual mean change based on the averaged dataset over the whole of South Korea. The results shown here provide beneficial information for understanding the general pattern of each dataset in South Korea. However, these findings cannot fully represent the feature of extremes for sub-scale data, such as daily precipitation, which is one of the vital parameters in climate impact assessment. Compared with gridded observations, an advantage of reanalysis data such as ERA-20c is that they can provide daily climate records at a 0.125º×0.125º grid without downscaling. In this context, from Chapter 5, this thesis focuses more on reanalysis products at a 0.125°×0.125° grid, especially for precipitation.

CHAPTER 5 [1,2]Bias correction of ERA-20c daily precipitation with a limited observation network

5.1 Motivation

As stated in Chapter 1, this thesis adopts century-long reanalysis data for climate change analysis of South Korea, where observation records are limited. Reanalysis data typically include biases as shown in Chapter 4. Thus, bias correction should be considered before hydrological modelling. Among various climate variables of reanalysis, this chapter mainly deals with bias correction of precipitation, which is one of the most commonly adopted variables in hydrological applications. More specifically, this chapter aims to reduce biases of ERA-20c daily precipitation in terms of the mean and extreme in South Korea. ERA-20c has shown significant agreement with the observed for the monthly precipitation in Chapter 4, and it can provide daily data with the finest resolution of 0.125°×0.125°. However, as Chapter 4 mainly dealt with the monthly mean, the feature of daily data, especially for the heavy daily rainfalls (hereafter referred to as 'extreme rainfalls'), was not sufficiently explored in South Korea. For this reason, this chapter begins with evaluating ERA-20c daily precipitation in terms of both the mean and the extreme. It then focuses on its bias correction.

[1]Kim, D.-I., Kwon, H.-H., and Han, D., 2018. Exploring the Long-Term Reanalysis of Precipitation and the Contribution of Bias Correction to the Reduction of Uncertainty over South Korea: A Composite Gamma-Pareto Distribution Approach to the Bias Correction. Hydrol. Earth Syst. Sci. Discuss., https://doi.org/10.5194/hess-2018-36

[2]Kim, D.-I., Kwon, H.-H., and Han, D., Exploring the long-term reanalysis of precipitation and its bias correction using a composite gamma-Pareto distribution approach over South Korea. Hydrol. Res. (accepted with minor revision)

As stated in Section 2.3, there are various bias correction concepts – from simple mean-based methods to more complex procedures – but QM method has been widely applied for the bias correction of precipitation. (Fang et al., 2015; Maraun and Widmann, 2018; Teutschbein and Seibert, 2012; Themeßl et al., 2012).

QM method commonly uses a gamma distribution as a transfer function for daily precipitation. However, this gamma-based QM approach (gQM) often fails to reproduce extreme rainfalls, which are mainly described by the upper tail of the distribution (Hundecha et al., 2009; Volosciuk et al., 2017; Vrac and Naveau, 2007; Wilks, 1999). One may intuitively consider heavy-tailed distributions such as extreme value distribution (e.g. GEV, Gumbel, and Weibull). Nonetheless, bias correction through heavy-tailed distribution can result in overestimation of daily rainfall in the lower part of the distribution. In these contexts, several recent studies have applied a composite distribution based on two different distributions to the QM approach, especially for the correction of climate change scenarios (Gutjahr and Heinemann, 2013; Nyunt et al., 2016; Smith et al., 2014; Volosciuk et al., 2017). However, comparatively little attention has been given to the bias correction of century-long reanalysis such as ERA-20c. Thus, this chapter aims to introduce a quantile mapping approach based on a composite distribution to bias correction of reanalysis data.

The conventional QM method is also limited in that it cannot be applied directly to the ungauged basin, where a one-to-one mapping between the observed and modelled data does not exist. That is, modellers can only obtain a transfer function of a set of grid points for the paired precipitation data. Thus, an alternative method needs to be established for the synthesis of unpaired data. A common approach to deal with this problem would be the interpolation of *in situ* data by the IDW or the kriging method. The interpolated values can be used to obtain the transfer function for ungauged areas. For example, Gutjahr and Heinemann (2013) applied the IDW method to reproduce spatially continuous estimates of the daily precipitation for the spatial bias correction. However, the systematic error in the process of the spatial interpolation of daily rainfall can be propagated through to the parameter estimation in the QM approach. Thus, one of the primary topics in the current bias correction analysis is whether the QM method can reliably improve ERA-20c daily precipitation, especially for extreme value, over 100 years when including the ungauged areas. To deal with this issue, this chapter proposes a new spatial interpolation method based on the parameter contour maps (IM-PCM) and evaluates the performances.

In brief, this chapter consists of three main parts. First, I examine the statistical behaviours of the ERA-20c data and analyse the biases (i.e. errors) in the mean and extreme precipitation. Second, the QM approach is explored using a combined gamma-Pareto distribution in 48 stations. Then, the corrected data are evaluated compared with the observation. Finally, I explore bias correction of ERA-20c data in the ungauged catchment by adopting the IM-PCM approach newly proposed in this thesis.

5.2 Data

5.2.1 Local gauged data

To correct reanalysis data in all grid points over South Korea, this chapter uses a larger number of weather stations (48 stations) than 13 stations in Chapter 4. However, due to data availability, the data period is limited to 1973–2010. That is, daily precipitation sequences for the period of 1973–2010 were obtained and compiled from the KMA. The local gauging stations used in this chapter are illustrated in Figure 5-1, and the detailed for the stations is summarised in Table 5-1.

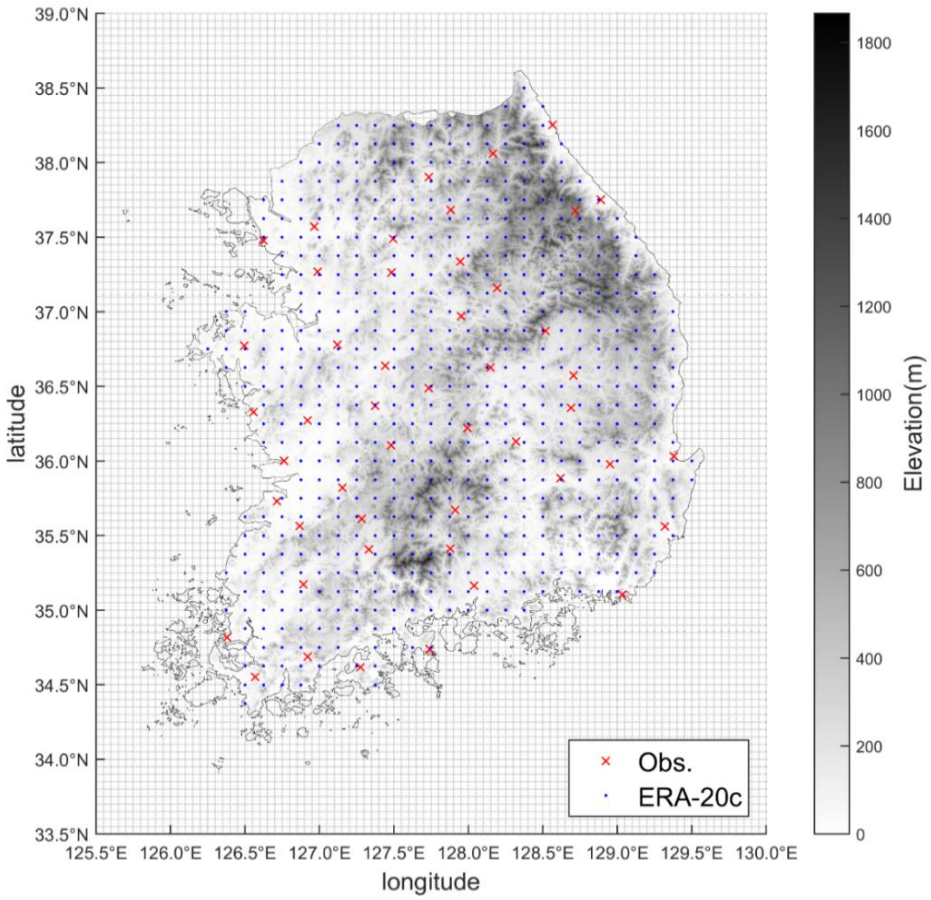

Figure 5-1 A map showing the study area, local gauging stations, and grid points of ERA-20c in Chapter 5. The grey shading on the map indicates elevations.

Table 5-1 The local rainfall stations used in Chapter 5.

No.	Name	Latitude (°N)	Longitude (°E)	Elevation (m. asl)	Annual rainfall(mm)*
St. 1	Sokcho	38.2508	128.5644	19.5	1,374.6
St. 2	Daegwallyeong	37.6769	128.7181	774.0	1,736.4
St. 3	Chuncheon	37.9025	127.7356	79.1	1,304.9
St. 4	Gangneung	37.7514	128.8908	27.4	1,436.6
St. 5	Seoul	37.5714	126.9656	11.1	1,386.8
St. 6	Incheon	37.4775	126.6247	69.6	1,183.0
St. 7	Wonju	37.3375	127.9464	150.0	1,318.6
St. 8	Suwon	37.2700	126.9875	38.3	1,274.9
St. 9	Chungju	36.9700	127.9525	116.5	1,202.0
St. 10	Seosan	36.7736	126.4958	30.3	1,254.9
St. 11	Cheongju	36.6361	127.4428	58.6	1,229.7
St. 12	Daejeon	36.3689	127.3742	70.3	1,353.0
St. 13	Chupungyeong	36.2197	127.9944	246.1	1,171.5
St. 14	Andong	36.5728	128.7072	141.5	1,017.3
St. 15	Pohang	36.0325	129.3794	3.7	1,145.4
St. 16	Gunsan	36.0019	126.7631	24.6	1,210.8
St. 17	Daegu	35.8850	128.6189	65.5	1,047.0
St. 18	Jeonju	35.8214	127.1547	54.8	1,291.6
St. 19	Ulsan	35.5600	129.3200	36.0	1,265.5
St. 20	Gwangju	35.1728	126.8914	73.8	1,387.9
St. 21	Busan	35.1044	129.0319	71.0	1,500.2
St. 22	Mokpo	34.8167	126.3811	39.4	1,139.4
St. 23	Yeosu	34.7392	127.7406	66.0	1,420.1
St. 24	Jinju	35.1636	128.0400	31.6	1,504.8
St. 25	Yangpyeong	37.4886	127.4944	49.4	1,359.6
St. 26	Icheon	37.2639	127.4842	79.4	1,330.9
St. 27	Inje	38.0600	128.1669	201.6	1,167.8
St. 28	Hongcheon	37.6833	127.8803	142.3	1,353.2
St. 29	Jecheon	37.1592	128.1942	265.0	1,345.8
St. 30	Boeun	36.4875	127.7339	176.4	1,275.0
St. 31	Cheonan	36.7794	127.1211	24.0	1,229.4
St. 32	Boryeong	36.3269	126.5572	16.9	1,219.6
St. 33	Buyeo	36.2722	126.9206	12.7	1,323.3
St. 34	Geumsan	36.1056	127.4817	171.7	1,277.1
St. 35	Buan	35.7294	126.7164	13.4	1,249.8
St. 36	Imsil	35.6122	127.2853	249.3	1,340.2
St. 37	Jeongeup	35.5631	126.8658	46.0	1,317.1
St. 38	Namwon	35.4053	127.3328	91.7	1,351.0
St. 39	Jangheung	34.6886	126.9194	46.4	1,493.7
St. 40	Haenam	34.5533	126.5689	14.4	1,322.4
St. 41	Goheung	34.6181	127.2756	54.5	1,459.2
St. 42	Yeongju	36.8717	128.5167	212.2	1,268.1
St. 43	Mungyeong	36.6272	128.1486	172.0	1,241.5
St. 44	Uiseong	36.3558	128.6883	83.2	1,016.5
St. 45	Gumi	36.1306	128.3206	50.3	1,051.1
St. 46	Yeongcheon	35.9772	128.9514	95.0	1,039.3
St. 47	Geochang	35.6711	127.9108	222.4	1,298.9
St. 48	Sancheong	35.4128	127.8789	0.8	1,512.7

** Annual mean precipitation estimated from 1973 to 2010*

5.2.2 ERA-20c daily precipitation

As stated in Section 2.2.2, ERA-20c daily precipitation is one of the longest reanalysis data covering the entire 20th century (Donat et al., 2016; Poli et al., 2016). The ERA reanalysis system is based on a set of data assimilation schemes, and the system provides relatively high-resolution gridded datasets, including daily total precipitation from 1900 to 2010 via the ECMWF web server. In this analysis, I focused on the data on the mainland of South Korea from January 1973 to December 2010 with its highest resolution, 0.125°×0.125° (approximately 13.8 km×11.2 km), which consists of 603 grid points in South Korea. The specific gridded points for ERA-20c are illustrated in Figure 5-1.

It is necessary to understand the features of the model biases to improve the modelled reanalysis data. Thus, this chapter first examines some of the general features of ERA-20c daily precipitation over South Korea in terms of the mean and the extreme values. For the mean precipitation, this analysis compared the intra-seasonal variability within the annual cycle by exploring the monthly means and the 10-day running means between the observed and ERA-20c precipitation (as shown in Figure 5-2) averaged over all 48 stations during the baseline period (1973–2010). The model performance was evaluated by both the Nash-Sutcliffe efficiency (NSE) and root-mean-square error (RMSE), which are well known goodness-of-fit measures for model evaluation in the field of hydrology (Legates and McCabe Jr., 1999; Ritter and Muñoz-carpena, 2013). Since this thesis pays more attention to the suitability of probability distribution of the modelled data, the following evaluations for the modelled values are also performed by both NSE and RMSE. These are provided in Eq. 5-1 and 5-2:

$$RMSE = \sqrt{\frac{\sum_{i=1}^{n}\left(Y_i^{obs} - Y_i^{sim}\right)^2}{n}} \tag{5-1}$$

$$NSE = 1 - \left[\frac{\sum_{i=1}^{n}\left(Y_i^{obs} - Y_i^{sim}\right)^2}{\sum_{i=1}^{n}\left(Y_i^{obs} - Y_i^{mean}\right)^2}\right] \tag{5-2}$$

Here, Y_i^{obs} is the i-th observation, Y_i^{mean} is the mean of the observation, while Y_i^{sim} is the modelled data, and n is the number of observations. For the NSE, the dataset accuracy improves as the efficiency approaches 1.

The results confirmed that ERA-20c could reproduce the mean values quite well, while there was a significant difference between modelled and observed precipitation during the summer season (i.e. July to September), which may lead to an underestimation of extreme rainfall.

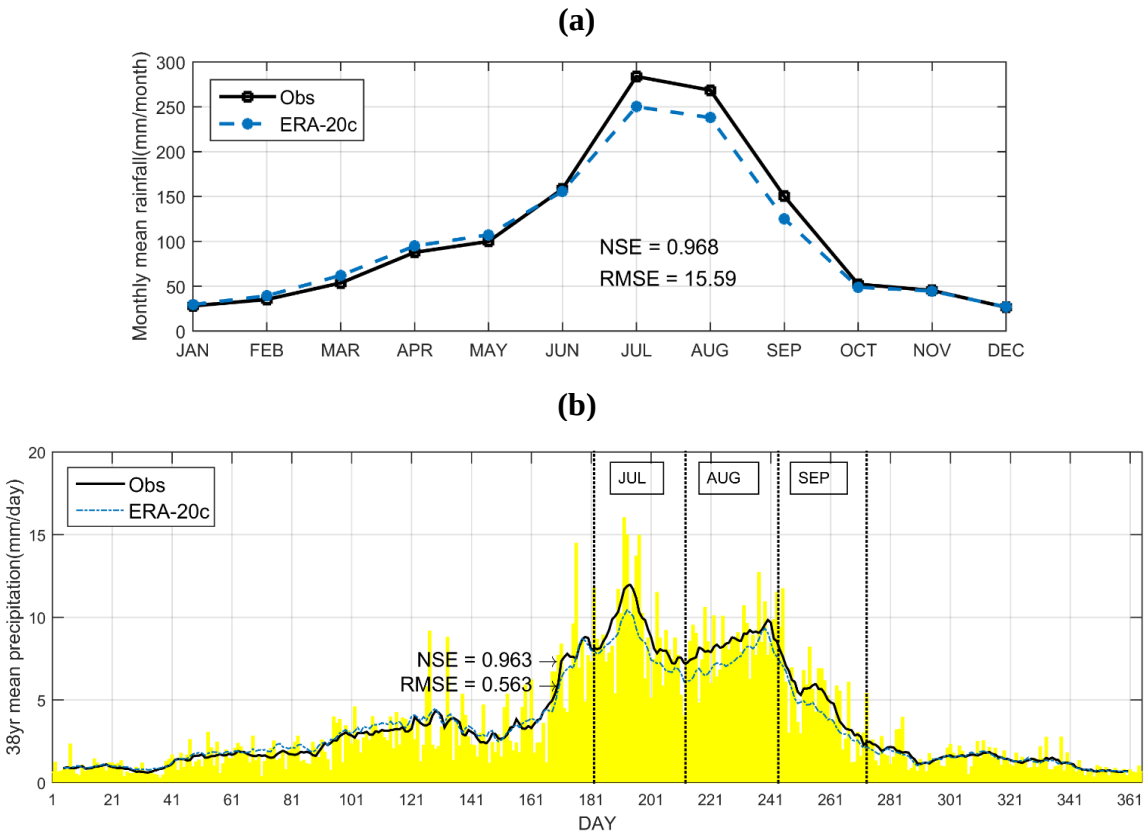

Figure 5-2 A comparison of the mean values of ERA-20c daily precipitation on an annual basis. (a) Monthly mean comparison between the observed (Obs) and ERA-20c, and (b) observed 38-year (1973-2010) mean of daily precipitation (yellow bar) and its 10-day running mean (black solid line) along with 10-day running mean estimated from ERA-20c (blue dotted line) for all 48 stations

In terms of the extreme rainfall episodes, the 50 top events in each station were extracted for the baseline period, and an underestimation of extremes in the ERA-20c was clearly identified, as illustrated in Figure 5-3. The deviations are generally significant, even for relatively larger upper tail parts of the distribution with -1.088 for NSE and 76.69 mm for RMSE (Figure 5-3(a)). On the one hand, the deviations are quite systematic in the sense of the bias correction. The relationships between the 50 top extreme rainfalls showed that the discrepancies were primarily attributed to

differences in summer rainfall, as seen in Figure 5-2. The overall relationships are similar for 48 stations, so the comparisons in St.4, St.16, St.28, and St.40 are representatively illustrated in Figure 5-3(b). The biases in extreme values are generally proportional to the amount of rainfall, and the biases are likely to be higher in the upper tails of the distribution than that of the middle layer.

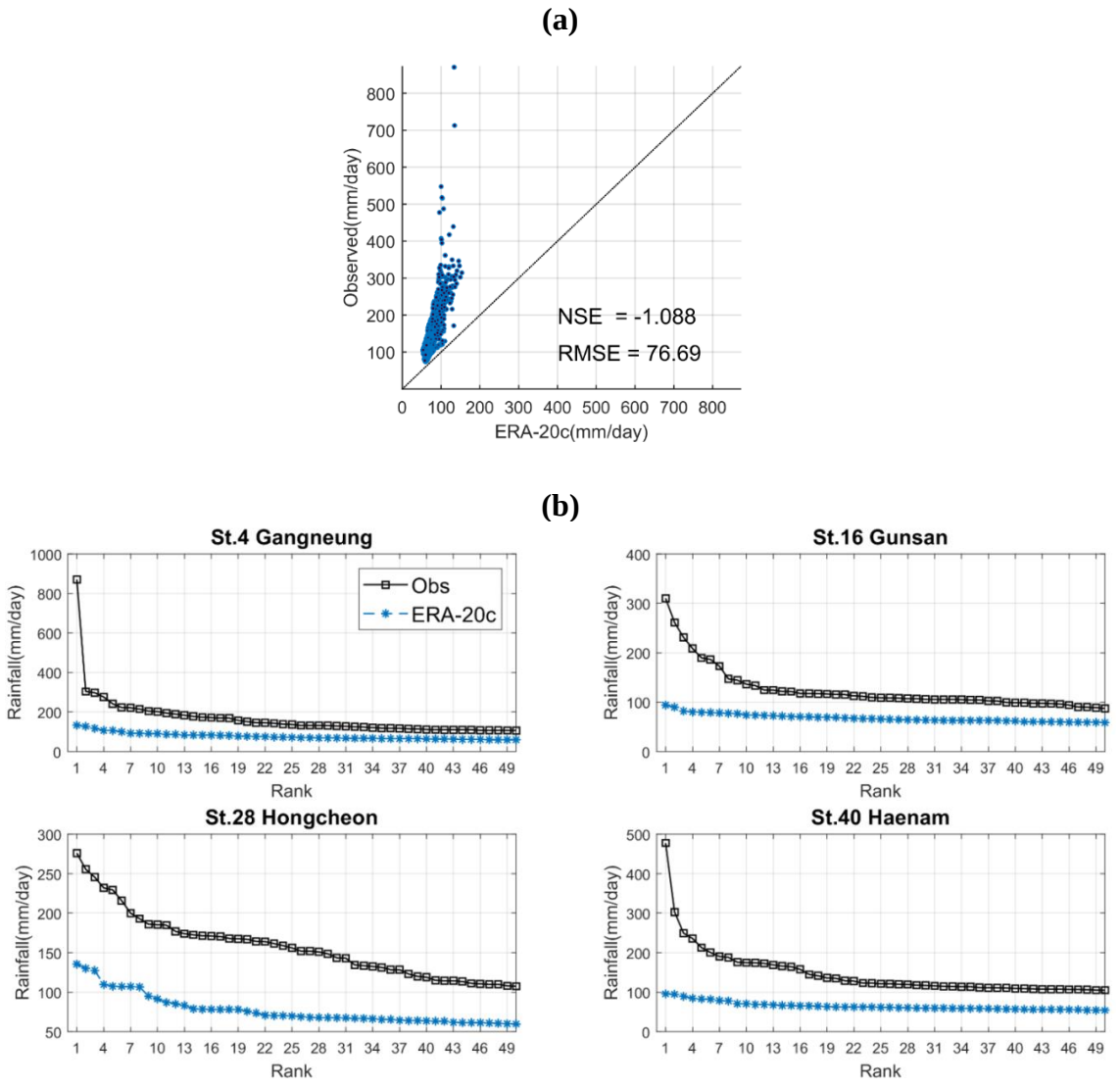

Figure 5-3 Evaluation of bias associated with 50 top extreme rainfall events. (a) Scatter plot of the extremes between the observed and ERA-20c over South Korea and (b) comparison of the deviation corresponding to the rank for St.4, St.16, St.28, and St.40 for the baseline period 1973-2010.

In summary, the ERA-20c precipitation data can reliably reproduce the monthly mean values with 0.968 for NSE and 15.59mm for RMSE (Figure 5-2(a)), while the extreme values in the 50 top events are consistently underestimated with -1.088 for NSE and 76.69mm for RMSE (Figure 5-3(a)). The results obtained in this analysis could indicate that although the ERA-20c modelling process adequately represents the mean climate of the historical period, heavy rainfalls in the summer season can be significantly underestimated due to the fact that intensive rainfall events driven by convective storms may not be effectively resolved by the current climate modelling approach and spatial resolution (Son et al., 2017). On the other hand, as shown in Figure 5-4, ERA-20c exhibits a much higher monthly frequency of wet-days (>0mm/day), varying from 11.75 to 26.64 days per month, than that of observation (6.07 to 14.5 days) for all months in South Korea. The overestimated frequency of light precipitation in climate models is a well-known problem, and it may partially cause the underestimation of the extremes. In these contexts, a two-stage bias correction approach to daily precipitation is typically applied to first adjust the overestimated wet-day frequency and then rectify the biases associated with both the mean and extreme values.

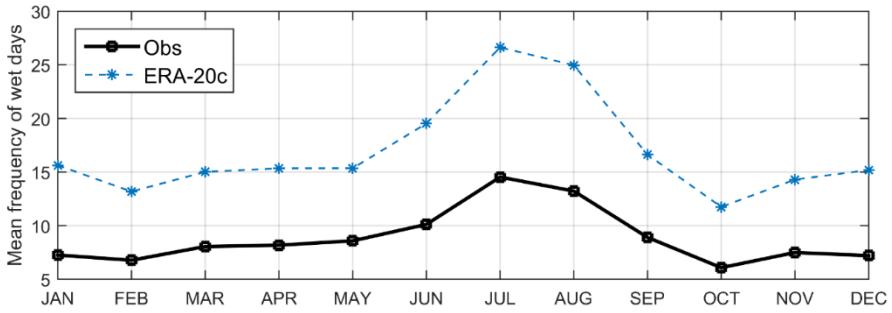

Figure 5-4 Monthly wet-day frequency for the observed (black solid line) and ERA-20c (blue dotted line) for all 48 stations for the baseline period (1973-2010).

5.3 Methodology

As illustrated in the previous section, two deficiencies in the ERA-20c became evident: the overestimation of the wet-day frequency and underestimation of the extreme values. To correct the biases, I adopted a two-stage bias correction scheme that consists of the wet-day frequency

correction scheme and the composite distribution-based QM approach. The proposed methods and their assumptions used in this approach are provided in this section.

5.3.1 Wet-day frequency correction scheme

It is well known that the wet-day frequencies of the simulated precipitation data from climate models are typically exaggerated due to the generation of small precipitation amounts near 0.1 mm/day (Kim et al., 2015b; Nyunt et al., 2016; Piani et al., 2010). For this reason, a cut-off threshold (TH) approach has been commonly applied to adjust the overestimated wet-day frequency in the bias correction for daily precipitation using various criteria (Kim et al., 2015a, 2015b; Nyunt et al., 2016; Piani et al., 2010; Rabiei and Haberlandt, 2015; Schmidli et al., 2006b; Themeßl et al., 2012; Volosciuk et al., 2017). For example, Piani et al.(2010) and Volosciuk et al. (2017) adopted 0.1 mm/day as the threshold, whereas in some studies the wet-day frequency of simulated precipitation was set equal to that of the observed (Kim et al., 2015a, 2015b; Nyunt et al., 2016). Rabiei and Haberlandt (2015) compared five different thresholds (0 mm/hr, 0.02 mm/hr, 0.05 mm/hr, 0.07 mm/hr, and 0.1 mm/hr) for spatial bias correction of hourly radar data and concluded that the threshold of 0.05 mm/hr performed the best among the five in terms of the reduction of biases.

In this chapter, a set of predetermined thresholds were used to adjust the wet-day frequency of the modelled daily precipitation from ERA-20c. I considered four different thresholds to identify an optimal threshold for the ERA-20c: (TH1) 0 mm/day, (TH2) 0.1 mm/day, (TH3) 1 mm/day, and (TH4) the thresholds with the assumption that the frequency of wet days of ERA-20c is equal to that of the observed value on a monthly basis, which varied from 0 to 4.66mm/day. The specific process for TH4 is shown in Figure 5-5. On the other hand, changes in the wet-day frequency can affect the overall performance in the bias correction process through the QM approach, because a transfer function between the simulated and observed precipitation is established based on non-zero precipitation. In this context, the optimum threshold was evaluated through the experiment with gQM for a pair of daily rainfall series for each station. Note that daily rainfalls below the thresholds were set to zero for ERA-20c. Among four different thresholds, the determined threshold was then adopted in the next steps.

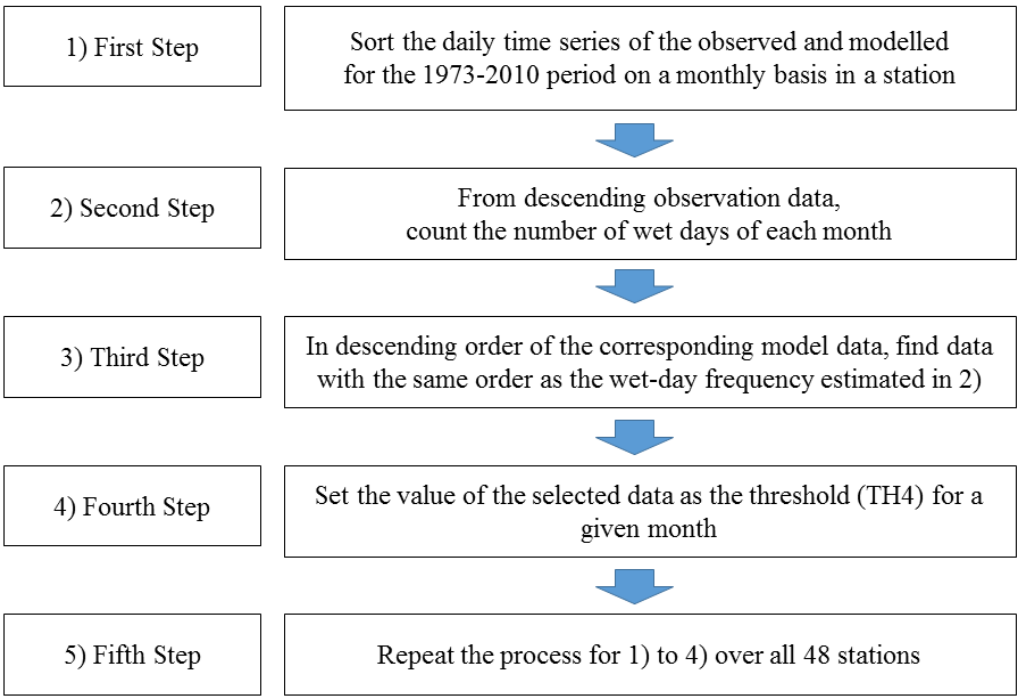

Figure 5-5 A flowchart of wet-day frequency correction scheme for TH4.

5.3.2 Statistical bias correction model: QM with a composite distribution

A main concept of QM is to map the modelled data to the observed data in the probability space. More generally, cumulative distribution functions (CDFs) of the modelled data are mapped to that of the observed, which is considered 'true' (Rabiei and Haberlandt, 2015; Teutschbein and Seibert, 2012). In other words, the distribution of simulated values is fitted to the true distribution, the relationship of which is established in the advanced stages of bias correction. As stated in Section 2.3.4, previous studies have commonly adopted a gamma distribution with two parameters. However, the gQM approach often fails to represent the extreme values.

To effectively improve the bias in the extreme rainfall for ERA-20c, this chapter proposes the QM approach based on two different distributions. More specifically, the extreme value distribution can be adopted for the upper tail of the distribution, while a gamma distribution is applied for the interior part of the distribution. For extremes, the 95^{th} or 99^{th} percentiles have been applied as an upper threshold in numerous studies because the distribution of excesses over the high thresholds

is asymptotically approximated by a generalised Pareto distribution (GPD) (Acero et al., 2011; Chan et al., 2015; Gutjahr and Heinemann, 2013; Manton et al., 2001; Nyunt et al., 2016; Wilson and Toumi, 2005). In this analysis, I apply both the 95th and 99th percentiles as the upper thresholds.

The GPD has been widely applied to the peak-over-threshold (POT) series for the selection of the best-fit distribution for the extreme rainfalls (Gutjahr and Heinemann, 2013; Hundecha et al., 2009; Nyunt et al., 2016; Volosciuk et al., 2017; Vrac and Naveau, 2007), although there have been a considerable number of studies using other extreme value distributions including GEV, Weibull (WEI), Gumbel (GUM), and Log-normal (LOGN). To ensure the suitability of the GPD, this chapter evaluated six different distributions, GPD, GEV, GUM, WEI, LOGN, and gamma, for the extremes in both the observed and ERA-20c over the 95th and 99th percentiles using the Akaike Information Criterion (AIC) and Bayesian Information Criterion (BIC). The distribution with the lowest AIC and BIC is preferred, as the best-fit distribution. The values of AIC and BIC was shown in Appendix A. For a given threshold, the GPD was selected as the best-fit distribution for the extremes as shown in Table 5-2. The values in Table 5-2 indicate the number of stations which belong to a certain distribution.

Table 5-2 The selected distributions among six distributions based on AIC and BIC values for the extremes from observed and ERA-20c daily precipitation over the 95th and 99th percentiles for all 48 stations.

Percentile	Data	GPD	GEV	LOGN	WBL	GUM	GAM
95th	Observation	47	1	0	0	0	0
	ERA-20c	48	0	0	0	0	0
99th	Observation	47	1	0	0	0	0
	ERA-20c	47	1	0	0	0	0

As previously mentioned, the GPD is separately adopted to the extreme values defined by the 95th and 99th thresholds at each station as a transfer function, whereas the gamma distribution is mainly applied to the interior part of the distribution, as illustrated in Eq. 5-3 (Gutjahr and Heinemann, 2013).

$$x_{cor} = \begin{cases} F_{o,gam}^{-1}\left(F_{m,gam}\right), & \text{if } x \leq 95 \text{ th or } 99 \text{ th percentile} \\ F_{o,GPD}^{-1}\left(F_{m,GPD}\right), & \text{if } x > 95 \text{ th or } 99 \text{ th percentile} \end{cases} \quad (5\text{-}3)$$

Here, $F_{m,gam}$ and $F_{m,GPD}$ are the CDFs of the ERA-20c model for gamma and GPD. Similarly, $F_{o,gam}^{-1}$ and $F_{o,GPD}^{-1}$ are the inverse (or quantile) function of CDFs of observations for gamma and GPD, respectively. The heavy-tailed distribution for POTs is defined as follows for a GPD with a high upper threshold (u) (Coles, 2001; Gutjahr and Heinemann, 2013):

$$F(x) = P_r(X - u \leq x \,|X > u) = \begin{cases} 1 - \left(1 + \frac{\xi x}{\theta}\right)^{-\frac{1}{\xi}} & for\ \xi \neq 0 \\ 1 - \exp\left(-\frac{x}{\theta}\right) & for\ \xi = 0 \end{cases} \quad (5\text{-}4)$$

Here, $\theta = \sigma + \xi(u - \mu)$ is the reparametrised scale parameter, and ξ is the shape parameter. In this analysis, the upper thresholds u (the 95th or 99th percentile) for observed and modelled precipitation were derived at each station.

In this approach, the four parameters to be estimated are the shape (α) and scale (β) parameters for the gamma distribution, and the shape (ξ) and scale (θ) parameter for GPD, while the upper thresholds are assumed to be known for the given 95th or 99th percentile. The parameters for gamma distribution are estimated on a monthly basis, whereas the parameters of GPD are estimated using entire POTs for all months in each station. Here, the maximum likelihood method is used to estimate all the parameters. Hereafter, the proposed method with a composite distribution of gamma and GPD is referred to as gpQM. Moreover, the gpQM with the 95th and 99th upper thresholds were abbreviated as gpQM95 and gpQM99, respectively. For comparison, the conventional bias correction using a gamma distribution (i.e. gQM) was also applied and compared in terms of the accuracy of both the extreme and the mean value.

5.3.3 Spatial Interpolation by parameter contour maps

In the gpQM approach, a pair of observed and modelled data are required to estimate the six parameters (TH, α, β, θ, ξ and u). However, because there is a limited number of available weather stations, the transfer function for the QM could not be established for all grid points. For this reason, this thesis introduces an interpolation method based on parameter contour maps (IM-PCM) which consist of three steps as summarised in Figure 5-6. For gpQM95 and gpQM99, the

six parameters (TH, α, β, θ, ξ and u) were first estimated for each station as already noted in the Sections 5.3.1 and 5.3.2. Secondly, a contour map for each parameter was then constructed using a scattered data interpolation method in Matlab (Amidror, 2002) as shown in Figure 5-7. Finally, a set of parameters for the gpQM were taken from the maps to construct the transfer function for all grid points. Note that the TH in Figure 5-7(c) represents the whole number of wet days for the reference period (1973-2010) and u in Figure 5-7(d) means daily rainfalls (mm/day) corresponding to the 99th percentiles. The TH is the first interpolated variable, and the maps of shape (α) and scale (β) parameters for the gamma distribution were then generated on a monthly basis, while the shape (θ), scale (ξ) and upper threshold (u) parameter maps of the GPD were created by using the entire POTs on an annual basis. For the gQM, a similar process to the one described above was used to produce three parameter (TH, α, and β) maps for the transfer function.

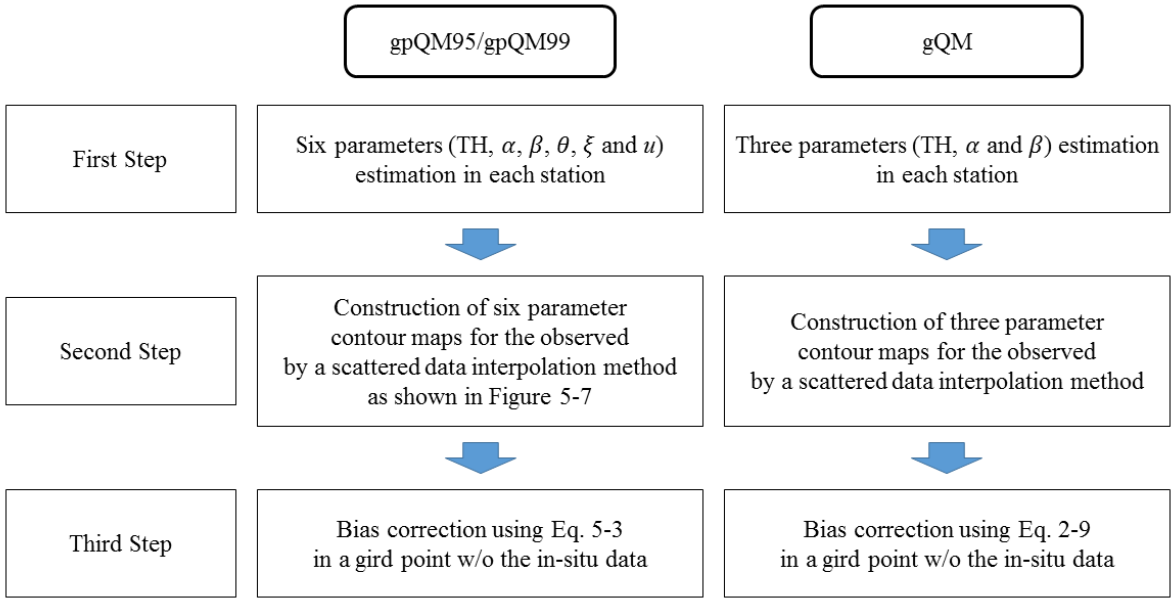

Figure 5-6 A flowchart of the proposed QM approaches (gpQM95/gpQM99 and gQM) based on the parameter contour maps (IM-PCM).

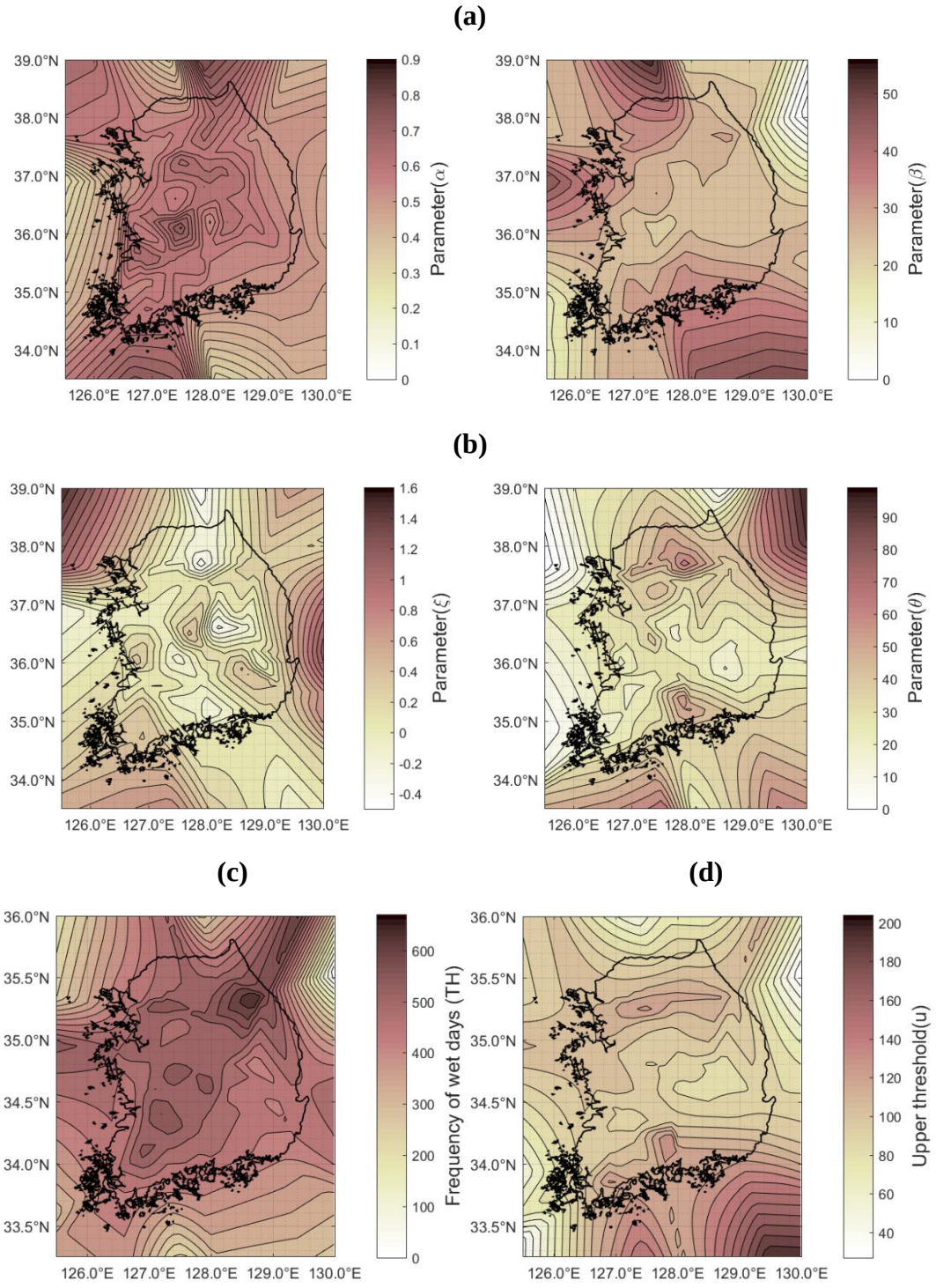

Figure 5-7 Parameter contour maps for the gpQM99 approach: (a) Maps of shape (α) and scale (β) parameter of the gamma distribution in August; (b) maps of shape (ξ) and scale (θ) parameter of the GPD; (c) a map of frequency of wet-days corresponding to the cut-off threshold (TH) in August; and (d) a map of upper threshold (u) for the GPD.

5.3.4 Evaluation criteria

This chapter evaluates the bias-corrected ERA-20c in terms of both the extreme and the mean values. For the extremes, I compared the rainfalls for a given 99^{th} threshold between three different QM approaches including gQM, gpQM95, and gpQM99. In addition, the annual maximum rainfall (AMR) series for all stations were extracted and compared with that of the corrected ERA-20c. For the mean values, both the monthly mean and 10-day running means between the observed and ERA-20c precipitation were analysed in the context of the intra-seasonal variability. The model performances for the extreme and mean values were evaluated by RMSE and NSE as described in Eq. 5-1 and 5-2.

The performance of the proposed interpolation method was evaluated by a leave-one-out procedure within a cross-validation framework as follows: (1) this approach estimates a set of parameters for the observation of daily precipitation for 47 stations out of 48 stations, and (2) the estimated parameters were further used to build contour maps as shown in Figure 5-7. (3) The set of parameters of the grid point corresponding to the excluded station were derived from the maps, and (4) the proposed bias correction approaches were then applied. (5) The process from (1) to (4) was repeated for all 48 stations in turn. Again, note that the model performances for the extreme and mean values were evaluated with regard to RMSE and NSE.

5.4 Results and discussion

5.4.1 Evaluation of the lower threshold

This chapter examined four different thresholds (TH1, TH2, TH3, and TH4) for adjustment of the wet-day frequency of ERA-20c daily precipitation through an experiment with the gQM approach in terms of both the mean and extreme values. I investigated the intra-seasonal variability within the annual cycle by comparing the monthly means and the 10-day running means as an overall evaluation of the bias-corrected precipitation. Here, all the values were averaged over all 48 stations during the baseline period (1973–2010) as illustrated in Figure 5-8. This analysis showed that TH4 performed the best results among the four different thresholds in terms of monthly mean, as summarised in Figure 5-8(a) and Table 5-3. Again, note that TH4 is the case where the

frequency of wet days of ERA-20c is set equal to that of the observed. On the other hand, the other thresholds, TH1, TH2, and TH3, showed a significant overestimation, whereas the uncorrected ERA-20c showed a relatively small bias. These results suggest that improper thresholds for the wet-day frequency may affect bias correction results, leading to a significant overestimation of daily rainfall. Such discrepancies may arise from the significantly different thresholds used to adjust the wet-day frequency. As described in Section 5.3.1, TH4 was varied over the range 0–4.66 mm while the thresholds assumed in TH1, TH2 and TH3 were much lower than the values measured in TH4, especially for the summer season (July–September). The comparison in the 10-day moving mean suggests the similar result, as shown in Figure 5-8(b) and Table 5-3. More specifically, the bias associated with the cut-off thresholds significantly varied within a specific season, especially in the summer. In Figure 5-8(b), the biases for both TH1 and TH2 range from 2.21 to 10.49 mm/day and from 1.92 to 10.09 mm/day during the summer, respectively. Meanwhile, TH3 and TH4 varied from 0.16 to 6.27 mm/day and from -1.06 to 2.97 mm/day, respectively.

(a)

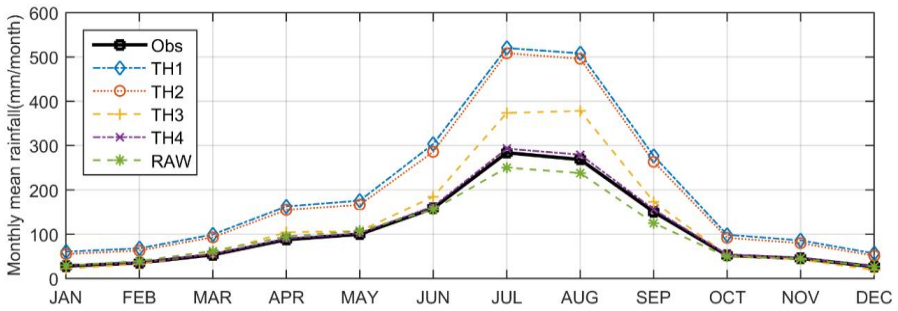

(b)

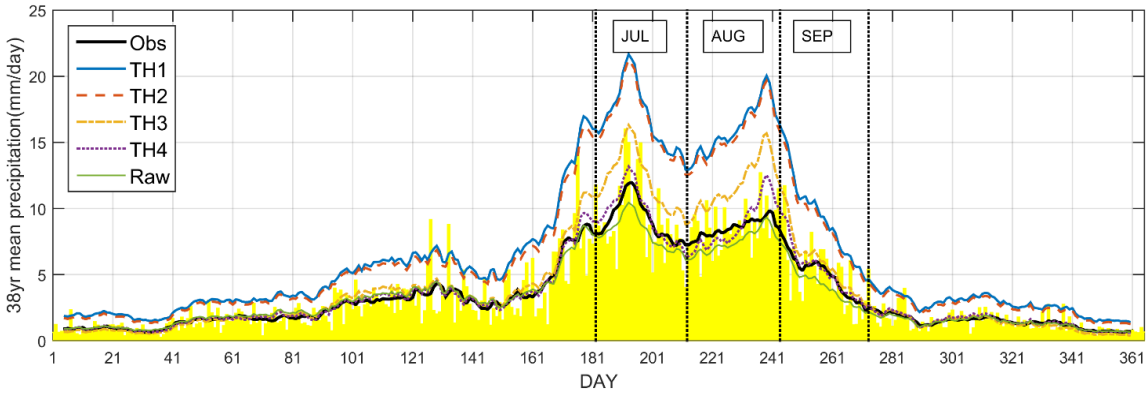

Figure 5-8 A comparison of mean rainfall between the observation and the corrected ERA-20c with different thresholds [TH1(>0mm/day), TH2(>0.1mm/day), TH3(>1mm/day), and TH4(Frequency adjustment)] and the uncorrected ERA-20c (RAW)) on the annual basis. All values are averaged over all 48 stations from 1973 to 2010. (a) Monthly mean comparison between different thresholds, and (b) observed 38-year (1973-2010) mean of daily precipitation (yellow bar) and its 10-day running mean (black solid line), along with a set of 10-day running means estimated from bias corrected ERA-20c daily precipitations using four different thresholds for all 48 stations.

Table 5-3 RMSE (mm) and NSE for the corrected ERA-20c with different thresholds [TH1 (>0mm/day), TH2 (>0.1mm/day), TH3 (>1mm/day) and TH4 (frequency adjustment)], and the uncorrected ERA-20c (RAW), compared with the observed.

Data	Measures	TH1	TH2	TH3	TH4	RAW
Monthly mean (mm/month)	RMSE (mm)	119.24	110.50	42.57	4.77	15.59
	NSE	-0.899	-0.631	0.758	0.997	0.968
10-days running mean. (mm/day)	RMSE (mm)	4.03	3.74	1.49	0.51	0.56
	NSE	-0.886	-0.622	0.744	0.970	0.963

For the evaluation of the extreme rainfalls associated with different THs, I extracted rainfall events exceeding a given 99th threshold and then compared the four different thresholds for all stations. As illustrated in Figure 5-9, the improvements appear to result from the reduction of the bias associated with extreme values regardless of the threshold, although there still exists a significant underestimation of heavy extremes in the ERA-20c. Specifically, TH4 performs the best with 0.755 for NSE and 27.33 mm for RMSE, followed by TH3, TH2, and TH1. The errors may be largely attributed to their number of data with different thresholds for a given time series. To be more specific, the lower threshold allows a relatively large number of data, while the higher threshold could reduce the number of available data. Given these results, TH4 could be the most reliable cut-off threshold for the ERA-20c under the gQM approach. On the other hand, there remains considerable potential for improving extremes, especially over 300 mm/day. Thus, I will further explore the bias correction approach for the upper tail of the distribution.

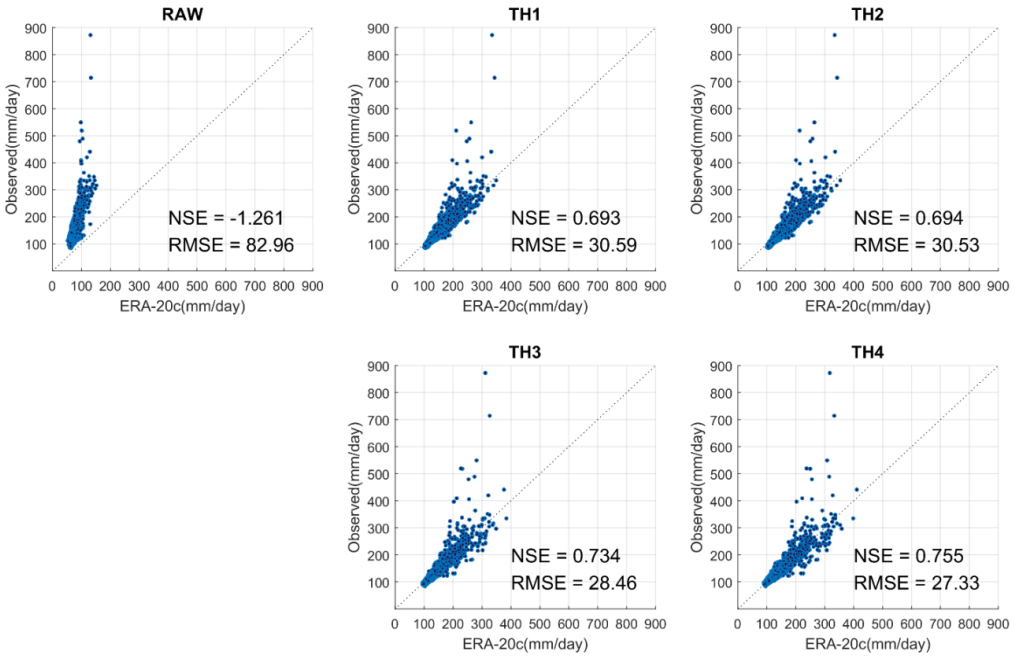

Figure 5-9 Scatter plots between the observed and the modelled extreme rainfalls associated with different thresholds over the 99th percentile for all 48 stations. RAW indicates the uncorrected ERA-20c and the others represent the results from the corrected ERA-20c by gQM with different thresholds [TH1(>0mm/day), TH2(>0.1mm/day), TH3(>1mm/day), and TH4(Frequency adjustment)].

5.4.2 Bias correction based on a composite gamma-GP distribution

This chapter applied a composite distribution-based QM approach which consists of gamma distribution and GPD, for a given set of thresholds. Here, after adopting TH4 as the lower threshold, the 95th or 99th quantile was considered the upper threshold for the correction of extremes (gpQM95 and gpQM99). The composite distribution approach was evaluated by comparing the obtained extreme rainfalls from modelled ERA-20c with the ones observed for the baseline, as shown in Figure 5-10. In comparison with the extreme daily rainfalls over the 99th percentile, the GPD based bias correction schemes (i.e. gpQM99 and gpQM95) demonstrate better performance in terms of reproducing the extremes than gQM (Figure 5-10(a)). gpQM99 shows the best performance in terms of NSE with an efficiency of 0.906, and a good agreement was achieved with 0.879 in gpQM95, whereas the gQM was 0.755. For RMSE, gpQM99 (i.e. 16.92 mm) and gpQM95 (i.e. 19.16 mm) showed a significant reduction of the errors by 38.1% and 29.9% relative

to gQM (27.33 mm). Moreover, a comparison of the AMRs also confirmed that gpQM99 and gpQM95 were capable of reproducing rainfall characteristics observed in the AMRs more effectively than gQM (Figure 5-10(b)). Specifically, gpQM99 showed the best performance with 0.912 for NSE and 18.80 mm for RMSE, whereas gpQM95 was 0.892 for NSE and 20.77 mm for RMSE. The results obtained in this analysis suggest that the gpQM approach is more appropriate to reduce the systematic errors in estimating extreme rainfalls than gQM.

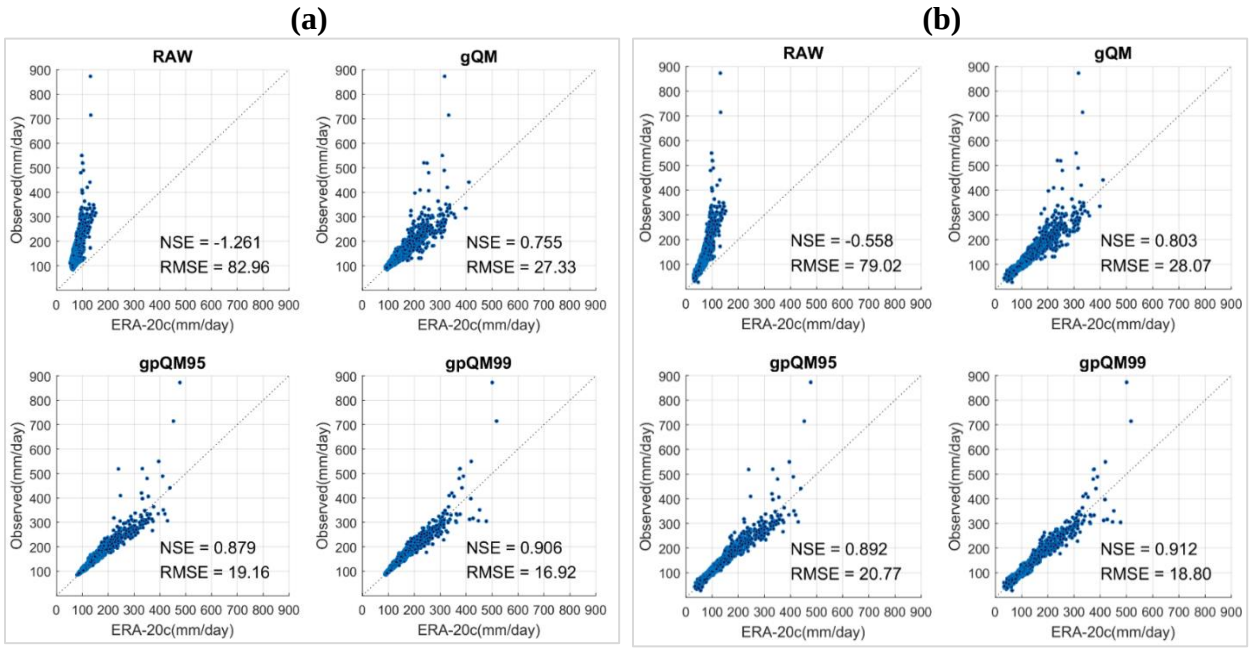

Figure 5-10 Scatter plots for (a) the extreme rainfalls over the 99th percentile and (b) the AMRs extracted from the observed and the bias-corrected ERA-20c daily precipitation over 48 stations.

Apart from evaluating the models in extreme cases, it is important to ensure that the proposed bias correction model with the GPD can reproduce the mean values as well. Again, I evaluate both the monthly mean and 10-day moving mean of the corrected daily precipitation as shown in Figure 5-11 and Table 5-4. For the monthly mean, gQM and gpQM99 give the best performance (Figure 5-11(a)), leading to the highest efficiency for NSE of 0.997 for both methods, and the lowest RMSE, about 4.77 to 5.12 mm/month, respectively (Table 5-4). For gpQM95, the efficiency for NSE is close to one, but the RMSE, 9.41 mm/month, is almost twice those of gQM and gpQM99. Regarding the 10-day moving mean, the results have shown that all QM approaches work equally well, although gpQM99 offers the best performance (Table 5-4). More generally, the gpQM99

approach can effectively correct the biases associated with the upper tails of the distribution without a loss in the efficiency of the bias correction process.

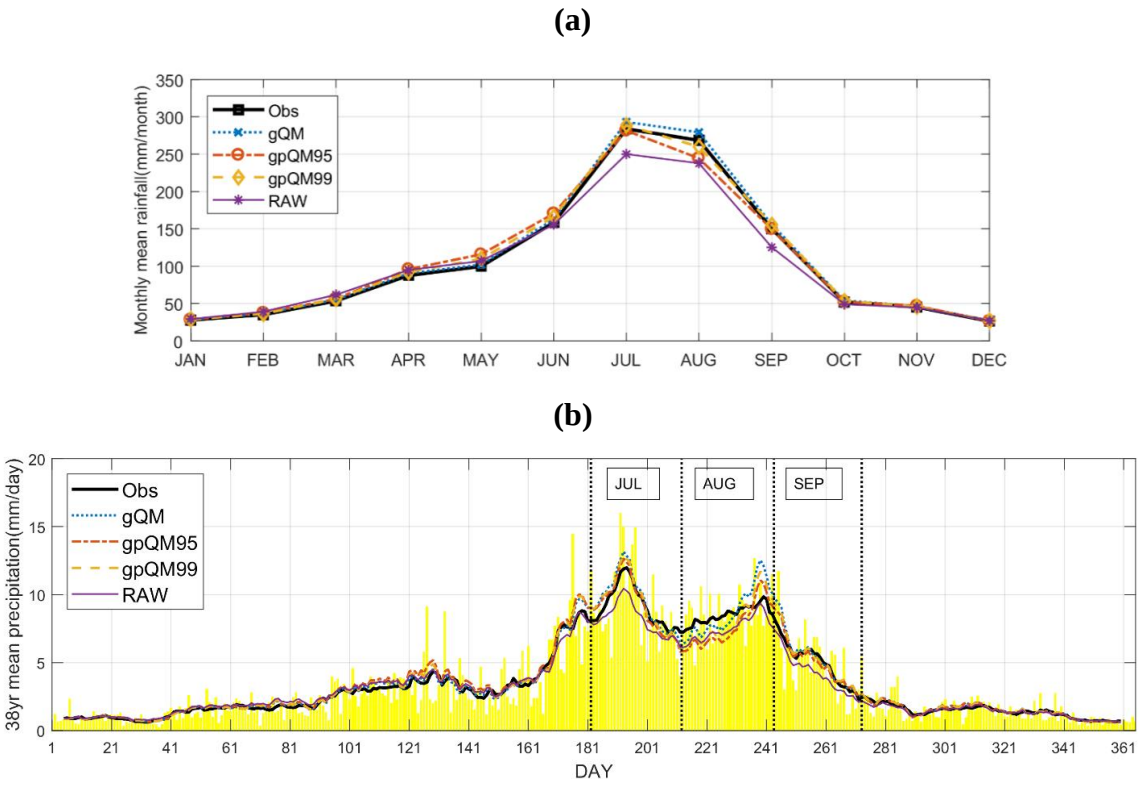

Figure 5-11 A comparison of mean rainfall between the observation and the corrected ERA-20c with different QM approaches. (a) Monthly mean comparison between different QMs and (b) observed 38-year (1973-2010) mean of daily precipitation (yellow bar) and its 10-day running mean (black solid line), along with a set of 10-day running means estimated from bias corrected ERA-20c daily precipitations using three different QM approaches for all 48 stations.

Table 5-4 A comparison of the mean values between the observed and modelled data (the corrected ERA-20c by gQM, gpQM95 and gpQM99, and the uncorrected ERA-20c(RAW)).

Data	Measures	gQM	gpQM95	gpQM99	RAW
Monthly mean (mm/month)	RMSE (mm)	4.77	9.41	5.12	15.59
	NSE	0.997	0.988	0.997	0.968
10-days running mean. (mm/day)	RMSE (mm)	0.507	0.545	0.497	0.563
	NSE	0.970	0.966	0.971	0.963

It should be noted that the bias remains substantial in the summer season as seen in the 10-day moving mean. The difference was mainly attributed to the discrepancies in the seasonal or monthly distribution of the heavy rainfall events between the observed and modelled data (Nyunt et al., 2016). In other words, there is a clear difference in the monthly number of extreme events over the 95th or 99th thresholds between the observed and ERA-20c (Figure 5-12), and this is considered to be the main source of the bias in terms of extremes in the intra-seasonal band. The results obtained in these experiments imply that the upper thresholds could be different (or updated) for each month to better represent the intra-seasonal change. The scale gap between the observed and the modelled can also result in biases (Maraun, 2013). Since the proposed QM approaches in this chapter matched the transfer function between the observation with point-scale and the model data with grid-scale, the bias-corrected value may include errors.

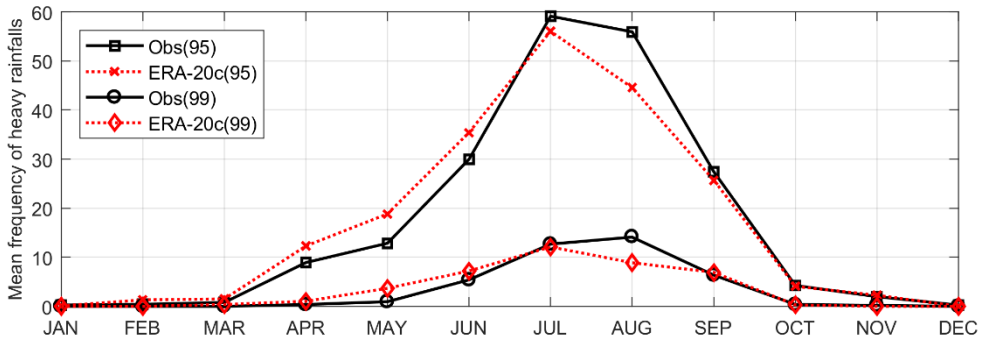

Figure 5-12 Monthly mean frequency of the heavy rainfalls over the 95th and 99th percentile from the observed (Obs) and ERA-20c daily precipitation. Here, the mean frequency is averaged over 48 stations from 1973 to 2010.

5.4.3 Spatial interpolation on bias correction parameters

The proposed IM-PCM approach is validated by leave-one-out cross validation. In this analysis, I estimated a set of parameters for the observation of daily precipitation, and the estimated parameters were then used to build contour maps. For extreme values of the interpolated daily precipitation, POTs exceeding a given 99th percentile and AMRs in 48 stations were first calculated and compared between three different QM approaches (gQM, gpQM95, and gpQM99). Note again that all results were obtained from the leave-one-out cross-validation procedure. As illustrated in Figure 5-13(a), the corrected extremes using an interpolated set of parameters by IM-PCM showed

good agreement with the observed values for the three QMs. Among them, gpQM95 and gpQM99 gave the best performance for the given POTs (Figure 5-13(a)) with 0.781 for NSE, and 0.714 for gQM. Similar results were obtained for the RMSE. Moreover, the proposed gpQM99 approach using the interpolated parameters was capable of reproducing the AMRs with 26.35 mm for RMSE and 0.827 for NSE (Figure 5-13(b)). However, it should be noted that an increased bias exists, which is mainly attributable to the parameter interpolation process. For example, the RMSE in AMRs using gpQM99 with IM-PCM increased from 18.80 to 26.35 mm when compared with a pointwise bias correction as already seen in Figure 5-10(b). A similar increase (i.e. 20.77 to 26.30 mm) was also observed in the gpQM95. Nevertheless, the RMSE for the corrected AMRs by IM-PCM with gpQM99, 26.35 mm, is still smaller than that of the pointwise bias correction from gQM, 28.07 mm.

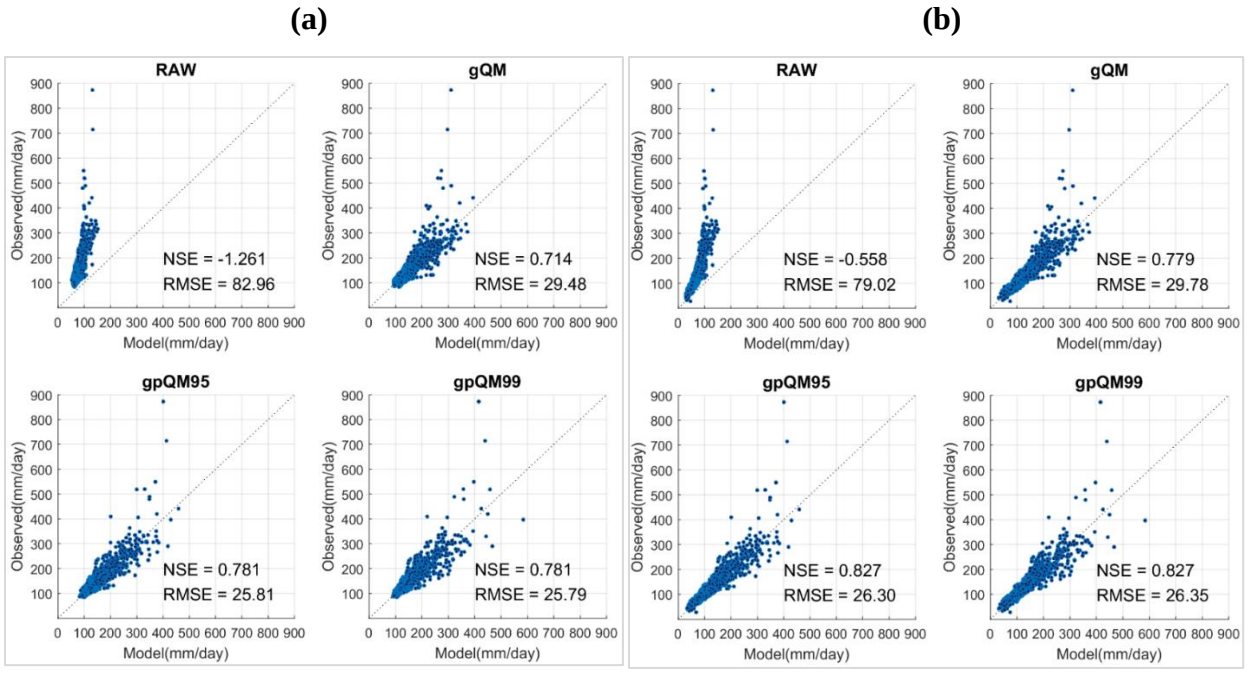

Figure 5-13 Scatter plots for (a) the extreme rainfalls over the 99th percentile and (b) AMRs extracted from the observed and the bias-corrected ERA-20c daily precipitation over all 48 stations. All the results presented here are obtained by leave-one-out cross validation.

In terms of the mean precipitation, the monthly mean and 10-day moving average of bias-corrected rainfall using a set of parameters obtained from IM-PCM were evaluated (Figure 5-14 and Table 5-5). Although all three QM approaches yielded slightly different estimates, overall favourable

performance was obtained for the monthly mean with a model efficiency over 0.98 for NSE. Among the options, gQM and gpQM99 performed the best and showed the lowest RMSE (Figure 5-14(a) and Table 5-5). Figure 5-14(b) shows a similar result for the 10-day moving average with an efficiency over 0.96 for NSE.

(a)

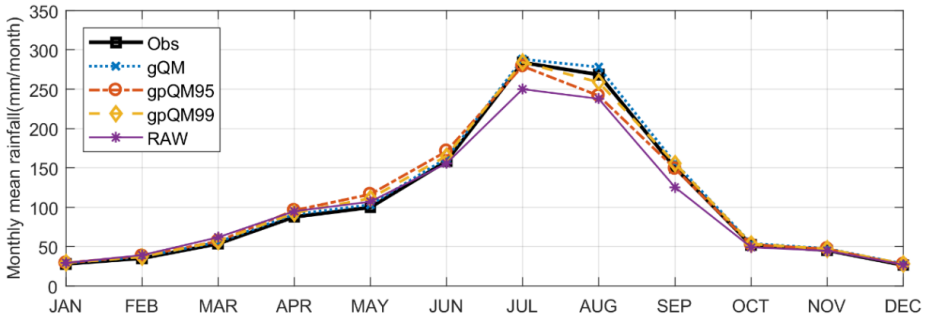

(b)

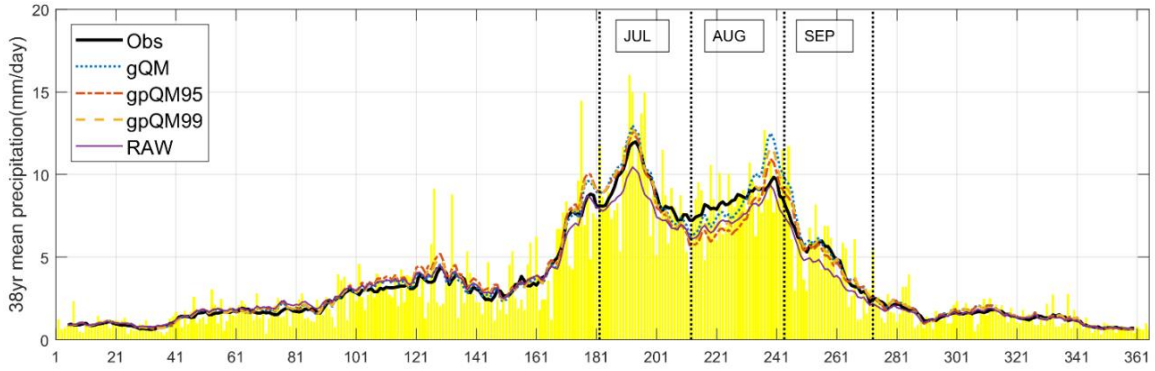

Figure 5-14 A comparison of cross validation results for the mean rainfall between the observation and the corrected ERA-20c with different QM approaches. (a) Monthly mean comparison between different QMs and (b) observed 38-year (1973–2010) mean of daily precipitation (yellow bar) and its 10-day running mean (black solid line), along with a set of 10-day running means estimated from bias corrected ERA-20c daily precipitations using three different QM approaches for all 48 stations. All the results presented here are obtained by leave-one-out cross validation.

Table 5-5 A comparison of the mean values between the observed and the modelled precipitation for three different approaches by using a set of parameters interpolated from IM-PCM within the leave-one-out cross validation framework.

Data	Measures	gQM	gpQM95	gpQM99	RAW
Monthly mean (mm/month)	RMSE (mm)	4.14	10.31	5.27	15.59
	NSE	0.998	0.986	0.996	0.968
10-days running mean. (mm/day)	RMSE (mm)	0.502	0.562	0.498	0.563
	NSE	0.971	0.963	0.971	0.963

For a more specific analysis in each weather station in the context of cross validation, I generated a map showing the spatial errors in both AMR and mean. The errors for AMRs were evaluated by RMSE and NSE in Figure 5-15. For the mean, this chapter additionally evaluated the IM-PCM method by estimating the relative error between the observed and modelled in Figure 5-16. As shown in the figures, for the AMRs, gpQM95 and gpQM99 generally perform well except for a few stations. Most stations showed NSE over 0.8 and RMSE less than 30mm. For the mean daily rainfall, the relative errors are generally below 10%. Given these results, the proposed gpQM approaches, especially for gpQM99, with IM-PCM can effectively rectify the spatial-temporal bias of the ERA-20c model data without a significant loss in efficiency for the mean values.

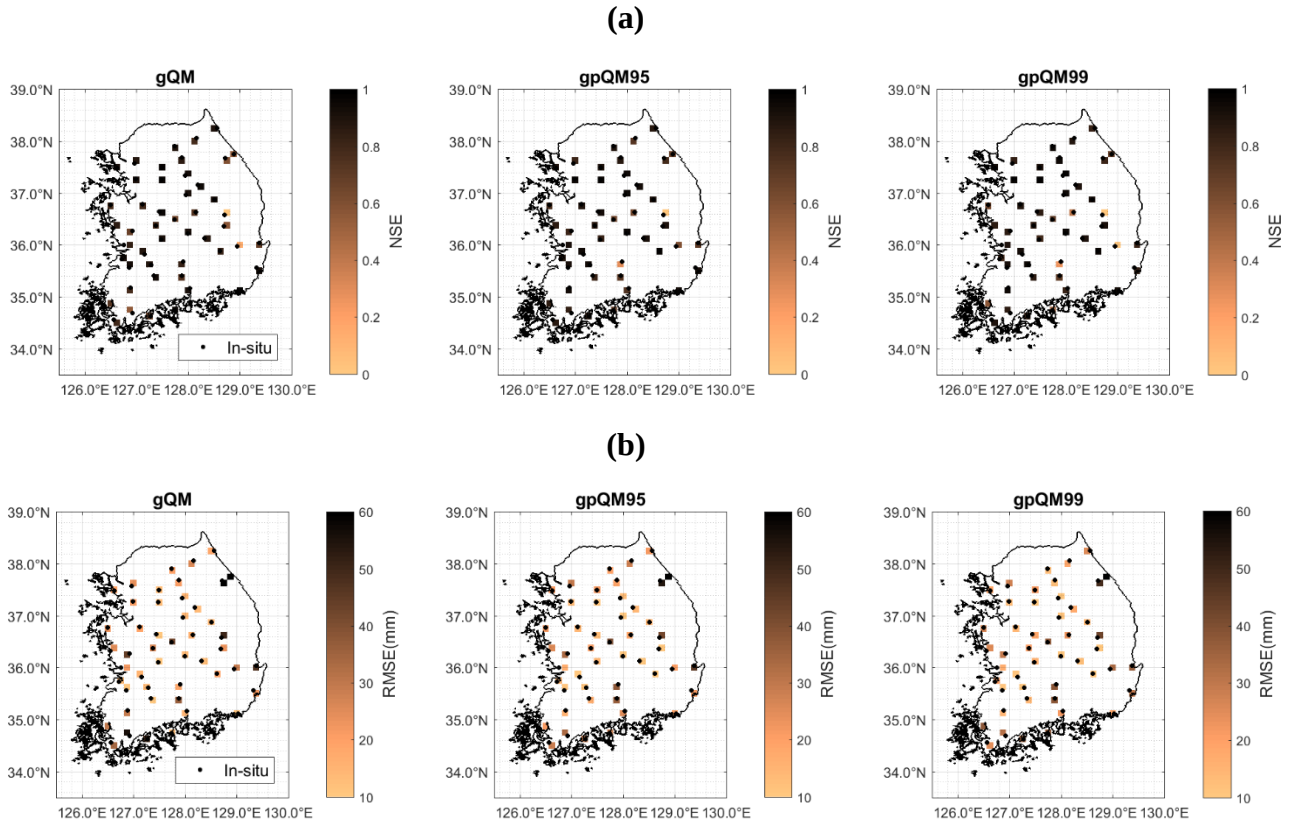

Figure 5-15 Cross validation results of the IM-PCM for the AMRs of the bias-corrected data by QM approaches (gQM, gpQM95, and gpQM99) over 48 grid points. (a) Nash-Sutcliffe efficiency (NSE) and (b) root-mean-square-error (RMSE).

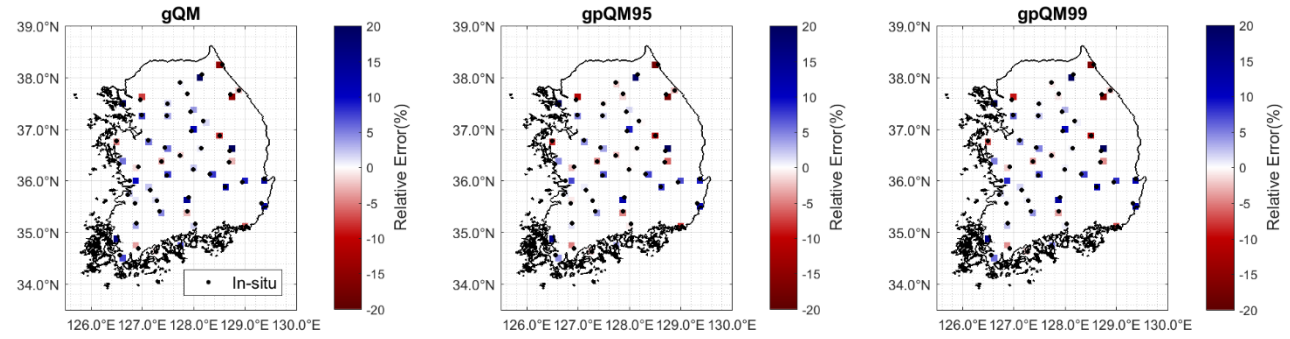

Figure 5-16 Relative error of the bias-corrected mean rainfalls by QM approaches (gQM, gpQM95, and gpQM99) in 48 grid points compared with the corresponding *in situ* records.

It is well known that precipitation is mainly influenced by the topology in mountainous areas, so numerous studies have used elevation as an exogenous factor for rainfall interpolation (Adhikary et al., 2017; Goovaerts, 2000; Lloyd, 2005). Thus, this chapter further explored the relationship

between the elevation and parameters for all 48 stations by using Pearson's correlation coefficient (*r*). As summarised in Table 5-6, the *r* values were not statistically significant, leading to a weak dependence between the elevation and parameters. The results imply that the elevation may not be important in terms of the interpolation of the parameter. In summary, the proposed interpolation scheme for the QM approach provided bias-corrected long-term precipitation data, especially for ungauged catchments. On the other hand, the proposed approach was easy to use and may help to reduce bias associated with the interpolation of daily precipitation. Moreover, this approach can be further used to obtain a century-long daily precipitation series over the Korean peninsula, which could be useful in terms of reducing uncertainty in the parameter estimation of rainfall frequency analysis.

Table 5-6 Pearson's correlation coefficients(r) between elevations and parameters for gQM, gpQM95, and gpQM99 for all 48 stations.

Type	Gamma Distribution													GPD	
	Para.	*r*												Para.	*r*
		Jan	Feb	Mar	Apr	May	Jun	Jul	Aug	Sep	Oct	Nov	Dec		
gQM	α	-0.40	-0.14	0.06	0.18	0.07	0.16	0.22	0.06	0.15	0.00	-0.06	-0.14	ξ	-
gpQM95		-0.37	-0.13	0.05	0.17	0.09	0.19	0.26	0.09	0.15	0.12	-0.13	-0.18		-0.01
gpQM99		-0.40	-0.14	0.06	0.18	0.07	0.16	0.24	0.08	0.14	0.03	-0.08	-0.14		-0.05
gQM	β	0.09	-0.15	-0.25	-0.22	-0.14	-0.20	-0.11	-0.11	-0.02	0.17	-0.02	-0.11	θ	-
gpQM95		0.02	-0.16	-0.22	-0.23	-0.20	-0.25	-0.18	-0.14	-0.08	-0.10	0.02	-0.08		-0.05
gpQM99		0.09	-0.14	-0.25	-0.23	-0.17	-0.21	-0.13	-0.16	-0.03	0.09	-0.03	-0.11		-0.01

The bias correction methods developed in this chapter statistically improved the quality of the data and could extend daily precipitation over the 20th century in South Korea. More specifically, this chapter further utilises the derived transfer function for the baseline period of 1973–2010 to provide the daily precipitation for the period of 1900–2010 under the stationary assumption. Finally, I roughly explored changes in the mean and extreme using the gpQM99 approach for three different periods (1900–1972, 1973–2010, and 1900–2010) in the context of a retrospective analysis. In Figure 5-17, the results in three different periods were denoted by gpQM99-1 (1900–1972), gpQM99-2 (1973–2010), and gpQM99-3 (1900–2010), respectively. As shown in Figure

5-17(a), the evaluation results for the monthly mean show a very noticeable and sudden increase in the recent period, especially for the summer season (July–September), while no significant changes were observed for dry season (October–April). Figure 5-17(b) shows boxplots representing a distribution of the AMRs for the three periods. The distribution of the AMRs derived from the gpQM99 approach for the period of 1973–2010 was almost identical to that of the observed, which indicates that the proposed gpQM99 was capable of reproducing the extremes of daily precipitations. As expected from the changes in summer rainfall, the distribution of the AMRs for the recent period of 1973–2010 (i.e. gpQM99-2) is much broader than that of the period of 1900–1972 (i.e. gpQM99-1), especially for the upper tail of the distribution. This difference between the two periods implies the recent increase of rainfall intensity, which may lead to an increase in design rainfalls for a specific return period. On the other hand, the distribution of the AMRs for the entire period of 1900–2010 is quite similar to that of the observed in terms of median AMR, while its range is relatively narrower than the recent period.

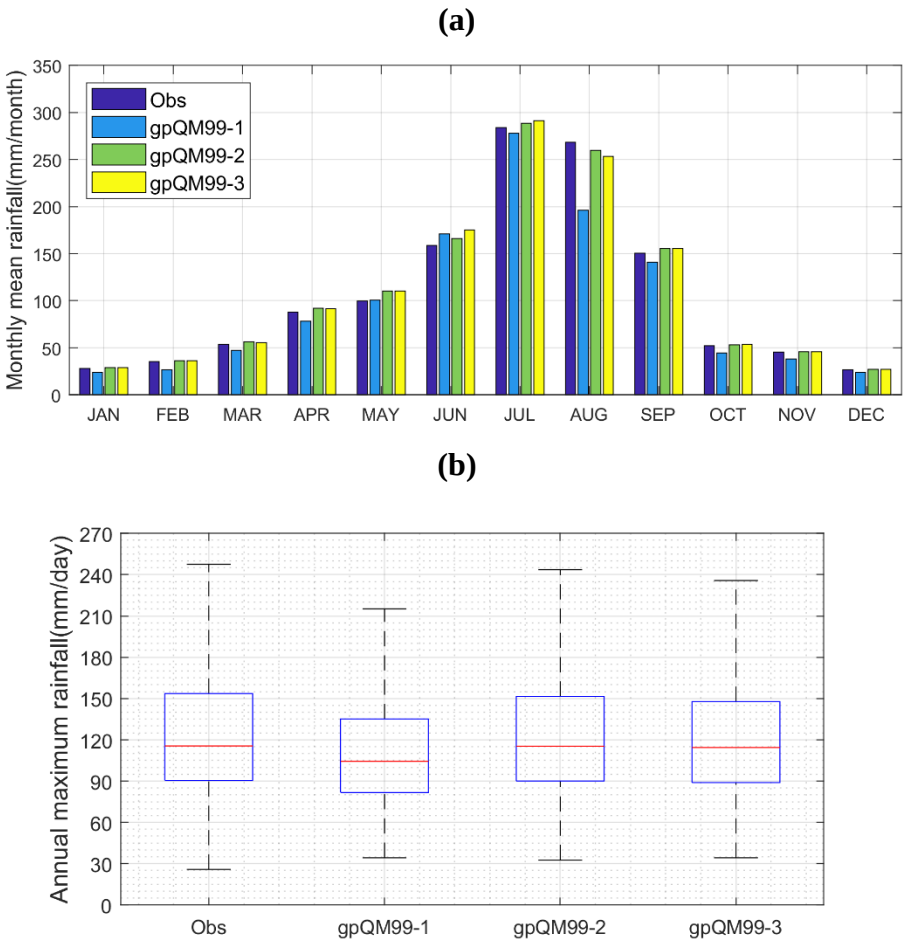

Figure 5-17 A retrospective analysis for a comparison between the observed precipitation (1973–2010) and the corrected ERA-20c by gpQM99 with three different periods: 1900–1972 (gpQM99-1), 1973–2010 (gpQM99-2), and 1900–2010 (gpQM99-3). (a) Monthly mean rainfalls and (b) box plot of the AMRs.

5.5 Conclusions

The main objective of this chapter was to explore the century-long reanalysis data, ERA-20c, especially for daily precipitation in South Korea in the context of bias correction. I first investigated the suitability of the ERA-20c data as proxy data in South Korea for hydrological applications. I then further examined several issues concerning the aspects of the bias correction that influence the use of modelled data in practice. This analysis found that there was a fairly good agreement between the observed and ERA reanalysis data for the baseline period of 1973–2010.

On the one hand, the results obtained here have also shown that ERA-20c precipitation data still have their own systematic biases, particularly in the frequency of wet-days and the extreme upper tail of the distribution. Given these results, this chapter proposed a two-stage bias correction approach to daily precipitation, which consists of two distinct parts: (1) a model for adjusting the overestimated wet-day frequency and (2) a model for reducing the biases associated with extreme values. To adjust the wet-day frequency, this thesis explored four different thresholds through an experiment with the gQM approach. In terms of extremes, a composite gamma-GPD distribution-based QM approach was introduced. Finally, this chapter proposed an IM-PCM approach as an alternative to constructing the transfer function for the ungauged catchment. The main findings obtained in this analysis are summarised as follows:

1. This chapter's analysis confirmed that ERA-20c data can well reproduce the monthly mean and annual cycle of daily precipitation of South Korea as observed. However, considerable underestimation of heavy rainfalls was consistently seen in the ERA-20c, especially during the summer season. Another issue for ERA-20c daily precipitation is that the simulated data have a much higher frequency of wet-days than that of the observed, which may in turn influence the underestimation of extremes.

2. Regarding the wet-day frequency adjustment, this chapter examined four different types of thresholds (i.e. TH1, TH2, TH3, and TH4) to identify an optimal threshold. Among the four, TH4 (setting the frequency of wet-days of ERA-20c equal to that of the observed) produced the best results. This analysis indicates that inappropriate thresholds for wet-day frequency may significantly influence bias correction results.

3. To better represent the bias in extreme rainfall, this chapter proposed a composite distribution-based QM approach, which consists of the gamma distribution and GPD for the two thresholds (i.e. the 95^{th} and 99^{th} percentiles). Given the efficiency gains, the findings suggest that the gpQM approach is more appropriate to reduce the systematic errors in estimating extreme rainfalls than gQM. To be more specific, the gpQM99 approach can effectively reduce the biases in the upper tails of the distribution without a significant loss of efficiency in the overall bias correction process. However, a certain degree of bias still exists in the summer season. Thus, the extremes derived from the bias-corrected values through the gpQM99 method might

not perfectly reflect the specific regional patterns associated with extreme rainfall in South Korea.

4. This chapter explored an alternative (i.e. IM-PCM) to obtain the transfer function of the QM approach for ungauged catchments in the context of the cross-validation process. The corrected daily precipitation based on the IM-PCM method showed good agreement with the observed precipitation. Particularly, the proposed gpQM99 with the IM-PCM performed the best in terms of reducing the spatial-temporal bias of the ERA-20c model data without a significant loss of efficiency. The analysis of the relationship between elevation and parameters suggested that the elevation may not be an essential variable for the interpolation of the parameters in South Korea.

5. This chapter finally adopted the derived transfer function for the baseline period of 1973–2010 to extend the daily precipitation for the period 1900–2010 under the stationary assumption. It also examined the changes in daily precipitation for three different periods (1900–1972, 1973–2010 and 1900–2010) as a retrospective analysis. In this analysis, a very noticeable and sudden increase in the recent period was observed during the summer season (July to September).

The findings in this chapter help to understand the knowledge gaps about the bias correction of century-long reanalysis, ERA-20c, as well as the critical characteristics of daily precipitation in South Korea. Furthermore, the results obtained here can provide a useful perspective on the spatial bias correction of the modelled data in the reanalysis and regional climate modelling systems for regional-scale analysis with a limited network of rainfall stations.

This chapter mainly dealt with the bias-correction technique for ERA-20c daily data in South Korea for the reference period under the stationary assumption. In the following chapter, this thesis introduces a trend-preserving bias-correction scheme for ERA-20c data for the whole period (1900–2010). It then analyses the impact of century-long data on design rainfall estimation.

CHAPTER 6 [1]Trend-preserving bias correction of ERA-20c and the impact of longer data on design rainfall estimation

6.1 Motivation

In Chapter 5, this thesis addressed the bias correction scheme which can improve ERA-20c daily precipitation data with limited observation networks. However, as Chapter 5 mainly addressed bias correction schemes for the reference period (1973–2010), the long-term trend of rainfall data was not deeply considered in the bias correction process. More specifically, a fundamental assumption of the applied QM approaches in Chapter 5 was that the biases in the model data were stationary for the baseline period. However, climate variables including precipitation are often viewed as nonstationary and previous studies have also documented that there is a significant increasing trend in South Korea, especially in the summer as discussed in Chapter 4 (Cannon et al., 2015; Chang and Kwon, 2007; Choi et al., 2009; Eum and Cannon, 2017; Jung et al., 2011; Miao et al., 2016; Nahar et al., 2017). Thus, the question of how to consider this time-dependent feature is one major issue in bias correction of long-term data such as century-long ERA-20c products.

Recently, bias correction methods including the consideration of nonstationarity have been proposed to better represent climate variables. Bürger et al. (2013) suggested the detrended quantile mapping (DQM) approach, removing the trends for future climate. Li et al. (2010) proposed an equidistant QM algorithm to reduce biases. Cannon et al. (2015) proposed a trend-preserving approach – namely, quantile delta mapping (QDM) approach – and documented that QDM was generally better in terms of reducing the uncertainty in GCMs for the future period than DQM or the conventional QM. From this perspective, this chapter adopts the QDM algorithm as well as the classic stationary QM approach (SQM) for the bias correction of century-long data.

[1] Kim, D.-I., Kwon, H.-H., and Han, D., Exploration of intensity change in daily precipitation using bias-corrected ERA-20c in South Korea for the 20th century (1900-2010). Clim. Dyn. (in review)

After reducing the errors in the reanalysis products, Chapter 6 aims to analyse the impact of the long-term data on hydrological applications – especially for rainfall frequency analysis. Rainfall frequency analysis has been routinely adopted for the estimation of design rainfall for a given specific return period. The AMRs of the observed data are generally used for frequency analysis based on the BM principle. However, there are significant uncertainties in the estimated design rainfall due to sampling error, which is related to a limited number of AMRs and the use of an improper distribution (Huard et al., 2010). In other words, the use of reliable long-term data in hydrologic frequency analysis may substantially reduce the uncertainty of design rainfall estimation (Coles et al., 2003; Huard et al., 2010; Overeem et al., 2008; Tung and Wong, 2014; Van de Vyver, 2015). In this context, century-long reanalysis products can be applied to reduce the uncertainty of design rainfall estimation in rainfall frequency analysis. Here, to quantitatively analyse change of uncertainty, this thesis has applied a Bayesian framework that estimates the range of design rainfall uncertainty based on a set of parameters of probability distribution (Huard et al., 2010; Kwon et al., 2008, 2011; Reis and Stedinger, 2005; Van de Vyver, 2015).

On the one hand, extended AMRs derived from bias-corrected data allow modellers to explore climate change impact on design rainfall quantiles throughout the 20th century which cannot be reached through the limited observation period. Since design quantile with a target return period is associated with the safety of a certain project, one of the goals of this chapter is to analyse how much design rainfalls have changed for the 20th century by using the bias-corrected AMRs.

6.2 Data

6.2.1 Weather station data

This chapter employs daily precipitation derived from the KMA in 48 stations over South Korea as in Chapter 5. However, since this chapter adopts a trend-preserving bias correction scheme, the reference period used for the observed in this chapter is slightly adjusted. More specifically, to remove biases in ERA-20c daily precipitation for the entire 20th century (1900–2010), I apply quantile delta mapping (QDM) method which needs the relative change of quantiles between the reference period and the simulation period, which are set to the same length. As ERA-20c data is

111-years-long, this chapter first sets the reference period to 1974–2010 (37 years) and then divides the past simulation period (1900–1973) into two periods (i.e. 1900–1936 and 1937–1973) to make the intervals equal to the reference period. Consequently, for bias correction, Chapter 6 adopts the local gauged daily records in 48 stations from 1974 to 2010, not the 1973–2010 (38 years) period as in Chapter 5.

Of 48 stations, this chapter also uses 7 stations with a more extended period of historical records for the evaluation: St 4. Gangneung (1912–2010), St. 5 Seoul (1910–2010), St. 6 Incheon (1910–2010), St. 17 Daegu (1912–2010), St. 18 Jeonju (1919–2010), St 21. Busan (1912–2010), and St 22. Mokpo (1910–2010). The specific locations of weather stations used in this chapter are found out in Figure 6-1, and the information about the stations is shown in Table 5-1.

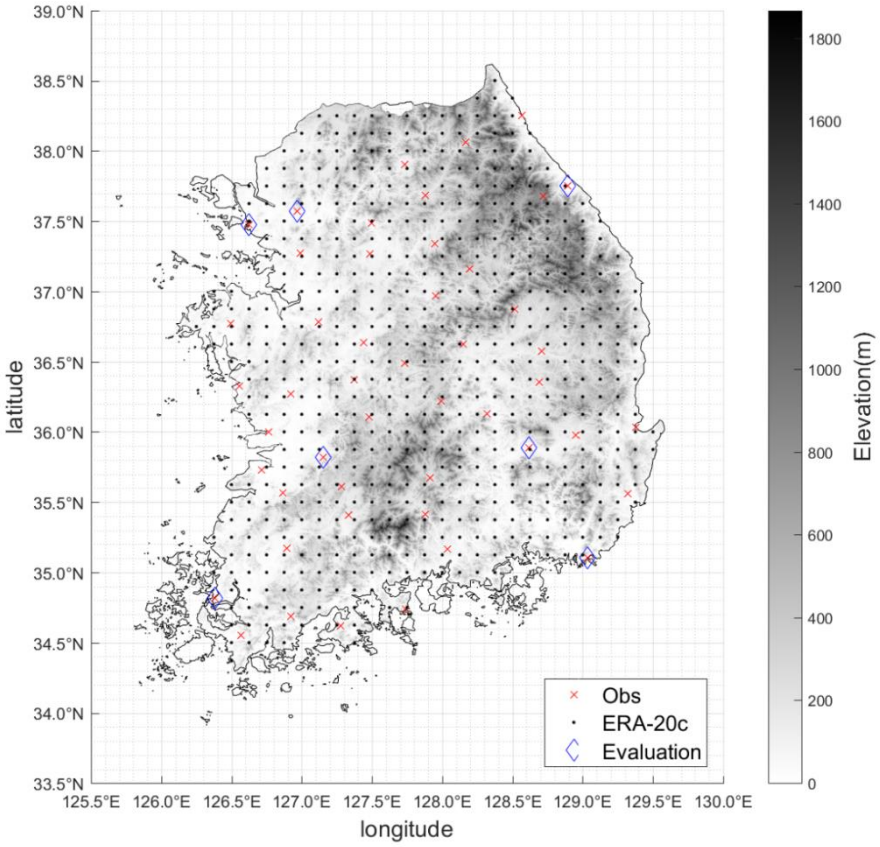

Figure 6-1 A map showing the study area, local gauging stations, grid points of ERA-20c and evaluation points in Chapter 6. The grey shading on the map indicates elevations.

6.2.2 ERA-20c daily precipitation

As same in Chapter 5, this chapter collected ERA-20c daily precipitation over South Korea for the period 1900–2010, via the ECMWF web server on the finest grid, 0.125°×0.125°. Again, note that the ERA-20c reanalysis data were finally obtained as a single simulation, without providing a large ensemble that accounts for uncertainties. The grid points of ERA-20c along with the locations of weather stations used in this chapter are illustrated in Figure 6-1. Here, the nearest grid centred at the target station was extracted for the subsequent analysis.

6.3 Methodology

In this section, three main approaches are demonstrated. First, the QDM, as well as SQM, is presented for bias correction of century-long daily precipitation with a primary focus on the use of composite distribution as a transfer function. Second, a Bayesian parameter estimation approach to rainfall frequency analysis is briefly introduced. Finally, an approach to estimate spatio-temporal change of design rainfall is described.

6.3.1 Quantile delta mapping with a composite distribution

This chapter adopts the parametric QM based on a composite distribution of gamma and GPD, which are addressed in Chapter 5. As stated in Section 5.2, this approach assumes that the CDF of all wet-day data (F_m) for the observed and the modelled follows a composite distribution of GPD for the heavy rainfall over the upper threshold and gamma for the events below the threshold.

Conceptually, the conventional QM algorithm used in Chapter 5 assumes that the degree of bias in the climate model is stationary for the entire simulation period (Cannon et al., 2015; Teutschbein and Seibert, 2012), and the stationary QM (SQM) algorithm is specifically designed to reduce bias in the climate model in the probability space. In this approach, CDFs of the historical records are constructed for the reference period, and climate model outputs for the entire simulation period are then mapped to that of the observed as follows:

$$\hat{x}_{m,p} = F_{o,r}^{-1}[F_{m,r}\{x_{m,p}(t)\}] \quad (6\text{-}1)$$

Here, $F_{o,r}$ and $F_{m,r}$ are the CDFs of the observed and modelled data for the reference period, respectively, and $\hat{x}_{m,p}(t)$ and $x_{m.p}$ mean the bias-corrected and uncorrected (or modelled) data at time *t* over the simulation period. Here, the model data, observation data, reference period, and simulation period are denoted by subscripts *m*, *o*, *r*, and *p*, respectively. For SQM, historical records from 1974 to 2010 in 48 stations and their corresponding values in the climate model were used as reference data, while the period from 1900 to 2010 was considered the entire simulation period.

Firstly, this chapter corrected the wet day frequency error, namely the 'drizzle effect', from the ERA-20c reanalysis data. As in Chapter 5, the SQM approach adopted a cut-off threshold that sets the wet-day frequency in the modelled precipitation equal to that of the observed. More specifically, the whole duration was divided into three different periods of the same length (1900–1936, 1937–1973, and 1974–2010) because climate is usually defined with 30 or more years, and the wet-day frequency of the modelled precipitation for each period was set equal to that of the observed for the reference period (1974–2010). After adjusting for the wet-day frequency, a gamma-GPD composite distribution was used to construct the CDFs in Eq. 6-1. The SQM approaches with the 95th and 99th thresholds were named SQM95 and SQM99, respectively. For SQM, several extremes for the simulation period may be beyond the range of the model data for the reference period, resulting in exceptionally high bias-corrected values for the extremes. To reduce over-estimation of the bias-corrected extremes, several extrapolation techniques have been proposed (Eum and Cannon, 2017; Li et al., 2017; Themeßl et al., 2012). Among these, this chapter used a constant extrapolation scheme over the high quantiles, as suggested by Themeßl et al. (2011).

One major issue in this SQM method is that this approach cannot consider the long-term trend of the target climate variable. As discussed in Section 6.1, there may be significant long-term trend for precipitation in many regions including South Korea. Thus, the QDM approach that is effective in preserving the long-term trend was employed for correcting the bias of the ERA-20c precipitation in terms of mean and extreme (Cannon et al., 2015; Eum and Cannon, 2017; Li et al., 2010; Miao et al., 2016). The only difference from the QDM proposed by Cannon et al. (2015) is that I superimpose the delta change for the past period, not future period. I begin with adjusting the wet-day frequency with the same TH used in SQM, and the QDM algorithm is subsequently applied for bias correction of the ERA-20c daily precipitation ranging from 1900 to 2010. As noted in the previous paragraph, ERA-20c daily precipitation was first divided into three periods with

the same data length, and the bias in precipitation in each period was then corrected by the QDM approach, as follows (Cannon et al., 2015; Eum and Cannon, 2017):

$$\tau_{m,p}\,(t) = F_{m,p}^{(t)}\left[x_{m,p}(t)\right], \qquad \tau_{m,p}(t) \in \{0, 1\} \tag{6-2}$$

$$\Delta_m(t) = \frac{F_{m,p}^{-1}\left(\tau_{m,p}(t)\right)}{F_{m,r}^{-1}\left(\tau_{m,p}(t)\right)} = \frac{x_{m,p}(t)}{F_{m,r}^{-1}[F_{m,p}(x_{m,p}(t))]} \tag{6-3}$$

$$\hat{x}_{m,p} = F_{o,r}^{-1}[\tau_{m,p}(t)] \times \Delta_m(t) = F_{o,r}^{-1}[F_{m,p}\{x_{m,p}(t)\}] \times \Delta_m(t) \tag{6-4}$$

Here, $\tau_{m,p}(t)$ is the nonexceedance probability associated with the value at time t, $\Delta_m(t)$ is the relative change in quantiles between the reference period (1974–2010) and the simulation period (1900–1936 or 1937–1973), and $F_{m,r}$ and $F_{m,p}$ are the CDFs of the modelled for the reference period and simulation period, respectively. A composite distribution described in Eq. 6-1 was adopted for estimating the CDFs in Eq. 6-2 to 6-4. Here, the QDMs with the 95th and 99th upper thresholds were abbreviated as QDM95 and QDM99, respectively. More specific information on the QDM can be found in an earlier study (Cannon et al., 2015).

For evaluation of the proposed models (SQM95, SQM99, QDM95, and QDM99), two efficiency measures, i.e. RMSE and NSE, are considered, as shown in Eq. 5-1 and 5-2. More specifically, this chapter evaluated the bias-corrected AMRs that are typically used in design rainfall estimation over a century-long historical record (1910–2010) for 7 out of 48 stations (St.4 Gangneung, St.5 Seoul, St.6 Incheon, St.17 Daegu, St.18 Jeonju, St.21 Busan, and St.22 Mokpo) and over the last four decades (1974–2010) for 48 stations. To find out how well the bias-corrected AMRs can represent the observed values in each period, the AMRs over three different periods (1974–2010, 1937–1973, and 1910–1973) were additionally evaluated for 7 stations.

6.3.2 Bayesian parameter estimation

As stated in Section 2.5, extreme precipitation is commonly characterised with the BM method of the extreme value theory. Specifically, AMRs were first obtained and fitted to a GEV distribution. Suppose that **R** indicates the AMRs in a given daily precipitation, and the PDF of the GEV distribution is then defined as bellows:

$$f(\mathbf{R};\mu,\alpha,\xi)=\begin{cases}\left(\frac{1}{\sigma}\right)\left(1+\frac{\xi(\mathbf{R}-\mu)}{\sigma}\right)^{-\frac{1}{\xi}-1}exp\left\{-\left[1+\frac{\xi(\mathbf{R}-\mu)}{\sigma}\right]^{-\frac{1}{\xi}}\right\}, & \xi\neq 0\\ \left(\frac{1}{\sigma}\right)exp\left\{-exp\left[-\frac{(\mathbf{R}-\mu)}{\sigma}\right]-\frac{(\mathbf{R}-\mu)}{\sigma}\right\} & \xi=0\end{cases} \quad (6\text{-}5)$$

where μ, σ, and ξ are the location, scale, and shape parameters, respectively.

In this chapter, the parameters of distribution functions were estimated within a Bayesian modelling framework, as seen in Eq. 2-10. The joint posterior distribution function $p(\boldsymbol{\theta}|\mathbf{R})$ for the rainfall frequency model can be formulated by combining the GEV likelihood function and prior distribution as follows:

$$p(\boldsymbol{\theta}|\mathbf{R}) \propto \prod_{i=1}^{n} GEV(\mathbf{R}|\mu,\sigma,\xi) \times N(\mu|0,10^3) \times N(\sigma|0,10^3) \times N(\xi|0,10^3) \quad (6\text{-}6)$$

The posterior distribution for the parameters of GEV distribution was obtained by maximising the joint posterior distribution as illustrated in Eq. 6-6, via the Markov Chain Monte Carlo (MCMC) algorithm, especially the Metropolis-Hastings (MH) sampler. The MH method generates a sequence of random samples from a proposal density function, which subsequently approximate the desired distribution. Here, Gaussian distributions with a zero mean and variance of 10^3 are used as prior distributions and the Markov chain eventually converges to the desired distribution through the rejection-acceptance process. The detailed information on the MCMC method can be found in Van de Vyver (2015). In this analysis, after 10,000 iterations, the second half of the chains was applied for estimation of design rainfall over all weather stations and the corresponding grid points. Design rainfalls with three different return levels (30-year, 50-year and 100-year return periods) were estimated for individual 5,000 parameter chains. Finally, the range of design rainfalls derived form 5,000 parameter chains at given return periods was compared in the form of boxplots.

6.3.3 Spatio-temporal change in design rainfall

To explore the spatio-temporal changes in design rainfall by using reanalysis products, it is essential to obtain the corrected data in all grid points. Here, I applied the IM-PCM approach proposed in Section 5.3.3 to correct ERA-20c daily precipitation with the limited observation.

To implement the QDM approaches based on a composite distribution suggested in Section 6.3.1, the six parameters (TH, α, β, θ, ξ and u) should be estimated for a pair of observed and modelled precipitation. Thus, I create contour maps using the estimated parameters based on a scattered data interpolation method in Matlab (Amidror, 2002), and then extract a set of distribution parameters covering the entire range. A flowchart for the proposed QDM procedure is illustrated in Figure 6-2. To evaluate the effectiveness of the interpolation approach, a leave-one-out cross validation framework is applied for the reference period (1974–2010). Specifically, one station was repeatedly excluded and validated using the estimated set of parameters from the remaining 47 stations. The AMRs in 48 stations were taken from the bias-corrected daily precipitation and evaluated by RMSE and NSE.

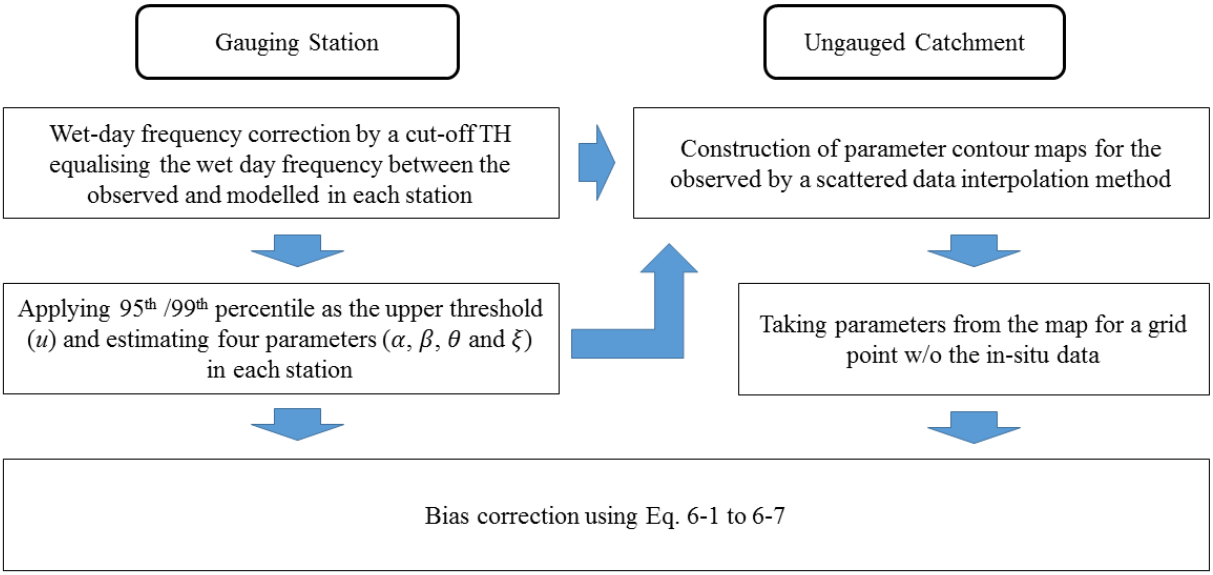

Figure 6-2 A flowchart of the QDM approach with a composite distribution in gauging stations and ungauged catchment.

With the spatially corrected reanalysis data, I explored the spatio-temporal changes in design rainfalls for a 100-year return period over South Korea. To be more specific, this chapter analysed the relative change (*RC*, %) in the observed and modelled design rainfalls for the three periods, 1900-1936, 1937-1973 and 1974-2010, as follows:

$$RC(\%) = \frac{D_r^{mod} - D_p^{obs}}{D_r^{obs}} \times 100 \quad (6\text{-}7)$$

Here, D_r^{obs} represents the design rainfall using the observed AMRs for the reference period (1974–2010), while D_p^{mod} indicates the design rainfalls based on the bias-corrected AMRs for the three periods. Note that I estimated the design rainfalls by fitting the bias-corrected AMRs of each period to GEV distribution, and those of the observed AMRs for the reference period (1974–2010) were obtained by an IDW method, which is commonly used in practice.

In addition, I conducted a retrospective analysis to explore the temporal changes in design rainfall for a given 100-year return period using bias-corrected century-long data. More specifically, the design rainfalls obtained from the bias-corrected AMRs for the whole period (1900–2010) were compared with those by the observed for the reference period (1974–2010) over South Korea.

6.4 Results and discussion

6.4.1 Evaluation for the bias-corrected ERA-20c

To evaluate the performance of the proposed QDM approach for heavy rainfalls, especially for heavy rainfalls, this chapter collected the bias-corrected AMRs and statistically compared them with those of the observed as illustrated in Figure 6-3. More specifically, Figure 6-3(a) describes the comparison between the raw ERA-20c and the bias-corrected values over all stations for the reference period 1974–2010. The QM approaches with the 95th and 99th percentiles performed reasonably well, 0.891 and 0.914 for NSE and 20.93mm and 18.65mm for RMSE, respectively, while the raw ERA-20c showed -0.579 for NSE and 79.81 for RMSE. Here, QDM and SQM with the same upper threshold conceptually gave the same error for the reference period. For a comparison with the century-long data for 7 stations, a significant reduction in bias was identified by QDM and SQM, as shown in Figure 6-3(b). It can be shown that QDM approaches performed slightly better than the corresponding SQMs. For QDM99, the agreement with the observed was 27.11mm for RMSE and 0.824 for NSE, indicating the better performance than SQM99 with 28.12mm for RMSE and 0.810 for NSE. For QDM95, the model efficiency in terms of NSE was comparable to that of the SQM95, but RMSE was slightly smaller than that of the SQM95. These

results suggest that the QM approaches applied in this chapter can significantly reduce the bias in daily precipitation for the whole 20th century, and QDM approaches are more efficient than SQM schemes, especially for the AMRs, during the whole 20th century.

(a)

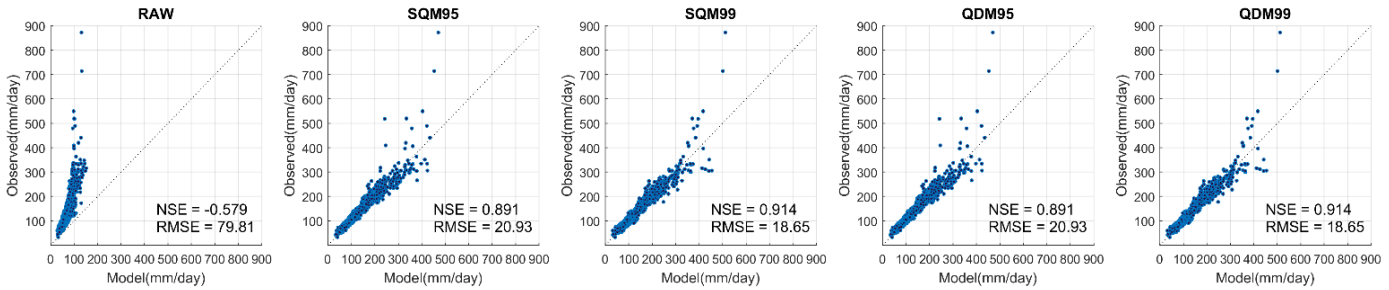

(b)

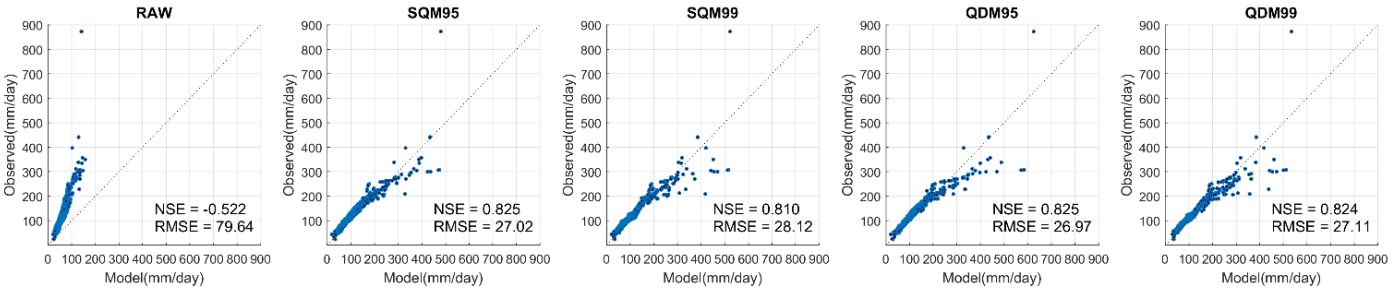

Figure 6-3 Scatter plots between the AMRs of the observed and the bias-corrected ERA-20c over (a) all 48 stations for the reference period (1974-2010) and (b) for 7 stations from 1910 to 2010.

However, the validation results in three different periods showed that the proposed bias correction scheme has a limitation in reproducing extreme values of each period as shown in Figure 6-4. As illustrated in Figure 6-4(a), the AMRs over 7 stations during the period of 1974–2010 are reasonably well reproduced and comparable to that of the observed in Figure 6-3(a). On the other hand, a relative increase in bias in AMRs is clearly seen in the period of 1937–1973, as shown in Figure 6-4(b).

(a)

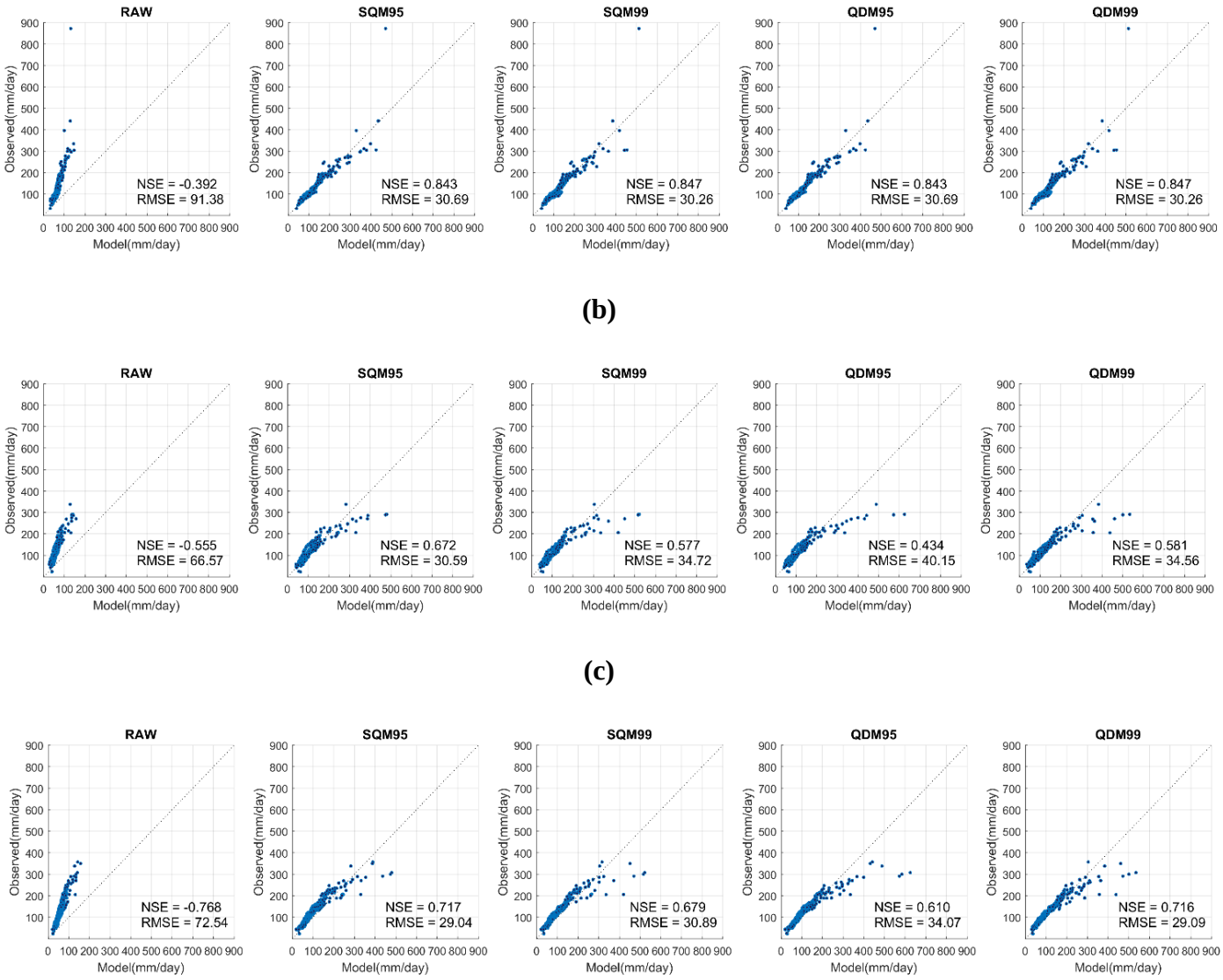

Figure 6-4 Scatter plots between the AMRs of the observed and the bias-corrected ERA-20c during (a) 1974–2010, (b) 1937–1973, and (c) 1910–1973 in 7 stations.

The bias-corrected ERA-20c was significantly overestimated in the upper tail in QDM approaches, as illustrated in Figures 6-4(b) and 6-4(c). The significant deviations in the top 5% of extremes between the observed (Δ_o) and modelled (Δ_m), which can be estimated from Eq. 6-3, were most likely responsible for the overestimation. Conceptually, the QDM begins with the premise that the relative change in the modelled precipitation over the reference and simulation periods is identical to these transformations of the observed. However, the relative changes for a few specific quantiles in the modelled were notably higher than the observed, especially for the high extremes, which can lead to the overestimation identified in Figure 6-4. More specifically, Figure 6-5 represents the

relative change in descending order of extreme rainfalls between the reference period (1974–2010) and the past period (1937–1973) for the observed and raw ERA-20c. The relative changes generally showed a similar trend with a ratio of around 1 in both the observed and modelled, but the large deviations were identified for high extremes. For example, the relative change of the highest rank at St.17 Daegu station was about 1.3 for the modelled, while the value for the observed was less than 1. Under the assumption of QDM approaches, the bias-corrected data for the past period increased by 1.3, leading to increased deviation in AMRs between the *in situ* and modelled data. Apart from the misrepresentation of high extremes, other aspects could also affect the differences. The significant inconsistency in the long-term trend, especially for the extreme in the first half of the 20th century, could also result in bias (Befort et al., 2016; Donat et al., 2016).

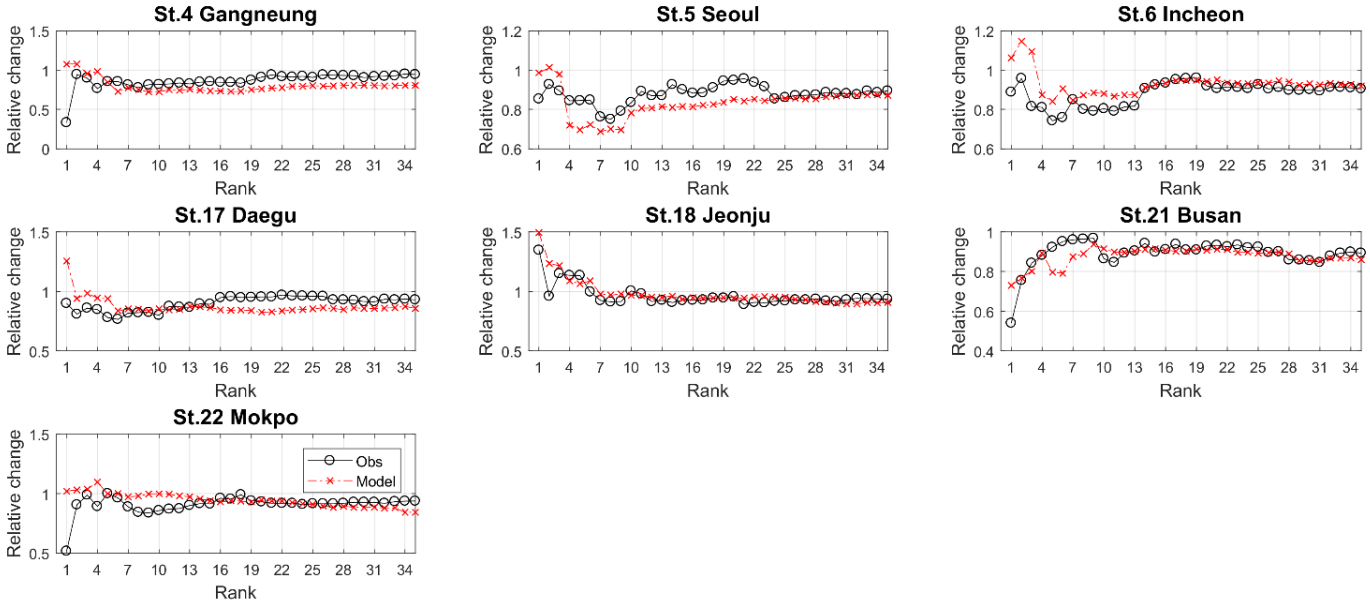

Figure 6-5 Relative changes in descending-ordered extreme rainfalls between the reference period (1974–2010) and the past period (1937–1973) for the observation (Obs) in 7 stations and the raw ERA-20c (Model) in the corresponding 7 grid points.

6.4.2 Uncertainty reduction in design rainfall using ERA-20c

Although the suggested QM approaches still have biases in the high extremes, the bias-corrected AMRs showed a significant reduction in bias across four different periods. Among the periods, the 1900-2010 period and the reference period (1974-2010) showed better performance than the other periods. Here, I explore changes in design rainfalls and their uncertainties in the context of a century precipitation data (i.e. the bias-corrected ERA-20c from 1900 to 2010). In many countries, the estimation of design rainfall is based on AMRs collected over a relatively short period of time and can lead to high uncertainty in estimating parameters for a given distribution. For this purpose, I evaluated the uncertainties of design rainfall with different return levels (30-year, 50-year and 100-year return periods) for both the observed and the bias-corrected ERA-20c by QDM approaches (QDM95 and QDM99) over 48 stations. Note that the uncertainties derived from the bias-corrected AMRs for the reference period (1974-2010) were named QDM95v1 and QDM99v1, respectively, and the uncertainties using the values from 1900 to 2010 were named QDM95v0 and QDM99v0, respectively. The uncertainty range of design rainfall for six stations (St. 5, St. 13, St. 21. St. 29, St. 37 and St. 43) for a representative experiment is illustrated in Figure 6-6. For the reference period, the median values of design rainfalls obtained from the bias-corrected ERA-20c are comparable to those of the observed while their uncertainty range is largely extended, except for Busan and Gumi stations. As seen in Figure 6-6, design rainfalls by the observed also have large uncertainties for the reference period. On the other hand, the uncertainty range of design rainfall using a century of precipitation data (QDM95v0 and QDM99v0) is much narrower than that for the reference period (QDM95v1 and QDM99v1). It is logical to assume that the uncertainty reduction in design rainfall is mainly attributed to the increase in sample size. Thus, despite a certain degree of errors, the long-term bias corrected rainfall has its own advantage in terms of the increase of the sample size, leading to an uncertainty reduction in design rainfall.

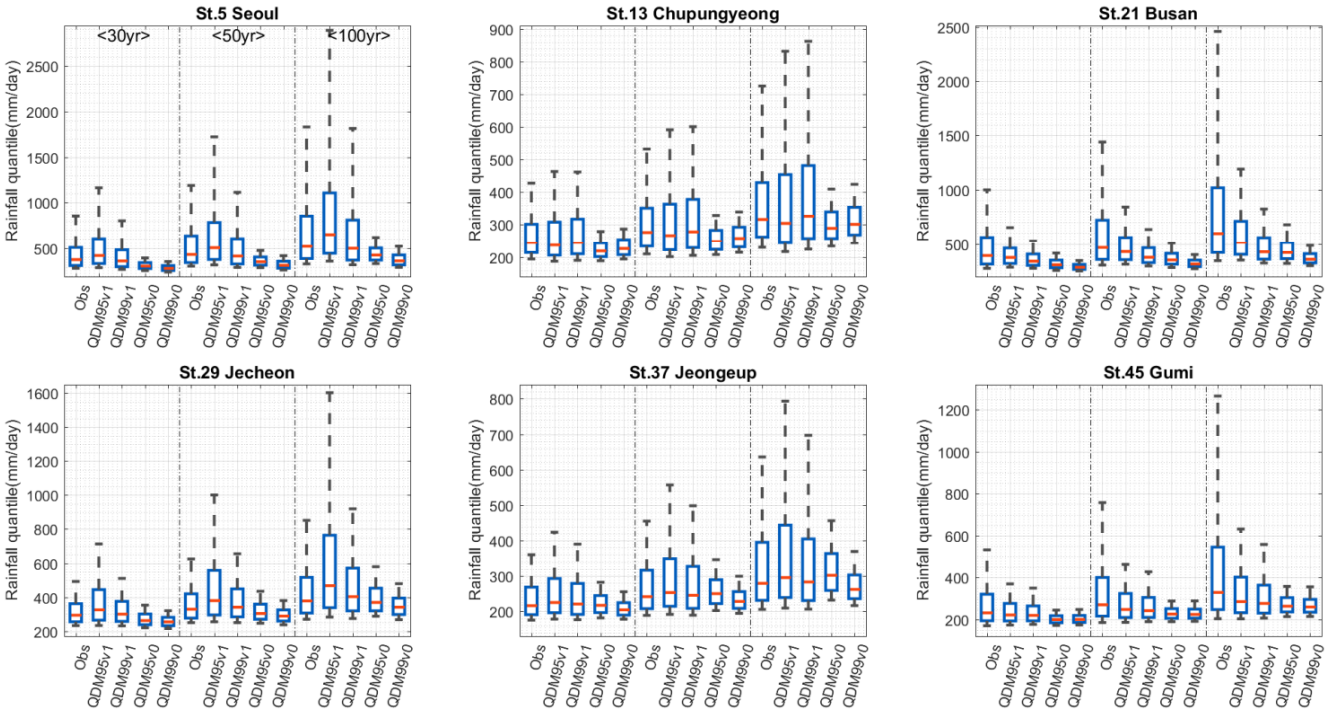

Figure 6-6 Boxplots of the uncertainties of design rainfalls with 30-year, 50-year, and 100-year return period for the observation (Obs) and the bias-corrected ERA-20c by QDM approaches in 6 stations (St.5 Seoul, St.13 Chupungyeong, St.21 Busan, St.29 Jecheon, St.37 Jeongeup, and St.45 Gumi). QDM95v1 and QDM99v1 represent the values estimated for the reference period (1974–2010), while QDM95v0 and QDM99v0 are derived from 1900 to 2010. Note that the ends of the whiskers in boxplots mean 9% and 91% of the simulated results by the MCMC approach.

The increase in uncertainty of design rainfall may be attributed to the GEV parameters, especially the shape parameter. This chapter assumes that use of long-term data could reduce the associated uncertainty. In this regard, I further explore the role of bias-corrected rainfall for uncertainty reduction in observation-based design rainfall in the context of prior information within a Bayesian framework. More specifically, the range of GEV parameters estimated from the bias-corrected century-long reanalysis data (QDM95v0 and QDM99v0) was considered the prior distribution for estimation of the distribution parameters within a Bayesian framework. That is, this chapter analysed the role of the prior distribution informed by the bias-corrected long-term reanalysis data on the uncertainty reduction in observation-based design rainfall. Three different cases for use of prior distributions were considered: (1) sole use of prior distribution for the shape parameter, (2)

use of prior distributions for both scale and location parameters, and (3) combined use of prior distributions for all three parameters within the QDMs. The first experiments with QDM95v0 and QDM99v0 were named Obs95a and Obs99a, respectively. The second experiments were named Obs95b and Obs99b, and the final experiments were named Obs95c and Obs99c, respectively. The comparison of three different experiments for the uncertainty reduction in design rainfall is illustrated in Figure 6-7. As shown in Figure 6-7, the median values are comparable over all cases presented, but a significant shrinkage of the uncertainty range is seen in most cases considering informative priors except for Obs95b and Obs99b in St.5. Among the three approaches, the combined use of prior distribution for all the parameters (Experiment 3) showed a greater reduction in uncertainty than either Experiment 1 or 2. More specifically, for St.5 Seoul, St.21 Busan and St. 45 Gumi, where the uncertainty range of design rainfall was exceptionally high, the degree of reduction in uncertainty for Experiment 1 (sole use of prior distribution for the shape parameter) is closely followed by that of Experiment 3, while Experiment 2 (use of prior distributions for the location and shape parameters) still has huge uncertainty. On the other hand, the reduction of uncertainty in the other three stations (St.13, St.29, and St.37) for Experiment 1 is nearly the same as that of Experiment 2. In these contexts, I conclude that the uncertainty reduction in design rainfall can be mainly attributed to the use of prior distribution for the shape parameter, informed by the long-term reanalysis data.

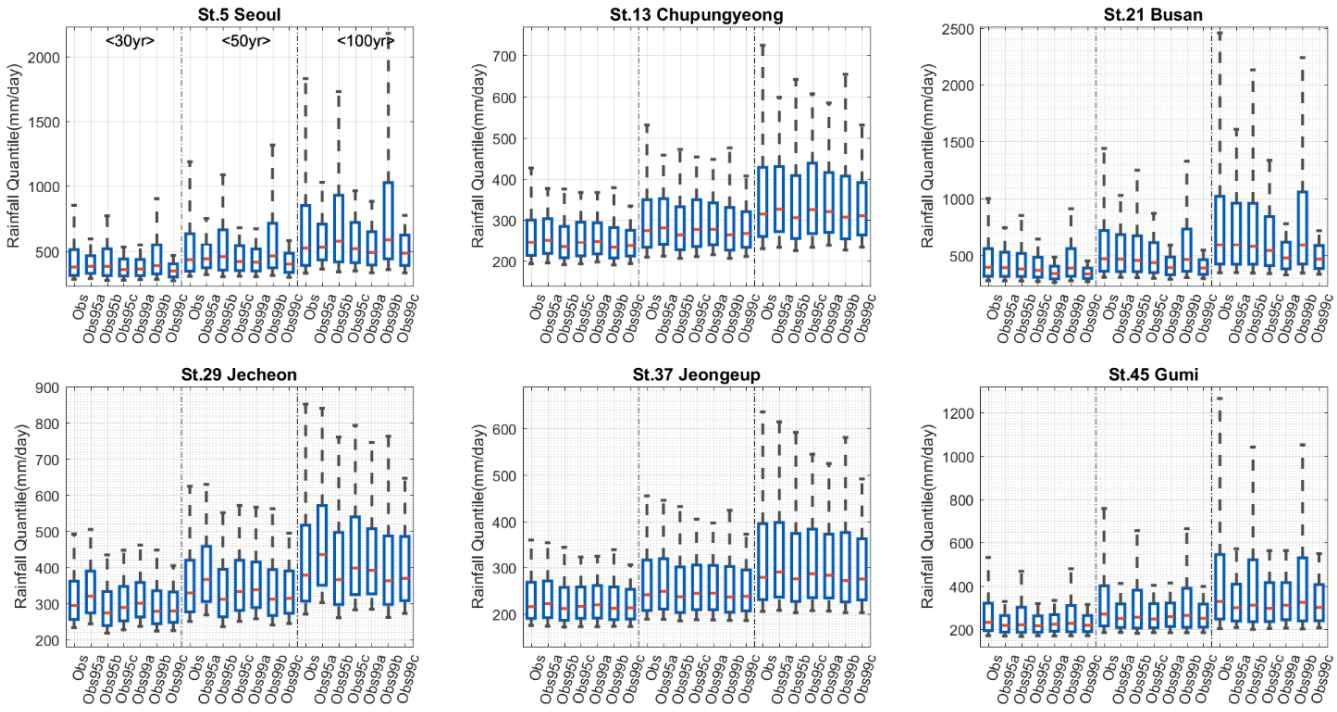

Figure 6-7 Boxplots of the uncertainties of design rainfalls with 30-year, 50-year, and 100-year return period for the observation using the prior information from the bias-corrected ERA-20c by QDM approaches in 6 stations (St.5 Seoul, St.13 Chupungyeong, St.21 Busan, St.29 Jecheon, St.37 Jeongeup, and St.45 Gumi). Here, Obs indicates the values based on the non-informative prior distribution; Obs95a and Obs99a were estimated by the shape parameter information from QDM95v0 and QDM99v0, respectively; Obs95b and Obs99b were based on the corresponding scale and location parameter information; and Obs95c and Obs99c were derived from the prior information of all parameters.

6.4.3 Spatio-temporal change in design rainfall

As the evaluation for IM-PCM approach has been done from 1973 to 2010 in Chapter 5, this chapter simply evaluated the spatial interpolation approach for ERA-20c within a leave-one-out cross validation scheme. The bias-corrected AMRs for the reference period of 1974–2010 were compared with the corresponding observation over 48 stations in terms of RMSE and NSE. In Figure 6-8, the result indicated that the bias-corrected AMRs were generally comparable to those from the observed, although slightly increased biases were observed, compared with the result in gauging stations in Figure 6-3(a). This analysis implies that the bias correction scheme based on a

set of interpolated parameters informed by the observed parameters could reliably provide spatially interpolated long-term data, especially for exploring changes in design rainfall. It should be noted that QDM and SQM have the same results for the reference period, and QM approaches with the 95th and 99th percentiles are labelled as QM95 and QM99 in Figure 6-8.

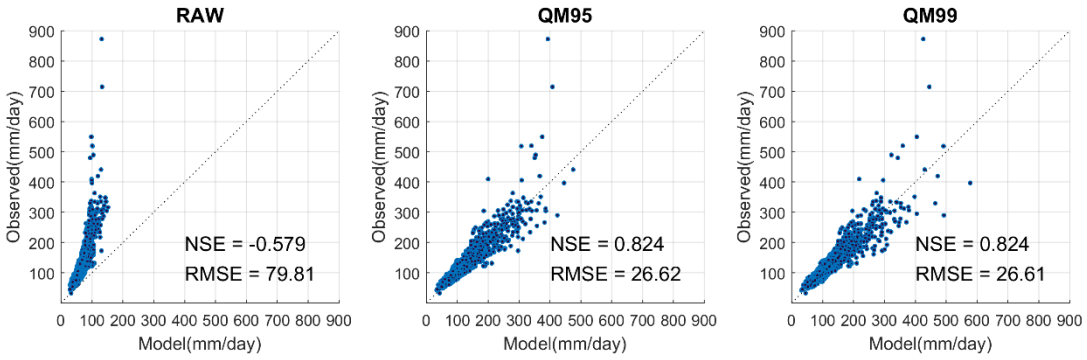

Figure 6-8 Scatter plots between the Annual maximum rainfalls of the observed and the bias-corrected ERA-20c by QM approaches (QM95 and QM99) over all 48 stations for the reference period (1974–2010). The results presented here are obtained by leave-one-out cross validation.

For exploration of spatio-temporal change in rainfall intensity over the 20th century, this chapter compared the relative change (%) in design rainfall between the observed for the reference period (1974–2010) and the modelled for three different periods (1900–1936, 1937–1973 and 1974–2010) as illustrated in Figures 6-9(a) to 6-9(c). For the reference period in Figure 6-9(a), the relative difference is generally limited within 10% in both QDM95 and QDM99 approaches, although the biases of particular areas slightly increase. The QDM99 shows better performance although the difference between the two approaches is not significant. Thus, the results based on the QDM99 are mainly considered for subsequent analysis on the spatial-temporal change in rainfall intensity over South Korea.

For the period from 1937 to 1973 as shown in Figure 6-9(b), changes in design rainfall vary spatially, and a noticeable change is observed in the southwest, suggesting a significant change in the rainfall intensity over the last three decades. On the other hand, an insignificant change in the rainfall intensity is identified in the other parts of South Korea for the period, compared with Figure

6-9(a). For the period of 1900–1936, the change in rainfall intensity relative to the current climate is illustrated in Figure 6-9(c), and reveals a similar pattern (i.e. negative values) over all areas, representing a noticeable increase in rainfall intensity over the last three decades over South Korea. This significant difference can imply the rainfall intensity change over time. However, reminding the errors remained in the heavy extreme values for the 1937–1973 period in Figure 6-4(b), it could be suggested that the gap may be attributed to not only the rainfall intensity change but also the errors in the bias-corrected AMRs. From these results, it can be concluded that the significant difference in rainfall intensity over different periods can lead to a misrepresentation of the design rainfall (or design flood) and are likely to misrepresent the flood risk, particularly at high return levels in the future. That is, this analysis implies that design rainfalls estimated by using bias-corrected model values based on a QDM method for a certain projected period (past or future) should be carefully interpreted in climate change impact studies.

Unlike the analyses in Figures 6-9(a) to 6-9(c), the AMRs over the entire period are used to explore the changes in design rainfall further, with that of the observed for the reference period (1974–2010), in Figure 6-9(d). As in the reference period in Figure 6-9(a), the overall relative changes in this period are similarly limited within 10%. However, the spatial distribution of relative change is slightly different from the changes based on the reference period from 1974 to 2010. More specifically, a negative change is more pronounced in the northern part of South Korea, confirming the role of the recent increase in rainfall intensity. However, a positive change remains in the south-western part of South Korea. This result implies that design rainfall estimated during the entire period can be significantly underestimated in broad areas of South Korea due to the recent increase in rainfall intensity, but conventional multi-decadal observation-based design rainfalls may also underestimate potential flood risk in some areas.

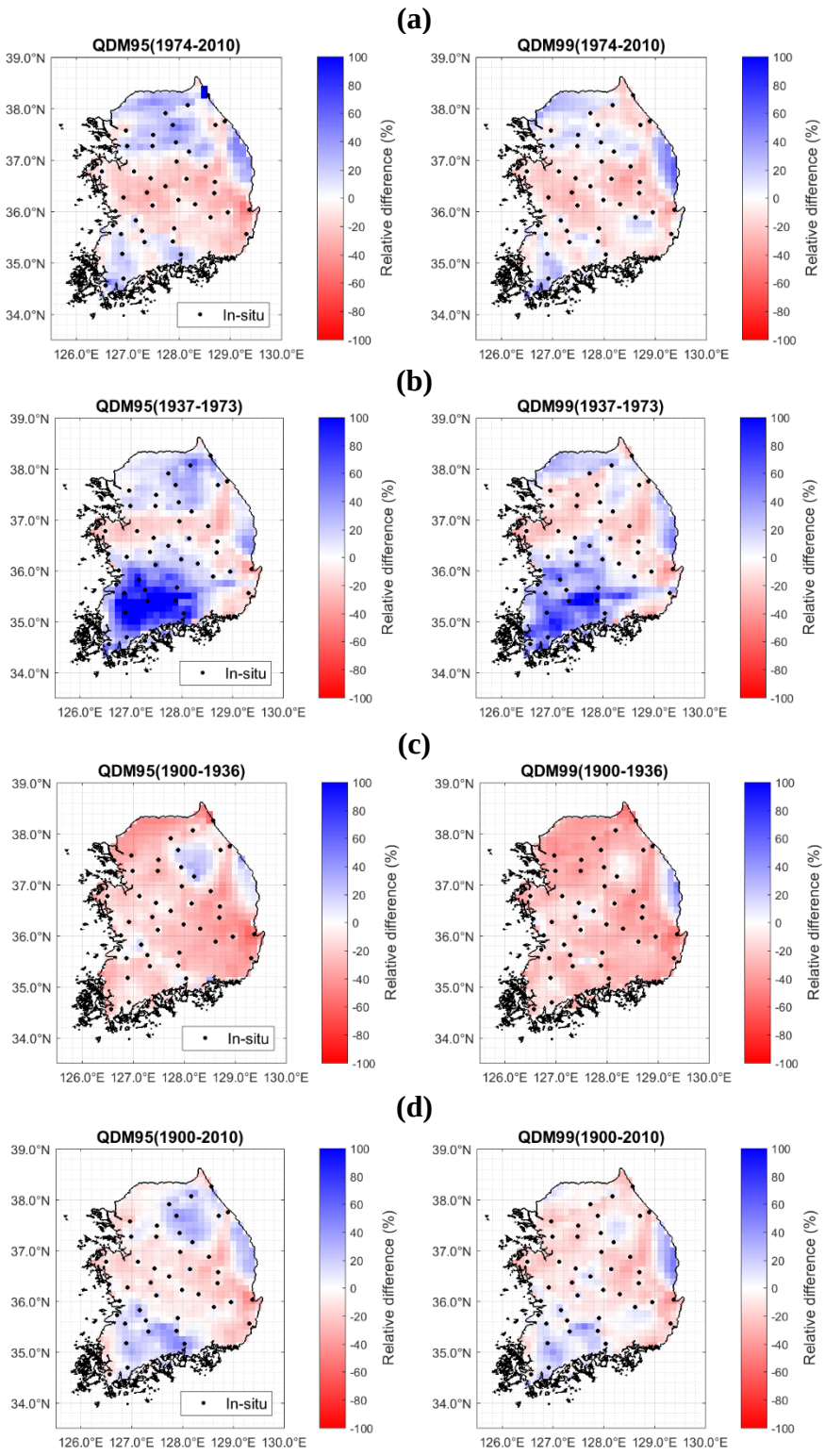

Figure 6-9 Relative change (%) in design rainfalls of the modelled data in four different periods, (a) 1974–2010, (b) 1937–1973, (c) 1900–1936, and (d) 1900–2010, compared with those of the observed for the reference period (1974–2010).

Estimating design rainfall in a certain area plays a vital role in managing the risk associated with water-related hazards. In many countries including South Korea, design rainfall is routinely estimated with limited data for a given return period exceeding the length of the data record for planning structural or non-structural measures. In this context, the estimated design rainfall can be significantly influenced by sampling error, leading to an increase in uncertainty. Numerous studies have shown that temporal change in extreme rainfall has been observed, and an increasing trend has been reported in many parts of the world (Jung et al., 2011; Mason et al., 1999; Park et al., 2011; Westra et al., 2014; Yilmaz et al., 2014). This nonstationarity in extreme rainfall is expected to continue in the future, and the current design practice may not be appropriate under the conditions. For this reason, guideline recommendations considering the potential impact of nonstationarity on either design rainfall or design flood have been proposed by various studies (Lawrence and Hisdal, 2011; Madsen et al., 2014; UK Environment Agency, 2017). These guidelines typically recommend employing a correction factor, corresponding to the expected change, in the estimation of design rainfall and design flood (Madsen et al., 2014). For instance, the Environment Agency (2017) in the UK recommended increasing the rainfall intensity from 5 % to 40% for the future period (2015–2115) over all of England and Wales. In Norway, a wider range of correction factors (0-40%) was similarly recommended for design flood (Lawrence and Hisdal, 2011). This approach may help to reduce the flood risk for a given region in a changing climate. However, in consideration of the wider range of uncertainty in design rainfall with the limited data as illustrated in Figure 6-6, the use of more extended data plays a crucial role in the reliable estimation of design rainfall with uncertainty reduction. Thus, the results of the proposed method in this thesis can be adopted as a reference in the decision-making process for climate change strategies such as flood prevention measurements.

6.5 Conclusions

The objective of this chapter was to effectively remove the bias in century-long ERA-20c data and to examine the impact of long-term data on design rainfall estimation in South Korea by using bias-corrected AMRs. In this context, this chapter first applied stationary and nonstationary QM approaches of using a composite distribution, referred to as QDM and SQM, respectively, to reduce

the biases. It then analysed the uncertainty change in design rainfall. More specifically, this chapter evaluated both the accuracy of bias-corrected AMRs and the uncertainty reduction in reanalysis-data-based design rainfalls within the Bayesian framework. Finally, this chapter explored the spatio-temporal changes in design rainfalls for the 20th century in South Korea. The major findings obtained in this analysis are summarised as follows:

1. QM approaches (i.e. SQM and QDM) are significantly effective in reducing the bias of daily precipitation from ERA-20c reanalysis data, and QDM approaches are more efficient than SQM schemes for the entirety of the 20th century, especially for AMRs. On the other hand, the validation results over different periods showed that the proposed bias correction scheme has a limitation in reproducing extreme values of each period. To be more specific, the AMRs during 1974–2010 are reasonably well reproduced and comparable with that of the observed data. However, the analysis for the past period (i.e. 1937–1973) indicated relatively significant biases. The deficiencies were mainly attributed to the mismatch of relative changes between the observed and modelled data in some high extreme quantiles (i.e. the top 5 events).

2. This chapter evaluated the uncertainties of design rainfalls with different return levels for both the observed data and bias-corrected ERA-20c using QDM approaches. The uncertainty range of design rainfall using century precipitation data is much narrower than that for the reference period (1974–2010) due to the increase in sample size. Thus, despite a certain degree of errors, the long-term bias-corrected rainfall has its own advantage in terms of the increase of the sample size, leading to uncertainty reduction in design rainfall. This thesis further explored the role of bias-corrected data for uncertainty reduction in design rainfall based on the observed data. This was done via three different experiments in the context of prior information within a Bayesian framework. A significant shrinkage in the uncertainty range is seen in most cases considering informative priors. This experimental analysis suggests that observation-based design rainfall can significantly reduce uncertainty by using prior distribution for the shape parameter, informed by the long-term reanalysis data.

3. There were significant changes in design intensity according to the periods (1900–1936, 1937–1973 and 1974–2010). More specially, the design quantiles for the 1900–1936 period were generally smaller than those by observation for the reference period. Meanwhile, the 1937–1973 period indicated a significant positive gap in southwest regions. The design rainfall

for the period of 1974-2010 had relatively small biases. The differences in design rainfalls may be attributed to both the biases which remained in the heavy extreme values for each period and the rainfall intensity change. This result implies that the design rainfalls estimated using bias-corrected model values based on a QDM approach for a certain projected period (past or future) should be carefully interpreted in climate change impact studies.

4. This chapter finally compared design rainfalls using the bias-corrected ERA-20c over the entire area for a given 100-year return period with those of the observation data for the reference period (1974–2010). The spatial distribution of relative change using the AMRs over the entire period is slightly different from the changes based on the reference period from 1974 to 2010. More specifically, a negative change is more pronounced in the northern part of South Korea, confirming that the recent increase in rainfall intensity should be considered in managing the risk associated with water-related hazards. However, positive changes remain in the south-western part of South Korea. These results imply that design rainfall estimated during the 1900–2010 period can be significantly underestimated in broad areas of South Korea. However, conventional multi-decadal observation-based design rainfall may also underestimate potential flood risk in some areas.

The findings obtained in this analysis provide a meaningful perspective on the use of long-term reanalysis data for uncertainty reduction in design rainfall. Furthermore, this analysis helps to better understand the long-term changes in rainfall intensity over the past century in South Korea, although design rainfall estimation was conducted under stationary assumption. In Chapter 7, this thesis deals with reanalysis-data-based nonstationary frequency analysis for estimating design rainfall.

CHAPTER 7 [1]Reanalysis-product-based nonstationary frequency analysis for estimating design rainfall

7.1 Motivation

In Chapter 6, this thesis carried out a trend-preserving bias correction scheme for century-long reanalysis daily precipitation and addressed the contribution of long-term data on design rainfall estimation. This chapter also discusses a similar issue, but it focuses more on nonstationary frequency analysis for estimating design rainfall.

As stated in Section 2.5, design rainfall plays a crucial role in planning a water-related infrastructure, and it has been commonly estimated from precipitation intensity-duration-frequency (IDF) relationship based on the historical records with the stationary assumption (Cheng and Aghakouchak, 2014; Li et al., 2017). However, recent researches have indicated that many regions over the world have experienced a pattern change of climatic extremes, especially for heavy rainfall (Alexander et al., 2006; IPCC, 2014). Remembering that a water-related project is designed under stationary condition in practice, the temporal change of extreme rainfalls (so-called 'nonstationarity') may significantly affect the safety of the infrastructure. In this context, Chapter 6 adopted a trend-preserving bias correction scheme, QDM, but the design rainfall analysis itself was carried out under the assumption that the distribution of the AMRs for the future period would be identical to those for the simulation period (1900–2010). However, since the long-term trend in extreme rainfalls may continue in the future, design rainfall under stationary condition can misrepresent the design rainfall which is linked to the flood risk in the future. That is, as an increasing trend in heavy rainfall can underestimate estimated future risk when an obvious trend exists in a target region, practitioners should consider this characteristic depending on time.

[1] Kim, D.-I., Han, D., and Lee, T., Reanalysis-product-based nonstationary frequency analysis for estimating extreme design rainfall. J. Hydrol. (in review)

As indicated in Chapter 6, the lack of data results in significant uncertainties in design rainfalls. In a BM approach, many regions (including South Korea) adopt less than 40- or 50-year AMRs for design rainfall estimation. Consequently, design quantiles produced by the AMRs must contain significant uncertainties, which are associated with sampling errors (Coles et al., 2003; Huard et al., 2010; Overeem et al., 2008; Tung and Wong, 2014; Van de Vyver, 2015). Moreover, the time-dependent nature of AMRs may not be sufficiently identified by the classic approach based on limited observations. For South Korea, Nadarajah and Choi (2007) showed that there was no clear evidence for the trend in the AMRs of the observed in 5 stations from 1961 to 2001. Meanwhile, other studies have indicated a clear increasing trend in summer rainfall (Cannon et al., 2015; Chang and Kwon, 2007; Choi et al., 2009; Eum and Cannon, 2017; Jung et al., 2011; Miao et al., 2016; Nahar et al., 2017). For these reasons, considering nonstationarity and extending the data length are critical factors for reliably preparing the future risk in areas such as South Korea where observation is limited. With this in mind, this chapter aims to reliably extend the data series, and it then seeks to explore South Korea's future risk change with the extended time series, which may depend on time (i.e. nonstationary condition).

As in Chapter 6, a QDM approach and SQM are applied for bias correction of reanalysis data. Since this chapter focuses on reanalysis-product-based nonstationary frequency analysis through the BM principle, I directly improve the AMRs of the reanalysis data without correcting all wet-day data as in Chapters 5 and 6. For nonstationarity, numerous studies have commonly adopted a time-varying parameter scheme (Cannon, 2010; Cunderlik and Burn, 2003; El Adlouni et al., 2007; Leclerc and Ouarda, 2007; Panagoulia et al., 2014; Son et al., 2017). Conceptually, this approach assumes that a climate variable like AMR has the same distribution function type (typically GEV distribution), but the parameters are dependent on time. Using the time-varying parameters, two main approaches have been performed to estimate design quantiles under nonstationary conditions: (1) the expected waiting time (EWT) approach and (2) the expected number of exceedance (ENE) approach (Du et al., 2015; Obeysekera et al., 2016; Read and Vogel, 2015; Salas et al., 2018; Salas ad Obeysekera, 2014). Both concepts are useful, but since the EWT method requires information beyond the design life of a project which can cause uncertainty (Du et al., 2015; Salas et al., 2018), this thesis carries out the nonstationary frequency analysis using the ENE interpretation.

7.2 Data

7.2.1 Local gauged data

To implement the QDM bias correction scheme, this chapter used 48 weather station data covering from 1974 to 2010, in South Korea as in Chapter 6. Since this chapter focuses on the AMR for estimating the design rainfall, only the AMRs of the *in situ* records for the period are derived from the KMA. To detect the time-dependent characteristic, the AMRs of the observed for the extended period of 1974–2017 are also adopted as well as for the period of 1974–2010. The weather stations chosen in this chapter are shown in Figure 7-1 and the detailed information about the stations is described in Table 5-1.

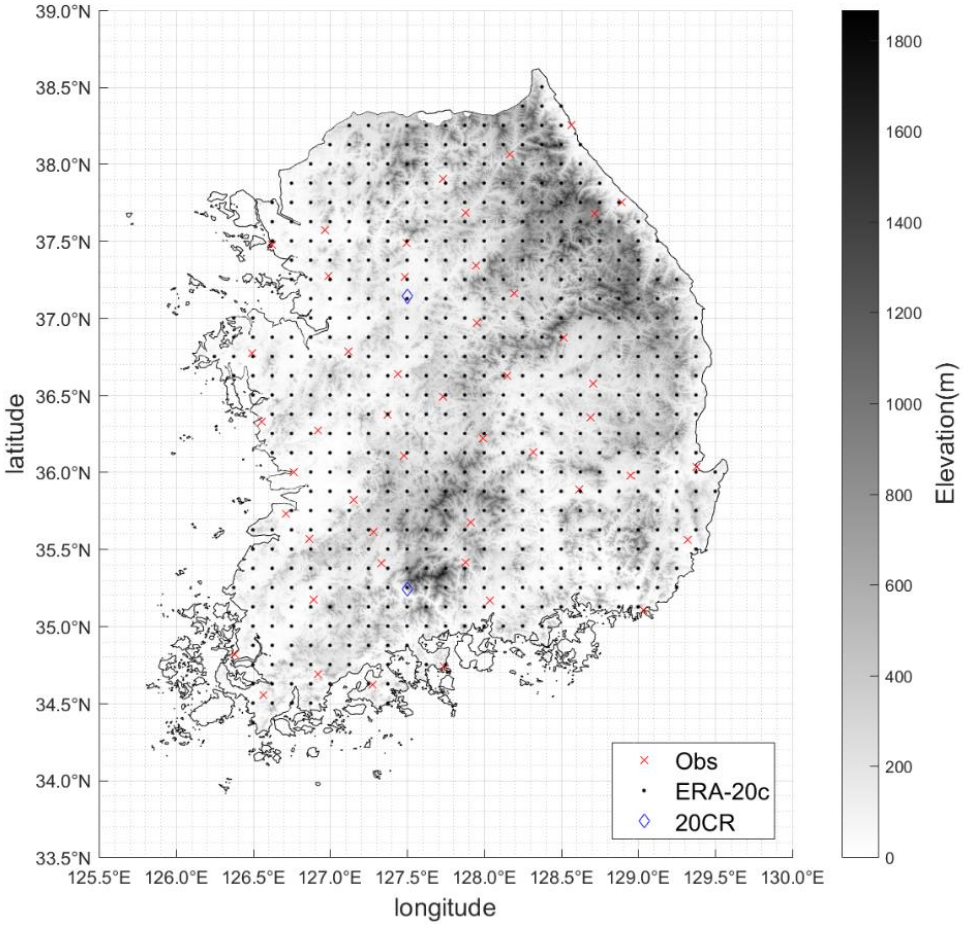

Figure 7-1 A map showing the study area, local gauging stations, grid points of ERA-20c and 20CR in Chapter 7. The grey shading on the map indicates elevations.

7.2.2 Reanalyses: ERA-20c and 20CR

In this chapter, I apply two representative century-long reanalysis products as ERA-20c by the ECMWF and 20CR by the NOAA. To confirm the significance of the long-term trend derived from the modelled data, I chose not only ERA-20c but also 20CR. As stated in Section 4.2.2, ERA-20c was produced by assimilation technique using observations of surface pressure and surface marine winds only, and the products can globally cover the period from 1900 to 2010 with the spatio-temporally various resolutions (Poli et al., 2016). On the other hand, 20CR, the first century-long reanalysis products by the NOAA, was assimilated with the Ensemble Kalman Filter technique using only surface pressure observations (Compo et al., 2011) and the latest version 2c could span the period from 1851 to 2014 with a spatial resolution of 1.875° ×1.9°. As the long-term climate records play an important role in the nonstationary analysis, this chapter collects daily rainfall data from these two century-long reanalysis products. More specifically, I extracted the daily precipitation records from 1900 to 2010 with the finest spatial resolution, 0.125° × 0.125° for ERA-20c and 1.875° × 1.9° for 20CR, respectively. From these daily rainfall series, this chapter derived the AMRs at grids in the mainland of South Korea from 1900 to 2010. The grid points over the sea were ignored in this analysis. The specific grid-scale points for ERA-20c and 20CR are shown in Figure 7-1. Note that only two grid points of 20CR covered the entire of South Korea due to its low spatial resolution.

7.3 Methodology

7.3.1 Bias correction

In design rainfall estimation, the BM approach using the AMRs is commonly adopted. To implement the reanalysis-products-based BM approach, bias-corrected AMRs should be collected. There are two approaches for it. Firstly, ones can correct all wet-day precipitation data by QM methods and then take the AMRs from the bias-corrected daily values as in Chapters 5 and 6. The other option is to directly improve the uncorrected AMRs by QM methods without considering the other rainfall data. If modellers are interested not only in AMRs but also in all daily rainfalls, it would be better to apply the first option. However, as this chapter only focuses on exploring the

nonstationary design rainfalls based on the BM, I utilise the latter option, which can reduce the error more efficiently than correcting the entire rainfall series (Li et al., 2017).

For the bias correction of the AMRs, this chapter applies parametric QM approaches based on a heavy-tailed single distribution. As this chapter requires the corrected AMRs only, the composite distribution proposed in Chapters 5 and 6 is not considered in the bias correction process. To find out the most fitted transfer function, I applied three representative distributions, gamma, Gumbel, and GEV, which have been commonly employed in a hydrological application and extreme study (Kim et al., 2015b; Koutsoyiannis, 2004; Rabiei and Haberlandt, 2015; Wilson and Toumi, 2005). As a QM approach is based on a one-to-one relationship, this chapter matches 48 weather stations with the closest grid points of the ERA-20c and 20CR, and the bias-corrected values are collected at each station. Here, I assumed that the difference of spatial resolution between datasets could be ignored.

For the bias correction for the period of 1900–2010 beyond the time range of the observation, this analysis applied the QDM approach described in Section 6.3.1. As in Chapter 6, I first set the reference period to 1974–2010, and then divided reanalysis data into three time periods with the same length (1900–1936, 1937–1973, and 1974–2010). The raw model data in each time period were improved by the QDM principle in Eq. 6-2 to 6-4. Here, the QDM schemes with three distributions, GEV, gamma, and Gumbel for estimating the CDFs in Eq. 6-2 to 6-4 were named as gevQDM, gamQDM, and gumQDM, respectively. For comparison, the conventional approach, SQM, is also implemented with the assumption that the climate records are stationary for the whole projected period. For SQM, the years from 1974 to 2010 were set as the reference period, while the whole period from 1900 to 2010 was considered as the simulation period in Eq. 6-1. Some heavy extreme values beyond the range of the reference period were also corrected by a constant extrapolation, which uses the correction values at the lowest and highest quantiles of the calibration range, suggested by Themeßl et al. (2012) as in Chapter 6. Note that the SQM approaches with the GEV, gamma, and Gumbel were abbreviated as gevSQM, gamSQM and gumSQM, respectively. Since the AMRs of the reanalysis datasets were directly corrected, a cut-off threshold for removing 'drizzle effect' was not considered in both SQM and QDM approaches.

For the distribution selection, this chapter uses the RMSE and NSE which are shown in Eq. 5-1 and 5-2. In this analysis, I compared the bias-corrected AMRs by QM approaches with the

observations in 48 stations for the reference period (1974-2010). As the results by QDM approaches are identical to those by SQM schemes for the reference period, the QDM results were used to evaluate the performances of three different curves for the bias correction scheme.

7.3.2 Detecting nonstationarity: Long-term trend test

As stated in Section 7.1, the conventional approach for bias correction is based on the stationary condition for climate model records, but the real climate may follow the nonstationary feature in terms of century-long trend. To find out the significance of the AMR trend over South Korea, this thesis evaluated the long-term trends of the observation and the bias-corrected reanalysis data. For the trend test, a non-parametric method, the Mann-Kendall test, was applied in this chapter. The significance of trends was evaluated by comparing the test statistic Z with the standard normal variate at the desired significance (Hamed and Rao, 1998), as shown in Eq. 4-5. When $|Z| > Z_{1-\alpha/2}$ for the standard normal deviate $Z_{1-\alpha/2}$ with the significance level α (= 0.05 in this analysis), the null hypothesis is rejected and a significant trend in a time series. For the slope, Theil-Sen approach (Sen, 1968; Theil, 1950) defined by the median among the ranked slope estimates is applied as described in Eq. 4-6.

This chapter first analysed the trends of the AMRs taken from both the observation and the bias-corrected reanalysis data for the reference period (1974–2010). For observation, the more extended data from 1974 to 2017 were also explored. Regarding the nonstationarity over the 20th century, this chapter tested the century-long trends of the bias-corrected AMRs from 1900 to 2010.

7.3.3 Rainfall frequency analysis with nonstationary condition

As addressed in Section 7.1, time-varying parameter schemes have been commonly adopted for nonstationarity analysis in hydrometeorological applications (Du et al., 2015; Leclerc and Ouarda, 2007; Ouarda and El-Adlouni, 2011; Panagoulia et al., 2014; Salas and Obeysekera, 2014; Son et al., 2017). As GEV family is typically applied for estimating design rainfalls based on the BM method in practice, I applied a GEV distribution with the time-varying location parameter(μ_t) while scale (σ) and shape (ξ) parameters set as constant. The location parameter is assumed as a time-depending linear function described in Eq. 7-1, and under the nonstationary condition, the CDF of GEV is described as Eq. 7-2.

$$\mu_t(t) = \mu_s t + \mu_i \tag{7-1}$$

$$F_z(z, \theta_t) = exp\left\{-\left[1 + \xi\left(\frac{z - \mu_t}{\sigma}\right)\right]^{-\frac{1}{\xi}}\right\} \tag{7-2}$$

Here, μ_i and μ_s are the interception and the slope of the location parameters, respectively, and $\theta_t = \{\mu_t, \sigma, \xi\}$ represents the time-varying parameter set of the GEV distribution.

To quantify the parameters for the GEV curve under nonstationary condition, this thesis applies the Bayesian principle suggested by Cheng et al. (2014). In this scheme, numerous parameter sets are estimated from the joint posterior distribution using the Differential Evolution Markov chain (DE-MC), which is based on the genetic algorithm differential evolution for global optimisation with the Markov Chain Monte Carlo (MCMC) principle (Cheng et al., 2014). In Eq. 2-10, the joint posterior distribution function $p(\boldsymbol{\theta}|\mathbf{R})$ can be formulated by combining the GEV likelihood function and prior distribution as follows:

$$p(\boldsymbol{\theta}|\mathbf{R}) \propto \prod_{i=1}^{n} GEV(\mathbf{R}|\mu_t, \sigma, \xi) \tag{7-3}$$

The posterior distribution for the parameters was obtained by maximising the joint posterior distribution as illustrated in Eq. 7-3, via MCMC scheme. Note that normal distributions are used for priors of parameters, and the prior distributions for all parameters are assumed to be independent (Cheng et al., 2014). Further information can be found in Cheng et al. (2014).

With the time-varying parameter chains, the next step is to estimate the return period for a given design quantile under nonstationary condition. As stated in Section 2.5, there were two main approaches to handle it: (1) the expected waiting time (EWT) method and (2) the expected number of exceedance (ENE) method (Du et al., 2015; Obeysekera and Salas, 2016, 2014; Read and Vogel, 2015; Salas et al., 2018; Salas and Obeysekera, 2014).

The EWT interpretation starts from estimating the probability for the first occurrence exceeding a design rainfall (z_{q0}). Under the nonstationary condition, the exceedance probabilities (p_t) are time-varying, and the first occurrence exceeding the design quantile (z_{q0}) at time x is described as follows (Du et al., 2015; Salas et al., 2018; Salas and Obeysekera, 2014):

$$f(x) = P(X = x) = (1 - p_1)(1 - p_2)(1 - p_3)\cdots(1 - p_{x-1})p_x$$
$$= p_x \prod_{t=1}^{x-1}(1 - p_t), \qquad x = 1, 2, \cdots, \infty \tag{7-4}$$

The expected waiting time for the first event exceeding z_{q0}, i.e. return period (T), is obtained as follows:

$$T = E(X) = \sum_{x=1}^{\infty} xf(x) = \sum_{x=1}^{\infty} xp_x \prod_{t=1}^{x-1}(1 - p_t) \tag{7-5}$$

Unlike the EWT scheme, the ENE approach focuses on the expected number of exceedances over the design life *T*. The number of events (*Y*) exceeding the design rainfall (z_{q0}) in *T* years can be expressed as follows (Du et al., 2015; Salas et al., 2018):

$$Y = \sum_{j=1}^{T} p_t \tag{7-6}$$

The return period (*T*) for the first event exceeding the design quantile (z_{q0}) can be numerically estimated by applying *Y* = 1 in Eq. 7-6. Here, the exceedance probability (p_t) corresponding to the design quantile (z_{q0}) is expressed for the GEV distribution as follows:

$$p_t = 1 - exp\left\{-\left[1 + \xi\left(\frac{z_{q0} - \mu_t}{\sigma}\right)\right]^{-\frac{1}{\xi}}\right\} \tag{7-7}$$

Both the EWT and ENE are applicable for nonstationary events, but the EWT approach has a drawback of conceptually requiring information beyond the design lifetime of a certain infrastructure in order to numerically solve the problem (Du et al., 2015; Salas et al., 2018). For this reason, this thesis adopts the ENE interpretation for estimating the design quantile (z_{q0}) with the return period from 10-year to 200-year.

In the proposed approach, four parameters (μ_s, μ_i, σ, and ξ) of a GEV distribution are required to estimate design rainfalls under nonstationary condition. By using the Bayesian principle in Eq. 7-3, I have collected the time-varying parameter sets ($\mu_{s,m}$, $\mu_{i,m}$, σ_m, and ξ_m) based on the bias-corrected AMRs of ERA-20c and 20CR from 1900 to 2010. However, as the bias-corrected values may still have errors of a certain magnitude, the future risk estimation by the model parameters are also able to misrepresent the future risk. On the other hand, the conventional approach based

on the observations may not sufficiently represent the long-term change of the AMRs due to the lack of data in certain regions including South Korea. For this reason, despite the errors, I carried out nonstationary design rainfall estimation by using all parameter sets ($\mu_{s,m}$, $\mu_{i,m}$, σ_m, and ξ_m) derived from the bias-corrected AMRs of ERA-20c and 20CR in 48 stations. More specifically, this chapter explored the design quantiles with return period from 10-year to 200-year by applying the median and 90% confidence interval of the four parameter chains generated by Eq. 7-3. Note that in this analysis, I considered 2011 the beginning year (t_1) for a target return period in Eq. 7-6. A flowchart for the nonstationary analysis is illustrated in Figure 7-2.

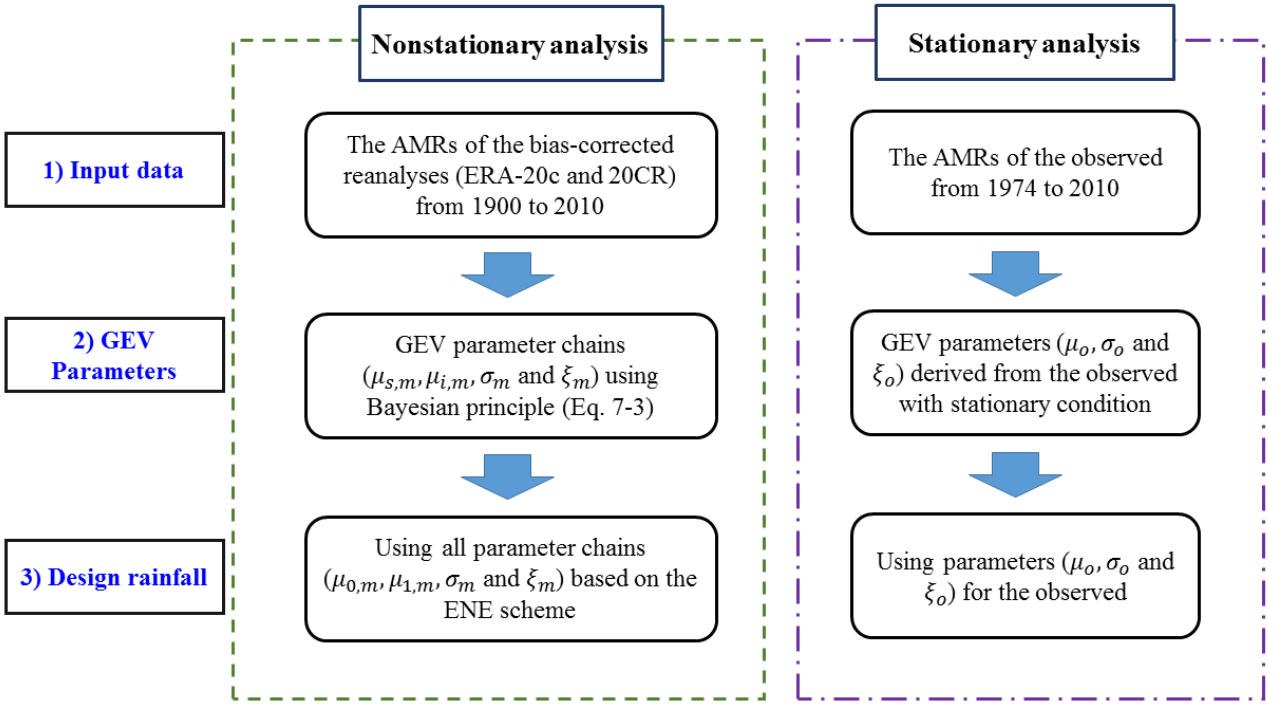

Figure 7-2 A flowchart for estimating design rainfall with the nonstationary condition and stationary condition.

Using the nonstationary interpretations over 48 stations, this chapter finally explores the spatial change in design rainfall with a 100-year return period over South Korea. After interpolating design rainfalls for the nonstationary model and the stationary model based on a scattered data interpolation method in Matlab (Amidror, 2002), this thesis spatially assesses the relative change (RC, %) of the modelled design rainfalls compared with the conventional values by Eq. 6-7. Here, design rainfalls for the nonstationary models are estimated from the median values of parameter

chains for GEV distribution, while the classic design rainfalls are obtained from the observed for the reference period (i.e. 1974–2010).

7.4 Results and discussion

7.4.1 Bias correction

To improve the uncorrected AMRs of ERA-20c and 20CR, I applied QM approaches based on three different distributions (i.e. gamma, Gumbel and GEV). The overall bias-corrected values over 48 stations for the reference period (1974–2010) were assessed by RMSE(mm) and NSE as illustrated in Figure 7-3 and Table 7-1. Conceptually, the bias-corrected values by QDM and SQM methods with the same distribution are identical for the reference period. Thus, the outputs by three different distributions were denoted as gevQM, gamQM, and gumQM. The overall comparison between the observed and the modelled indicated the significant reduction of errors in all QM schemes. The result showed that GEV distribution performed the best in both ERA-20c and 20CR. The bias-corrected ERA-20c by gevQM had 17.56mm for RMSE and 0.924 for NSE, while the values by gamQM and gumQM were from 22.34mm to 26.08mm for RMSE and from 0.831 to 0.876 for NSE. For 20CR, the model efficiency by gevQM with 20.63mm for RMSE and 0.894 for NSE dominated those by gamQM and gumQM with from 22.46mm to 26.86mm for RMSE and from 0.821 to 0.875 for NSE.

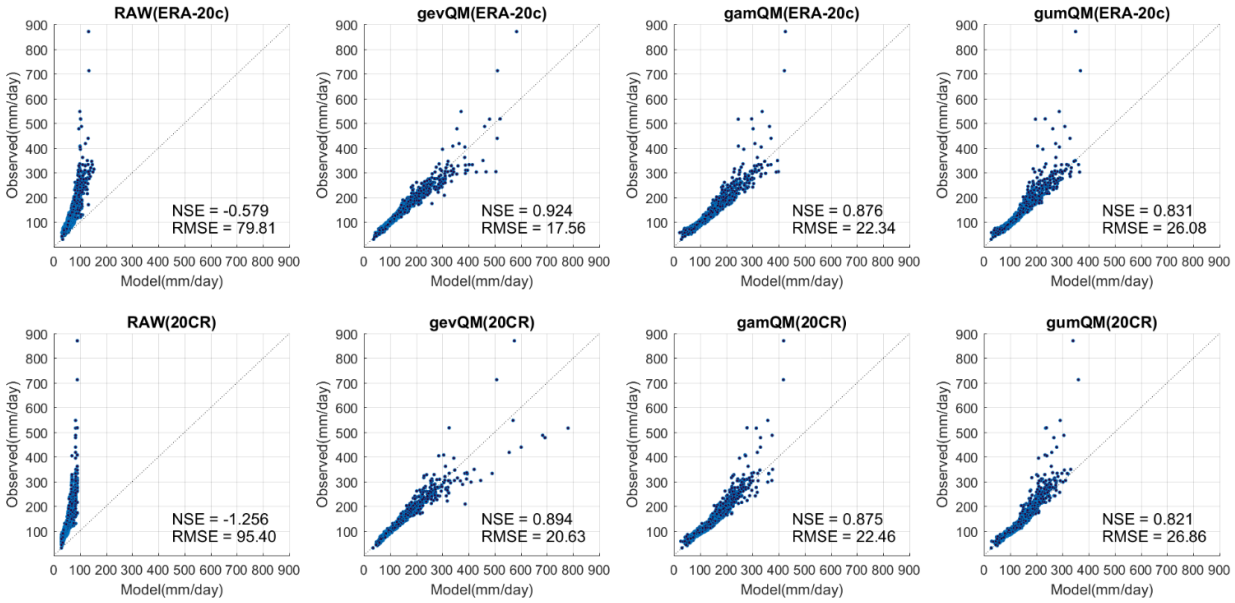

Figure 7-3 Scatter plots between the AMRs of the observation and the model data [the raw reanalyses (RAW(ERA-20c) and RAW (20CR)) and the bias-corrected reanaylses (i.e. ERA-20c and 20CR) by the QM approaches with GEV, gamma and Gumbel distributions (gevQM, gamQM, and gumQM)] over 48 stations from 1974 to 2010.

Table 7-1 Error estimation results of RMSE(mm) and NSE for the uncorrected (RAW) ERA-20c and 20CR, and the bias-corrected reanalyses (i.e. ERA-20c and 20CR) by the QM approaches with GEV, gamma, and Gumbel distributions (gevQM, gamQM, and gumQM)] over 48 stations from 1974 to 2010.

Method	ERA-20c		20CR	
	RMSE (mm)	NSE	RMSE (mm)	NSE
RAW	79.81	-0.579	95.40	-1.256
gevQM	17.56	0.924	20.63	0.894
gamQM	22.34	0.876	22.46	0.875
gumQM	26.08	0.831	26.86	0.821

To spatially evaluate the performance, this thesis also implemented the error estimation in individual stations as shown in Figures 7-4 and 7-5 for NSE and RMSE, respectively. Figure 7-4 illustrates NSE values for the AMRs of the bias-corrected ERA-20c and 20CR based on QM approaches (i.e. gevQM, gamQM and gumQM) in 48 stations, whereas Figure 7-5 indicates RMSE values. The model efficiencies were generally over 0.8 for NSE in all model values except a few stations. For RMSE, the most error estimates were less than 30 mm, which indicates the significant reduction of the bias. In order to clarify the range of the model values, this thesis used a boxplot scheme based on the individual error estimates in 48 stations as illustrated in Figure 7-6 and compared the mean values of the error estimation results in individual stations as described in Table 7-2. The boxplot for NSE in Figure 7-6(a) indicated that the median values were over 0.9 in all QM approaches and the most values were within the range from 0.6 to 1. Especially, gevQM for ERA-20c showed the best efficiencies among three QM schemes, whereas for 20CR, gevQM and gamQM had a better performance than gumQM. The analysis on RMSE also showed a similar result (Figure 7-6(b)). The median values were generally within 10 to 15mm in all bias-corrected values. gevQM for ERA-20c performed the best, and gevQM for 20CR and gamQM for ERA-20c and 20CR closely followed. In terms of the mean, gevQM for ERA-20c showed the best efficiencies with 14.30mm for RMSE and 0.933 for NSE as described in Table 7-2. For 20CR, NSE values for gevQM and gamQM were similar but RMSE for gevQM, 16.69mm, was slightly smaller than that of gamQM, 17.48mm. These results suggest that the applied QM approaches can significantly reduce the error in the AMRs of reanalyses (i.e. ERA-20c and 20CR), and among three different transfer functions, GEV distribution could be the best option for bias correction of the AMRs, especially for ERA-20c.

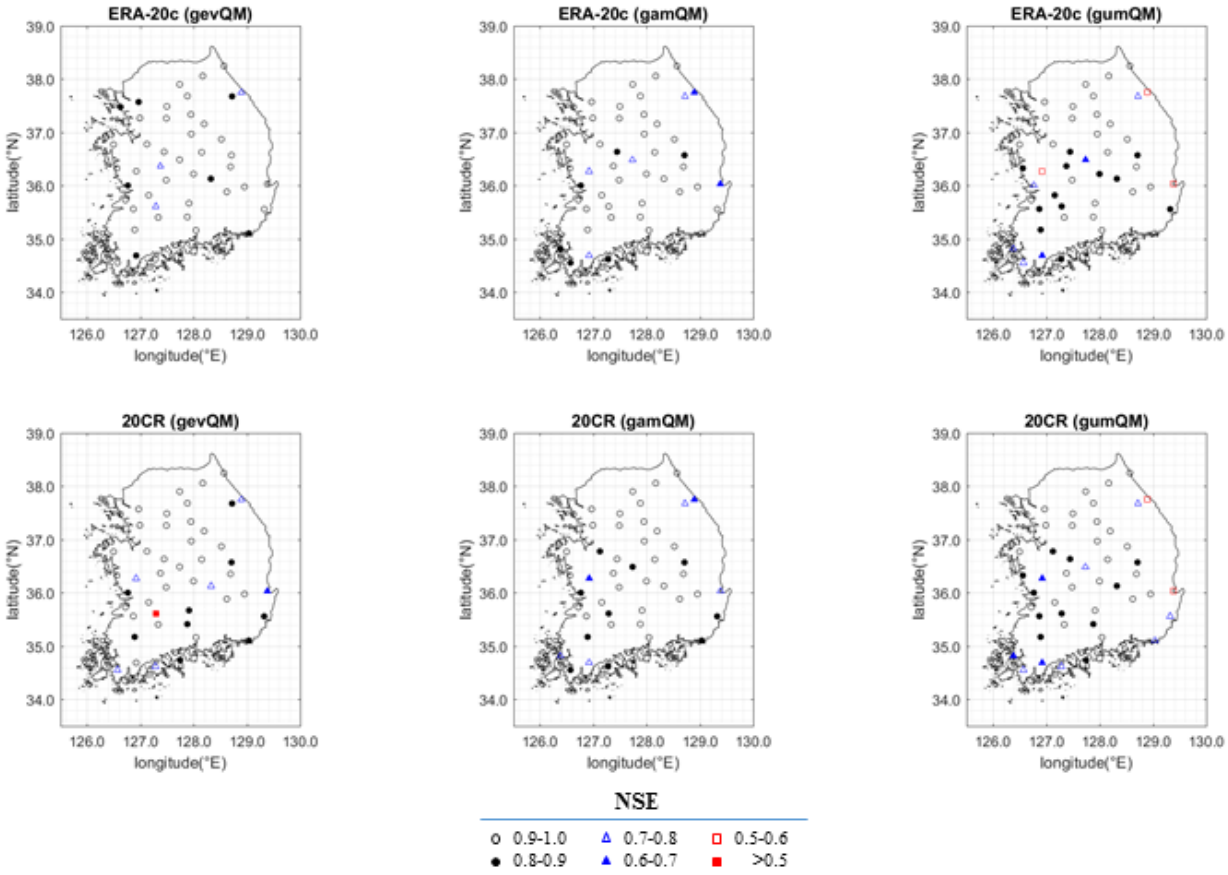

Figure 7-4 NSE results for the AMRs of the bias-corrected ERA-20c (above) and 20CR (bottom) by QM approaches (gevQM, gamQM, and gumQM) in 48 stations for the reference period (1974–2010).

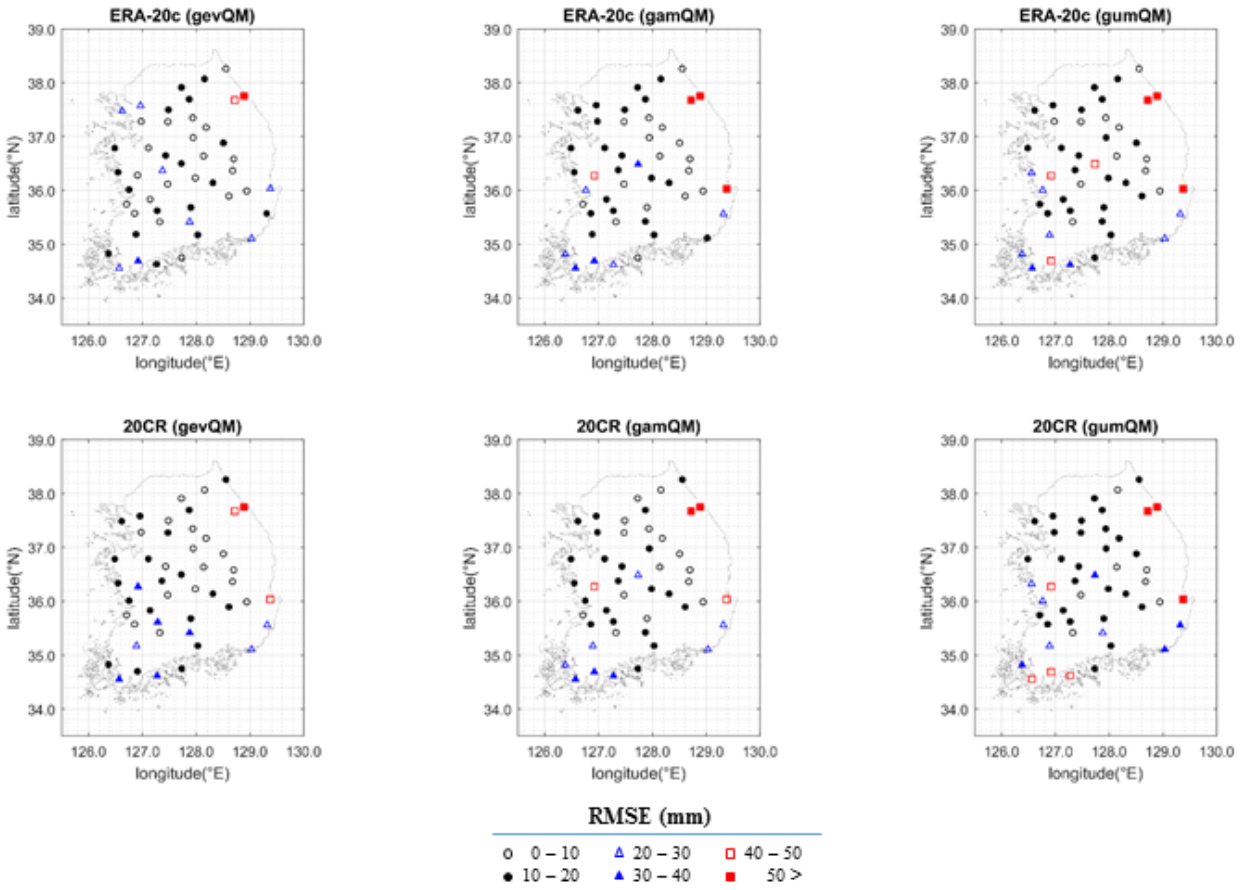

Figure 7-5 RMSE (mm) results for the AMRs of the bias-corrected ERA-20c (above) and 20CR (bottom) by QM approaches (gevQM, gamQM and gumQM) in 48 stations for the reference period (1974–2010).

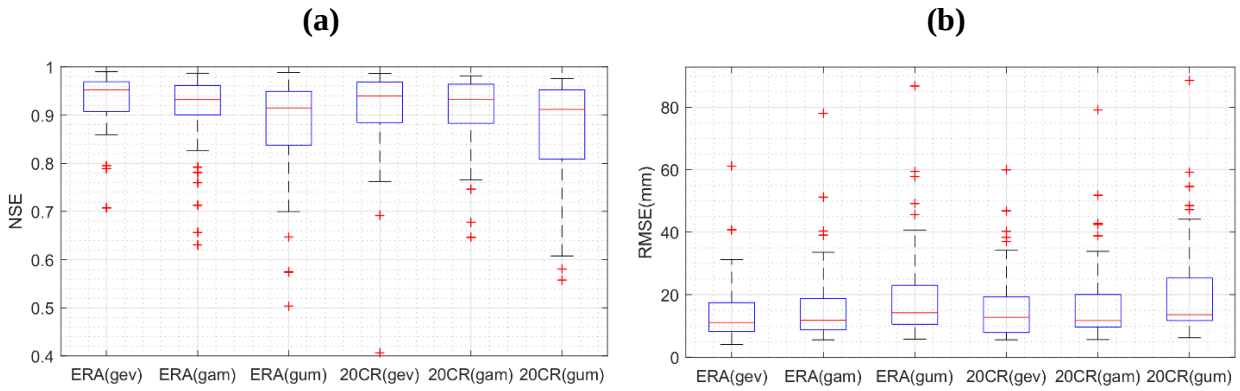

Figure 7-6 Boxplots of (a) NSE and (b) RMSE (mm) results for the AMRs of the bias-corrected ERA-20c (ERA) and 20CR by QM approaches with GEV (gev), gamma (gam), and Gumbel (gum) distributions in 48 stations from 1974 to 2010.

Table 7-2 Mean of error estimation results (RMSE(mm) and NSE) for the AMRs of the bias-corrected ERA-20c and 20CR by the QM approaches with GEV, gamma, and Gumbel distributions (gevQM, gamQM, and gumQM) in 48 stations from 1974 to 2010.

Method	ERA-20c		20CR	
	RMSE (mm)	NSE	RMSE (mm)	NSE
gevQM	14.30	0.933	16.69	0.905
gamQM	17.29	0.909	17.48	0.907
gumQM	20.31	0.871	21.09	0.864

7.4.2 Long-term trend

To consider the nonstationary condition in rainfall frequency analysis, the long-term trend of the AMRs should be necessarily detected. For this purpose, this thesis analysed the long-term trend of AMRs for the observed (Obs) and the bias-corrected for the reference period (i.e. 1974–2010) using a non-parametric method, the Mann-Kendall test, as shown in Figure 7-7. To further evaluate the observed trend, this chapter additionally analysed the AMRs of the observation for an extended period, from 1974 to 2017 (Obs0). The results in both Obs and Obs0 had no significant trend at the 0.05 significant level except a few stations. More specifically, among 48 stations, only five stations for Obs and two stations for Obs0 presented a significant trend, respectively. The performances for the bias-corrected reanalyses showed similar results. The AMRs of the bias-corrected reanalysis data (ERA-20c and 20CR) by QM approaches as well as the raw values (RAW) had no significant trends at the 0.05 significance level in all comparisons. These results suggest that the recent 40 years' data do not illustrate any significant data in the observation as well as in the reanalysis data.

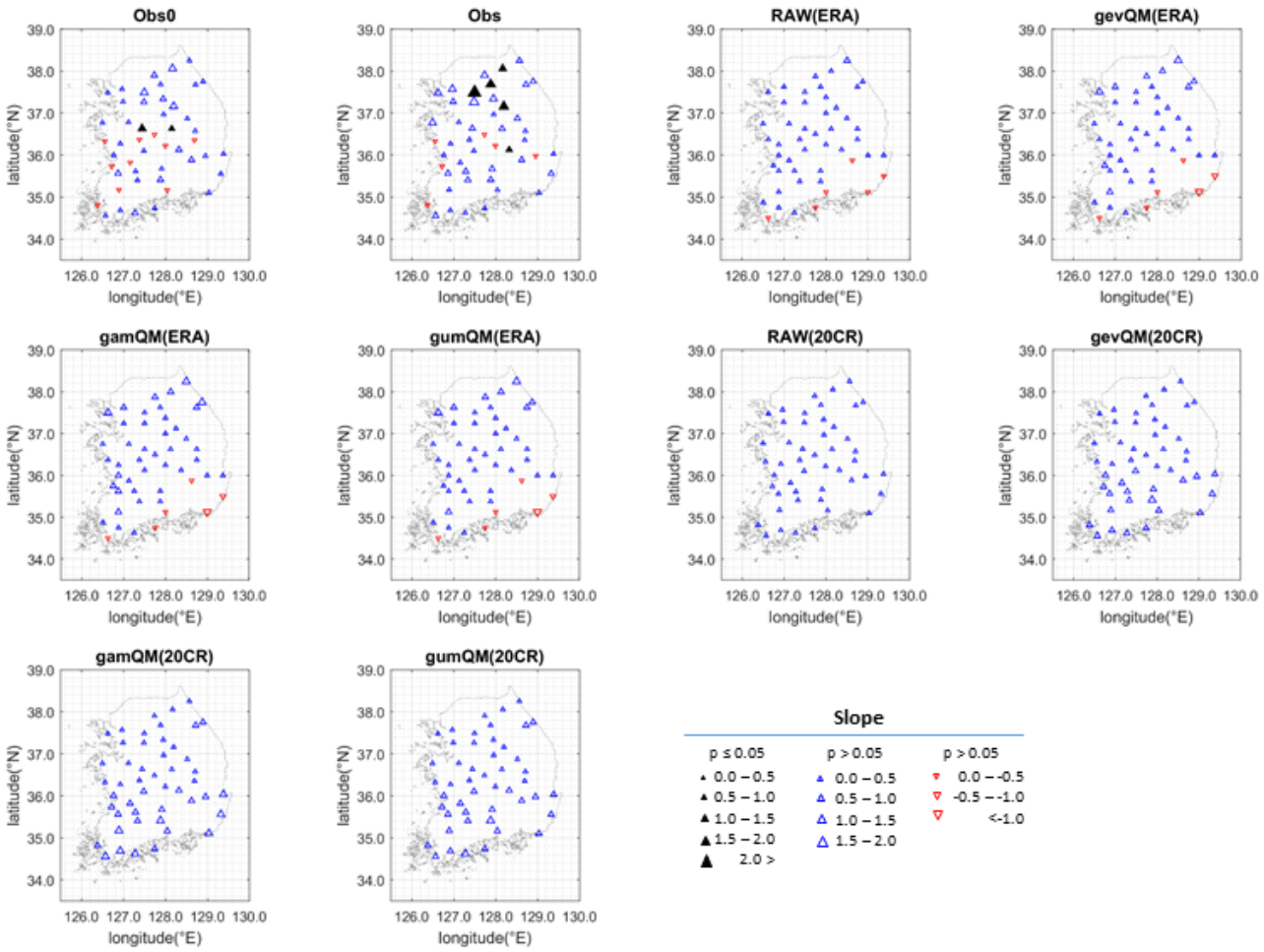

Figure 7-7 Trends in the AMRs of the observation for 1974–2017(Obs0) and 1974–2010(Obs), respectively, and the AMRs of the raw reanalyses (RAW) and the bias-corrected values by QM approaches (gevQM, gamQM, and gumQM) for the reference period (1974–2010). ERA and 20CR mean the data from the ERA-20c and 20CR in this figure. Note that solid triangles represent significant trends at the 95% confidence levels, while hollow triangles mean no significant trends. The upward-pointing triangle and downward-pointing indicate increasing slope and decreasing slope, respectively, whereas the size of the triangle represents the magnitude of trends.

To estimate nonstationarity over the 20th century, this thesis also checked a century-long trend using the bias-corrected AMRs of ERA-20c and 20CR from 1900 to 2010 instead of the observation periods Obs and Obs0. Figure 7-8 illustrates trend test results for the AMRs of the bias-corrected reanalyses in 48 stations from 1900 to 2010. For ERA-20c, the corrected values by

SQM approaches (gevSQM, gamSQM, and gumSQM) had obvious increasing trends in all stations, and the QDM algorithms (gevQDM, gamQDM and gumQDM) also indicated the significant increasing trends at 0.05 significance level except a few points. The results for 20CR were similar to those for ERA-20c. The bias-corrected values demonstrated the obvious increasing trends for both SQM and QDM schemes of the whole 20th century. These results imply that the AMRs in South Korea may have an increasing trend over the 20th century, although the AMRs in recent decades are not able to clarify the nonstationary characteristic.

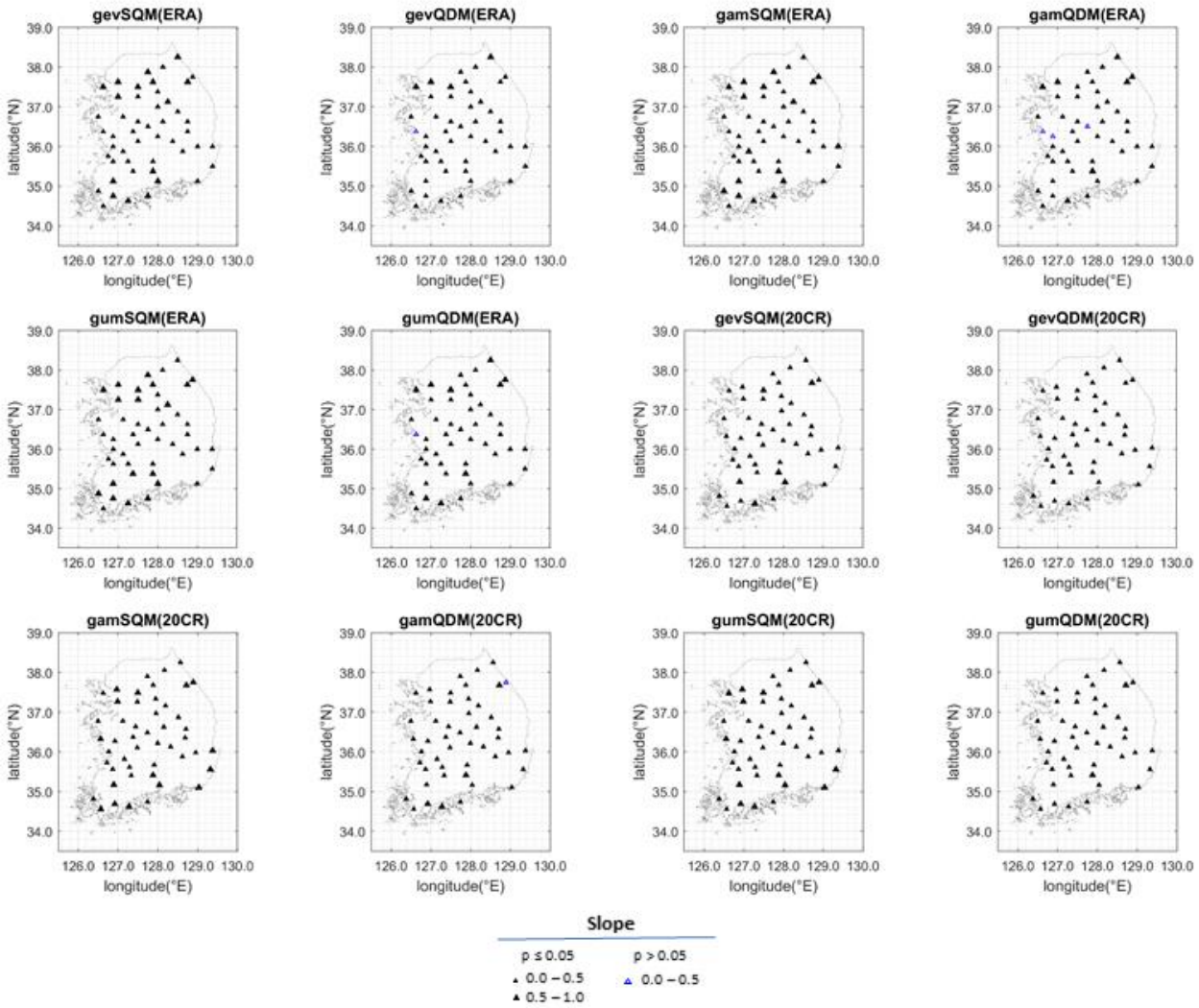

Figure 7-8 Trends in the AMRs of the bias-corrected ERA-20c and 20CR by QM approaches as in Figure 7-7, but the data period is covered from 1900 to 2010.

To evaluate the magnitude of the trends, inter-annual variabilities over 48 stations from 1900 to 2010 were also analysed as illustrated in Figure 7-9. Individual values for each station are

presented with thin weak blue and red lines for ERA-20c and 20CR, respectively, while the means of 48 stations are presented with thick strong blue and red lines. The straight lines represent the linear fit to AMRs from 1900 to 2010. Although there was the difference in specific movements between ERA-20c and 20CR, the trends of the overall means for 48 stations (which are indicated by bold blue straight lines for ERA-20c and bold red straight lines for 20CR) illustrate the significant increasing trends for both cases. To find out the variability on an individual station basis, I additionally illustrated inter-annual movements in four different stations, St.5, St.18, St.21 and St.27 in Figures 7-10 to 7-12. They also indicated significant trends for ERA-20c and 20CR.

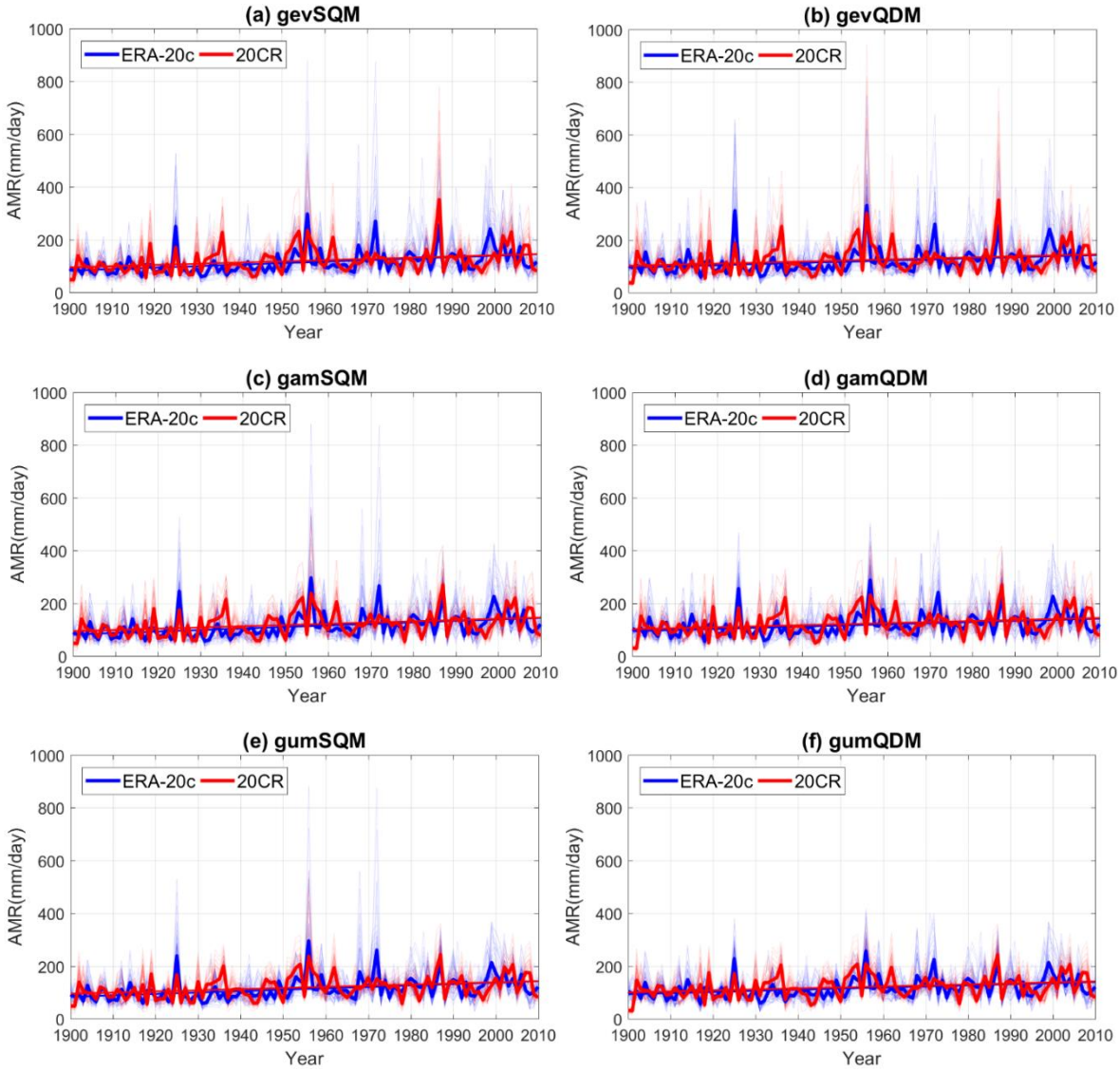

Figure 7-9 Inter-annual change of the AMRs of the bias-corrected ERA-20c and 20CR by QM approaches [(a) gevSQM, (b) gevQDM, (c) gamSQM, (d) gamQDM, (e) gumSQM, and (f) gumQDM].

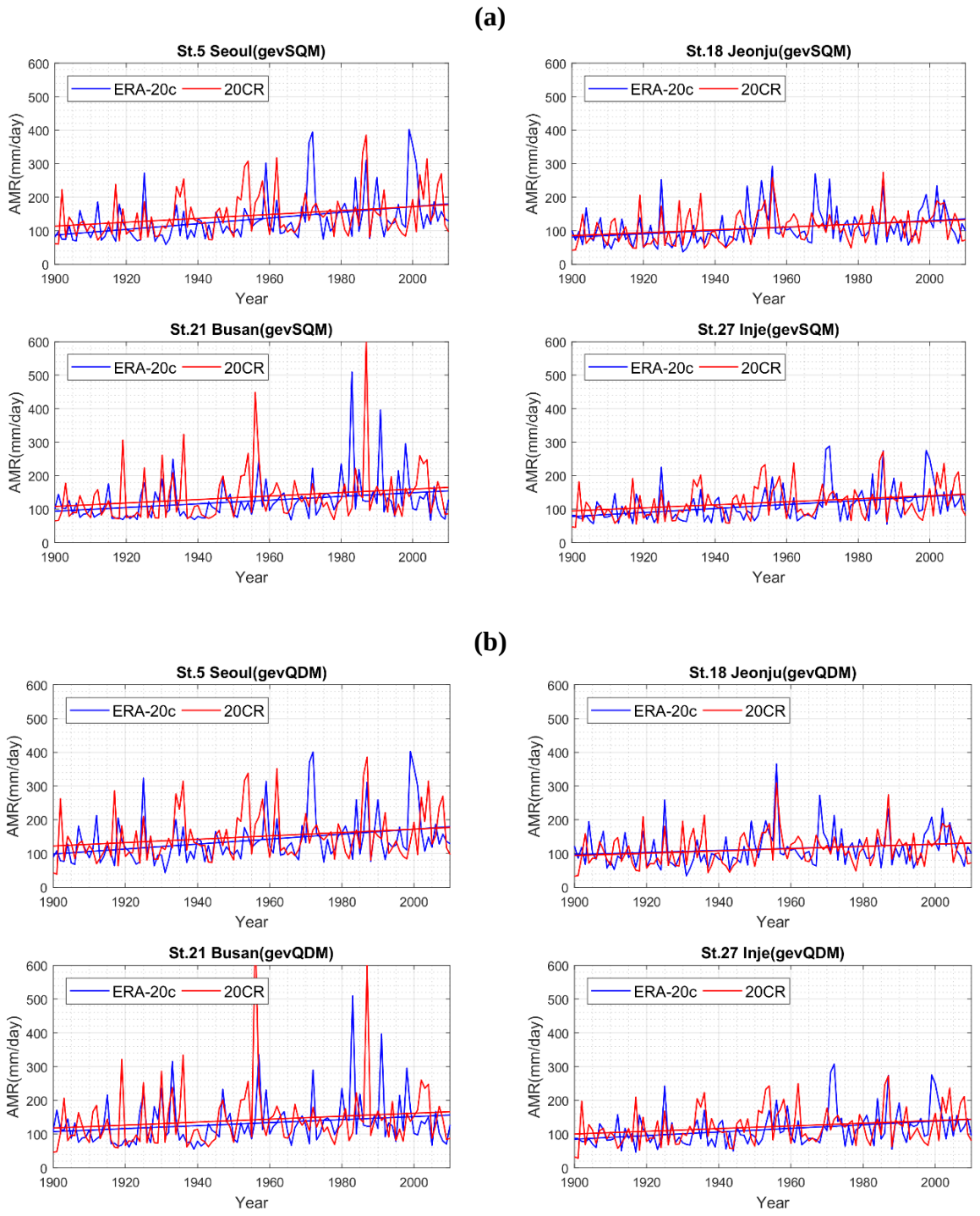

Figure 7-10 Inter-annual change of the AMRs of the bias-corrected ERA-20c and 20CR by (a) gevSQM, and (b) gevQDM in four different stations (St.5 Seoul, St.18 Jeonju, St.21 Busan, and St.27 Inje).

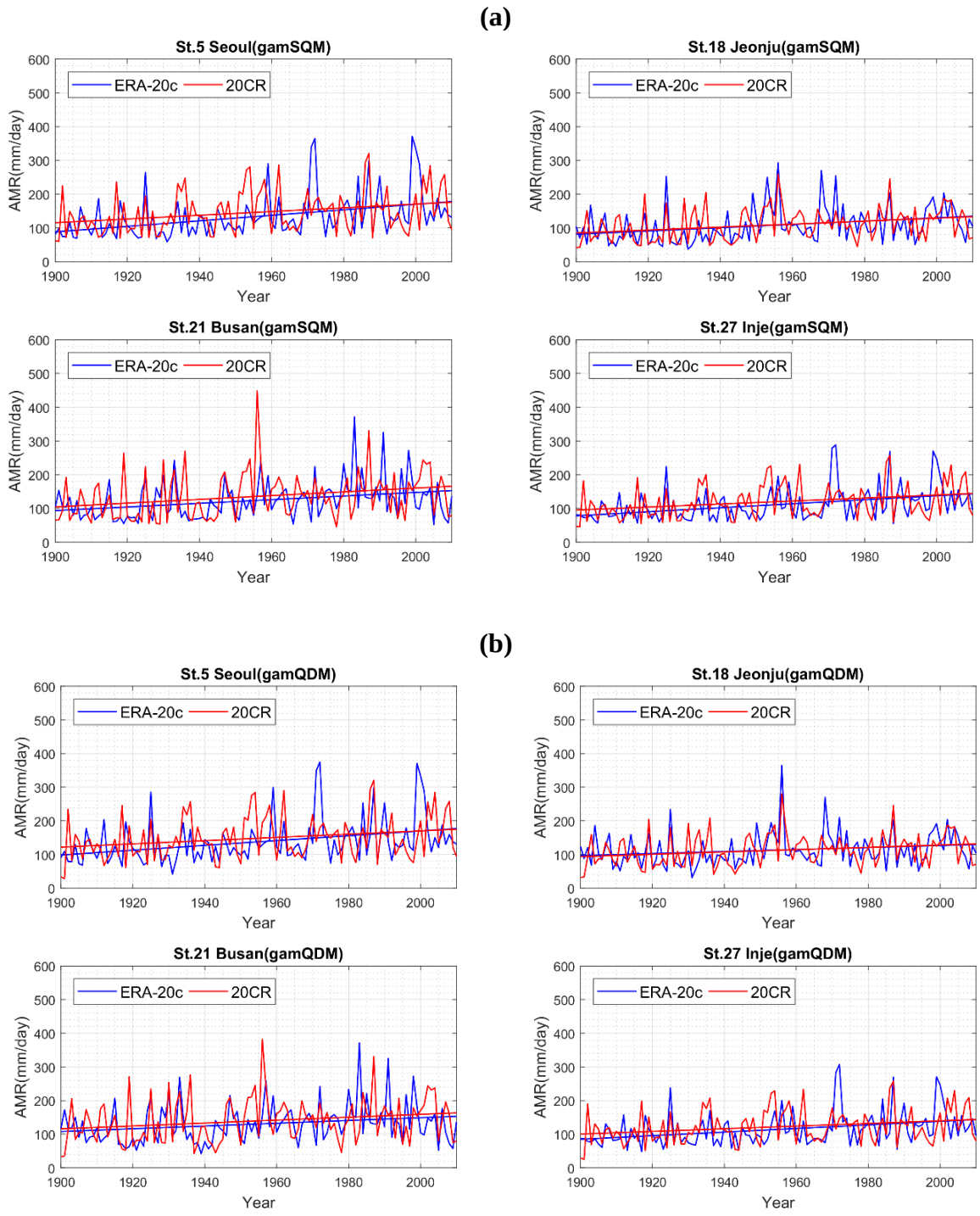

Figure 7-11 Inter-annual change of the AMRs of the bias-corrected ERA-20c and 20CR by (a) gamSQM, and (b) gamQDM in four different stations (St.5 Seoul, St.18 Jeonju, St.21 Busan, and St.27 Inje).

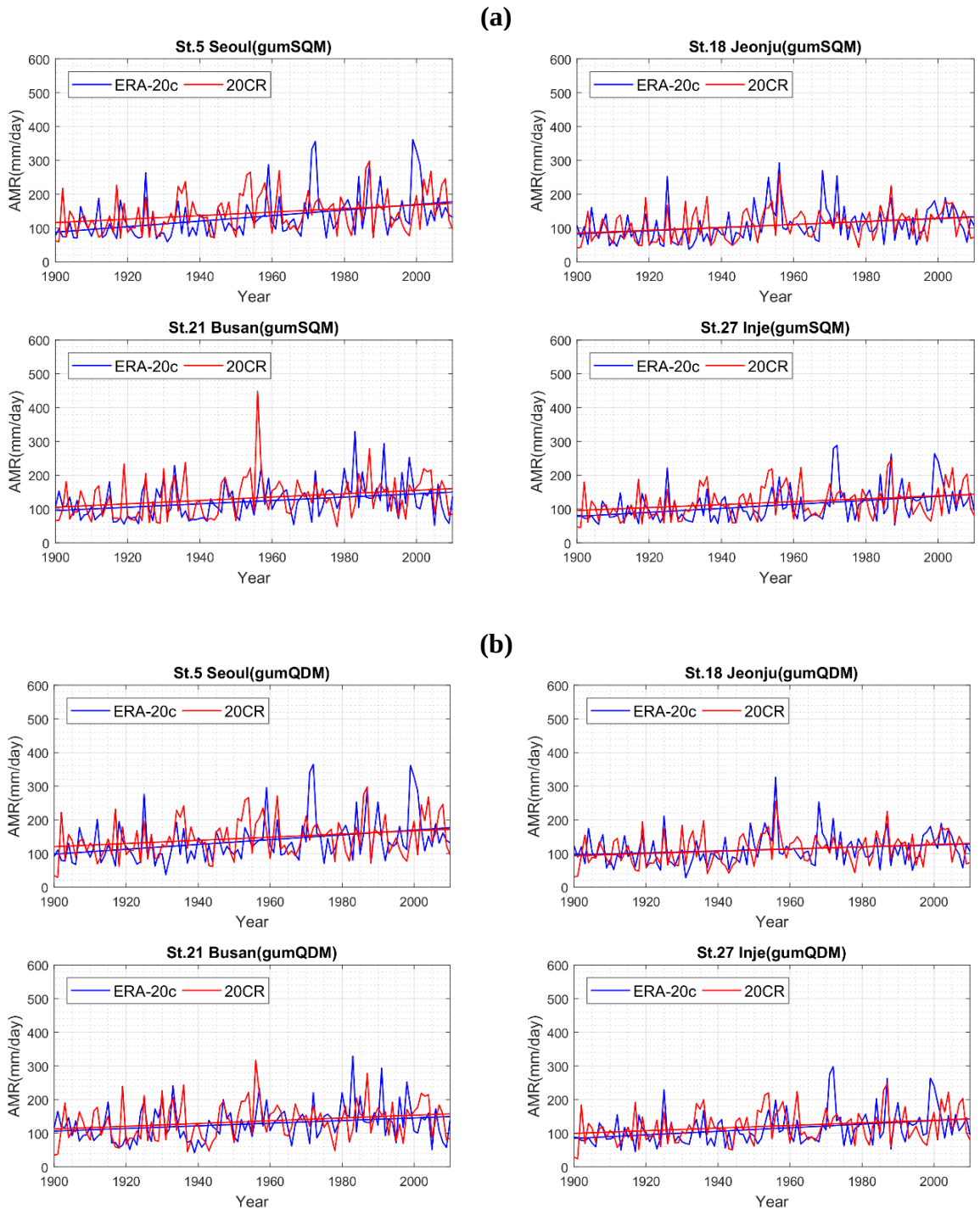

Figure 7-12 Inter-annual change of the AMRs of the bias-corrected ERA-20c and 20CR by (a) gumSQM, and (b) gumQDM in four different stations (St.5 Seoul, St.18 Jeonju, St.21 Busan, and St.27 Inje).

The slopes of the means for ERA-20c in Figure 7-9 were within the range from 0.40 mm/year to 0.55 mm/year, whereas the means for 20CR had a bit fewer slopes from 0.34 to 0.45 mm/year as described in Table 7-3. In comparison between SQM and QDM approaches, the trends by QDM schemes were lower than those by the corresponding SQM methods in both ERA-20c and 20CR. With the assumption that two reanalyses, ERA-20c and 20CR, could plausibly reproduce the long-term trend, these temporal patterns imply the clear nonstationarity of the AMRs in South Korea from 1900 to 2010.

Table 7-3 Mann-Kendall test results for the mean of the AMRs of the bias-corrected ERA-20c and 20CR by QM approaches from 1900 to 2010 as illustrated in Figure 7-9. Note that *z* and *b* (mm/year) values represent the standardised test statistics and the slope of the trend, respectively, and *z* values over 1.96 indicate a significant trend at the 0.05 significance level in this test.

Method	ERA-20c		20CR	
	z	*b*	*z*	*b*
gevSQM	5.51	0.50	3.43	0.38
gevQDM	4.21	0.40	2.67	0.34
gamSQM	5.56	0.55	3.53	0.45
gamQDM	4.06	0.41	2.71	0.37
gumSQM	5.50	0.52	3.59	0.42
gumQDM	4.30	0.40	2.91	0.36

It is surprising that the slopes of all stations based on the two different reanalysis products present the similar increasing trend in the AMRs, unlike the mean-based trend in Chapter 4. This result implies that the extreme data over South Korea might have a significant increasing trend that the current observed data with the limited period such as 1974–2010 and 1974–2017 cannot capture. Therefore, the abstraction of these trends might be beneficial in estimating the future extreme design rainfall over South Korea with nonstationary frequency analysis. The following study was conducted accordingly to employ the derived overall trend that might be more feasible to occur in nature even though a certain degree of uncertainties is included.

7.4.3 Design rainfalls with nonstationary condition

To explore design rainfalls with the nonstationary condition by using the bias-corrected AMRs from 1900 to 2010, this chapter estimated time-varying parameters of GEV distribution. Nonstationary design rainfalls were estimated by the BM approach based on the GEV parameters ($\mu_{s,\mathrm{m}}, \mu_{i,\mathrm{m}}, \sigma_m$, and ξ_m) derived from the bias-corrected AMRs. Here, the bias-corrected AMRs were collected from QM approaches with GEV distribution (gevSQM and gevQDM), which showed the best performance in Section 7.4.1.

To find out the impact of nonstationary condition, this chapter representatively illustrated design rainfall comparisons in the selected 4 stations, St.5, St.18, St.21, and St.27 in Figure 7-13. Note that Figure 7-13 adopted the median values and 90% confidence interval (5^{th} percentile to 95^{th} percentile) of parameters for ERA-20c and 20CR derived by the Bayesian approach in Section 7.3.2 to illustrate precipitation quantiles. The specific values used in Figure 7-13 is found at appendix B. In the comparisons, design quantiles showed the significant range of uncertainties, which had an upper bound of approximately 1.3 to 2.0 times higher than the design rainfalls by the observed and a lower bound of about 7–45% lower. For example, for St.5 Seoul, the precipitation quantiles with 100-year return period derived from ERA-20C varied from about 327mm to 815mm for gevSQM, and from 346mm to 852mm for gevQDM, while the classic quantile by the observation was 483mm. This characteristic is also shown in the other stations.

For the median values, the design quantiles of the reanalyses with long return periods such as 100-year and 200-year were generally higher than those by the observations except st.21 Busan, while the design rainfalls with short return periods, i.e. 10-year and 20-year, have little difference from the observed. For instance, St.18 Jeonju had a small gap in 10-year design quantiles between the observation and the reanalyses, but the longer the return period, the more gap there exists, especially for ERA-20c. St.5 Seoul and St.27 Inje also showed the similar characteristic with the design rainfall for the reanalyses exceeding those for the observed as the return period became longer. On the other hand, St.21 Busan had no clear feature compared with the other stations, and even the design rainfall for the observed exceeded those by the bias-corrected reanalyses for gevSQM. Although reanalysis-products-based design rainfall estimation includes a certain degree of uncertainty, these results imply that the nonstationary design rainfall would influence on

estimating the future risk of extreme precipitation and the strength of the impact depends on the target return period and location.

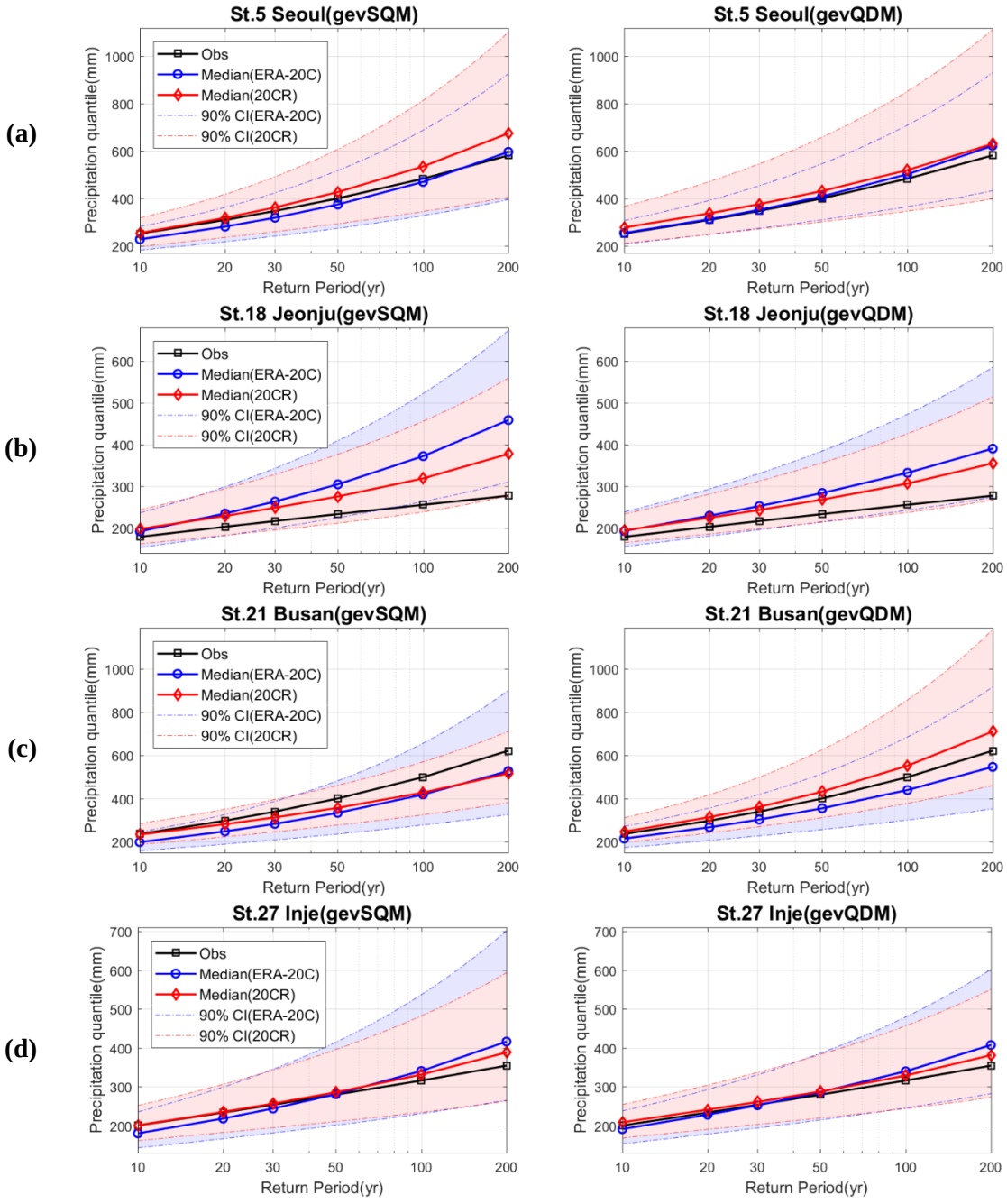

Figure 7-13 Precipitation quantiles by the conventional GEV model using the AMRs of observation (black line) for the reference period (1974–2010) and the nonstationary GEV models using the bias-corrected ERA-20c and 20CR derived from gevSQM and gevQDM in 4 stations. (a) St.5 Seoul, (b) St.18 Jeonju, (c) St.21 Busan, and (d) St.27 Inje.

To find out the spatial influence of nonstationarity in design rainfall, this thesis estimated the relative change (%) of design rainfall with 100-year return period based on the median values of the generated parameter chains in 48 stations. The relative change in 48 stations varied from -38.1% to 58.4% for gevSQM, and from -30.8 to 42.8% for gevQDM, respectively, but the spatial comparisons in Figure 7-14 illustrated the increase of the relative change (%) in many regions over South Korea.

Furthermore, the spatial area presenting lower or higher than the observation-based quantiles is more similar in case of the QDM for ERA-20c and 20CR than SQM. The results of the gevQDM relative change shown at the bottom panels of Figure 7-14 (i.e. Figure 7-14(b)) present that the southern and middle regions have higher design rainfall estimation than the observed one. Meanwhile, the northern region and the edges of the southeast and southwest present lower design rainfall from the gevQDM than from the observed one.

Despite the uncertainty range, these results suggest that conventional stationary approach based on the multi-decadal observation may lead to significant underestimation of future risk in some regions. For example, southwest parts within 35-36°N and 126.5-127.5°E had relative change within approximately 10 to 50% in all comparisons.

Compared with reanalysis-product-based design quantile changes under stationary condition in Figure 6-9(d), design rainfall change in Figure 7-14 reconfirms the effects of nonstationarity of the AMRs. More specifically, the stationary model using century-long ERA-20c data demonstrated a moderate decrease of design rainfall in most areas in Figure 6-9(d). Meanwhile, the nonstationary model based on the bias corrected ERA-20c by gevQDM in Figure 7-14(b) indicated the significant increase of rainfall intensity in most regions. Even though there are the difference in the specific bias correction scheme between two models, this gap implies the significant impact of climate change on rainfall intensity in South Korea.

It is evident that there still exists a certain degree of errors in design rainfall taken from the bias-corrected reanalyses. Nevertheless, if practitioners want to design a project but only have a limited observation, this result can provide meaningful information for a project plan with long-term lifespan.

(a)

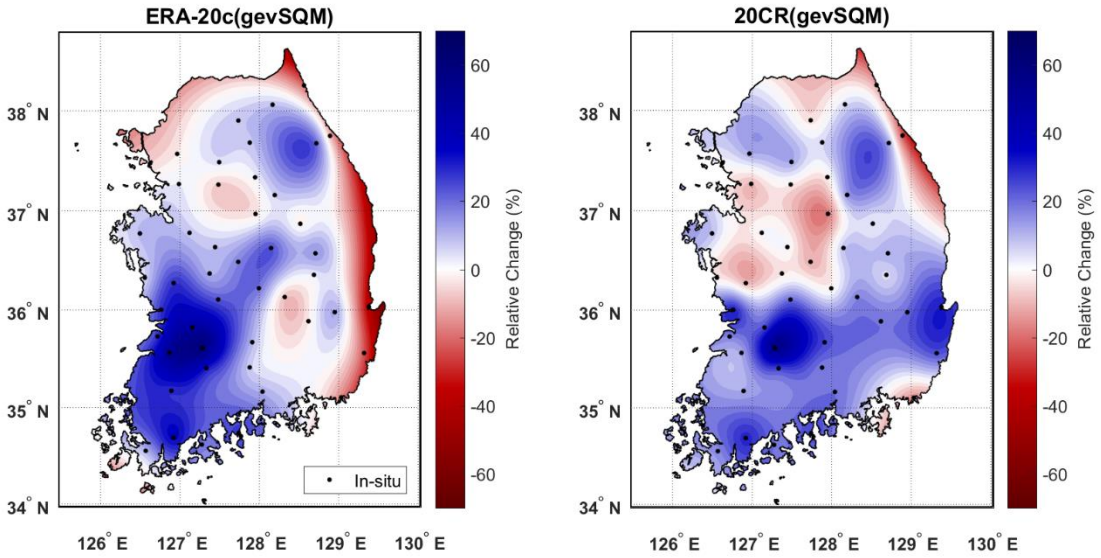

(b)

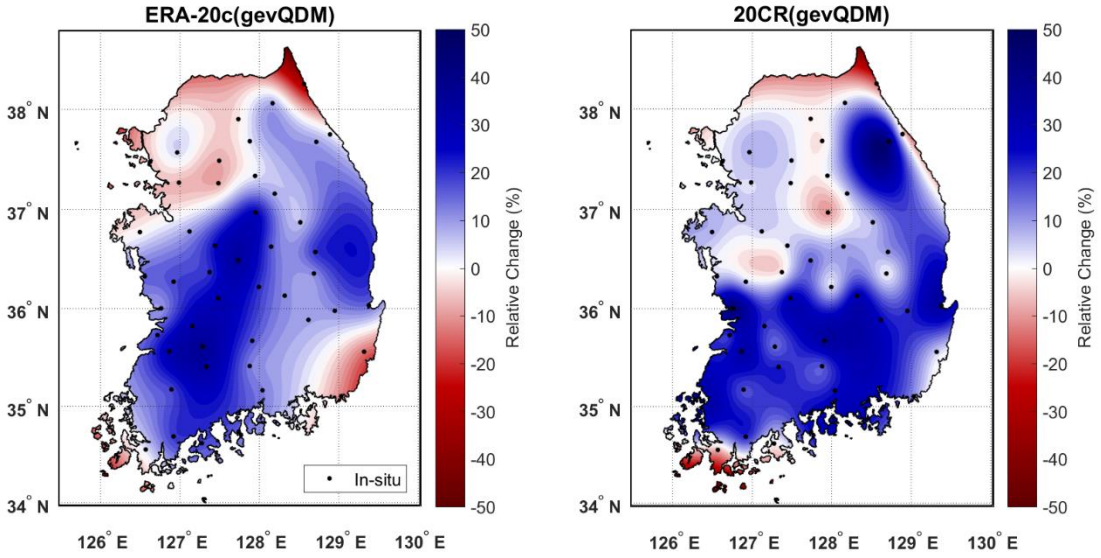

Figure 7-14 Relative change (%) of design rainfalls with 100-year return period between stationary condition and nonstationary condition. (a) indicates on the relative change for the bias-corrected AMRs by gevSQM, while (b) means the results for the bias-corrected AMRs by gevQDM.

7.5 Discussion

Despite the meaningful information, the proposed methods contain errors for various reasons. Basically, long-term reanalyses for daily precipitation have systematic errors which vary spatio-temporally (Bao and Zhang, 2013; Bosilovich et al., 2008; Gao et al., 2016; Ma et al., 2009). Previous studies have documented that century-long reanalyses such as ERA-20c and 20CR can mislead long-term trends, and a considerable bias may exist for the first half of the twentieth century (Befort et al., 2016; Brands et al., 2012; Donat et al., 2016; Krueger et al., 2013; Poli et al., 2013). The proposed bias correction methods, SQM and QDM, also have limitations. As a QM approach cannot exactly correct the climate change trend (Maraun, 2016), the potential error in the raw data's long-term trend may propagate the bias into the bias-corrected value. Moreover, a QM approach based on a single distribution can underestimate highly extreme rainfalls, which are mainly described by the upper tail of the distribution (Hundecha et al., 2009; Volosciuk et al., 2017; Vrac and Naveau, 2007; Wilks, 1999). The scale gap between the observed and the modelled can result in biases (Maraun, 2013). In other words, as the proposed QM approaches in this chapter matched the transfer function between the observation with point-scale and the model data with grid-scale, the bias-corrected value may include errors.

In design rainfall estimation with nonstationary condition, the problem of how to define time-varying parameters is also a major issue. This thesis assumed the linearly time-dependent location parameter, which has been commonly adopted in nonstationary studies. Nonetheless, several studies have also suggested non-linear location parameter or time-varying scale parameter (Cheng et al., 2014; Leclerc and Ouarda, 2007; Obeysekera and Salas, 2016, 2014; Son et al., 2017).

Likewise, various causes may result in substantial errors for the design rainfall interpretation in this study. Nevertheless, the proposed analysis suggests meaningful information to help to forecast future risk under the climate change environment. As rainfall intensity is expected to increase in the future, the conventional approach with stationary assumption may underestimate future risk. As discussed in Section 6.4.3, several studies and authorities have suggested a guideline for design rainfall and design flood considering potential impact (Lawrence and Hisdal, 2011; Madsen et al., 2014; UK Environment Agency, 2017). However, these guidelines typically suggested adding a correction factor into design rainfall or design flood estimated under stationary condition (Madsen et al., 2014). For instance, the UK Environment Agency (2017) recommended increasing the peak

rainfall intensity from 5 % to 40% for the future period (2015–2115), compared with the data for the baseline period (1961–1990). Furthermore, those suggestions are generally based on the analysis of future climate change scenarios which also include significant biases, and the nonstationary analysis based on the observation is constrained by lack of data. I.e., this correction factor approach has inherent uncertainties in the estimation of the correction factor and design quantile. Thus, despite the substantial errors, the proposed approach in this chapter can be a viable option to obtain supplementary information for estimating future risk in rainfall. I.e., in the case of a flood management plan, especially with a long-term lifespan plan such as 100 years, the design quantiles derived by the proposed method can be considered in comparison with the correction factor approach.

7.6 Conclusion

This chapter aimed to explore design rainfalls under nonstationary condition using century-long reanalyses, ERA-20 and 20CR, for South Korea. For this purpose, I first improved the AMRs of the reanalyses from 1900 to 2010 using a trend preserving method – QDM – compared with the conventional stationary QM scheme – SQM. After bias correction, this chapter assessed the long-term trend of the bias-corrected AMRs for the entire 20^{th} century to confirm the nonstationarity. With the improved values of ERA-20c and 20CR, design rainfalls under nonstationary condition were estimated based on the ENE approach in 48 stations. Finally, this thesis explored the spatial change in design rainfalls between the nonstationary approach applied in this chapter and the conventional approach. The major results obtained in this analysis are summarised as follows:

1. The applied QM approaches (gevQM, gamQM, and gumQM) based on a single distribution significantly improved the AMRs of ERA-20c and 20CR for the reference period. Among the applied QM approaches, gevQM performed the best for reducing the biases of the AMRs in terms of RMSE and NSE.

2. For long-term trend, no significant trend for the AMRs of the observed and reanalyses could be found during the observational period. However, the century-long AMRs of the bias-corrected ERA-20c and 20CR indicated obvious increasing trends. This result implies that the

AMRs might have a time-dependent characteristic. Also, the trend in the long-term reanalysis datasets could be beneficial in estimating South Korea's future extreme design rainfall with nonstationary frequency analysis.

3. The design rainfalls estimated under nonstationary condition were influenced in estimating the future risk of extreme precipitation. Also, the strength of the impact depends on the target return period and location. More specifically, the nonstationary design rainfalls in many parts of South Korea exceeded the classic design rainfalls by the observed – unlike the stationary model values in Chapter 6. This result implies that the nonstationarity in the AMRs that the short-term observation often fails to detect could deteriorate the confidence of a project based on the observed data for future risk in South Korea.

The findings obtained in this analysis provide a meaningful perspective on the applicability of century-long reanalysis products in a region with limited observation network – especially for nonstationary rainfall frequency analysis. Despite a certain degree of errors, the proposed scheme with employing the reanalysis products can be beneficial to predict the future evolution of extreme precipitation and to estimate the design rainfall accordingly.

The analysis dealt with in this chapter is a preliminary trial to deal with both the lack of data and nonstationarity of climate variables in hydrological applications. Further researches should tackle this issue to reliably assess future risk under climate change environments.

CHAPTER 8 Conclusions and recommendations

8.1 Conclusions

This thesis aims to substitute the limited local records for long-term reanalysis and evaluate its applicability in hydrological applications – especially in design rainfall frequency analysis. The main topics of this thesis can be divided into three parts. In the first part (Chapter 4), this thesis assessed the quality of long-term retrospective datasets at the regional scale. The second part (Chapters 5 and 6) dealt with the bias-correction scheme with a spatio-temporally limited observation and analysed the contribution of long-term data on the reduction of design rainfall uncertainty. Finally, the reanalysis-product-based nonstationary frequency analysis for design rainfall estimation was addressed in the third part (Chapter 7).

More specifically, the goal of the first part was to evaluate the reliability of retrospective datasets – especially for reanalysis data covering the whole 20th century – as an alternative to the local gauged data in regional-scale climate change studies. Here, this thesis first evaluated the suitability of century-long retrospective datasets in South Korea for precipitation and temperature. To discover the suitability, Chapter 4 assessed multi-decadal reanalyses (ERA-20cm, ERA-20c, ERA-40, and 20CR) and gridded observations (CRUv3.23 and GPCCv7) for monthly mean precipitation and temperature in South Korea. To obtain the characteristics of reanalysis ensemble that account for the uncertainty, an additional analysis for ERA-20cm ensemble was also carried out. The evaluation was mainly conducted within the context of temporal variability, long-term trend and statistical agreement. For ERA-20cm ensemble, the goodness of the ensemble spread and the relationship between the spread and the ENSO were also explored. The evaluation results not only help to fill in the knowledge gaps about these datasets in South Korea but also provide a useful guideline for the applicability of the global datasets in different parts of the world.

The key findings of this part are described below:

(1) For gridded observations, GPCCv7 and CRUv3.23 for precipitation showed the best agreement in all comparisons, while CRUv3.23 for temperature showed a clear gap compared

with the observation in South Korea. This result suggests that not only reanalyses but also gridded observations (which have been generally accepted as the true values in global climate change studies) could be substantially biased.

(2) Reanalysis datasets excepting ERA-20cm (i.e. ERA-40, ERA-20c, and 20CR) have significant agreements to the observation in terms of temporal and statistical comparisons. ERA-20c for precipitation showed better results than the others, and ERA-40 for temperature performed the best. However, they still include a certain degree of errors, so substantial improvement of the quality should be conducted before hydrological applications. It was also suggested that the accuracy of reanalysis data may vary depending on the region – especially for ERA-20cm.

(3) ERA-20cm has difficulty in providing useful information on long-term trend and temporal variability for temperature and precipitation in South Korea, although the temperature ensemble has a partial relationship with the observation. Statistically, all ensemble predictions showed significant agreements with the observed, but they still required a certain degree of improvement for the application in South Korea.

(4) It is found that the ERA-20cm mean may not represent ten individual members, even in the statistical estimate. The ensemble did not spread well enough to cover all observations – especially for temperature. Additionally, there was no relationship between the spread and ENSO. This result implies that researchers who want to apply ERA-20cm mean to a regional-scale study should treat this dataset with caution.

The second part of this study focused on the bias-correction of ERA-20c daily precipitation in South Korea with limited observations. The century-long bias-corrected data have not been used in regional scale analysis before. In Chapter 5, after the preliminary investigation for the bias types of ERA-20c daily precipitation, this thesis suggested a QM scheme based on a combined gamma-GPD distribution to efficiently correct the raw ERA-20c data – especially for the extremes. For the bias-correction in ungauged catchments, the transfer functions were estimated based on the IM-PCM approach. This was newly proposed in this thesis. As the applied bias-correction scheme in Chapter 5 was mainly explored for the reference period (1973–2010) under stationary condition, a trend preserving bias-correction scheme (i.e. QDM) was adopted to the bias correction for the

whole data period (1900–2010) in Chapter 6. With the bias-corrected century-long data, this chapter analysed both the reduction of design rainfall uncertainty and the rainfall intensity change over the 20th century. The findings in this study has suggested that the proposed approach can provide a useful alternative to the bias correction of a regional-scale modelled data with a limited network of rain gauges. Meanwhile, the use of bias-corrected data can reduce uncertainties in design rainfall compared with the observation-based analysis. The key findings of this part are described below:

(5) ERA-20c daily products well represent the monthly mean and annual cycle of daily precipitation in South Korea. However, considerable underestimation of heavy rainfalls was consistently observed in the ERA-20c, especially during the summer season. Furthermore, ERA-20c daily precipitation had a much higher frequency of wet-days than that of the observed, which may in turn influence the underestimation of the extremes.

(6) Regarding the wet-day frequency adjustment, a cut-off TH setting the frequency of wet-days of ERA-20c equal to that of the observed reduced the errors more effectively than the other pre-determined THs, such as 0.1mm/day and 1mm/day. This analysis suggests that inappropriate thresholds for the wet-day frequency may significantly influence the bias correction results.

(7) Concerning the bias correction of extreme rainfalls, a composite distribution-based QM (gpQM) approach was more appropriate for reducing the systematic errors in extreme values than the conventional gQM approach for the reference period (1973–2010). Especially, gpQM99 showed the best performance. However, a certain degree of bias still existed in the summer season when South Korea had the highest rainfall intensity. This analysis implies that bias-corrected ERA-20c data using the gpQM99 method may not perfectly reflect the specific regional patterns associated with extreme rainfall in South Korea.

(8) The corrected daily precipitation series using the IM-PCM showed good agreement with the observed precipitation for the 1973–2010 period. Particularly, the proposed gpQM99 with the IM-PCM performed the best in terms of reducing the spatial-temporal bias of the ERA-20c model data without a significant loss of efficiency for the period of 1973–2010. In the IM-

PCM approach, the elevation may not be an essential variable for the interpolation of the parameters in South Korea.

(9) The QDM approach based on a combined gamma-GPD distribution significantly reduces the error in terms of AMRs for the whole simulation period of 1910–2010 and the reference period of 1974–2010. However, this analysis indicates that the QDM method might not guarantee the accuracy of the AMRs for a certain past period (e.g. 1937–1973). The deficiencies were mainly attributed to the mismatch of relative changes between the observed and modelled in some high extreme quantiles.

(10) In design rainfall estimation, using bias-corrected century precipitation data significantly reduced the uncertainty in design rainfalls compared with the classic approach based on a limited observation period. The uncertainty reduction is attributed to the increase of sample size. This thesis also showed that the usage of informative prior distribution for the shape parameter of GEV informed by the century-long reanalysis data could effectively reduce the uncertainty in the conventional observation-based design rainfall estimation.

(11) There were significant changes in design intensity according to the periods (1900–1936, 1937–1973 and 1974–2010) in South Korea. More specially, the design quantiles for the 1900–1936 period were generally smaller than those by observation for the reference period. The 1937–1973 period indicated a significant positive gap in southwest regions. The design rainfall for the period of 1974–2010 had relatively small biases. The differences in design rainfalls may be attributed to both the biases which remained in the heavy extreme values for each period and the rainfall intensity changes. This result implies that the design rainfalls estimated using bias-corrected model values based on a QDM approach for a certain projected period (past or future) should be carefully interpreted in climate change impact studies.

(12) The spatial distribution of relative change using century-long AMRs showed that a negative change is more pronounced in the northern part of South Korea. This confirms its role of the recent increase in rainfall intensity, which should be considered in managing the risk associated with water-related hazards. However, positive changes remain in the south-western part of South Korea. These results imply that design rainfall estimated during the 1900–2010 period can be significantly underestimated in broad areas of South Korea. However,

conventional multi-decadal observation-based design rainfall may also underestimate potential flood risk in some areas.

In the third part (Chapter 7), this thesis focused on analysing design rainfall change under nonstationary condition using century-long reanalysis products, which has not been tried in previous studies. For this purpose, I directly improved the AMRs of the reanalyses (ERA-20 and 20CR) from 1900 to 2010 by QDM and SQM. After bias correction, this thesis detected the long-term trend of the AMRs for the observed and the reanalysis data to discover the nonstationarity. With the improved values of ERA-20c and 20CR, design rainfalls under nonstationary condition were estimated based on the ENE approach in 48 stations. Finally, this thesis examined the spatial change in design rainfalls between the nonstationary approach applied in this thesis and the conventional approach. The results showed that the proposed scheme with employing the reanalysis product might be beneficial to predict the future evolution of extreme precipitation and to estimate the design rainfall accordingly. The major findings of this part are summarised as follows:

(13) The applied QM approaches (gevQM, gamQM, and gumQM) based on a single distribution significantly improved the AMRs of ERA-20c and 20CR. Among the applied QM approaches, gevQM performed the best for reducing the biases of the AMRs in terms of RMSE and NSE.

(14) For long-term trend, there was no significant trend for the AMRs of the observed and the reanalyses (i.e. ERA-20c and 20CR) during the observational periods (1974–2010 and 1974–2017). However, the century-long AMRs of the bias-corrected ERA-20c and 20CR indicated obvious increasing trends. This result implies that the AMRs might have a time-dependent characteristic. Also, the trend in the long-term reanalysis datasets could be beneficial in estimating future extreme design rainfall in South Korea using nonstationary frequency analysis.

(15) The design rainfalls estimated under nonstationary condition were influenced in estimating the future risk of extreme precipitation. The strength of the impact depends on the target return period and location. Unlike stationary model in Chapter 6, the nonstationary design rainfalls in many parts of South Korea exceeded the classic design rainfalls by the observed. This result implies that the nonstationarity in the AMRs that the short-term observation often fails to

detect could deteriorate the confidence of a project based on the observed data for the future risk in South Korea.

8.2 Limitations and recommendations

The issues addressed in this thesis are novel and valuable to the hydrology community. However, due to time and resource constraints, it is not possible to thoroughly address all related factors in one PhD study. Thus, it is necessary to point out the limitations of this thesis and to suggest the following recommendations for future work.

(1) Although this thesis aims to fill in knowledge gaps for century-long reanalysis data and its applicability in regional-scale studies, the applied analyses have been conducted in only one region (i.e. South Korea). The findings in this thesis can provide useful information to researchers in different countries over the world, but further studies in more than two different regions would be able to provide more perspectives.

(2) Chapter 4 assessed various global data sources in terms of the mean over South Korea. The mean value can help to understand the general feature of individual datasets in South Korea, but the extremes of climate variables can show different characteristics from those of the means. Although this thesis analysed ERA-20c daily precipitation in Chapter 5, further assessment is needed for the extremes taken from the various global datasets to comprehensively understand the characteristics of individual reanalysis datasets.

(3) In Chapter 4, a comparative study on several global datasets was carried out with the assumption that the grid scale difference between 20CR and the other datasets could be ignored. As this assessment was based on the mean values averaged over all regions, the results in this analysis could provide robust information. However, to specifically evaluate spatial pattern in a study region using reanalysis data such as 20CR, reanalysis data with a finer resolution should be considered. In this context, further assessment with the downscaled data is recommended as the next step.

(4) The bias correction schemes applied in Chapters 5 to 7 were based on the relationship between the grid-scale reanalysis data and the corresponding point-scale *in situ* data in gauged catchments. This scale mismatch between the model outputs and the observation has typically been neglected in bias correction studies, but it is also true that a certain degree of biases can be attributed to the scale difference. One can attempt to solve the scale gap problem by creating gridded observation derived from the point-scale data, but as discussed in Chapters 4 and 5, the gridded observation may involve systematic errors caused by its interpolation scheme. Thus, it is quite complex to reduce the influence of the scale difference in bias correction which will be dealt with in further study.

(5) The QM approaches applied in this thesis were conceptually based on a univariate algorithm for daily precipitation. This is because this PhD work mainly focused on the applicability of bias-corrected values to rainfall frequency analysis. However, many hydrological models require more than one variable, and these different input variables typically have dependence. As reanalysis products can provide several variables such as temperature, wind, soil moisture and precipitation, the multivariate bias correction approach would be beneficial to researchers who deal with hydrological applications based on several climate variables.

(6) In the practical engineering field, design rainfalls are commonly estimated from the IDF relationship in a target area. This IDF curve typically involves the design rainfall and return period relationship for various time scales from 1 to 48 hours. It is then applied to future flood risk estimation. However, this thesis carried out reanalysis-product-based rainfall intensity analysis for only daily precipitation. Thus, further explorations with the different time scales by downscaling are recommended in the future to better understand the impact of the extended data on the future flood risk.

(7) In Chapter 7, this thesis concluded that despite a certain degree of uncertainty, the increasing trend of extreme rainfall could accelerate future risk in many parts of South Korea. As discussed in Section 7.5, previous studies have also presented a similar conclusion based on future climate change scenarios. The GCM-RCM outputs under future climate scenarios are typically used to predict the future climate change in a region. Since the outputs include biases, a bias correction method is applied to improve the data. In this process, the observation period is set as the reference period and the future period data are improved by a bias correction

method. However, as shown in Chapter 7, local observations (i.e. reference period data) often fails to detect the nonstationarity. Thus, the bias-corrected GCM-RCM data using local observations can misrepresent the future change. On the other hand, the proposed method in the thesis allows modellers to collect reliable data (i.e. bias-corrected reanalysis data) covering the entire 20th century in a region lacking local observations such as South Korea. More specifically, the bias-corrected data can help to estimate the long-term statistical change of daily precipitation. I.e., the future climate estimated by the proposed reanalysis products-based trend may provide the supplementary information to accurately predict future climate change by comparing them with the bias-corrected GCM-RCM outputs for the future period. However, this thesis has not quantitatively evaluated the similarity between reanalysis-data-based interpretation applied in this PhD work and climate change scenario-based interpretation. If two different approaches are compared quantitatively, the results can help to evaluate the reliability of the approaches in estimating future risk changes.

(8) To adapt and mitigate climate change, it is essential to discover changes not only in hazards such as heavy rainfall, but also in vulnerability associated with human activity such as land use and population density. More specifically, since climate change strategies in a certain area are generally results of decision-making based on a combination of vulnerability and hazard, it is important to fully understand the future change of the two different factors. However, the reanalysis-product-based frequency analysis applied in this thesis mainly analysed the change of rainfall intensity (i.e. hazard change) in South Korea. Thus, to better predict future risk under climate change, it would be crucial to evaluate both the hazard change and the vulnerability change in future study.

APPENDIX

Appendix A. AIC and BIC values of six distributions for the extremes in Table 5-2

Table A1 AIC and BIC values for the extremes over the 95th percentiles of observations

No.	AIC						BIC					
	GPD	**GEV**	**LOGN**	**WBL**	**GUM**	**GAM**	**GPD**	**GEV**	**LOGN**	**WBL**	**GUM**	**GAM**
St. 1	1,915	1,947	2,139	2,077	2,038	2,042	1,925	1,957	2,048	2,146	2,045	2,084
St. 2	2,564	2,591	2,877	2,785	2,718	2,741	2,575	2,602	2,748	2,885	2,726	2,792
St. 3	1,878	1,909	2,056	2,004	1,975	1,978	1,888	1,919	1,984	2,063	1,982	2,011
St. 4	1,974	2,002	2,251	2,172	2,106	2,132	1,984	2,012	2,139	2,257	2,112	2,178
St. 5	1,939	1,965	2,139	2,080	2,043	2,045	1,949	1,975	2,052	2,146	2,049	2,087
St. 6	1,781	1,808	1,953	1,900	1,867	1,872	1,791	1,817	1,879	1,959	1,874	1,906
St. 7	1,938	1,967	2,138	2,075	2,040	2,040	1,949	1,977	2,047	2,144	2,047	2,081
St. 8	1,899	1,928	2,100	2,044	2,008	2,014	1,909	1,938	2,020	2,107	2,015	2,050
St. 9	1,820	1,845	2,003	1,940	1,909	1,905	1,830	1,855	1,916	2,010	1,912	1,947
St. 10	1,982	2,017	2,138	2,083	2,059	2,057	1,992	2,027	2,066	2,145	2,064	2,089
St. 11	1,895	1,925	2,113	2,040	2,006	2,000	1,905	1,936	2,012	2,120	2,006	2,047
St. 12	1,995	2,024	2,201	2,135	2,101	2,098	2,005	2,034	2,108	2,208	2,105	2,141
St. 13	1,897	1,922	2,106	2,028	1,991	1,984	1,908	1,933	1,998	2,113	1,991	2,035
St. 14	1,365	1,397	1,485	1,441	1,427	1,417	1,374	1,407	1,433	1,491	1,423	1,447
St. 15	1,659	1,675	1,924	1,839	1,782	1,785	1,668	1,685	1,792	1,930	1,788	1,846
St. 16	1,911	1,928	2,147	2,064	2,023	2,013	1,921	1,938	2,029	2,153	2,020	2,071
St. 17	1,535	1,563	1,714	1,655	1,628	1,620	1,545	1,573	1,634	1,720	1,627	1,662
St. 18	2,030	2,067	2,239	2,175	2,142	2,142	2,040	2,077	2,149	2,246	2,148	2,182
St. 19	1,672	1,685	1,900	1,827	1,784	1,782	1,681	1,695	1,791	1,906	1,788	1,834
St. 20	2,092	2,113	2,344	2,257	2,212	2,205	2,102	2,123	2,219	2,351	2,212	2,264
St. 21	1,747	1,772	1,952	1,884	1,850	1,846	1,757	1,782	1,857	1,958	1,852	1,891
St. 22	1,969	1,999	2,193	2,110	2,069	2,070	1,979	2,010	2,077	2,200	2,076	2,117
St. 23	1,764	1,789	1,936	1,880	1,853	1,848	1,773	1,799	1,859	1,943	1,854	1,887
St. 24	1,701	1,736	1,890	1,838	1,813	1,806	1,711	1,746	1,820	1,897	1,813	1,845
St. 25	1,828	1,855	2,006	1,952	1,922	1,924	1,838	1,864	1,930	2,013	1,929	1,959
St. 26	1,730	1,728	1,938	1,869	1,832	1,820	1,738	1,740	1,838	1,944	1,826	1,875
St. 27	1,807	1,836	1,970	1,924	1,897	1,903	1,817	1,846	1,910	1,977	1,904	1,931
St. 28	1,808	1,839	1,972	1,927	1,902	1,905	1,817	1,849	1,911	1,978	1,908	1,934
St. 29	1,848	1,877	2,047	1,985	1,953	1,948	1,858	1,887	1,959	2,054	1,955	1,991
St. 30	1,855	1,876	2,115	2,026	1,977	1,971	1,865	1,886	1,983	2,122	1,977	2,033
St. 31	1,851	1,888	2,011	1,954	1,930	1,927	1,861	1,898	1,937	2,018	1,934	1,961
St. 32	1,893	1,921	2,092	2,033	1,996	2,004	1,903	1,931	2,011	2,099	2,003	2,040
St. 33	1,795	1,823	2,019	1,935	1,893	1,892	1,805	1,833	1,899	2,025	1,899	1,942
St. 34	1,772	1,804	1,911	1,860	1,841	1,833	1,782	1,814	1,848	1,918	1,840	1,867
St. 35	1,816	1,840	1,987	1,925	1,899	1,890	1,826	1,850	1,906	1,994	1,897	1,932
St. 36	1,937	1,979	2,165	2,088	2,057	2,042	1,947	1,990	2,064	2,172	2,049	2,095
St. 37	1,790	1,819	1,993	1,920	1,893	1,877	1,800	1,829	1,900	2,000	1,884	1,927
St. 38	1,854	1,887	2,023	1,962	1,939	1,927	1,864	1,897	1,946	2,030	1,933	1,969
St. 39	1,947	1,974	2,145	2,072	2,033	2,037	1,957	1,984	2,043	2,152	2,040	2,079
St. 40	1,976	2,002	2,196	2,121	2,077	2,082	1,986	2,012	2,089	2,202	2,084	2,128
St. 41	1,746	1,770	1,942	1,876	1,838	1,840	1,756	1,780	1,847	1,948	1,844	1,883
St. 42	1,618	1,647	1,796	1,733	1,707	1,694	1,628	1,657	1,714	1,803	1,701	1,739
St. 43	1,609	1,641	1,762	1,705	1,687	1,670	1,618	1,651	1,694	1,768	1,676	1,711
St. 44	1,451	1,464	1,577	1,519	1,499	1,488	1,460	1,473	1,505	1,583	1,494	1,525
St. 45	1,467	1,491	1,664	1,601	1,572	1,558	1,476	1,501	1,579	1,670	1,565	1,607
St. 46	1,432	1,468	1,583	1,536	1,518	1,508	1,441	1,477	1,524	1,590	1,515	1,542
St. 47	1,644	1,660	1,814	1,749	1,723	1,706	1,654	1,670	1,729	1,821	1,713	1,755
St. 48	1,762	1,794	1,925	1,879	1,851	1,855	1,772	1,803	1,861	1,931	1,857	1,885

Table A2 AIC and BIC values for the extremes over the 95th percentiles of ERA-20c

No.	AIC						BIC					
	GPD	**GEV**	**LOGN**	**WBL**	**GUM**	**GAM**	**GPD**	**GEV**	**LOGN**	**WBL**	**GUM**	**GAM**
St. 1	1,635	1,657	1,837	1,771	1,737	1,728	1,645	1,667	1,843	1,778	1,744	1,735
St. 2	2,098	2,144	2,331	2,251	2,220	2,206	2,108	2,154	2,338	2,258	2,227	2,213
St. 3	1,530	1,551	1,727	1,650	1,624	1,599	1,540	1,560	1,733	1,656	1,631	1,606
St. 4	1,634	1,671	1,813	1,748	1,726	1,711	1,644	1,681	1,819	1,755	1,732	1,717
St. 5	1,579	1,604	1,785	1,707	1,680	1,656	1,589	1,614	1,792	1,713	1,687	1,663
St. 6	1,424	1,453	1,629	1,554	1,531	1,506	1,434	1,463	1,635	1,561	1,538	1,513
St. 7	1,615	1,639	1,794	1,720	1,697	1,674	1,625	1,649	1,801	1,726	1,703	1,681
St. 8	1,520	1,545	1,740	1,658	1,632	1,602	1,530	1,555	1,747	1,665	1,639	1,609
St. 9	1,487	1,514	1,663	1,592	1,574	1,548	1,497	1,524	1,669	1,599	1,581	1,554
St. 10	1,552	1,575	1,766	1,677	1,653	1,620	1,562	1,585	1,773	1,683	1,660	1,626
St. 11	1,551	1,588	1,761	1,684	1,665	1,633	1,561	1,599	1,768	1,691	1,672	1,639
St. 12	1,608	1,639	1,790	1,720	1,704	1,675	1,618	1,650	1,797	1,727	1,711	1,682
St. 13	1,591	1,631	1,764	1,700	1,685	1,662	1,601	1,641	1,771	1,707	1,692	1,669
St. 14	1,244	1,264	1,387	1,330	1,313	1,294	1,253	1,274	1,394	1,336	1,320	1,300
St. 15	1,390	1,428	1,569	1,511	1,495	1,474	1,400	1,438	1,575	1,518	1,501	1,480
St. 16	1,547	1,593	1,706	1,645	1,633	1,610	1,557	1,603	1,713	1,652	1,640	1,617
St. 17	1,322	1,355	1,470	1,418	1,405	1,386	1,332	1,364	1,477	1,424	1,411	1,392
St. 18	1,663	1,707	1,801	1,743	1,732	1,714	1,673	1,718	1,808	1,750	1,739	1,721
St. 19	1,390	1,415	1,566	1,499	1,477	1,456	1,400	1,425	1,573	1,505	1,484	1,463
St. 20	1,747	1,775	1,886	1,822	1,808	1,787	1,758	1,786	1,893	1,828	1,815	1,794
St. 21	1,364	1,387	1,557	1,476	1,454	1,425	1,374	1,397	1,563	1,483	1,460	1,432
St. 22	1,604	1,648	1,762	1,697	1,683	1,662	1,614	1,658	1,768	1,703	1,690	1,669
St. 23	1,401	1,427	1,552	1,493	1,479	1,455	1,411	1,436	1,559	1,499	1,485	1,462
St. 24	1,388	1,415	1,535	1,478	1,464	1,443	1,397	1,425	1,541	1,484	1,470	1,449
St. 25	1,495	1,518	1,692	1,618	1,592	1,568	1,505	1,528	1,698	1,624	1,598	1,574
St. 26	1,434	1,455	1,634	1,558	1,534	1,505	1,444	1,465	1,641	1,565	1,540	1,512
St. 27	1,458	1,488	1,649	1,579	1,557	1,535	1,468	1,498	1,656	1,586	1,564	1,542
St. 28	1,474	1,500	1,655	1,584	1,560	1,538	1,484	1,509	1,662	1,590	1,567	1,545
St. 29	1,511	1,543	1,678	1,613	1,595	1,573	1,521	1,553	1,685	1,620	1,602	1,580
St. 30	1,525	1,561	1,712	1,644	1,628	1,600	1,535	1,571	1,718	1,651	1,635	1,607
St. 31	1,470	1,498	1,671	1,592	1,572	1,540	1,480	1,508	1,677	1,598	1,579	1,547
St. 32	1,464	1,493	1,653	1,577	1,560	1,529	1,473	1,503	1,659	1,584	1,567	1,535
St. 33	1,409	1,438	1,569	1,505	1,492	1,466	1,418	1,448	1,575	1,512	1,499	1,472
St. 34	1,434	1,468	1,582	1,524	1,512	1,489	1,444	1,478	1,588	1,531	1,519	1,495
St. 35	1,470	1,496	1,583	1,530	1,520	1,502	1,480	1,506	1,589	1,536	1,527	1,508
St. 36	1,655	1,685	1,787	1,727	1,716	1,694	1,666	1,695	1,794	1,734	1,722	1,701
St. 37	1,515	1,540	1,633	1,578	1,569	1,548	1,525	1,550	1,640	1,585	1,575	1,555
St. 38	1,582	1,608	1,712	1,652	1,640	1,619	1,592	1,619	1,719	1,659	1,646	1,626
St. 39	1,476	1,500	1,617	1,554	1,542	1,519	1,486	1,510	1,624	1,561	1,548	1,525
St. 40	1,516	1,543	1,682	1,608	1,592	1,566	1,526	1,554	1,688	1,615	1,599	1,573
St. 41	1,319	1,352	1,473	1,413	1,400	1,377	1,328	1,362	1,480	1,419	1,407	1,383
St. 42	1,369	1,395	1,519	1,458	1,442	1,422	1,379	1,405	1,526	1,465	1,449	1,429
St. 43	1,371	1,415	1,546	1,486	1,472	1,449	1,380	1,424	1,553	1,493	1,478	1,456
St. 44	1,283	1,314	1,442	1,387	1,371	1,351	1,292	1,323	1,448	1,393	1,377	1,357
St. 45	1,282	1,315	1,429	1,376	1,364	1,345	1,292	1,325	1,435	1,382	1,370	1,351
St. 46	1,260	1,286	1,409	1,358	1,344	1,325	1,270	1,296	1,415	1,364	1,350	1,331
St. 47	1,330	1,373	1,481	1,427	1,416	1,395	1,340	1,382	1,488	1,433	1,423	1,401
St. 48	1,347	1,373	1,487	1,431	1,419	1,397	1,357	1,382	1,493	1,438	1,425	1,403

Table A3 AIC and BIC values for the extremes over the 99th percentiles of observations

No.	AIC						BIC					
	GPD	**GEV**	**LOGN**	**WBL**	**GUM**	**GAM**	**GPD**	**GEV**	**LOGN**	**WBL**	**GUM**	**GAM**
St. 1	418	426	458	447	443	439	423	431	462	451	446	443
St. 2	546	554	629	604	590	586	552	560	633	608	594	590
St. 3	397	399	421	409	406	402	402	404	424	412	409	405
St. 4	440	445	502	485	470	472	445	451	506	488	474	475
St. 5	416	426	450	441	438	436	421	431	453	445	441	439
St. 6	373	381	413	404	401	398	378	386	416	407	404	401
St. 7	408	410	456	442	437	431	413	416	459	445	440	434
St. 8	401	411	443	431	427	424	407	416	446	435	431	427
St. 9	379	386	425	413	409	404	384	392	428	417	412	408
St. 10	391	397	434	415	410	402	396	402	437	418	414	406
St. 11	390	396	445	428	422	414	395	401	449	431	425	417
St. 12	419	423	456	440	435	429	424	429	460	443	439	433
St. 13	395	402	452	434	427	419	400	407	455	437	431	423
St. 14	274	281	298	286	284	281	278	286	301	289	287	284
St. 15	360	361	428	412	400	399	365	366	431	416	404	402
St. 16	395	398	465	447	440	431	400	403	468	451	443	434
St. 17	317	323	365	354	350	345	322	328	368	357	353	348
St. 18	417	424	465	449	445	438	423	429	469	453	448	442
St. 19	361	367	411	397	390	385	365	372	415	400	393	389
St. 20	435	443	505	487	479	472	441	449	509	491	483	475
St. 21	374	379	423	406	399	393	379	384	426	409	403	396
St. 22	397	402	478	454	443	433	403	408	482	457	446	436
St. 23	364	373	400	389	386	381	369	378	403	392	389	384
St. 24	358	366	382	374	372	369	362	371	386	377	375	372
St. 25	382	387	424	411	407	401	387	392	427	414	410	404
St. 26	380	388	412	403	399	397	385	393	415	406	402	400
St. 27	374	382	402	392	389	385	379	387	406	395	392	388
St. 28	374	377	390	380	378	376	379	382	393	383	382	379
St. 29	397	406	432	421	418	414	402	411	436	425	421	417
St. 30	390	393	461	444	435	430	395	398	464	447	438	433
St. 31	379	378	416	397	393	384	384	384	419	401	396	388
St. 32	399	407	444	429	423	418	404	413	448	432	427	422
St. 33	375	378	447	424	413	404	381	383	450	428	416	407
St. 34	350	362	380	370	368	363	355	367	384	373	371	367
St. 35	368	373	407	390	387	379	373	378	410	394	390	383
St. 36	405	412	457	441	436	428	411	418	461	445	440	432
St. 37	358	365	414	394	389	378	363	370	417	397	392	382
St. 38	366	372	405	391	388	381	371	377	408	394	391	384
St. 39	394	400	468	448	438	430	399	406	471	451	442	434
St. 40	417	422	481	464	455	452	422	428	485	467	459	455
St. 41	373	378	425	411	403	399	378	382	428	414	407	403
St. 42	341	345	379	367	363	357	346	350	382	370	367	361
St. 43	325	334	347	337	336	333	330	338	350	341	339	336
St. 44	292	294	330	315	311	303	297	299	333	318	314	306
St. 45	312	317	351	340	336	331	317	322	354	343	339	334
St. 46	289	297	320	308	306	301	294	301	323	312	309	304
St. 47	342	349	375	364	362	358	347	354	378	368	365	361
St. 48	366	377	394	388	386	384	371	382	397	391	389	387

Table A4 AIC and BIC values for the extremes over the 99th percentiles of ERA-20c

No.	AIC						BIC					
	GPD	**GEV**	**LOGN**	**WBL**	**GUM**	**GAM**	**GPD**	**GEV**	**LOGN**	**WBL**	**GUM**	**GAM**
St. 1	366	379	389	381	379	378	371	384	393	385	383	382
St. 2	429	437	475	457	453	445	434	443	478	461	457	449
St. 3	311	315	357	343	339	330	316	320	360	346	342	334
St. 4	329	339	369	355	352	346	334	344	372	358	356	349
St. 5	323	327	372	359	355	346	328	332	376	362	358	350
St. 6	296	301	339	323	320	312	301	306	342	327	323	315
St. 7	338	345	373	360	358	351	343	350	377	364	361	355
St. 8	321	327	364	350	346	338	326	332	367	353	350	342
St. 9	299	305	336	323	321	313	304	311	339	326	324	316
St. 10	315	319	364	347	344	333	320	325	367	351	347	336
St. 11	312	322	348	333	331	324	317	328	352	337	335	328
St. 12	315	317	343	328	326	318	320	322	346	331	329	322
St. 13	299	307	344	328	326	316	304	312	347	332	330	320
St. 14	256	262	286	275	273	267	260	266	289	278	276	270
St. 15	274	284	303	293	291	285	279	289	307	296	294	289
St. 16	287	295	322	306	305	296	292	300	325	310	308	300
St. 17	260	268	288	277	275	269	265	273	291	280	279	273
St. 18	302	312	330	319	317	312	307	318	334	322	321	315
St. 19	285	292	321	308	305	299	289	297	324	311	308	302
St. 20	313	324	361	344	342	332	319	330	364	348	346	335
St. 21	280	283	330	313	309	297	285	288	334	316	312	300
St. 22	305	313	343	324	322	314	310	318	346	328	326	317
St. 23	261	267	300	285	283	273	266	272	304	288	286	276
St. 24	264	270	298	283	281	273	269	275	301	287	285	276
St. 25	323	327	359	347	344	338	328	332	362	351	347	341
St. 26	297	306	340	328	325	319	302	311	343	331	328	322
St. 27	302	301	338	323	320	310	307	306	341	326	323	314
St. 28	304	310	342	331	328	323	309	315	345	334	332	326
St. 29	308	320	338	328	326	322	313	325	341	331	329	325
St. 30	295	305	331	319	317	310	301	310	334	323	321	313
St. 31	297	302	341	325	322	313	302	307	344	329	326	316
St. 32	285	294	330	314	312	303	290	299	333	318	315	306
St. 33	271	277	307	291	289	280	276	282	311	294	293	283
St. 34	261	273	298	285	284	276	266	278	301	289	287	280
St. 35	251	258	288	274	272	263	256	263	292	277	276	266
St. 36	301	307	333	316	315	306	307	312	337	320	319	310
St. 37	266	272	295	280	279	272	271	277	298	284	283	275
St. 38	284	290	324	310	308	298	289	295	327	313	312	301
St. 39	271	280	316	299	297	286	277	285	319	303	301	290
St. 40	289	296	337	321	318	307	294	301	341	325	322	310
St. 41	235	240	290	274	272	259	240	245	294	277	275	262
St. 42	269	274	308	294	292	284	274	279	311	297	295	287
St. 43	268	273	304	292	290	281	273	278	307	295	293	284
St. 44	262	271	291	281	279	275	266	275	294	284	282	278
St. 45	246	254	279	267	265	258	251	258	282	270	268	261
St. 46	249	256	275	265	264	258	253	260	278	268	267	261
St. 47	251	253	279	264	263	254	256	258	282	267	266	258
St. 48	255	256	283	269	268	259	260	261	286	272	271	262

Appendix B. GEV parameter values used in Figure 7-13.

No.	Method	Index	ERA-20c				20CR			
			μ_i	μ_s	σ	ξ	μ_i	μ_s	σ	ξ
St.5	gevSQM	Median	83.4	0.357	30.6	0.327	98.0	0.266	38.1	0.315
		Low[1)]	76.0	0.237	26.6	0.220	89.6	0.143	33.0	0.173
		Upper[2)]	90.5	0.481	35.0	0.438	107.1	0.387	42.7	0.444
	gevQDM	Median	89.1	0.372	39.5	0.262	99.8	0.368	46.7	0.208
		Low	80.2	0.238	37.0	0.151	85.2	0.181	42.2	0.073
		Upper	96.5	0.509	42.3	0.382	113.9	0.532	54.5	0.366
St.18	gevSQM	Median	66.4	0.296	30.3	0.244	65.2	0.423	34.2	0.065
		Low	59.8	0.193	26.9	0.135	56.8	0.352	30.3	-0.056
		Upper	73.3	0.397	34.4	0.341	73.8	0.497	38.9	0.208
	gevQDM	Median	79.0	0.199	34.3	0.138	74.3	0.301	35.8	0.044
		Low	71.3	0.084	31.7	0.033	71.9	0.215	32.1	-0.057
		Upper	85.7	0.328	37.4	0.262	77.0	0.392	40.0	0.178
St.21	gevSQM	Median	91.4	0.095	28.5	0.334	90.2	0.304	37.7	0.203
		Low	86.9	0.002	24.7	0.207	80.0	0.157	33.3	0.147
		Upper	96.0	0.190	31.5	0.479	100.2	0.434	42.7	0.279
	gevQDM	Median	90.0	0.158	33.3	0.293	84.4	0.310	37.0	0.345
		Low	84.8	0.065	29.1	0.174	76.4	0.216	32.4	0.232
		Upper	95.5	0.262	38.6	0.423	92.2	0.409	42.8	0.469
St.27	gevSQM	Median	75.7	0.200	26.6	0.253	79.0	0.296	34.3	0.106
		Low	68.4	0.107	24.0	0.113	72.6	0.189	30.7	-0.036
		Upper	82.4	0.344	31.5	0.384	87.5	0.408	39.0	0.240
	gevQDM	Median	76.3	0.254	30.3	0.189	80.9	0.324	37.6	0.050
		Low	68.7	0.147	27.0	0.087	72.4	0.194	34.5	-0.058
		Upper	84.2	0.381	34.1	0.295	90.8	0.411	41.4	0.183

[1)] 'Low' = the lower bound (i.e. 5th percentile of parameters).
[2)] 'Upper' = the upper bound (i.e. 95th percentile of parameters).

REFERENCES

Acero, F.J., García, J.A., Gallego, M.C., 2011. Peaks-over-threshold study of trends in extreme rainfall over the Iberian Peninsula. J. Clim. 24, 1089–1105. https://doi.org/10.1175/2010JCLI3627.1

Adhikary, S.K., Muttil, N., Yilmaz, A.G., 2017. Cokriging for enhanced spatial interpolation of rainfall in two Australian catchments. Hydrol. Process. 31, 2143–2161. https://doi.org/10.1002/hyp.11163

Alexander, L. V., Zhang, X., Peterson, T.C., Caesar, J., Gleason, B., Klein Tank, A.M.G., Haylock, M., Collins, D., Trewin, B., Rahimzadeh, F., Tagipour, A., Rupa Kumar, K., Revadekar, J., Griffiths, G., Vincent, L., Stephenson, D.B., Burn, J., Aguilar, E., Brunet, M., Taylor, M., New, M., Zhai, P., Rusticucci, M., Vazquez-Aguirre, J.L., 2006. Global observed changes in daily climate extremes of temperature and precipitation. J. Geophys. Res. Atmos. 111, 1–22. https://doi.org/10.1029/2005JD006290

Amidror, I., 2002. Scattered data interpolation methods for electronic imaging systems: a survey. J. Electron. Imaging 11, 157. https://doi.org/10.1117/1.1455013

Babak, O., Deutsch, C. V, 2009. Statistical approach to inverse distance interpolation. Stoch. Environ. Res. Risk Assess. 23, 543–553. https://doi.org/10.1007/s00477-008-0226-6

Bae, D., Jung, I., Chang, H., 2008. Long-term trend of precipitation and runoff in Korean river basins. Hydrol. Process. 22, 2644–2656.

Bao, X., Zhang, F., 2013. Evaluation of NCEP–CFSR, NCEP–NCAR, ERA-Interim, and ERA-40 reanalysis datasets against independent sounding observations over the Tibetan Plateau. J. Clim. 26, 206–214.

Becker, A., Finger, P., Meyer-Christoffer, A., Rudolf, B., Schamm, K., Schneider, U., Ziese, M., 2013. A description of the global land-surface precipitation data products of the Global Precipitation Climatology Centre with sample applications including centennial (trend) analysis from 1901-present. Earth Syst. Sci. Data 5, 71–99. https://doi.org/10.5194/essd-5-71-2013

Befort, D.J., Wild, S., Kruschke, T., Ulbrich, U., Leckebusch, G.C., 2016. Different long-term trends of extra-tropical cyclones and windstorms in ERA-20C and NOAA-20CR reanalyses. Atmos. Sci. Lett. 17, 586–595. https://doi.org/10.1002/asl.694

Beven, K., 2006. On undermining the science? Hydrol. Process. 20, 3141–3146. https://doi.org/10.1002/hyp.6396

Beven, K., Binley, A., 1992. The future of distributed models: Model calibration and uncertainty prediction. Hydrol. Process. 6, 279–298. https://doi.org/10.1002/hyp.3360060305

Beven, K., Smith, P., Freer, J., 2007. Comment on "Hydrological forecasting uncertainty assessment: Incoherence of the GLUE methodology" by Pietro Mantovan and Ezio Todini. J.

Hydrol. 338, 315–318. https://doi.org/10.1016/j.jhydrol.2007.02.023

Beven, K.J., Smith, P.J., Freer, J.E., 2008. So just why would a modeller choose to be incoherent? J. Hydrol. 354, 15–32. https://doi.org/10.1016/j.jhydrol.2008.02.007

Bosilovich, M.G., Chen, J., Robertson, F.R., Adler, R.F., 2008. Evaluation of global precipitation in reanalyses. J. Appl. Meteorol. Climatol. 47, 2279–2299.

Brands, S., Gutiérrez, J.M., Herrera, S., Cofiño, A.S., 2012. On the use of reanalysis data for downscaling. J. Clim. 25, 2517–2526. https://doi.org/10.1175/JCLI-D-11-00251.1

Bürger, G., Sobie, S.R., Cannon, A.J., Werner, A.T., Murdock, T.Q., 2013. Downscaling extremes: An intercomparison of multiple methods for future climate. J. Clim. 26, 3429–3449. https://doi.org/10.1175/JCLI-D-12-00249.1

Cannon, A.J., 2010. A flexible nonlinear modelling framework for nonstationary generalized extreme value analysis in hydroclimatology. Hydrol. Process. 24, 673–685. https://doi.org/10.1002/hyp.7506

Cannon, A.J., Sobie, S.R., Murdock, T.Q., 2015. Bias correction of GCM precipitation by quantile mapping: How well do methods preserve changes in quantiles and extremes? J. Clim. 28, 6938–6959.

Chan, S.C., Kendon, E.J., Roberts, N.M., Fowler, H.J., Blenkinsop, S., 2015. Downturn in scaling of UK extreme rainfall with temperature for future hottest days. Nat. Geosci. 9, 24–28. https://doi.org/10.1038/ngeo2596

Chang, C.L., Lo, S.L., Yu, S.L., 2006. The parameter optimization in the inverse distance method by genetic algorithm for estimating precipitation. Environ. Monit. Assess. 117, 145–155. https://doi.org/10.1007/s10661-006-8498-0

Chang, H., Kwon, W.-T., 2007. Spatial variations of summer precipitation trends in South Korea, 1973–2005. Environ. Res. Lett. 2, 45012.

Chen, M., Xie, P., Janowiak, J.E., Arkin, P.A., 2002. Global land precipitation: A 50-yr monthly analysis based on gauge observations. J. Hydrometeorol. 3, 249–266.

Cheng, L., Aghakouchak, A., 2014. Nonstationary precipitation intensity-duration-frequency curves for infrastructure design in a changing climate. Sci. Rep. 4, 1–6. https://doi.org/10.1038/srep07093

Cheng, L., AghaKouchak, A., Gilleland, E., Katz, R.W., 2014. Non-stationary extreme value analysis in a changing climate. Clim. Change 127, 353–369. https://doi.org/10.1007/s10584-014-1254-5

Choi, G., Collins, D., Ren, G., Trewin, B., Baldi, M., Fukuda, Y., Afzaal, M., Pianmana, T., Gomboluudev, P., Huong, P.T.T., 2009. Changes in means and extreme events of temperature and precipitation in the Asia-Pacific Network region, 1955–2007. Int. J. Climatol. 29, 1906–1925.

Choi, K.-S., Kim, B.-J., Zhang, R., Nam, J.-C., Park, K.-J., Kim, J.-Y., Kim, D.-W., 2016. Possible influence of South Asian high on summer rainfall variability in Korea. Clim. Dyn. 46, 833–846.

Chung, Y.S., Yoon, M.B., 2000. Interpretation of recent temperature and precipitationtrends observed in Korea. Theor. Appl. Climatol. 67, 171–180.

Coles, S., Pericchi, L.R., Sisson, S., 2003. A fully probabilistic approach to extreme rainfall modeling. J. Hydrol. 273, 35–50. https://doi.org/10.1016/S0022-1694(02)00353-0

Coles, S.G., 2001. An introduction to Statistical Modeling of Extreme Values, Springer. Springer, London. https://doi.org/10.1007/978-1-4471-3675-0

Compo, G.P., Whitaker, J.S., Sardeshmukh, P.D., Matsui, N., Allan, R.J., Yin, X., Gleason, B.E., Vose, R.S., Rutledge, G., Bessemoulin, P., 2011. The twentieth century reanalysis project. Q. J. R. Meteorol. Soc. 137, 1–28.

Cunderlik, J.M., Burn, D.H., 2003. Non-stationary pooled flood frequency analysis. J. Hydrol. 276, 210–223. https://doi.org/10.1016/S0022-1694(03)00062-3

Dai, Q., 2014. Radar rainfall uncertainty analysis for hydrological applications. University of Bristol.

Dee, D.P., Uppala, S.M., Simmons, A.J., Berrisford, P., Poli, P., Kobayashi, S., Andrae, U., Balmaseda, M.A., Balsamo, G., Bauer, P., 2011. The ERA-Interim reanalysis: Configuration and performance of the data assimilation system. Q. J. R. Meteorol. Soc. 137, 553–597.

Deser, C., Phillips, A.S., Hurrell, J.W., 2004. Pacific interdecadal climate variability: Linkages between the tropics and the North Pacific during boreal winter since 1900. J. Clim. 17, 3109–3124. https://doi.org/10.1175/1520-0442(2004)017<3109:PICVLB>2.0.CO;2

Dickinson, R.E., Oleson, K.W., Bonan, G., Hoffman, F., Thornton, P., Vertenstein, M., Yang, Z.L., Zeng, X.B., 2006. The Community Land Model and its climate statistics as a component of the Community Climate System Model. J. Clim. 19, 2302–2324. https://doi.org/Doi 10.1175/Jcli3742.1

Dinku, T., Connor, S.J., Ceccato, P., Ropelewski, C.F., 2008. Comparison of global gridded precipitation products over a mountainous region of Africa. Int. J. Climatol. 28, 1627–1638.

Donat, M.G., Alexander, L. V, Herold, N., Dittus, A.J., 2016. Temperature and precipitation extremes in century-long gridded observations, reanalyses, and atmospheric model simulations. J. Geophys. Res. Atmos. 121.

Donat, M.G., Sillmann, J., Wild, S., Alexander, L. V, Lippmann, T., Zwiers, F.W., 2014. Consistency of temperature and precipitation extremes across various global gridded in situ and reanalysis datasets. J. Clim. 27, 5019–5035.

Du, T., Xiong, L., Xu, C.Y., Gippel, C.J., Guo, S., Liu, P., 2015. Return period and risk analysis of nonstationary low-flow series under climate change. J. Hydrol. 527, 234–250. https://doi.org/10.1016/j.jhydrol.2015.04.041

El Adlouni, S., Ouarda, T.B.M.J., Zhang, X., Roy, R., Bobée, B., 2007. Generalized maximum likelihood estimators for the nonstationary generalized extreme value model. Water Resour. Res. 43, 1–13. https://doi.org/10.1029/2005WR004545

Eum, H. Il, Cannon, A.J., 2017. Intercomparison of projected changes in climate extremes for South Korea: application of trend preserving statistical downscaling methods to the CMIP5 ensemble. Int. J. Climatol. 37, 3381–3397. https://doi.org/10.1002/joc.4924

Fang, G., Yang, J., Chen, Y.N., Zammit, C., 2015. Comparing bias correction methods in downscaling meteorological variables for a hydrologic impact study in an arid area in China. Hydrol. Earth Syst. Sci. 19, 2547–2559.

Fekete, B.M., Vörösmarty, C.J., Roads, J.O., Willmott, C.J., 2004. Uncertainties in precipitation and their impacts on runoff estimates. J. Clim. 17, 294–304.

Ferguson, C.R., Villarini, G., 2012. Detecting inhomogeneities in the Twentieth Century Reanalysis over the central United States. J. Geophys. Res. Atmos. 117.

Gao, L., Bernhardt, M., Schulz, K., Chen, X., 2012. Elevation correction of ERA-Interim temperature data in the Tibetan Plateau. Int. J. Climatol. 37, 3540–3552. https://doi.org/10.1002/joc.4935

Gao, L., Bernhardt, M., Schulz, K., Chen, X.W., Chen, Y., Liu, M.B., 2016. A First Evaluation of ERA-20CM over China. Mon. Weather Rev. 144, 45–57. https://doi.org/10.1175/Mwr-D-15-0195.1

Gao, L., Hao, L., Chen, X.W., 2014a. Evaluation of ERA-interim monthly temperature data over the Tibetan Plateau. J. Mt. Sci. 11, 1154–1168. https://doi.org/10.1007/s11629-014-3013-5

Gao, L., Schulz, K., Bernhardt, M., 2014b. Statistical downscaling of ERA-interim forecast precipitation data in complex terrain using lasso algorithm. Adv. Meteorol. 2014, 16–21. https://doi.org/10.1155/2014/472741

Gholami, V., Chau, K.W., Fadaee, F., Torkaman, J., Ghaffari, A., 2015. Modeling of groundwater level fluctuations using dendrochronology in alluvial aquifers. J. Hydrol. 529, 1060–1069. https://doi.org/10.1016/j.jhydrol.2015.09.028

Goovaerts, P., 2000. Geostatistical approaches for incorporating elevation into the spatial interpolation of rainfall. J. Hydrol. 228, 113–129. https://doi.org/10.1016/S0022-1694(00)00144-X

Gutjahr, O., Heinemann, G., 2013. Comparing precipitation bias correction methods for high-resolution regional climate simulations using COSMO-CLM. Theor. Appl. Climatol. 114, 511–529. https://doi.org/10.1007/s00704-013-0834-z

Hall, J.W., Manning, L.J., Hankin, R.K.S., 2011. Bayesian calibration of a flood inundation model using spatial data. Water Resour. Res. 47, 1–14. https://doi.org/10.1029/2009WR008541

Hamed, K.H., Rao, A.R., 1998. A modified Mann-Kendall trend test for autocorrelated data. J. Hydrol. 204, 182–196.

Harris, I., Jones, P.D., Osborn, T.J., Lister, D.H., 2014. Updated high-resolution grids of monthly climatic observations - the CRU TS3.10 Dataset. Int. J. Climatol. 34, 623–642. https://doi.org/10.1002/joc.3711

Hayes, K.R., 2011. Uncertainty and uncertainty analysis methods. CSIRO.

Herrmann, S.M., Anyamba, A., Tucker, C.J., 2005. Recent trends in vegetation dynamics in the African Sahel and their relationship to climate. Glob. Environ. Chang. 15, 394–404. https://doi.org/10.1016/j.gloenvcha.2005.08.004

Hersbach, H., Peubey, C., Simmons, A., Berrisford, P., Poli, P., Dee, D., 2015. ERA-20CM: a twentieth-century atmospheric model ensemble. Q. J. R. Meteorol. Soc. 141, 2350–2375.

Ho, C., Lee, J., Ahn, M., Lee, H., 2003. A sudden change in summer rainfall characteristics in Korea during the late 1970s. Int. J. Climatol. 23, 117–128.

Huard, D., Mailhot, A., Duchesne, S., 2010. Bayesian estimation of intensity-duration-frequency curves and of the return period associated to a given rainfall event. Stoch. Environ. Res. Risk Assess. 24, 337–347. https://doi.org/10.1007/s00477-009-0323-1

Huffman, G.J., Adler, R.F., Arkin, P., Chang, A., Ferraro, R., Gruber, A., Janowiak, J., McNab, A., Rudolf, B., Schneider, U., 1997. The Global Precipitation Climatology Project (GPCP) Combined Precipitation Dataset. Bull. Am. Meteorol. Soc. 78, 5–20. https://doi.org/10.1175/1520-0477(1997)078<0005:TGPCPG>2.0.CO;2

Hundecha, Y., Pahlow, M., Schumann, A., 2009. Modeling of daily precipitation at multiple locations using a mixture of distributions to characterize the extremes. Water Resour. Res. 45, 1–15. https://doi.org/10.1029/2008WR007453

IPCC, 2014. Climate Change 2014–Impacts, Adaptation and Vulnerability: Regional Aspects. Cambridge University Press.

Jeong, M., Kim, J., Oh, S.M., Moon, Y., 2015. Sensitivity of summer precipitation over the Korean Peninsula to temperature gradients. Int. J. Climatol. 35, 836–845.

Jung, H., Choi, Y., Oh, J., Lim, G., 2002. Recent trends in temperature and precipitation over South Korea. Int. J. Climatol. 22, 1327–1337.

Jung, I.-W., Chang, H., Bae, D.-H., 2013. Spatially-explicit assessment of flood risk caused by climate change in South Korea. KSCE J. Civ. Eng. 17, 233–243.

Jung, I.W., Bae, D.H., Kim, G., 2011. Recent trends of mean and extreme precipitation in Korea. Int. J. Climatol. 31, 359–370. https://doi.org/10.1002/joc.2068

Kalnay, E., Kanamitsu, M., Kistler, R., Collins, W., Deaven, D., Gandin, L., Iredell, M., Saha, S., White, G., Woollen, J., 1996. The NCEP/NCAR 40-year reanalysis project. Bull. Am. Meteorol. Soc. 77, 437–471.

Kendall, M.G., 1955. Rank correlation methods, 2nd editio. ed. Griffin, London.

Kim, K.B., Bray, M., Han, D., 2015a. An improved bias correction scheme based on comparative

precipitation characteristics. Hydrol. Process. 29, 2258–2266. https://doi.org/10.1002/hyp.10366

Kim, K.B., Kwon, H.H., Han, D., 2015b. Bias correction methods for regional climate model simulations considering the distributional parametric uncertainty underlying the observations. J. Hydrol. 530, 568–579. https://doi.org/10.1016/j.jhydrol.2015.10.015

Koutsoyiannis, D., 2004. Statistics of extremes and estimation of extreme rainfall: I. Theoretical investigation. Hydrol. Sci. J. 49, 575–590. https://doi.org/10.1623/hysj.49.4.575.54430

Krueger, O., Schenk, F., Feser, F., Weisse, R., 2013. Inconsistencies between long-term trends in storminess derived from the 20CR reanalysis and observations. J. Clim. 26, 868–874. https://doi.org/10.1175/JCLI-D-12-00309.1

Kwon, H.-H., Brown, C., Lall, U., 2008. Climate informed flood frequency analysis and prediction in Montana using hierarchical Bayesian modeling. Geophys. Res. Lett. 35, L05404. https://doi.org/10.1029/2007GL032220

Kwon, H.H., Sivakumar, B., Moon, Y. Il, Kim, B.S., 2011. Assessment of change in design flood frequency under climate change using a multivariate downscaling model and a precipitation-runoff model. Stoch. Environ. Res. Risk Assess. 25, 567–581. https://doi.org/10.1007/s00477-010-0422-z

Langley, R.S., 2000. Unified approach to probabilistic and possibilistic analysis of uncertain system. J. Eng. Mech. 126, 1163–1172.

Lawrence, D., Hisdal, H., 2011. Hydrological projections for floods in Norway under a future climate, NVE Report. Norwegian Water Resources and Energy Directorate.

Leadbetter, M.R., 1983. Extremes and local dependence in stationary sequences. Probab. Theory Relat. Fields 65, 291–306. https://doi.org/10.1007/BF00532484

Leander, R., Buishand, T.A., 2007. Resampling of regional climate model output for the simulation of extreme river flows. J. Hydrol. 332, 487–496. https://doi.org/10.1016/j.jhydrol.2006.08.006

Leander, R., Buishand, T.A., van den Hurk, B.J.J.M., de Wit, M.J.M., 2008. Estimated changes in flood quantiles of the river Meuse from resampling of regional climate model output. J. Hydrol. 351, 331–343. https://doi.org/10.1016/j.jhydrol.2007.12.020

Leclerc, M., Ouarda, T.B.M.J., 2007. Non-stationary regional flood frequency analysis at ungauged sites. J. Hydrol. 343, 254–265. https://doi.org/10.1016/j.jhydrol.2007.06.021

Legates, D.R., McCabe Jr., G.J., 1999. Evaluating the Use of "Goodness of Fit" Measures in Hydrologic and Hydroclimatic Model Validation. Water Resour. Res. 35, 233–241. https://doi.org/10.1029/1998WR900018

Lenderink, G., Buishand, A., Van Deursen, W., 2007. Estimates of future discharges of the river Rhine using two scenario methodologies: Direct versus delta approach. Hydrol. Earth Syst. Sci. 11, 1145–1159. https://doi.org/10.5194/hess-11-1145-2007

Li, H., Sheffield, J., Wood, E.F., 2010. Bias correction of monthly precipitation and temperature fields from Intergovernmental Panel on Climate Change AR4 models using equidistant quantile matching. J. Geophys. Res. Atmos. 115.

Li, J., Evans, J., Johnson, F., Sharma, A., 2017. A comparison of methods for estimating climate change impact on design rainfall using a high-resolution RCM. J. Hydrol. 547, 413–427. https://doi.org/10.1016/j.jhydrol.2017.02.019

Lloyd, C.D., 2005. Assessing the effect of integrating elevation data into the estimation of monthly precipitation in Great Britain. J. Hydrol. 308, 128–150. https://doi.org/10.1016/j.jhydrol.2004.10.026

Lu, G.Y., Wong, D.W., 2008. An adaptive inverse-distance weighting spatial interpolation technique. Comput. Geosci. 34, 1044–1055. https://doi.org/10.1016/j.cageo.2007.07.010

Ma, L., Zhang, T., Frauenfeld, O.W., Ye, B., Yang, D., Qin, D., 2009. Evaluation of precipitation from the ERA-40, NCEP-1, and NCEP-2 Reanalyses and CMAP-1, CMAP-2, and GPCP-2 with ground-based measurements in China. J. Geophys. Res. Atmos. 114.

Madsen, H., Lawrence, D., Lang, M., Martinkova, M., Kjeldsen, T.R., 2014. Review of trend analysis and climate change projections of extreme precipitation and floods in Europe. J. Hydrol. 519, 3634–3650. https://doi.org/10.1016/j.jhydrol.2014.11.003

Mann, H.B., 1945. Nonparametric tests against trend. Econom. J. Econom. Soc. 245–259.

Manton, M.J., Haylock, M.R., Hennessy, K.J., Nicholls, N., Chambers, L.E., Collins, D.A., Daw, G., Finet, A., Gunawan, D., Inape, K., Isobe, H., Kestin, T.S., Lefale, P., Leyu, C.H., Lwin, T., Maitrepierre, L., Ouprasitwong, N., Page, C.M., Pahalad, J., Plummer, N., Salinger, M.J., Suppiah, R., Tran, V.L., Trewin, B., Tibig, I., Yee, D., 2001. Trends in Extreme Daily Rainfall and Temperature in Southeast Asia and the South Pacific : 1961 – 1998. Int. J. Climatol. 21, 269–284. https://doi.org/10.1002/joc.610

Mantovan, P., Todini, E., 2006. Hydrological forecasting uncertainty assessment: Incoherence of the GLUE methodology. J. Hydrol. 330, 368–381. https://doi.org/10.1016/j.jhydrol.2006.04.046

Maraun, D., 2016. Bias Correcting Climate Change Simulations - a Critical Review. Curr. Clim. Chang. Reports 2, 211–220. https://doi.org/10.1007/s40641-016-0050-x

Maraun, D., 2013. Bias Correction, Quantile Mapping, and Downscaling: Revisiting the Inflation Issue. J. Clim. 26, 2013–2014. https://doi.org/10.1175/JCLI-D-12-00821.1

Maraun, D., Widmann, M., 2018. Statistical Downscaling and Bias Correction for Climate Research. Cambridge University Press.

Mason, S., Waylen, P., Mimmack, G., Rajaratnam, B., Harrison, M., 1999. Changes in Extreme Rainfall Events in South Africa Simon. Clmatic Chang. 41, 249–257.

Merz, B., Thieken, A.H., 2005. Separating natural and epistemic uncertainty in flood frequency analysis. J. Hydrol. 309, 114–132. https://doi.org/10.1016/j.jhydrol.2004.11.015

Miao, C., Su, L., Sun, Q., Duan, Q., 2016. A nonstationary bias-correction technique to remove bias in GCM simulations. J. Geophys. Res. 121, 5718–5735. https://doi.org/10.1002/2015JD024159

MOLIT, 2013. Water Resoures in Korea.

Montanari, A., 2011. 2.17 Uncertainty of Hydrological Prediction, in: Treatise on Water Science. pp. 459–478. https://doi.org/10.1021/jp037247d

Montanari, A., 2007. What do we mean by "uncertainty"? The need for a consistent wording about uncertainty asseement in hydrology. Hydrol. Process. 21, 841–845.

Montanari, A., 2005. Large sample behaviors of the generalized likelihood uncertainty estimation (GLUE) in assessing the uncertainty of rainfall-runoff simulations. Water Resour. Res. 41, 1–13. https://doi.org/10.1029/2004WR003826

Montanari, A., Shoemaker, C.A., Van De Giesen, N., 2009. Introduction to special section on uncertainty assessment in surface and subsurface hydrology: An overview of issues and challenges. Water Resour. Res. 45, 2005–2008. https://doi.org/10.1029/2009WR008471

Nadarajah, S., Choi, D., 2007. Maximum daily rainfall in South Korea. J. Earth Syst. Sci. 116, 311–320. https://doi.org/10.1007/s12040-007-0028-0

Nahar, J., Johnson, F., Sharma, A., 2017. Assessing the extent of non-stationary biases in GCMs. J. Hydrol. 549, 148–162. https://doi.org/10.1016/j.jhydrol.2017.03.045

Nelson, G.C., Rosegrant, M.W., Koo, J., Robertson, R., Sulser, T., Zhu, T., Ringler, C., Msangi, S., Palazzo, A., Batka, M., 2009. Climate change: Impact on agriculture and costs of adaptation. International Food Policy Research Institute.

Nicholson, S.E., Some, B., McCollum, J., Nelkin, E., Klotter, D., Berte, Y., Diallo, B.M., Gaye, I., Kpabeba, G., Ndiaye, O., 2003. Validation of TRMM and other rainfall estimates with a high-density gauge dataset for West Africa. Part I: Validation of GPCC rainfall product and pre-TRMM satellite and blended products. J. Appl. Meteorol. 42, 1337–1354.

Nikulin, G., Jones, C., Giorgi, F., Asrar, G., Büchner, M., Cerezo-Mota, R., Christensen, O.B., Déqué, M., Fernandez, J., Hänsler, A., 2012. Precipitation climatology in an ensemble of CORDEX-Africa regional climate simulations. J. Clim. 25, 6057–6078.

Nyunt, C.T., Koike, T., Yamamoto, A., 2016. Statistical bias correction for climate change impact on the basin scale precipitation in Sri Lanka , Philippines , Japan and Tunisia. https://doi.org/10.5194/hess-2016-14

Obeysekera, J., Salas, J.D., 2016. Frequency of Recurrent Extremes under Nonstationarity. J. Hydrol. Eng. 21, 1–9. https://doi.org/10.1061/(ASCE)HE.1943-5584.0001339.

Obeysekera, J., Salas, J.D., 2014. Quantifying the Uncertainty of Design Floods under Nonstationary Conditions. J. Hydrol. Eng. 19, 1438–1446. https://doi.org/10.1061/(ASCE)HE.1943-5584.0000931

Onogi, K., Tsutsui, J., Koide, H., Sakamoto, M., Kobayashi, S., Hatsushika, H., Matsumoto, T., Yamazaki, N., Kamahori, H., Takahashi, K., Kadokura, S., Wada, K., Kato, K., Oyama, R., Ose, T., Mannoji, N., Taira, R., 2007. The JRA-25 Reanalysis. J. Meteorol. Soc. Japan. Ser. II 85, 369–432. https://doi.org/10.2151/jmsj.85.369

Ouarda, T.B.M.J., El-Adlouni, S., 2011. Bayesian nonstationary frequency analysis of hydrological variables. J. Am. Water Resour. Assoc. 47, 496–505. https://doi.org/10.1111/j.1752-1688.2011.00544.x

Overeem, A., Buishand, A., Holleman, I., 2008. Rainfall depth-duration-frequency curves and their uncertainties. J. Hydrol. 348, 124–134. https://doi.org/10.1016/j.jhydrol.2007.09.044

Panagoulia, D., Economou, P., Caroni, C., 2014. Stationary and nonstationary generalized extreme value modelling of extreme precipitation over a mountainous area under climate change. Environmetrics 25, 29–43. https://doi.org/10.1002/env.2252

Park, J.S., Kang, H.S., Lee, Y.S., Kim, M.K., 2011. Changes in the extreme daily rainfall in South Korea. Int. J. Climatol. 31, 2290–2299. https://doi.org/10.1002/joc.2236

Parker, W.S., 2016. Reanalyses and Observations: What's the difference?'. Bull. Am. Meteorol. Soc. 97, 1565–1572. https://doi.org/10.1175/BAMS-D-14-00226.1

Patz, J.A., Campbell-Lendrum, D., Holloway, T., Foley, J.A., 2005. Impact of regional climate change on human health. Nature 438, 310–317.

Perkins, S.E., Pitman, A.J., Holbrook, N.J., McAneney, J., 2007. Evaluation of the AR4 climate models' simulated daily maximum temperature, minimum temperature, and precipitation over Australia using probability density functions. J. Clim. 20, 4356–4376. https://doi.org/10.1175/Jcli4253.1

Piani, C., Haerter, J.O., Coppola, E., 2010. Statistical bias correction for daily precipitation in regional climate models over Europe. Theor. Appl. Climatol. 99, 187–192. https://doi.org/10.1007/s00704-009-0134-9

Poli, P., Hersbach, H., Dee, D.P., Berrisford, P., Simmons, A.J., Vitart, F., Laloyaux, P., Tan, D.G.H., Peubey, C., Thépaut, J.-N., 2016. ERA-20C: An Atmospheric Reanalysis of the Twentieth Century. J. Clim. 29, 4083–4097.

Poli, P., Hersbach, H., Tan, D., Dee, D., Thépaut, J.-N., Simmons, A., Peubey, C., Laloyaux, P., Komori, T., Berrisford, P., Dragani, R., Trémolet, Y., Holm, E., Bonavita, M., Isaksen, L., Fisher, M., 2013. The data assimilation system and initial performance evaluation of the ECMWF pilot reanalysis of the 20th-century assimilating surface observations only (ERA-20C), ERA report series.

Rabiei, E., Haberlandt, U., 2015. Applying bias correction for merging rain gauge and radar data. J. Hydrol. 522, 544–557.

Read, L.K., Vogel, R.M., 2015. Reliability, return periods, and risk under nonstationarity. Water Resour. Res. 51, 6381–6398. https://doi.org/10.1002/ 2015WR017089

Reis, D.S., Stedinger, J.R., 2005. Bayesian MCMC flood frequency analysis with historical information. J. Hydrol. 313, 97–116. https://doi.org/10.1016/j.jhydrol.2005.02.028

Salas, J.D., Obeysekera, J., 2014. Revisiting the Concepts of Return Period and Risk for Nonstationary Hydrologic Extreme Events. J. Hydrol. Eng. 19, 554–568. https://doi.org/10.1061/ (ASCE)HE.1943-5584.0000820

Salas, J.D., Obeysekera, J., Vogel, R.M., 2018. Techniques for assessing water infrastructure for nonstationary extreme events: a review. Hydrol. Sci. J. 63, 325–352. https://doi.org/10.1080/02626667.2018.1426858

Sayemuzzaman, M., Jha, M.K., 2014. Seasonal and annual precipitation time series trend analysis in North Carolina, United States. Atmos. Res. 137, 183–194.

Schmidli, J., Frei, C., Vidale, P.L., 2006a. Downscaling from GCM precipitation: A benchmark for dynamical and statistical downscaling methods. Int. J. Climatol. 26, 679–689. https://doi.org/10.1002/joc.1287

Schmidli, J., Frei, C., Vidale, P.L., 2006b. Downscaling from GCM precipitation: a benchmark for dynamical and statistical downscaling methods. Int. J. Climatol. 26, 679–689.

Schneider, U., Becker, A., Finger, P., Meyer-Christoffer, A., Rudolf, B., Ziese, M., 2015. GPCC Full Data Reanalysis Version 7.0 at 0.5°: Monthly Land-Surface Precipitation from Rain-Gauges built on GTS-based and Historic Data [WWW Document]. Res. Data Arch. Natl. Cent. Atmos. Res. https://doi.org/10.5065/D6000072

Sen, P.K., 1968. Estimates of the regression coefficient based on Kendall's tau. J. Am. Stat. Assoc. 63, 1379–1389.

Shadmani, M., Marofi, S., Roknian, M., 2012. Trend analysis in reference evapotranspiration using Mann-Kendall and Spearman's Rho tests in arid regions of Iran. Water Resour. Manag. 26, 211–224.

Sheffield, J., Wood, E.F., Roderick, M.L., 2012. Little change in global drought over the past 60 years. Nature 491, 435–438. https://doi.org/10.1038/nature11575

Simmons, A.J., Jones, P.D., Bechtold, V.D., Beljaars, A.C.M., Kallberg, P.W., Saarinen, S., Uppala, S.M., Viterbo, P., Wedi, N., 2004. Comparison of trends and low-frequency variability in CRU, ERA-40, and NCEP/NCAR analyses of surface air temperature. J. Geophys. Res. Atmos. 109. https://doi.org/10.1029/2004jd005306

Smith, A., Freer, J., Bates, P., Sampson, C., 2014. Comparing ensemble projections of flooding against flood estimation by continuous simulation. J. Hydrol. 511, 205–219. https://doi.org/10.1016/j.jhydrol.2014.01.045

Son, C., Lee, T., Kwon, H.H., 2017. Integrating nonstationary behaviors of typhoon and non-typhoon extreme rainfall events in East Asia. Sci. Rep. 7, 1–9. https://doi.org/10.1038/s41598-017-04629-1

Stephens, E., Bates, P., 2015. Assessing the reliability of probabilistic flood inundation model

predictions. Hydrol. Process. 29, 4264–4283. https://doi.org/10.1002/hyp.10451

Talagrand, O., 1997. Assimilation of Observations, an Introduction. J. Meteorol. Soc. Japan 75, 191–209.

Teegavarapu, R.S.V., Chandramouli, V., 2005. Improved weighting methods, deterministic and stochastic data-driven models for estimation of missing precipitation records. J. Hydrol. 312, 191–206. https://doi.org/10.1016/j.jhydrol.2005.02.015

Teng, J., Jakeman, A.J., Vaze, J., Croke, B.F.W., Dutta, D., Kim, S., 2017. Flood inundation modelling: A review of methods, recent advances and uncertainty analysis. Environ. Model. Softw. 90, 201–216. https://doi.org/10.1016/j.envsoft.2017.01.006

Teutschbein, C., Seibert, J., 2012. Bias correction of regional climate model simulations for hydrological climate-change impact studies: Review and evaluation of different methods. J. Hydrol. 456, 12–29.

Theil, H., 1950. A rank-invariant method of linear and polynomial regression analysis. I, II, III. Proc. K. Ned. Akad. van Wet. 53, 386–392, 521–525, 1397–1412.

Themeßl, M.J., Gobiet, A., Leuprecht, A., 2012. Empirical-statistical downscaling and error correction of daily precipitation from regional climate models. Int. J. Climatol. 31, 1530–1544. https://doi.org/10.1002/joc.2168

Thorne, P.W., Vose, R.S., 2010. Reanalyses Suitable for Characterizing Long-Term TrendsAre They Really Achievable? Are They Really Achievable? Bull. Am. Meteorol. Soc. 91, 353–361. https://doi.org/10.1175/2009BAMS2858.1

Tomczak, M., 1998. Spatial Interpolation and its Uncertainty Using Automated Anisotropic Inverse Distance Weighting (IDW) - Cross-Validation/Jackknife Approach. J. Geogr. Inf. Decis. … 2, 18–30.

Tung, Y. koung, Wong, C. leung, 2014. Assessment of design rainfall uncertainty for hydrologic engineering applications in Hong Kong. Stoch. Environ. Res. Risk Assess. 28, 583–592. https://doi.org/10.1007/s00477-013-0774-2

UK Environment Agency, 2017. Flood risk assessments: climate change allowances [WWW Document]. Environ. Agency. URL https://www.gov.uk/guidance/flood-risk-assessments-climate-change-allowances (accessed 6.25.18).

Uppala, S.M., Kållberg, P.W., Simmons, A.J., Andrae, U., Bechtold, V. d, Fiorino, M., Gibson, J.K., Haseler, J., Hernandez, A., Kelly, G.A., 2005. The ERA ‐ 40 re ‐ analysis. Q. J. R. Meteorol. Soc. 131, 2961–3012.

Van de Vyver, H., 2015. Bayesian estimation of rainfall intensity-duration-frequency relationships. J. Hydrol. 529, 1451–1463. https://doi.org/10.1016/j.jhydrol.2015.08.036

Volosciuk, C., Maraun, D., Vrac, M., Widmann, M., 2017. A combined statistical bias correction and stochastic downscaling method for precipitation. Hydrol. Earth Syst. Sci. 21, 1693–1719. https://doi.org/10.5194/hess-21-1693-2017

Vörösmarty, C.J., Green, P., Salisbury, J., Lammers, R.B., 2000. Global water resources: vulnerability from climate change and population growth. Science (80-.). 289, 284–288. https://doi.org/10.1126/science.289.5477.284

Vrac, M., Naveau, P., 2007. Stochastic downscaling of precipitation : From dry events to heavy rainfalls. Water Resour. Res. 43, 1–13. https://doi.org/10.1029/2006WR005308

Vrugt, J.A., ter Braak, C.J.F., Gupta, H. V., Robinson, B.A., 2009. Equifinality of formal (DREAM) and informal (GLUE) Bayesian approaches in hydrologic modeling? Stoch. Environ. Res. Risk Assess. 23, 1011–1026. https://doi.org/10.1007/s00477-008-0274-y

Wang, B., Ding, Q., Jhun, J., 2006. Trends in Seoul (1778–2004) summer precipitation. Geophys. Res. Lett. 33.

Wang, W. chuan, Chau, K. wing, Xu, D. mei, Chen, X.Y., 2015. Improving Forecasting Accuracy of Annual Runoff Time Series Using ARIMA Based on EEMD Decomposition. Water Resour. Manag. 29, 2655–2675. https://doi.org/10.1007/s11269-015-0962-6

Westra, S., Fowler, H.J., Evans, J.P., Alexander, L. V, Berg, P., Johnson, F., Kendon, E.J., Lenderink, G., Roberts, N.M., 2014. Future changes to the intensity and frequency of short-duration extreme rainfall. Rev. Geophys. 52, 522–555. https://doi.org/10.1002/2014RG000464

Wilks, D.S., 1999. Interannual variability and extreme-value characteristics of several stochastic daily precipitation models. Agric. For. Meteorol. 93, 153–169. https://doi.org/10.1016/S0168-1923(98)00125-7

Wilson, P.S., Toumi, R., 2005. A fundamental probability distribution for heavy rainfall. Geophys. Res. Lett. 32, 1–4. https://doi.org/10.1029/2005GL022465

Wu, C.L., Chau, K.W., Fan, C., 2010. Prediction of rainfall time series using modular artificial neural networks coupled with data-preprocessing techniques. J. Hydrol. 389, 146–167. https://doi.org/10.1016/j.jhydrol.2010.05.040

Xu, Z.X., Gong, T.L., Li, J.Y., 2008. Decadal trend of climate in the Tibetan Plateau—regional temperature and precipitation. Hydrol. Process. 22, 3056–3065.

Xu, Z.X., Takeuchi, K., Ishidaira, H., Li, J.Y., 2005. Long-term trend analysis for precipitation in Asian Pacific FRIEND river basins. Hydrol. Process. 19, 3517–3532.

Yilmaz, A.G., Hossain, I., Perera, B.J.C., 2014. Effect of climate change and variability on extreme rainfall intensity-frequency-duration relationships: A case study of Melbourne. Hydrol. Earth Syst. Sci. 18, 4065–4076. https://doi.org/10.5194/hess-18-4065-2014

Zang, C., Liu, J., 2013. Trend analysis for the flows of green and blue water in the Heihe River basin, northwestern China. J. Hydrol. 502, 27–36. https://doi.org/10.1016/j.jhydrol.2013.08.022

Zhang, L., Zhou, T., 2011. An assessment of monsoon precipitation changes during 1901–2001. Clim. Dyn. 37, 279–296.

Zhang, Z., Guo, W., Gong, D., Kim, S.J., 2013. Evaluation of the twentieth century reanalysis dataset in describing East Asian winter monsoon variability. Adv. Atmos. Sci. 30, 1645–1652. https://doi.org/10.1007/s00376-012-2226-1

Zhao, T., Fu, C., 2006. comparison of production from ERa-40, ncep-2, and cur for summer prec over china(2006).pdf. Adv. atmosheric Sci. 23, 593–604.